THE UNIVERSITY
of EDINBURGH

THE UNIVERSITY
of EDINBURGH

Comparing the hydrogeological prospectivity of three UK locations for deep radioactive waste disposal

Emma V. Hipkins

Thesis submitted in fulfilment of
the requirements for the degree of
Doctor of Philosophy
to the
University of Edinburgh
October 2018

Abstract

The UK has a large and growing inventory of higher activity radioactive waste awaiting safe long term disposal. The international consensus is to dispose of this radioactive and toxic waste within a deep geological repository, situated 200-1,000 metres beneath the ground surface.

The deep geological disposal facility is designed to be a series of engineered and natural barriers. Groundwater forms an integral component of the natural barrier because it 1) controls the flux of reactive components towards the engineered repository, and 2) forms one of the primary transport mechanism through which released radionuclides can be transported away from the repository. The timescale of protection provided by the natural barrier exceeds those provided by the engineered barriers. Knowledge of the regional hydrogeology is a vital step towards predicting the long term performance of any potential repository site. Topically, a UK government decision in 2017 to re-open a nation-wide repository location search has now created a renewed mandate for site exploration.

This research aims to determine the regional groundwater characteristics of three UK settings, selected to be hydrogeologically distinct, in order to determine which, if any, offers natural long term hydrogeological containment potential. The settings selected for analysis include Sellafield in West Cumbria, the Tynwald Basin within the East Irish Sea Basin, and Thetford within East Anglia. Site selection is based on diverse groundwater characteristics, and on previous research suggesting potential hydrogeological suitability at these locations. This research is novel in that it provides, for the first time, a direct comparison between the characteristics and qualities of different regional groundwater settings to contain and isolate radioactive waste, based on UK site specific data.

Large and detailed numerical models for the three sites, covering areas of 30 km length by 2-4 km depth have been developed using the open source finite element code ‘OpenGeoSys’. The models couple the physical processes of liquid flow and heat transport, in order to replicate regional scale groundwater flow patterns. Models are calibrated to measured rock properties, and predict groundwater behaviour 10,000 years into the future. Uncertain parameter ranges of lithological and fault permeabilities, and peak repository temperatures are tested to determine the possible range of groundwater outcomes. Geochemical retention is assessed separately and validated using the finite difference modelling software ‘GoldSim’. Worst case groundwater characteristics for containment and isolation at each site are compared to an ‘ideal’ benchmark far-field hydrogeological outflow scenario, and scored accordingly using a newly proposed method of assessment.

Results show that the Tynwald Basin offers the best potential of the three sites for natural radionuclide containment, performing between 3.5 and 4 times better than Sellafield, and between 1.7 and 4 times better than Thetford. The Tynwald Basin is characterised by 1) long and deep groundwater pathways, and 2) slow local and regional groundwater movement. Furthermore, the Tynwald Basin is located at a feasible tunnelling distance from the coast, adjacent to the UK's current nuclear stockpile at Sellafield, and thus could provide a simple solution to the current waste legacy problem.

Results from the Sellafield model indicate that this location cannot be considered to exhibit beneficial characteristics due to short and predictable groundwater pathways which ascend, from the repository, towards surface aquifers. Finally, Thetford within East Anglia has never been drilled to depth so that sub-surface rock properties of basement, located beneath layered sediments, are based on evidence inferred from around the UK. Uncertainties in rock properties has produced a wide range of groundwater characteristic possibilities, with results indicting prospective performance to range from 0 to 2.4 times better than Sellafield. As such, the hydrogeological suitability to host a potential deep geological repository is promising when modelled with most-likely permeability values, but cannot be accurately determined at present.

Consideration of decaying heat from the heat emitting waste packages at the three sites reveal that the natural groundwater flow patterns can be distorted up to as much as 7 km away from the theoretical repository, depending on setting. This thus changes the use of the term 'near-field' for safety assessments, as implying an area within the immediate vicinity of the excavated repository site.

The overarching findings from this research are that: 1) some locations have greater long term radionuclide containment and isolation prospectivity than others, due to variable quality far-field geological and hydrogeological characteristics; 2) the effect of radiogenic heat emission on the natural groundwater flow pattern is dependent on the site specific geological and hydrogeological characteristics, and therefore so is the area defined as the 'near-field'; and 3) a simple method of site comparison is possible for regional groundwater system under steadystate conditions.

Recommendations are for scoping models of regional groundwater settings to be used as a comparative tool, such as undertaken as part of this research, to differentiate between potential sites at an early stage of the current UK site selection programme.

Lay Summary

Radioactive material is produced from medical, military, industrial practice and research, but most of its tonnage is derived from nuclear power generation. When there is no possibility for the radioactive material to be re-used, the material is termed *'radioactive waste'*, and must be managed safely. The safe management of radioactive waste is a major challenge facing nuclear power nations due to the dangerously high levels of radioactivity (activity of single high level waste package up to 24,500 times higher than Public Health England radon action levels), long duration of existence (up to 1 million years), and high levels of heat emitted from some of the radioactive waste packages (100 °C).

The most common approach to dealing with this highly radioactive waste is to dispose of it underground at a depth of between 500 and 1,000 m, that's 1 and 3 times the height of 'The Shard'. The radioactive waste will be placed within a specially designed engineered facility termed a *'deep geological disposal facility'*. One of the containment strategies to ensure the radioactive waste remains underground for up to 1 million years, is by having multiple barriers located between the radioactive waste and the human environment at the surface. One of these barriers, which also happens to be the final barrier protecting the human environment from the radioactive waste, is the surrounding rock mass and its groundwater.

Groundwater can be static or can flow through small spaces in the rock mass termed *'pores'*. Understanding of this water flow is essential to predict how long the radioactive waste will remain underground. This is because groundwater is the one of the primary transport mechanism through which radioactive waste will be leached from a repository, and transported back towards the surface, just as coffee granules are dissolved and transported within water when making a cup of coffee.

The controls on the speed and direction of groundwater flow near to the deep geological disposal facility are however often determined by features much further away, such as a result of nearby mountain ranges, river basins, geological formations, and even the sea. Therefore, in order to understand how well a particular location might keep radioactive waste under the ground, it is necessary to consider the wider setting. This wider setting can extend over many kilometres, and in the case of this research, a length of 30 km has been selected for investigation, the distance between York and Leeds city centres.

The wider setting will however change over the 1 million year timeframe, most notably as a result of climate change, especially glaciation events. To put these timescales into context, the last glaciation event finish in Britain *circa* 15,000 years ago, and Homo-sapiens only

spread out from their homeland in the East African Rift Valley *circa.* 300,000 years ago. Challenges are thus associated with predicting deep geological disposal facility performance, and groundwater behaviour over these timescales.

The aim of this research is to understand the groundwater speed and direction across the underground geology in three different UK settings, and to work out which, if any, are likely to ensure radioactive waste remains underground for many thousands of years. The settings selected for analysis are Sellafield in West Cumbria, the Tynwald Basin beneath the Irish Sea, and near Thetford within East Anglia. The chosen sites are based on previous research which suggested these locations may have diverse groundwater characteristics.

Large and detailed computer models were run in order to predict the speed and direction of the groundwater within each of these settings. The models show where groundwater flows over timescales of 10,000 years, and how fast.

This research finds that: 1) the Tynwald Basin has the potential to perform between 3.5 and 4 times better than Sellafield, and between 1.7 and 4 times better than Thetford, and thus this research can conclude that some locations offer substantially better radionuclide containment and isolation potential than others; 2) the area of sub-surface affected by heat production (from the radioactive waste packages) varies significantly between locations, and thus should be assessed on a site-by-site basis; and 3) a simple method of groundwater speed and direction comparison between sites is possible.

Overarching recommendations from this research are that the quality of many more UK based regional groundwater settings should be compared. This should be undertaken as part of the current and on-going national deep geological disposal site selection programme, in order to aid decision making as to what is a comparatively *'good'* location to store the UK's nuclear waste legacy.

Declaration and attribution of work

I declare that this thesis has been composed solely by myself and that it has not been submitted, in whole or in part, in any previous application for a degree. Except where states otherwise by reference or acknowledgment, the work presented is entirely my own.

Emma V. Hipkins

October 2018

Additional Research Specific Declarations

The sites selected for analysis in this research have NOT been selected, nor are under investigation as potential deep geological facilities by the Nuclear Decommissioning Authority. Site selection within the research has been undertaken as a theoretical exercise at the discretion of the author, and does not reflect the current government position.

The findings from this research are not intended to replace the research undertaken, and currently being undertaken by the Nuclear Decommissioning Authority, but is instead intended to widen the discussion as to the role the regional groundwater setting should play in site selection.

The modelling undertaken of the Sellafield site has built on previous work undertaken by (Fraser Harris et al. 2015). The original model encompassed an area 6 km in length by 1.7 km depth within the immediate vicinity of the proposed rock characterisation facility (Nirex 1997b). This research has expanded that area out to 30 km in length, and 2.08 km depth. The repository footprint has been elongated in line with the generic design criteria (Nuclear Decommissioning Authority 2010a), and the Borrowdale Volcanic Group's Fleming Hall Formation, Bleawath Formation and Moorside Formation have been included.

Access to a GoldSim contaminant and radionuclide transport licence (GoldSim Technology Group 2017a; GoldSim Technology Group 2017b), in addition to technical and financial support has been provided by Golder Associates Ltd.

Emma V. Hipkins

October 2018

Acknowledgements

First and foremost I want to say a big thank you to Stuart Haszeldine (primary supervisor) and Chris McDermott (secondary supervisor) at the University of Edinburgh for granting me the opportunity to undertake this research. Their support and guidance throughout the four years has been absolutely invaluable, and I would not have progressed as far as I did without them.

Stuart has supported me in formulating my research ideas, providing historic context, insight, and vision into the political and contentious world of radioactive waste disposal. Chris has helped and guided me in numerical model development, teaching me the process and philosophy of numerical modelling, and the hydrogeological principles underlying them. Both have spent time reviewing work and providing almost continuous emotional support and encouragement.

I also want to thank the National Environmental Research Council (NERC) for their sponsorship, and admission onto the Doctoral Training Programme (DTP), which has offered many opportunities for wider development and learning. Without NERC this research could not have happened.

I also want to say a big thank you to Golder Associates for enabling me to undertake this research, and providing financial support. To James Dowle (industrial supervisor) at Golder who not only gave me my first job as a graduate hydrogeologist, but also introduced me to the issue of radioactive waste disposal through assignments at British Nuclear Power Stations, igniting my interest in the subject. During the research, James granted me the opportunity to use the GoldSim software, and has provided ongoing technical knowledge and guidance on geochemical modelling.

Next I would like to thank Mike Mineter at the University of Edinburgh for his seemingly infinite computational wisdom and expertise, without whom my numerical models would probably still be running today! Mike revolutionised my ability to run multiple models at once, saving vast amounts of time and energy, for which I am eternally grateful.

It is also important for me to thank Andrew Fraser-Harris (aka. Gus) at the University of Edinburgh, who had the unfortunate luck of learning OpenGeoSys before me, and as such, became a frequently visited sounding board. Gus has provided ongoing technical support over the past four years.

In addition, thanks must be made to Kate Heal (advisor), the Geoenergy Research Group, Ross, Justin and Magnus in IT, Stephanie and Pete from the DTP, Matt Ball, Mark Naylor and Alex Thomas, all of whom have contributed in some shape or form to this programme of study.

Moving on to family and friends, first and foremost I want to thank my Mum (Alison) and Dad (Steve). Through their relentless support and encouragement over the past 28 years I have developed, progressed and achieved far more than I ever thought possible. I am very lucky to have them as my parents, and I know their support and guidance will continue.

I also want to thank my brother Alex who has taken time to proof read my thesis, and who's unfiltered honestly has never failed to make me laugh: "Emma, this is categorically the most boring thing I have ever read...", "try writing it" I said.

Next I want to show appreciation for my friends; namely Anna, Amelia and Becky who I have spent may long hours with discussing all manner of issues: professional; personal; and miscellaneous. Their cheese and whisky parties have absolutely kept me going.

Last but certainly not least I would like to thank my partner Julien who, despite undertaking his own Ph.D. (which he successfully vivaed in June) has provided me with non-stop support and encouragement from day one. I am so proud of his achievement, as I know he is of mine.

Contents

List of Figures

Chapter 1 Introduction

Chapter 1 will present an overview of radioactive waste in the UK (section 1.1), including its life cycle (section 1.1.1), its volumes and the locations where it is stored (section 1.1.2), the chemical and radiological composition of the waste (section 1.1.3), the characteristics of higher activity waste (1.1.4), and finally the preferred disposal method (section 1.1.5). This will be followed by the position and importance of this research (section 1.2), the overarching aims and hypotheses (section 1.3), the general approached used to resolve the hypotheses (section 1.4), and finally the overall thesis layout and structure (section 1.5).

1.1 Background

1.1.1 Nuclear Energy to Radioactive Waste Disposal

Radioactive decay, originally discovered by Henri Becquerel in 1896 (Sekiya & Yamasaki 2015), is the process whereby an unstable atomic nucleus, termed the *'parent isotope'*, loses energy by emitting radiation in the form of alpha particles, beta particles or gamma rays to form a *'daughter isotope'*. Radioactivity is defined by the number of nuclei that decay and give off radiation per second, and is measured in Becquerel's (Bq) (Tuniz 2012). Energy in the form of heat is also given off by this process which, when part of a controlled fission decay chain, can be harnessed to produce electricity (Tuniz 2012).

A byproduct of this process is irradiated material, both direct in the form of the raw material used to fuel the fission reaction, and indirectly from neutron bombardment of surrounding material, such as reactor equipment. The irradiated material that cannot be re-used is termed *'radioactive waste'*. Dealing with radioactive waste safely is a major source of concern for nuclear producing nations given its cancerous properties, and as such, research into safe disposal has become an area of intense scientific interest.

The characteristics of the radioactive waste determine how it should be dealt with. For radioactive wastes with lower levels of radioactivity, disposal within permitted landfills or underground engineered *'near-surface disposal facilities'* is sufficient, however, for radioactive wastes with higher levels of radioactivity, the international consensus is to dispose of this waste deeper underground within *'deep geological disposal facilities'*, considered to offer greater protection.

The UK has near-surface disposal facilities for lower activity radioactive waste, but currently no deep geological disposal facility for higher activity radioactive waste. As a result, higher

activity wastes are currently held within temporary surface storage at various locations across the UK (Nuclear Decommissioning Authority 2014).

Internationally the progress towards selection of suitable deep geological facility locations is variable. The Waste Isolation Pilot Plant (USA) is operational and accepting military derived radioactive waste (Waste Isolation Pilot Plant 2018), but the Yucca Mountain site (USA) for civil nuclear power derived radioactive waste has stalled (U.S. Department of Energy 2010). Construction has also begun on deep geological disposal facilities at Forsmark in Sweden (SKB 2009) and Olkiluoto in Finland (Posiva Oy 2017), with final sites agreed at Kincardine in Canada for non heat producing higher activity wastes (Ontario Power Generation 2018), and Bure in France (Andra 2018a). No final site has thus far been agreed however for Germany, Switzerland, Italy, Japan, Korea or the UK, or for Canada's heat producing higher activity wastes (Ontario Power Generation 2018).

1.1.2 UK Radioactive Waste Stockpile

The UK opened the world's first commercial nuclear power station, Calder Hall, in West Cumbria in 1956. The UK currently obtains 21% of its total electricity production from nuclear power (Figure 1.1), produced over 8 separate sites (Department for Business 2017).

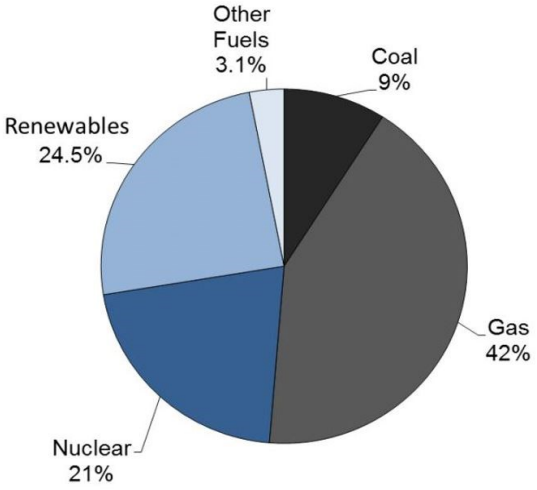

Figure 1.1: Summary of electricity generation in the UK in 2016 by fuel type (Department for Business 2017).

It is estimated that by 2125, when all the existing nuclear facilities have been decommissioned, the UK will have an estimated 4.77 million m^3 of packaged radioactive waste (Nuclear Decommissioning Authority 2017c), enough to fill Wembley Stadium 1.2 times. Although the vast majority of this waste is derived from the civil nuclear power, reprocessing and research industry (98%), small contributions (< 2%) are also made from medical and military practice (Nuclear Decommissioning Authority 2013c).

In 2008, the government announced investment in a new generation of nuclear power stations (Department for Business Enterprise & Regulatory Reform 2008), intended to contribute a further 16 gigawatts of nuclear power capacity to the energy grid by 2030, by the way of 12 new nuclear reactors (Department of Energy & Climate Change 2013b). The decision to pursue future nuclear power generation came as a response for the need to improve energy security by increasing national generation capacity (Department of Energy & Climate Change 2013b), and to invest in low CO_2 producing technologies following the Paris Climate Agreement (2015). The paris agreement aims to limit global temperature rise to 1.5 degrees over the next 100 years (United Nations 2017).

The new generation of nuclear power stations will lead to further, as yet unquantified, volumes of radioactive waste (Nuclear Decommissioning Authority 2017b). It is therefore crucial that a suitable UK location for deep geological facility development is found, especially given that the first bricks of Hinkley Point C, the first of the new generation of nuclear power stations, have already been laid (Department for Business 2017).

1.1.3 Radioactive Waste Classification

The international norm is to classify radioactive waste based on activity content, radioactive half-life and radiogenic heat emission, leading to three main classifications; high level waste (HLW), intermediate level waste (ILW) and low level waste (LLW) (International Atomic Energy Agency 2009a).

HLW is defined as waste with > 4 gigabecquerels per tonne (GBq/tonne) of alpha activity or > 12 GBq/tonne of beta or gamma activity, and for which the amount of radiogenic heat emitted requires consideration within the disposal facility design. ILW is defined the same as HLW, but for which radiogenic heat does not require consideration within the disposal facility design. LLW is classified as having < 4 GBq/tonne of alpha activity and < 12 GBq/tonne of beta or gamma activity. VLLW, itself a sub-division of LLW, is defined as waste for which each 0.1 m^3 of material has < 400 kilobecquerels (kBq) of total activity, or a single item contains < 40kBq of total activity (Nuclear Decommissioning Authority 2013a). For comparison, Public Health England guidelines are for homes with > 200 Bq/m^3 of radon (naturally produced radioactive gas) to improve ventilation (Public Health England 2017), that's 24,500 times less that the radioactivity given out by HLW (assuming air density of 1.225 kg/m^3). The levels of radiation produced by radioactive waste thus require management. A summary of UK waste origin, packaging and volumes by classification is presented within Figure 1.2.

Waste Classification	Image of waste packaged (HLW & ILW) and unpackaged (LLW)	Origin of waste	Conditioning and packaging of waste	Composition and mass of conditioned and packaged waste (1st April 2016)	Image of interim Storage (HLW & ILW) and Near-Surface Disposal Facility (LLW)
High Level Waste (HLW)		• Reprocessing of spent fuel	Vitrified into a borosilicate glass and emplaced within 150 L stainless steel canister	~3,000 tonnes total including: • Metals (~23 tonnes) • Inorganics (~3,000 tonnes)	
Intermediate Level Waste (ILW)		• Reprocessing of spent fuel • Reactor decommissioning	Encapsulated within cement or polymer based matrix, and then emplaced within either a 3 m^3 stainless streel box, or a 500 L stainless steel drum	~310,000 tonnes total including: • Metals (~95,000 tonnes) • Organics (~11,000 tonnes) • Inorganics (~181,000 tonnes) • Soil (~6.2 tonnes) • Other (~21,000 tonnes)	
Low Level Waste (LLW)		• Decommissioning of nuclear facilities	Encapsulated in cement and emplaced within large steel containers	~1.7 million tonnes total including: • Metals (~564,000 tonnes) • Organics (~111,000 tonnes) • Inorganics (~957,000 tonnes) • Soil (~69,000 tonnes) • Other (~33,000 tonnes)	

Figure 1.2: Summary of the main waste classifications, origin of the wastes, conditioning and packaging of the wastes, and the composition and mass of the conditioned and packaged waste as per 1st April 2016. Information and images compiled from (Nuclear Decommissioning Authority 2014; Nuclear Decommissioning Authority 2017c)

1.1.4 Higher Activity Radioactive Waste (HAW)

Radioactive waste intended for deep geological disposal is termed *'higher activity radioactive waste'* (HAW), and includes HLW, ILW, and some LLW (<1% of total LLW) for which near surface disposal is not considered suitable (Nuclear Decommissioning Authority 2017c; Nuclear Decommissioning Authority 2014).

Previous estimates have put the total UK volume of HAW at 650,000 m^3 (Nuclear Decommissioning Authority 2014), but this value does not include waste produced from the new generation of nuclear power stations, nor does it include materials not currently classified as waste due to reprocessing and enrichment activities, such as spent nuclear fuel, Uranium and Plutonium stocks (Nuclear Decommissioning Authority 2014). Reprocessing of spent fuel is expected to continue until 2020 (Nuclear Decommissioning Authority 2017c), after which it too will require disposal within a deep geological facility as HLW.

Interestingly, although HLW only accounts for 0.03% of the total packaged waste volume, it contains > 95% of the total activity, in comparison to LLW which accounts for 30 % of the total waste but only 0.00003 % of the total activity (Figure 1.3) (Nuclear Decommissioning Authority 2017b).

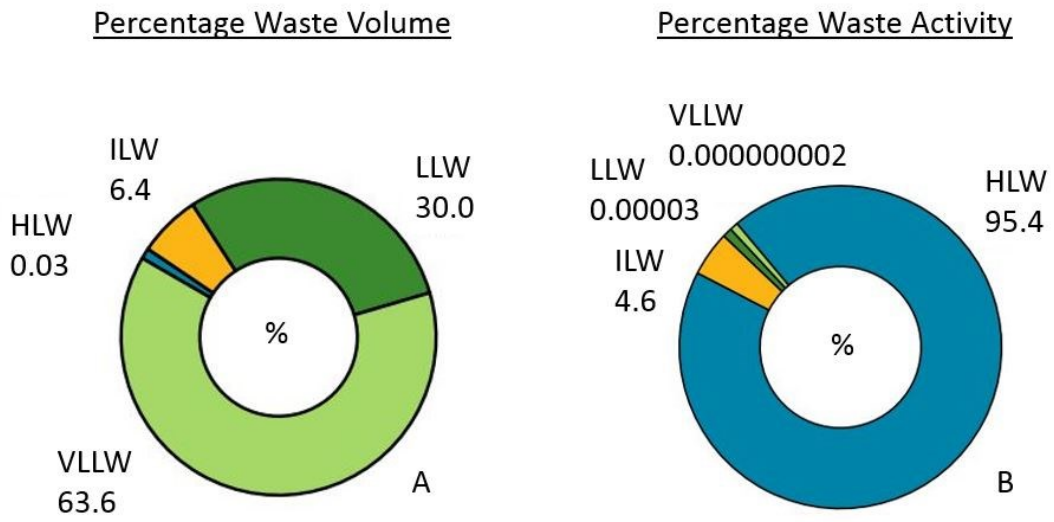

Figure 1.3: Comparison of HLW, ILW, LLW and VLLW: A) percentage contribution to total packaged waste volume, and B) percentage contribution to total waste activity (Nuclear Decommissioning Authority 2017b).

HLW releases the greatest amount of radioactivity over the first 1,000 years out of the three waste classifications (Figure 1.4) due to the decay of shorter lived radionuclides such as Americium-241 and Strontium-90, with ILW becoming the dominant contributor over the following 100 million years (although at much lower levels) due to longer lived radionuclides

such as Nickel-59 (Nuclear Decommissioning Authority 2017c). The relative contribution to total activity from LLW also increases with time, primarily due to very long lived radionuclides such as Uranium-235, Uranium-238, and Lead-210 (Nuclear Decommissioning Authority 2017c).

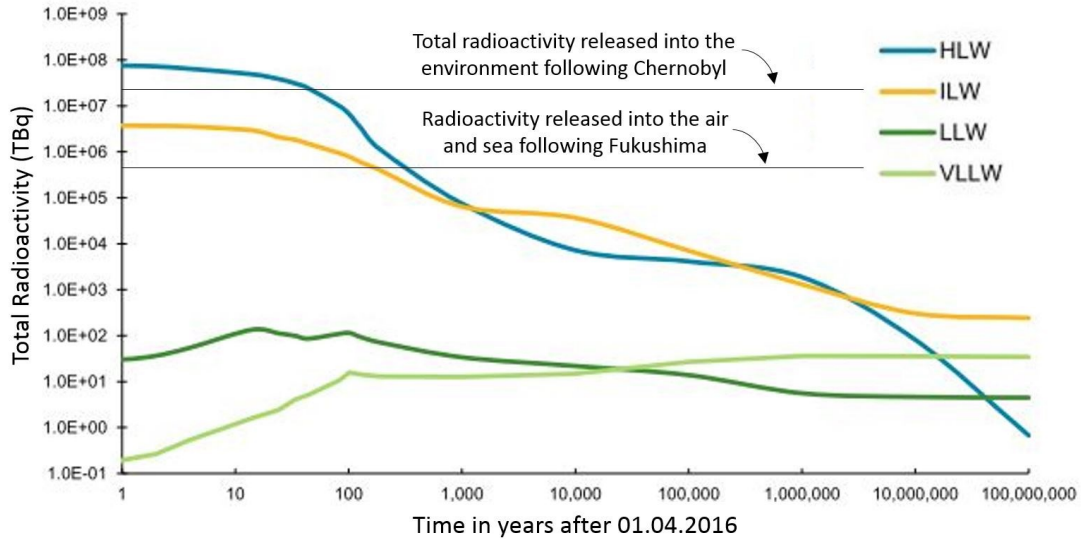

Figure 1.4: Total radioactivity as a function of time post 1st April 2016 (Nuclear Decommissioning Authority 2017c), with information of radioactivity comparisons from Chernobyl and Fukushima obtained from (Institute of Nuclear Power Operations 2011).

As a by-product of the rapid decay of many shorter lived radionuclides, HLW also produces a lot of heat. It is this heat production, most prevalent over the first 1,000 years post disposal (Figure 1.4), which requires consideration within the design of the final disposal facility.

Energy (heat) output estimates for HLW packages are variable, with (Nirex 2005d) predicting 1900 to 3200 W/canister at the time of construction, reducing down to 400 to 600 W/canister after 50 years. Similarly, (McGinnes 2002) predicts 1500 to 2100 W/canister 40 years after reactor discharge, decaying down to between 490 and 810 W/canister after 100 years. For comparison, a typical electric heater has an energy transfer rate of between 1500 and 2000 W.

Regardless of heat output uncertainty, HLW canisters should be designed as to ensure the temperature on the outside of the HLW waste package does not exceed 100 °C, as this could cause damage to the disposal facility (Nirex 2005d), and its ability to contain and isolate radioactive waste.

1.1.5 Deep Geological Disposal

The international consensus is to dispose of HAW within a deep geological disposal facility (Figure 1.5), situated 200-1,000 m below the ground surface (Nuclear Decommissioning

Authority 2013b; Streffer et al. 2011; International Atomic Energy Agency 2014; Nuclear Decommissioning Authority 2014).

Any deep geological disposal facility should be designed with a series of engineered barriers and a natural barrier (International Atomic Energy Agency 2011a), intended to contain and isolate the radioactive waste over many thousands of years, or longer (International Atomic Energy Agency 2011a). Although the engineered barrier system will likely provide radionuclide containment and isolation for 10's of thousands or even 100's of thousands of years (Radioactive Waste Management 2016a), the integrity of the engineered barriers will eventually be compromised due to chemical and mechanical degradation (Radioactive Waste Management 2016a; King et al. 2016). This will result in radionuclide containment and isolation being dependent solely on the natural barrier. Although the multiple barriers must complement each other, it is also important for the barriers to independently contain and isolate radioactive waste (International Atomic Energy Agency 2009b).

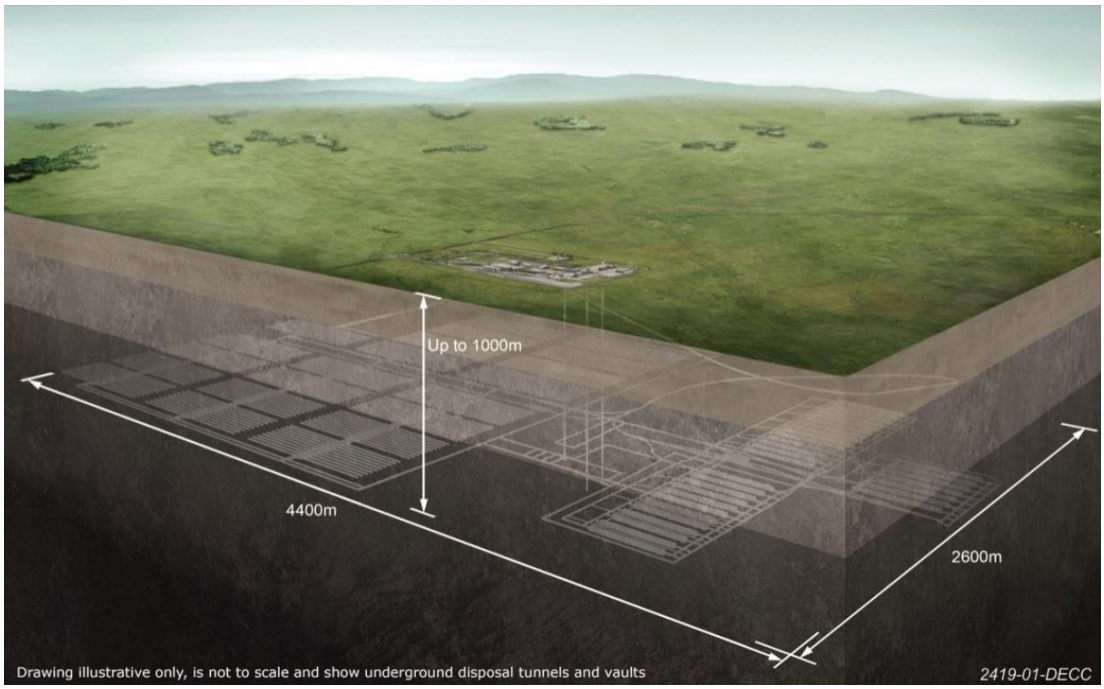

Figure 1.5: Illustration of an underground deep geological disposal facility (Nuclear Decommissioning Authority 2014).

Groundwater flow rates and chemistry directly affect the key components of the multi-barrier containment system. This is for three reasons: 1) it controls the corrosion rate of the engineered barriers by reducing the flow of reactive elements towards the waste packages (Nuclear Decommissioning Authority 2010b; Corkhill et al. 2013; Sharland et al. 2008; Gin 2014); 2) it limits the transport of released radionuclides away from the disposal facility

allowing more time for radionuclide decay and interactions with mineral surfaces (Radioactive Waste Management 2016b; Nuclear Decommissioning Authority 2010b); and 3) it allows for dispersion of the released radionuclides, reducing the concentration within the environment. Groundwater characterisation is therefore an important aspect of assessing the suitability of any potential disposal location.

Research undertaken by (Chapman et al. 1986) into suitable groundwater environments to store radioactive waste identified a series of regional groundwater characteristics considered of benefit for radionuclide containment and isolation (detailed within section 2.3.6). The research also identified locations across the UK where these groundwater characteristics could be found (see section 2.6). As no research has been undertaken to the contrary, it is the author's understanding that these groundwater characteristics and locations are still considered relevant today, and thus can be used a basis for this research.

The research by (Chapman et al. 1986) was however undertaken for ILW, rather than heat producing HLW. Radiogenic heat emission from 1) shorter lived radionuclide decay, and 2) gas generation from metal corrosion and microbial degradation of organic material within the waste packages both have the potential to affect groundwater flow (Sharland et al. 2008; Metcalfe et al. 2008), and therefore the performance of the natural barrier. Both processes require consideration within the context of regional groundwater characteristics however, only radiogenic heat emission will be assessed within this research, discussed within section 2.7.

1.2 Position & Importance of Research

Following the rejection of an application to develop a rock characterisation facility (underground laboratory for rock experiments) in West Cumbria in 1997, the UK has been left with no host community volunteering land for deep geological disposal investigation. The recent decision of Radioactive Waste Mangagement (implementors of deep geological disposal in the UK) to undertake a national geological screening programme (Radioactive Waste Management 2016b; Nuclear Decommissioning Authority 2014) has therefore once again re-opened the question of selecting an appropriate disposal location.

The historic UK focus on West Cumbria has resulted in little scientific research having been carried out on other locations (see section 2.3.1). To the knowledge of the author, there has never been a comparison of the regional groundwater characteristics of different locations, or a discussion of their relative natural attributes to contain and isolate radioactive waste.

This research therefore provides, for the first time, a direct comparison between the hydrogeological characteristics of different UK settings. It is this direct comparison that is

considered the real strength and contribution of this research. It is believed this comparison will: 1) widen the discussion as to the role the far-field natural barrier should play in site selection; 2) provide insight as to the type of natural groundwater settings the UK has to offer; and 3) aid decision making and understanding as to what is a comparatively *'good enough'* site.

1.3 Aims & Hypotheses

Section 1.3 will outline the overarching aims, individual aims and chosen hypotheses for this research as follows.

1.3.1 Overarching Aim

To investigate the hydrogeological suitability of three selected UK settings to host a theoretical deep geological facility.

1.3.2 Individual Aims

1. To assess the regional groundwater characteristics of three selected UK locations, based on the groundwater characteristics previously hypothesised by (Chapman et al. 1986)
2. To investigate the extent to which uncertainties in rock properties and radiogenic heat emission affect the regional groundwater characteristics, and
3. To score the regional groundwater characteristics of the three sites against an ideal benchmark groundwater scenario (i.e. a scenario with groundwater characteristics considered beneficial for long term radioactive waste containment).

1.3.3 Hypotheses

1. Do the regional geological and hydrogeological characteristics of some locations offer greater long term radionuclide containment and isolation potential than others?
2. Does the regional geological and hydrogeological setting control the effect of radiogenic heat emission on natural groundwater flow patterns?
3. Is a simple method of far-field natural barrier comparison possible, despite complex and detailed regional geological and hydrogeological characteristics?

1.4 Approach

Section 1.4 will present the chosen approach to resolve the outlined hypotheses (section 1.4.1), along with general procedure to be followed (section 1.4.2).

1.4.1 Method

Geological systems, including deep geological disposal facilities, can be represented mathematically through a series of coupled thermal, hydrological, mechanical and chemical processes, or a mixture thereof (Stephansson et al. 2004; Tsang 1987). The usefulness of undertaking coupled process numerical modelling, is the ability to interrogate the behaviour of systems, otherwise impossible using laboratory experiments, over the timescales of interest. This research will therefore utilise the coupled process modelling software *'OpenGeoSys'* (OpenGeoSys 2017), in conjunction with the reactive mass transport code *'GoldSim'* (GoldSim Technology Group 2017d) to predict the regional groundwater flow characteristics at different locations, and the migration of radionuclides through the natural barrier system. The chosen method is discussed in detail in Chapter 4.

1.4.2 General Procedure

The general procedure used to resolve the hypotheses will be as follows:

1. Selection of three UK based regional groundwater settings for comparison,
2. Identification of hydrogeological parameters that can be used to represent the hypothesised groundwater characteristics (Chapman et al. 1986) within a predictive numerical model,
3. Development of a benchmark hydrogeological scenario for the long term containment and isolation of radioactive material, based on previous work undertaken by (Chapman et al. 1986), against which the chosen hydrogeological parameters of the selected sites can be later compared,
4. Develop a hydrogeological conceptual model for each of the three selected sites,
5. Construct and run a numerical groundwater flow model, using OpenGeoSys, for each of the three selected sites based on publically available geological and hydrogeological information,
6. Vary regional fault and lithological permeabilities to determine the change in hydrogeological parameters within the numerical models (and by extension, the hydrogeological characteristics),
7. Determine chemical retardation potential of the three sites,
8. Compare the hydrogeological parameters of the three modelled locations, against those of the ideal scenario, and finally

9. Simulate the effect of radiogenic heat emission from waste packages to determine the change in groundwater speed and direction.

1.5 Thesis Layout

This thesis will cover the principles and processes underlying the natural barrier as part of a deep geological disposal facility (Chapter 2), the development and use of coupled process models for natural barrier evaluation (Chapter 3), model development, results and discussion for the three selected sites (Chapters 4 to 6), a brief comparison of the findings from the three sites (Chapter 7), findings from the effect of radiogenic heat simulation on the natural barrier (Chapter 8), a discussion of the challenges of far-field groundwater flow simulation (Chapter 9), and finally overall conclusions and recommendations (Chapter 10). Supplementary and supporting information will be provided in Appendix A to G, including a discussion of the feasibility of deep geological repository development offshore (Appendix G).

Chapter 2 Principles and Processes of the Natural Barrier for Deep Geological Disposal

This chapter will outline the overarching safety principles associated with deep geological disposal (section 2.1); the concept of multiple barriers (section 2.2); the principles and processes associated with the natural barrier (section 2.3); the use of natural analogues in deep geological disposal research (section 2.4); the principles and processes of the natural barrier that drive and characterise international site selection (section 2.5), locations within the UK identified has having potentially suitable natural barrier settings (section 2.6); the main uncertainties in natural barrier performance (section 2.7); the representation of natural barrier processes through coupled mathematical processes (section 2.8); and finally, a summary of the main points of the literature review underpinning the thesis (section 2.9).

2.1 Safety Principles & Safety Functions

Section 2.1 will introduce the three key safety principles associated with deep geological disposal which include *'multiple barriers'*, *'defence in depth'* and *'safety margins'* (International Atomic Energy Agency 2009a) as now discussed.

The principle of 'multiple barriers' (section 2.2) ensures that undue reliance is not placed upon a single physical, chemical or operational barrier (International Atomic Energy Agency 2011a). The 'defence in depth' principle is designed to minimise the opportunity for the multiple barriers to be compromised by locating the facility at depth, away from the near-surface human environment. And finally, the principle of 'safety margins' is to ensure long term multiple barrier performance, despite uncertainties, such as parameter or geodynamic phenomena, which could affect barrier performance (section 2.7). All three principles are designed to work together to *contain* and *isolate* radioactive waste (International Atomic Energy Agency 2011a).

Containment and *isolation* should be ensured over the repository performance assessment timeframe, covering thousands of years and longer (International Atomic Energy Agency 2011b), but performance assessments generally extend up to about 1 million years (Metcalfe et al. 2008). These longer timeframes ensure the decay of the most radioactive shorter lived radionuclides.

The International Atomic Energy Agency specify that performance of the disposal system should be achieved through a number of barrier specific '*safety functions'*, which include: impermeability to water; resistance to corrosion; limited solubility; limited dissolution; limited

leach rate; good retention of radionuclides; and effective retardation of radionuclide migration (International Atomic Energy Agency 2011a).

Furthermore, the performance of the barriers should not be compromised by features, events or processes, such as resulting from waste emplacement, tectonic or climatic changes (Metcalfe et al. 2008; International Atomic Energy Agency 2011a). Finally the safety functions and barrier performance must be proven within a *'safety assessment',* prior to any facility development (International Atomic Energy Agency 2011a), with the risk remaining below one death in a million per annum (Environment Agency 2009).

These safety principles lay the foundation for all research assessing the performance of deep geological disposal facility barriers. Of particular interest to this research is the radionuclide retention and retardation safety functions which are operational within the natural barrier.

2.2 Multiple Barriers

Section 2.2 will described in more detail the 'multiple barrier' safety principle, and how it comprises a series of engineered barriers and a natural barrier.

Internationally multiple barrier containment systems typically include the waste form itself, waste canister material, the over pack container, backfill and buffer material to surround and support the canister/container, and the surrounding geological barrier (Harley et al. 2016). The barriers should be chosen, or designed, to perform one or more of the specific safety functions (Nuclear Energy Agency 2008; International Atomic Energy Agency 2011a), as outlined in section 2.1.

The Nuclear Decommissioning Authority (NDA) have opted specifically for a Swedish style multiple barrier containment system, named KSB-3V (Nirex 2005d). It is the understanding of the author that selection of the Swedish KSB-3V concept by the NDA is due to the apparent success of Sweden's implementers (SKB) in final deep geological disposal site selection (discussed further in section 2.4).

The KSB-3V concept states that high level waste will be vitrified in a borosilicate glass, packaged within copper canisters with cast iron inserts for mechanical strength, or stainless steel canisters within the case of the UK (Nirex 2005d). Canisters will be located within deposition holes, surrounded by swelling bentonite clay, to separate the canisters from the surrounding rock mass (Nuclear Decommissioning Authority 2014). Deposition tunnels, central tunnels, access tunnels, and shafts will be backfilled with crushed rock or bentonite

clay (Posiva Oy 2012), and the entire engineered facility will be situated within the 'geosphere' or 'natural barrier' at a depth of 200 - 1,000 m (Figure 2.1).

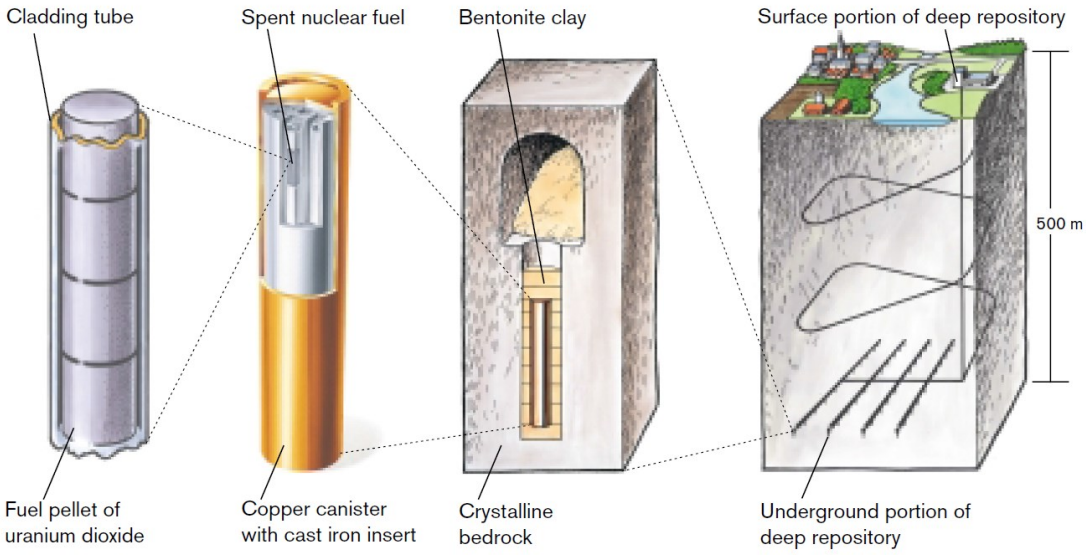

Figure 2.1: KSB-3 style protective barrier in the deep repository. Image obtained from (SKB 2001).

Intermediate level waste will however be treated slightly differently by being conditioned, placed within stainless steel containers and surrounded by a cementitious backfill material. The backfill is designed to limit the ingress of water (Nuclear Decommissioning Authority 2014). A comparison between ILW and HLW packaging is presented within Figure 2.2.

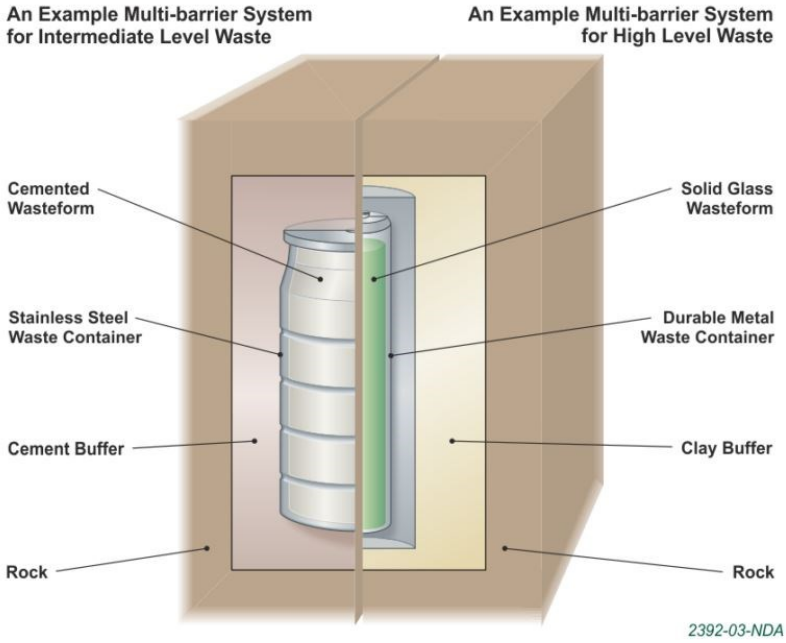

Figure 2.2: Illustration of the containment system for intermediate level radioactive waste and high level radioactive waste. Image obtained from (Nuclear Decommissioning Authority 2014).

The natural barrier can most simply be described as the rock mass surrounding the engineered facility, of which groundwater is a key aspect (Radioactive Waste Management 2016b). The natural barrier can also be described through a series of geologically and hydrogeologically dependent coupled physical and chemical processes, discussed further in section 2.8. Although the multiple barriers should be complimentary, each barrier should be able to independently perform its safety functions, as far as practicable (International Atomic Energy Agency 2009b) to ensure long duration containment, and to minimise the risk of knock-on barrier failure.

Thus far within the UK, no study has examined and compared the characteristics of different natural barriers, as independent barriers to radionuclide migration (section 2.3), which will form the focus of this research moving forward.

Finally, for clarification, although the groundwater within the surrounding rock mass can be treated as a receptor i.e. as soon as radionuclides are released into the groundwater the performance of the deep geological disposal facility has failed, this research will instead consider groundwater as a pathway. The pathway can thus provide containment and isolation functions, with the receptor becoming any human or ecological dependent groundwater resource.

2.3 Natural Barrier

This section will discuss host rock classifications and characteristics (section 2.3.1); the controls on radionuclide migration rates including sorption and solubility (section 2.3.2); the classification of the natural barrier into the near-field and far-field domain (section 2.3.4); the importance of the far-field in ensuring long term radionuclide containment (section 2.3.5); specific groundwater characteristics considered of benefit for radionuclide containment (section 2.3.6); and identified far-field hydrogeological regimes which encompass these groundwater characteristics (section 2.3.7).

2.3.1 Rock Type: Classifications & Characteristics

Three types of ‘host rock formations’ (geological formations in which the engineered barriers will be emplaced) have been identified as being suitable to host a deep geological disposal facility. These include ‘higher strength’, ‘lower strength’ and ‘evaporitic’ rocks (Radioactive Waste Management 2016b; Nuclear Decommissioning Authority 2014). The geological and hydrogeological characteristics of these host rock formations will now be discussed.

Higher strength rocks, e.g. granites, are characterised by a low permeability matrix leading to groundwater being facilitated along intersecting fractures. Solute transport is often via advective groundwater through fractures (faster, pressure driven) but via diffusion through the matrix (very slow concentration driven) (Table 2.1). Higher strength rocks have high mechanical strength, making them easier to tunnel through, and medium thermal conductivity allowing some heat dissipation (Table 2.1). The majority of sorption (uptake of migrating radionuclide from the groundwater onto the solid) occurs onto minerals such as phyllosilicates, carbonates and iron-oxides (Domenico & Schwartz 1997), which line fracture surfaces (Berry et al. 1999; Nuclear Decommissioning Authority 2010c). Anion/ion exclusion and molecular filtration (see Figure 2.7b) are also considered important processes, blocking matrix pore spaces and further reducing sorption within the matrix (Nuclear Decommissioning Authority 2010c). Sorption and retardation (the degree to which migrating radionuclides are slowed down compared to groundwater) in higher strength rocks is therefore dependent on the characteristics of the fracture network (Nuclear Decommissioning Authority 2010c).

Lower strength rocks, e.g. clays, are characterised by sedimentary layers, with solutes transported by a mixture of matrix diffusion and advective groundwater through fractures. Fractures are often parallel to bedding. Lower strength rocks have low to medium mechanical strength, making them more challenging to tunnel through, with low thermal conductivity (Table 2.1). These rocks, due to their high phyllosilicate mineral content strongly sorb contaminants (Figure 2.7c), contributing significantly to sorption, and therefore increasing retardation (Nuclear Decommissioning Authority 2010c; Metcalfe & Rochelle 1999). Physical filtration (blocking) of larger molecules (see Figure 2.7b) is also an active process in lower strength rocks. Selection of a site with abundant clay is therefore considered advantageous for radionuclide retention (Apted & Ahn 2017).

Evaporitic rocks, e.g. layered salt deposits, are rarely associated with effective groundwater flow due to their intrinsically low permeabilities. As such solute transport is often via solid state diffusion. Evaporitic rocks exhibit self-healing creep properties, and have high thermal conductivities (Table 2.1). Evaporitic rocks have very low sorption potential (Radioactive Waste Management 2016b) due to competition for sorption sites from the high percentage of dissolved ions within the brines (Nuclear Decommissioning Authority 2010c). The main defence to radionuclide migration within these rocks are therefore the physical processes, such as isolated and static groundwater pockets, rather than chemical processes.

Table 2.1: Summary table of the key characteristics and features of potential host rocks relevant for disposal: Rock Salt, Argillaceous Formations and Crystalline Rocks. Information complied from (International Atomic Energy Agency 2003) and (Streffer et al. 2011).

Feature	**Rock Salt**	**Argillaceous Formations**	**Crystalline Granites**
Host Rock	*Bedded Salt, Salt Domes*	*Strongly Consolidated Clays; Claystone; Mudstone. Consolidated Clays; Shales; Marls; Plastic Clays*	*Granite, Gneiss*
Thermal Conductivity	*High*	*Low*	*Medium*
Hydraulic Conductivity	*Practically impermeable*	*Very low to low*	*Very low (un-fractured) to conductive (fractured)*
Mechanical Strength	*Medium*	*Low to medium*	*High*
Deformation Behaviour	*Viscous (Creep)*	*Plastic to brittle*	*Brittle*
Solubility	*High*	*Very low*	*Very low*
Sorption Behaviour	*Very Low*	*Very high*	*Medium to high*
Heat Resistance	*High*	*Low (depending on rock)*	*High*

Legend: Green = favourable feature**;** Yellow = medium; Red = unfavourable feature.

The only host rock formation properly investigated within the UK is the Borrowdale Volcanic Group within West Cumbria (section 2.5.6), classified as a 'higher strength rock' (Nirex 1997a; Nirex 1997b; Nirex 1997c; Nirex 1997d). Other minor scoping studies were also undertaken on the 'higher strength' Strath Halladale Granite in Caithness (Mather J. D 1985) and the 'lower strength' Cretaceous-Jurassic mudstone sequence beneath Harwell in Oxfordshire (Mather J. D 1985). However, these locations were side-lined in favour of further investigation in the Borrowdale Volcanic Group in the 1990's (section 2.5.6). A subsequent review undertaken by (Metcalfe et al. 2008) suggests an under representation of investigative studies of gas migration in lower strength and evaporitic rocks within the UK, and by extension groundwater studies. This research will therefore consider a range of geological host rock types, including UK based lower strength and evaporitic formations.

2.3.2 Solute Transport Mechanisms

Solutes, including released radionuclides, can be transported via two main mechanisms: advection (based on Darcy's Law) and/or diffusion (based on Fick's Law). This section will outline the mechanisms of these two processes (sections 2.3.2.1 to 2.3.2.3), and will discuss their relative importance to natural barrier prospectivity assessments (section 2.3.2.4).

2.3.2.1 Advection

Advection is the transport of solutes within free flowing groundwater. Groundwater itself most commonly moves because of a pressure gradient, described through Darcy's Law (section A.1.1). The flux of solutes through a medium $F_{sol,A}$ (kg/m^{2}s), transported due to advecting groundwater can be described as Equ.2.1 (Domenico & Schwartz 1997), where F_{gw} is the groundwater flux (m/s), described in Equ.A.1, and C_s is the solute concentration (kg/m^3).

$$F_{sol,A} = F_{gw} C_s \qquad (2.1)$$

The distance solutes move due to advection over time can be determined by Equ.2.2, where x is the distance travelled (m), F_{gw} is the groundwater flux (m/s) as described above, n_e is the effective porosity (-) and t is time (s). Equ.2.2 comprises an advective velocity component (see section A.4.1), and a component of time.

$$x = \frac{F_{gw}}{n_e} t \qquad (2.2)$$

2.3.2.2 Diffusion

Diffusion is the transport of solutes due to a solute concentration gradient. The flux of solutes through a medium $F_{sol,D}$ (kg/m^{2}s), transported due to a solute concentration difference can be described as Equ.2.3 in the x direction, where D_e is the effective diffusion coefficient (m^2/s),

as detailed within Appendix A.1.2 and is a function of both the physical characteristics of the solute and those of the medium, C_s is the solute concentration (kg/m^3) and *x* is the distance in the x-direction (m).

$$F_{sol,D} = D_e \frac{\partial C_s}{\partial x} \quad (2.3)$$

The distance solutes move due to diffusion over time can be determined by Equ.2.4 (Atkins 2001), where x is the distance travelled (m), D_e is the effective diffusion coefficient (m^2/s) as described above, and t is time (s).

$$x = \sqrt{2D_e t} \quad (2.4)$$

2.3.2.3 Advection vs Diffusion

The relationship between solute transport distance, x, and time, t, is linear in Equ.2.2 and non-linear in Equ.2.4. The increase in distance travelled by solutes via diffusion reduces with time, whilst it remains constant with time when transported via advection (Figure 2.3). Thus, when a solute concentration gradient is present, diffusion can dominate over shorter timescales, whilst advection solute transportation mechanisms can dominate over longer timescales. The cross-over point, if present, depends on the advective velocity of the groundwater, and the effective diffusion coefficient (Figure 2.3).

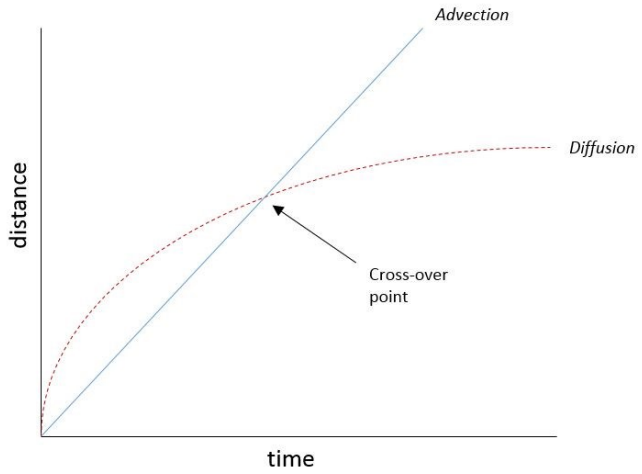

Figure 2.3: Schematic illustration of solute transport distance via advection and diffusion with respect to time.

(Fetter 2001) suggests that in general, assuming a solute concentration gradient, diffusion based solute transport tends to dominate advection driven solute transport at effective diffusivities of 1.00E-09 m^2/s (value used in Figure 2.4). Effective diffusion coefficients have however been reported to range from 9.31E-09 m^2/s for H^+ in seawater and deep-sea sediments (Domenico & Schwartz 1997), down to less than 1.00E-14 m^2/s for selected ionic solutes in porous medium (Domenico & Schwartz 1997) i.e. 6 orders of magnitude.

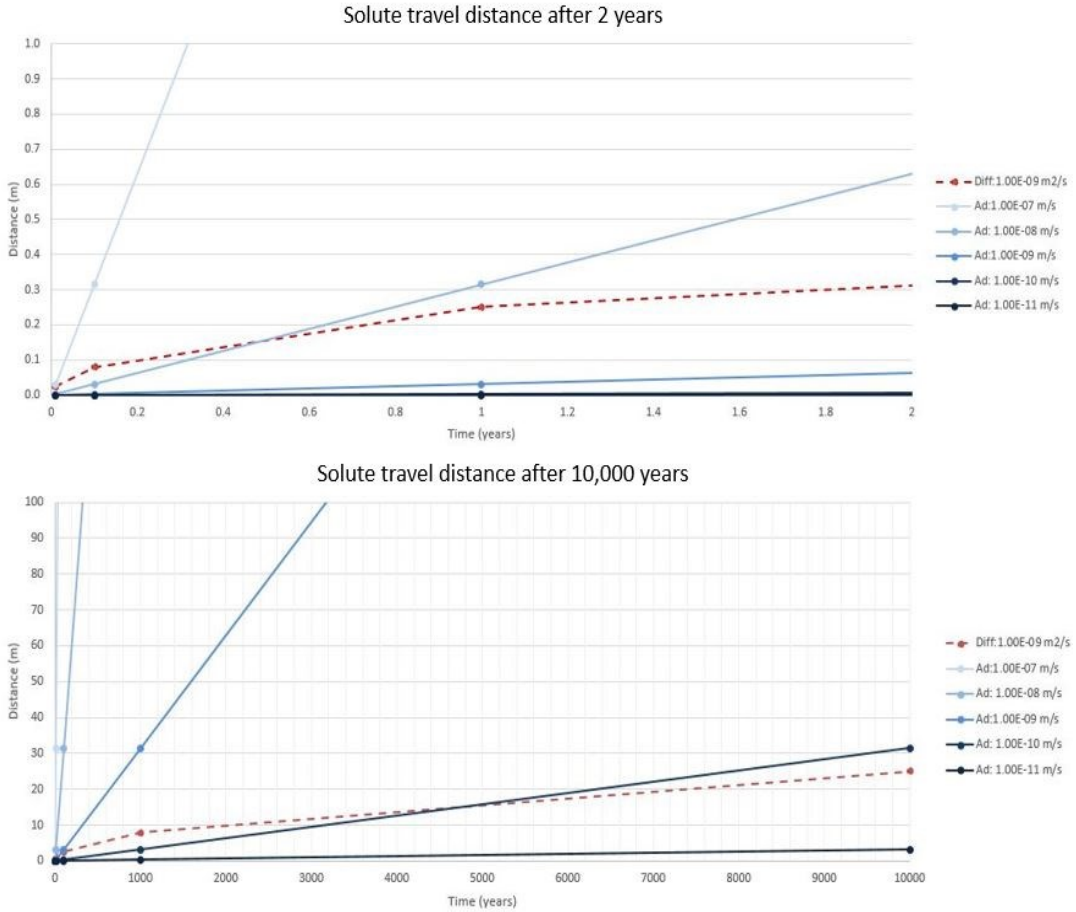

Figure 2.4: [Top] Solute travel distance over 2 years as a result of diffusion with a D_e of 1.00E-09 m^2/s (red), and advection with a V_a of 1.00E-07, 1.00E-08, 1.00E-09, 1.00E-10 and 1.00E-11 m/s (blue). [Bottom] Solute travel distance over 10,000 years.

Due to the low rates of solute transport via diffusion, advection is often the solute transportation mechanism of most concern within contaminant transportation studies.

2.3.2.4 Importance of solute transport mechanisms to deep geological disposal

Advection driven solute transport tends to operate in one predominant direction, whilst diffusion spreads solutes out radially, and thus controls the primary solute transportation pathway (Figure 2.5). As low permeability formations are targets for deep geological disposal (Domenico & Schwartz 1997), advective velocity is often very low, and diffusion has a chance to dominate solute transportation. Released radionuclides (solutes) may therefore follow a different pathway to that of the advective groundwater (Figure 2.5), which must be considered within deep geological disposal prospectivity assessments.

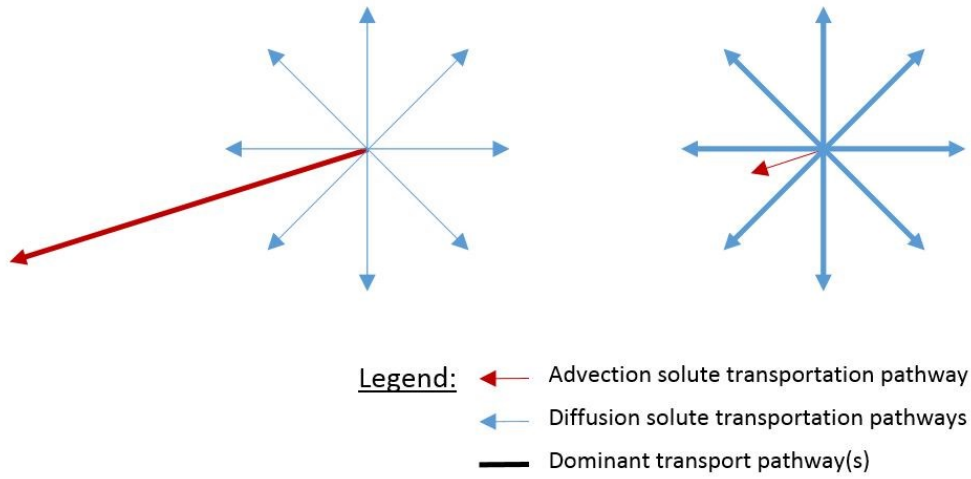

Figure 2.5: [Left] Advection dominated solute transportation. [Right] Diffusion dominated solute transportation.

2.3.3 Radionuclide Migration Controls: Sorption & Solubility

Once radionuclides have been released from the engineered barriers into the groundwater within the surrounding rock mass, their migration rates, relative to groundwater (retardation), can be controlled by a couple of different processes. Firstly, physio-chemical processes such as diffusion into dead end pores; molecular filtration; or ion exclusion (Figure 2.7a&b), and/or secondly chemical processes such as sorption; or precipitation (Figure 2.7c&d). Figure 2.6 presents an illustration of how different physio-chemical processes can affect the relative radionuclide/solute concentrations and its migratory rate (retardation factor) relative to groundwater.

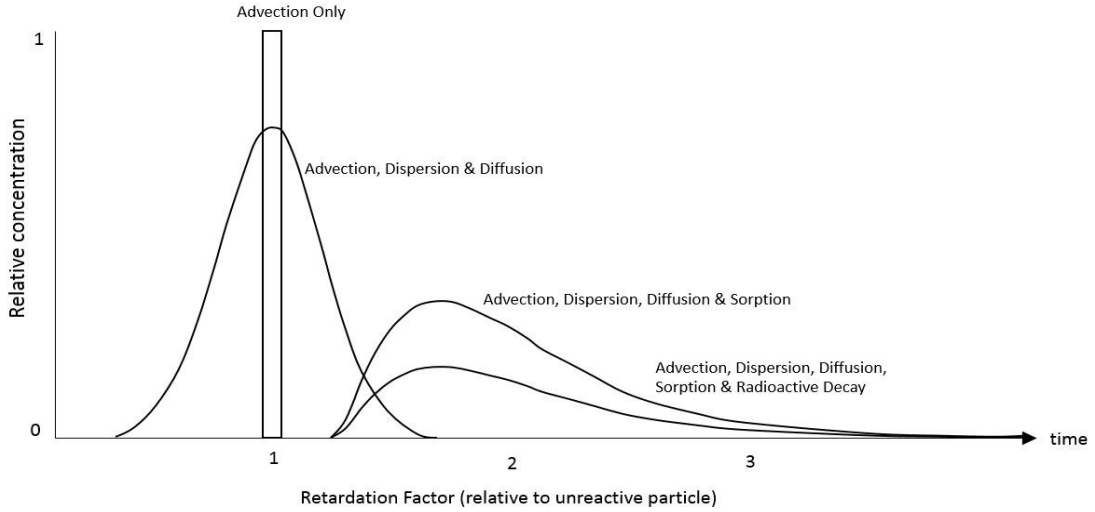

Figure 2.6: Image of breakthrough curves for contaminants transported via 1) advection only, 2) advection, dispersion & diffusion, 3) advection, dispersion, diffusion & sorption, and 4) advection, dispersion, diffusion, sorption & radioactive decay.

The most important chemical process is sorption (Domenico & Schwartz 1997). This is because sorption is an effective process re-distributing contaminants between the liquid phase (water), and the solid phase (rock) (Domenico & Schwartz 1997). This is achieved via the processes of 1) ion exchange or 2) surface complexation (Radioactive Waste Management 2012). Ion exchange describes the uptake of a cation (positively charged particle) onto a negatively charged mineral surface, whilst surface complexation involves the formation of a chemical complex of an ion in solution with a mineral surface (Figure 2.7c) (Radioactive Waste Management 2012). Sorption processes change the radionuclide concentrations within groundwater and migration rates, and thus 'have an extremely important bearing on the suitability of a given nuclear waste disposal site' (Domenico & Schwartz 1997).

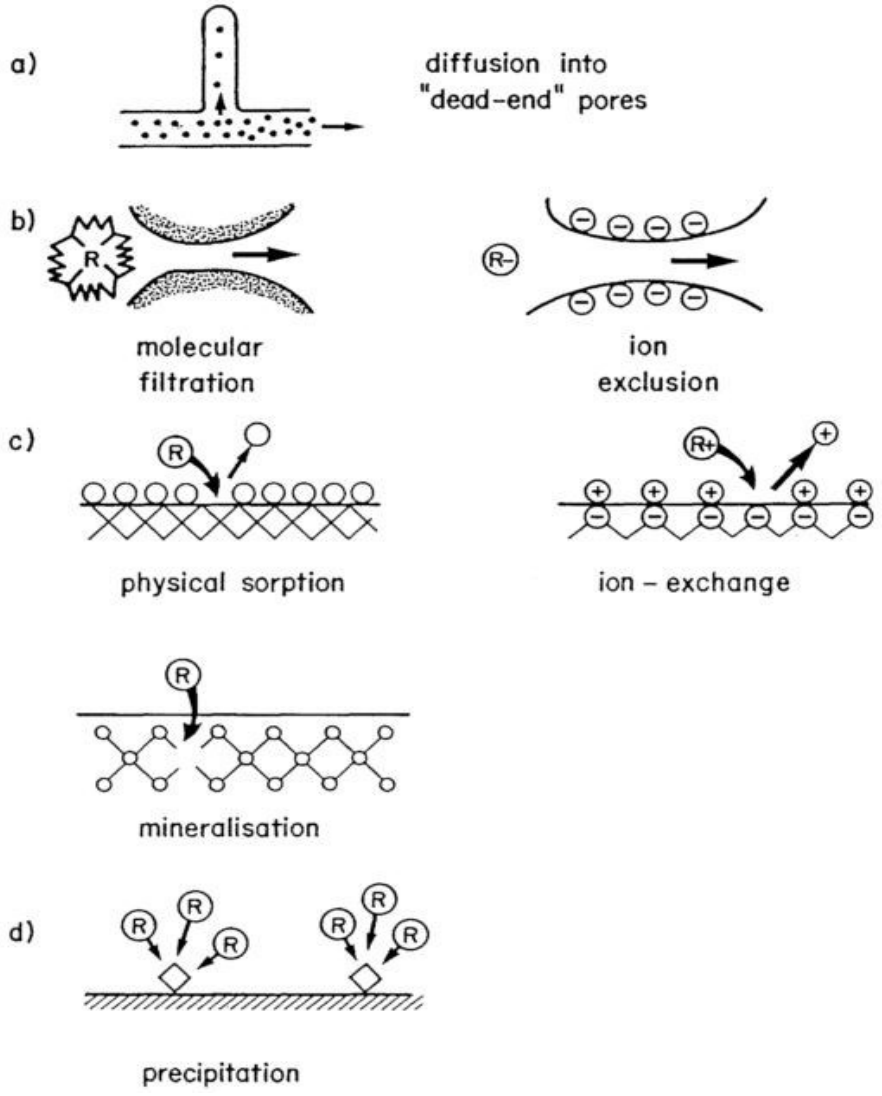

Figure 2.7: Retardation mechanisms affecting radionuclide transportation in groundwaters: a) & b) occur in dynamic systems and retard solute transport; whilst c) & d) are sorption processes that occur in either dynamic or static systems. Image obtained from (Miller et al. 1994).

Chemical factors influencing sorption processes include 1) radionuclide species, 2) radionuclide concentration, 3) mineralogical composition of the rock mass (discussed in section 2.3.1), and 4) temperature of the sub-surface environment (Domenico & Schwartz 1997). The role/importance of chemical processes in controlling radionuclide migration rates, over that of the ambient groundwater flow rate, is variable and setting dependent, and will be explored for each selected site as part of this research.

The remainder of this section will present a discussion of the role of radionuclide species, concentration and temperature on radionuclide migration rates through the natural barrier, in preparation for numerical model simulation.

2.3.3.1 Radionuclide Species

As it is not necessary (or practical) to simulate all released radionuclides, radionuclides species can be grouped into similar sub-surface fate and transport behaviours (chemical analogues) for the purpose of investigation. This can achieved based on their position within the periodic table. (Chapman et al. 1984) suggests that chemical analogies are greatest when similar valance states, complex formations, types of species and comparable ionic radiuses are achieved.

Important to this research is that: Nickel (Ni) can be considered chemically analogous to lead (Pb) (Chambers & Williams 2010); Selenium (Se) to Sulphur (S); Chlorine (Cl) to Iodine (I) (Nuclear Decommissioning Authority 2010c); the lanthanides with the exception of Europium (Eu) to the trivalent actinides; trivalent Americium (Am(III)) to other trivalent actinides including trivalent Plutonium (Pu(III)) and trivalent Curium (Cm(III)) (Miller et al. 1994); tetravalent Uranium (U(IV)) to tetravalent Neptunium (Np(IV)), tetravalent plutonium (Pu(IV)), tetravalent Thorium (Th(IV)) and pentavalent protactinium (Pa(V)) (Chapman et al. 1984; Miller et al. 1994); and hexavalent Uranium (U(VI)) to pentavalent Neptunium (Np(V)) and pentavalent Plutonium (Pu(V)) (Chapman et al. 1984).

Furthermore, parent radionuclides naturally decay to daughter products over time (section 1.1.1), each of which express different sub-surface behaviours. This makes prediction of radionuclide decay chain fate and transportation over time challenging. However, as the purpose of this research is to determine the degree to which chemical processes affect migrating radionuclides rates within different settings, and not to undertake a detailed fate and transportation risk assessment, selection of a variety of long-lived radionuclides, covering a range of sub-surface behaviours, is considered representative and sufficient for this purpose. Radioelements selected for investigation as part of this research are presented within Table B.0.1.

Finally chemical properties of stable elements can, under certain circumstances, be used as chemical analogues for radioactive isotopes of the same element. This due to their similar propensity for chemical reactions (Apted & Ahn 2017). Of particular interest to this research is the application of partition coefficients (K_d), a key parameter used to determine the retardation factor (see section A.3.3.1). These chemical analogues are however considered strongest when applied to isotopes with long half-lives due to decay effects (Miller et al. 1994). A list of partition coefficients applied to the selected radioelements is presented within Table B.0.2.

2.3.3.2 Radionuclide Concentrations

The concentration of radionuclides within the groundwater pathway also has a bearing on the amount of retardation (see section A.3.3.1), and therefore on the migration rates of radionuclides within the natural barrier. At equilibrium the increase in the radionuclide concentration, relative to the amount sorbed, causes a higher percentage of radionuclides to remain within groundwater. This reduces the retardation factor, and therefore increases the advective and diffusive mass flux (see Equ.A.16, Equ.A.18 and Equ.A.20).

The relationship between radionuclide concentration within groundwater, and the amount of mass sorbed to the rock mass, can be expressed either as a *linear* or *non-linear* sorption isotherm. *Linear* sorption isotherms assume 1) constant temperature, and that 2) the sorbed mass and the concentration within the groundwater are proportional. Linear sorption isotherms, such as the Freundlich-special case isotherm (presented in Equ.A.20 and Figure A.0.2) are the isotherms most commonly implemented within solute transport models due to their relative simplicity (Domenico & Schwartz 1997), or alternatively when limited site specific data is available.

Non-linear sorption isotherms, such as the Freundlich (general) and Langmuir isotherms (Domenico & Schwartz 1997) assume 1) constant temperature, but that 2) the sorbed mass and the equilibrium concentration are not proportional (see Figure A.0.2). This lack of proportionality can be a result of natural sub-surface heterogeneities in mineralogy; pore structures; ion concentration; pH of the water; amount of contaminant on the rock surface; and kinetics including water-rock contact time (e.g. equilibrium). Due to these complex dependencies, analytical sorption isotherms are often fitted to experimental data.

As experimental determination of the site specific sorption isotherms is beyond the scope of this project, this research will implement the Freundlich-special case *linear* sorption isotherm for simplicity. This approach is also justified as radionuclide concentrations are not anticipated to reach sorption limits within the pathway due low radionuclide leach rates from

the repository. It is however recommended any further research focuses on determining the site specific sorption isotherms for the individual radioelements.

2.3.3.3 Radionuclide Concentrations: Solubility Constraints

The radionuclide concentration released from the repository is controlled by characteristics and features of the engineered barriers, including: 1) the initial inventory composition; 2) inventory volumes; 3) waste package designs; 4) matrix disintegration rates (reported fractionally at 10^{-6}/year (Apted & Ahn 2017)); 5) radionuclide solubility; 6) buffer disintegration rate; and 7) flow-rate into the geosphere.

The purpose of this research is however to test the containment and isolation potential of the natural barrier, and not the engineered barrier. The only influence the engineered barriers will have on geospheric radionuclide migration rates, will therefore be to control the release rate of radionuclides. This will be achieved by using near-field solubility constraints (listed within Table B.0.2).

Solubility is dependent on the type and form of the species (Domenico & Schwartz 1997), and therefore also on the environmental conditions of the repository, including the pH (negative logarithm of the hydrogen ion concentration), Eh (oxidation potential), temperature and ionic strength (concentration of ions in solution). For example, Ni typically occurs in the Ni^{2+} form below pH 10, but the $Ni(OH)_2$ form above pH 10, with nickel becoming less soluble (considered advantageous for radionuclide containment) with increasing pH (Nuclear Decommissioning Authority 2010c). Organic material from the cellulose degradation of items within the repository such as paper and cardboard, can however act to increase solubility, by lowering the pH, due to the formation of organic complexants (Nirex 1997c). In order to mitigate the effect of organic complexants and to limit solubility, it is proposed that the repository will be backfilled with a Portland alkaline cement, designed to increase the pH and reduce the Eh of the repository porewater (Nirex 1997c). This research will therefore also conservatively consider the effect of organic complexants on solubility values.

2.3.4 Near-Field vs Far-Field Containment

Host rock formations (see section 2.3.1) are commonly only one lithological unit within a wider disposal setting, together which form the natural barrier. The natural barrier is commonly sub-divided into the near-field and the far-field for the purpose of investigation, the definitions of which will now be presented.

The near field is defined as the area *significantly affected by repository construction and waste emplacement* (Apted & Ahn 2017), whilst the far-field is defined as the area of the geosphere

where *the thermal, hydraulic, chemical and mechanical effects caused by the presence of the repository are small or negligible* (Apted & Ahn 2017).

Research on the near-field (see Figure 2.8) which covers the engineered barrier system, typically extends at the most a few tens of meters out into the natural barrier. This area covers the rock mass-engineered barrier system contact (Lunn et al. 2017), and the zone of excavation damage/disturbance (Tsang et al. 2005), such as a result of excavation derived mechanical disturbance to the rock mass (section 2.7.5), radiogenic heat emission (section 2.7.6) and/or gas generation (section 2.7.7).

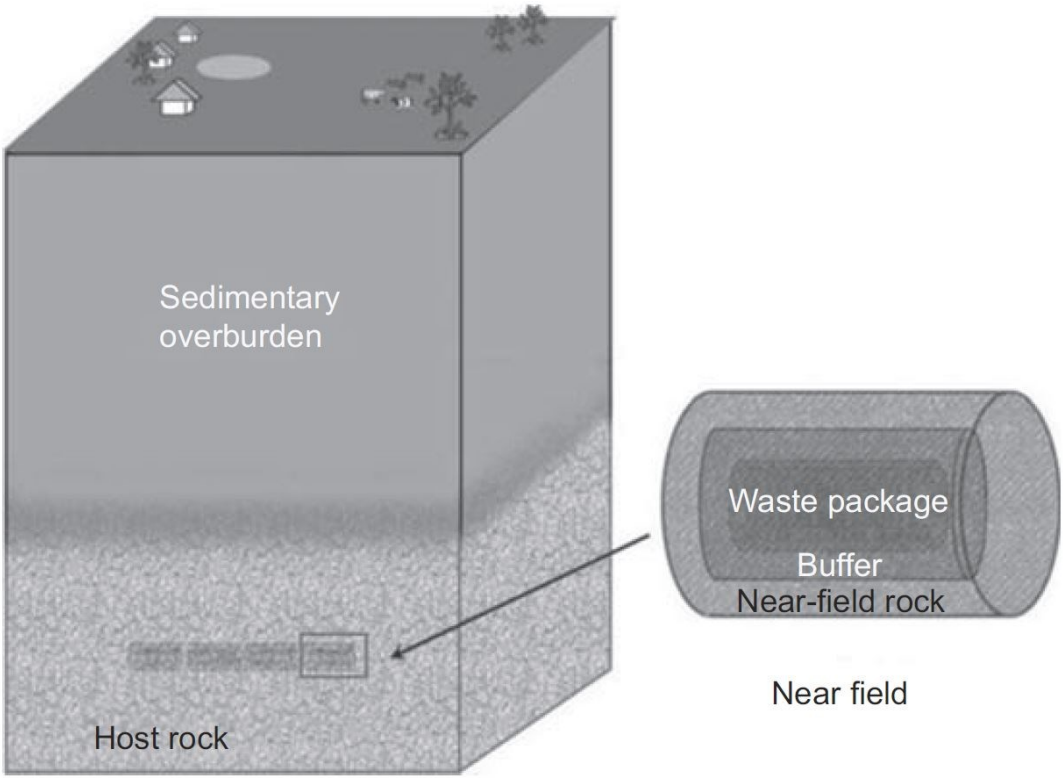

Figure 2.8: Illustration of the near-field of a deep geological repository for high level radioactive waste. Image obtained from (Apted & Ahn 2017).

Far-field studies, as the area outside the near-field, have extended up to *approx*. 3 km (Fraser Harris et al. 2015; Min et al. 2005), or 12 km in length (Nirex 1997c) from the proposed repository site at Sellafield, West Cumbria. Internationally, far-field studies for deep geological disposal have however covered much larger areas including up to *approx.* 70,000 km^2 (Cao et al. 2017), incorporating regional mountain chains and river basins.

This raises the question as to how far should 'far-field' investigations extend? Arguably the far-field should cover the major topographical and hydrogeological features which control regional groundwater movement i.e. as defined by (Tóth 1963) (see Figure 2.9), which can

range over tens to hundreds of km depending on the unique geological, topographic and hydrological features of the settings.

This research will therefore consider wider features considered to control regional/far-field groundwater movement at the chosen settings.

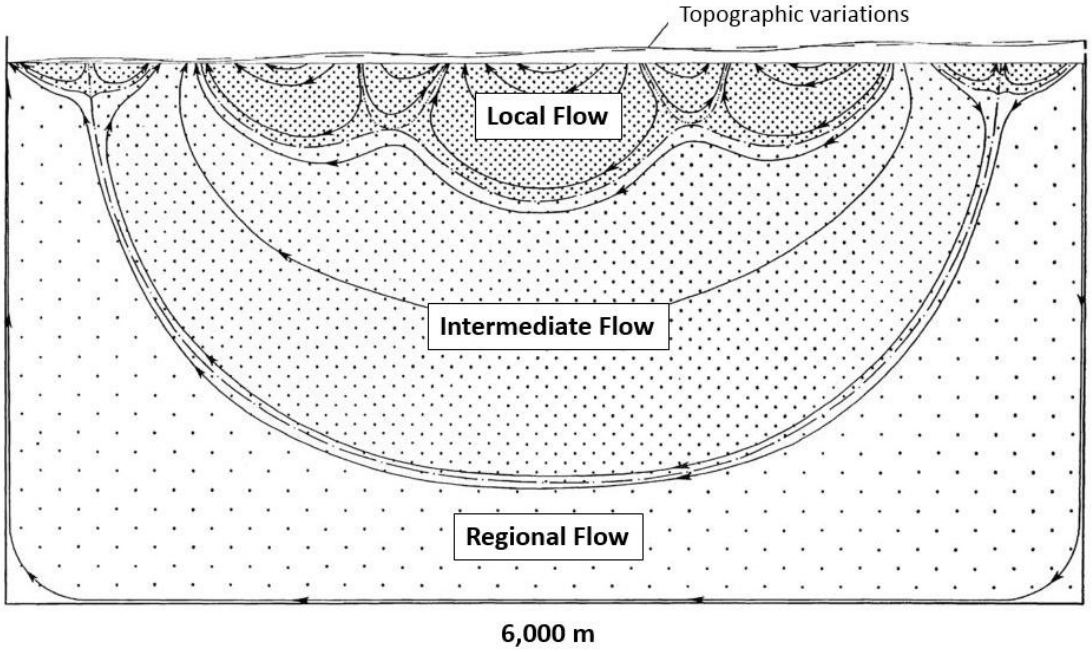

Figure 2.9: Image of local, intermediate and regional groundwater flow fields as defined (and image obtained from) (Tóth 1963)

Furthermore, research undertaken at Sellafield by (Fraser Harris et al. 2015) shows increases in groundwater velocities up to 1.5 times along adjacent faults as a result of radiogenic heat emission (i.e. waste emplacement), with changes to the natural groundwater flow pattern observed over 1 km away. This raises more questions; firstly, is the common use of the terms 'near-field' i.e. *'the area significantly affected by waste emplacement'*, as only extending a few tens/hundreds of meters into the natural barrier, fit for purpose? Secondly does the area and the degree to which the natural barrier is affected by waste emplacement vary between different disposal locations?

These questions will be addressed through this research by comparing the area and the degree to which sub-surface waste emplacement affects the natural barrier over different regional UK settings. This will be achieved through numerical model simulation of waste emplacement at three chosen settings. The waste emplacement process of interest to this research is radiogenic heat emission. The reasons for its selection are discussed further in section 2.7.6.

2.3.5 Importance of Far-field Containment

It is the opinion of the author that much more research has been undertaken on the near-field engineered barriers within the UK than that of the far-field natural barriers. Furthermore, understanding of the geological and hydrogeological characteristics of the natural barrier over the far-field domain is considered essential. This is because the far-field characteristics not only inform the characteristics of the near-field, but can also provide a naturally stable, and thus predictable disposal setting, enhancing the confidence in performance of the overall disposal system.

Geological formations only change slowly over millions of years and so are thus, relatively predictable when considering facility performance. Hydrogeological systems (within the upper 1 km) are however more dynamic, typically exhibiting groundwater residence times > 40 ka, beyond the range of ^{14}C dating (Darling et al. 1997). Some basins, such as the Wessex Basin and East Irish Sea Basin indicate pre-Quaternary (> 2.6 million years ago) recharge (Darling et al. 1997; Bath et al. 2006), although some degree of Holocene (< 10,000 years) and Pleistocene (< 2.6 million years) aged groundwater flushing is expected (Darling et al. 1997). These long residence, slow response, groundwater formations provide the best opportunity for long term radionuclide containment.

The characteristics of suitable hydrogeological regimes, as hypothesised by (Chapman et al. 1986), are detailed within the next section. It is these hydrogeological regimes, that if proven relatively stable through past geodynamic phenomena (section 2.7), will offer the greatest opportunity for long term radionuclide containment. This research will consider the characteristics of the far-field hydrogeological systems, but further research would be required to ascertain the groundwater residence times of the investigated sites.

2.3.6 Beneficial Groundwater Characteristics

This section will outline six groundwater characteristics identified as beneficial for waste containment within the natural barrier (Chapman et al. 1986) (justified within section 1.1.5), and include:

HC.1 Slow groundwater movement over the far-field,

HC.2 Long distance groundwater pathways from repository to discharge point,

HC.3 Shallow groundwater progressing downwards, and mixing with older deeper waters,

HC.4 Slow groundwater movement within the near-field,

HC.5 Predictable groundwater pathways, and

HC.6 Eventual very low volume discharge to the sea (only after hundreds of thousands of years or longer).

These hydrogeological characteristics are intended to: 1) ensure low rates of leaching from a repository; 2) leaching into a stable and predictable hydrogeological environment; 3) minimal radionuclide transportation rates within the geosphere; and 4) long distance pathways and timeframes prior to surface discharge. All of which enable time for radionuclide decay and concentration reduction. If/when surface discharge does occur, low volume seepage to the oceans has the potential to further dilute radionuclide concentrations. However, selection of a suitable natural barrier should minimise the risk of surface seepage to very long timescales, and any predicted seepage should be below current marine pollution regulatory thresholds.

In addition, decoupling, that is the separation of deeper from near-surface groundwater systems (see Figure 2.10), is also considered a beneficial hydrogeological characteristic (Radioactive Waste Management 2016b). This is because decoupling provides a predictable deeper groundwater system through future climatic changes, for which near-surface groundwater systems are considered most sensitive (see section 2.7). The depth of the geological features causing the groundwater decoupling vary between sites, but could realistically be located at depths of 200 m of greater.

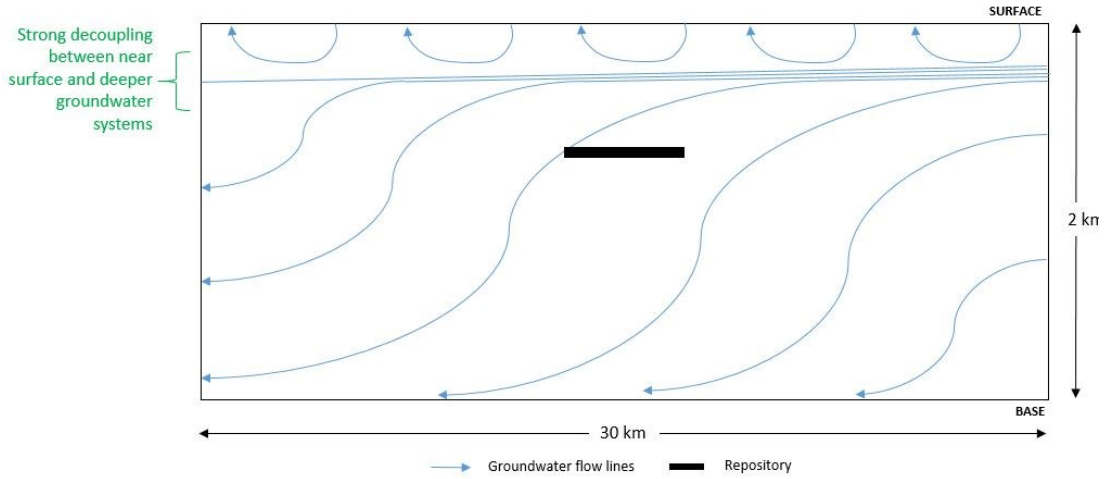

Figure 2.10: Illustration of shallow and deep groundwater decoupling. A repository should be located within a decoupled, deep groundwater system.

This research will therefore consider different far-field groundwater characteristics in reference to hydrogeological characteristics 1 to 4 (HC.1 to HC.4), and the degree of

decoupling between near surface and deeper systems, to assess their potential suitability to host a deep geological disposal facility.

Although the focus of this research is the far-field, this research will consider the characteristics of the near-field (HC.4) as an integral component of the natural barrier, and because the boundary between near-field and far-field is not clear cut (see section 2.3.4). Furthermore, the predictability of a far-field setting (HC.5) will be tested by running 'uncertainty scenarios' (see section 2.7), to look at the variance in hydrogeological characteristics at each setting. This will be used to inform a holistic discussion of the qualities of the individual natural barriers.

Finally, although there is a debate as to the relative benefits of 'low volume' discharge to the sea (HC.6), rapid return rates to the surface, either onshore or offshore, is a negative containment attribute, and will be considered as such within this research. A discussion on the relative merits of offshore vs onshore disposal is presented in Appendix G.

2.3.7 Idealised Hydrogeological Regimes

This section will discuss five far-field hydrogeological regimes, which encompass the hydrogeological characteristics (section 2.3.6) that have been hypothesised as being potentially suitable to host radioactive waste (Chapman et al. 1986). Unlike the official classification of suitable host rock formations (section 2.3.1), no official classification of suitable 'groundwater formations' has ever been produced, only these advised by (Chapman et al. 1986), which are also illustrated in Figure 2.11:

1. Inland Basin or a modified basin limb; downward dip, mixed sedimentary layers with a high proportion of those being of low permeability, water confined to more permeable layers and, low advective flux between layers,

2. Seaward dipping and offshore sediments; similar to 'Inland Basin or modified basin limb' but progressing offshore,

3. Basement rocks under sedimentary cover; low permeability basement rock overlain by newer sedimentary deposits, groundwater movement confined primarily to sedimentary cover, with little hydraulic connection between cover and basement. For clarification, 'basement' within the context of this research, is taken as any formation altered by the Caledonian Orogeny (490 - 390 million years ago).

4. Hard rock in low relief coastal terrain; hard rocks with a low matrix permeability, flat topography, and low hydraulic head groundwater drive, and

5. Small Island; repository below fresh-saline water interface where groundwater is essentially stagnant, large dilution potential of the sea.

It is also important for any selected hydrogeological regime to be geologically and hydrogeologically simple, as its response to various feature and process uncertainties (see section 2.7) should be easier to predict (International Atomic Energy Agency 2011b). For clarification, this research will compare the chosen settings to the above identified hydrogeological regimes for potential suitability.

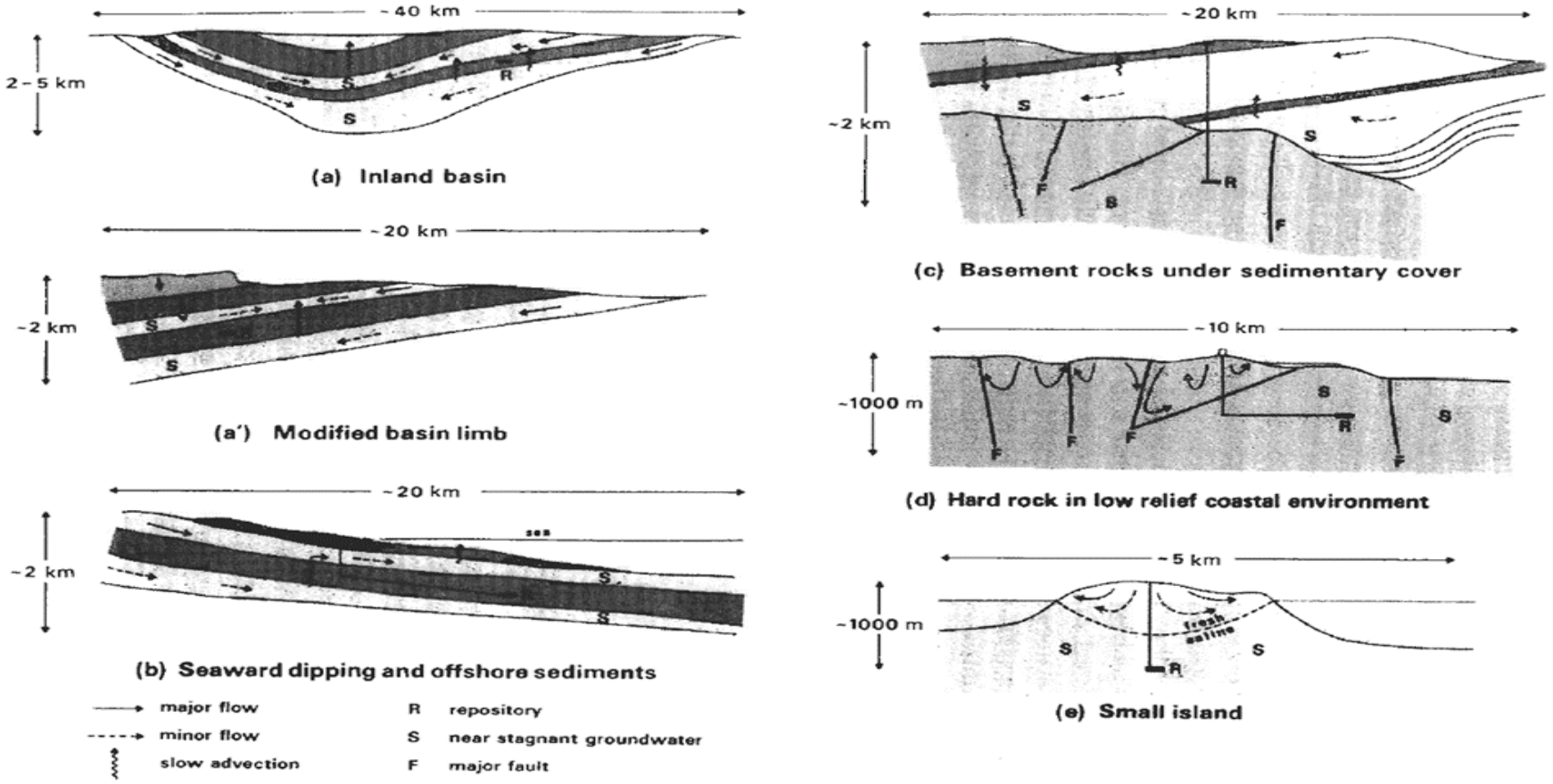

Figure 2.11: Hydrogeological environments considered most suitable for deep disposal of long-lived intermediate level wastes in the UK (Chapman et al. 1986).

2.4 Natural Analogues

This section will introduce the concept of natural analogues (section 2.4.1), the use of natural analogues in characterising radionuclide fate and transportation within host rock formations (section 2.4.2), and finally the relevance and limitations of natural analogues to deep geological disposal research (section 2.4.3).

2.4.1 Natural analogues introduced

Many of the processes which lead to the mobilisation of radionuclides within the natural barrier of a deep geological repository have analogues within nature i.e. natural analogues. These natural analogues provide a means through which the behaviour of processes, important to long term radionuclide containment and isolation can be explored. This has the benefit of providing insight into key processes to be modelled and assessed within deep geological disposal performance studies.

Natural analogues, specifically those exploring the fate and transport of radionuclides within the environment, can be based on entirely naturally occurring systems (such as the Oklo natural Uranium reactor, discussed later), or can utilise anthropogenic radiation releases, such as from the Chernobyl (Gustafsson et al 1987) or Windscale nuclear incidents (Chapman et al 1984, Miller et al 1994).

The Olko natural Uranium reactors, located in Gabon, are the most famous natural analogues for deep geological disposal research. This is because the Uranium, contained within ore bodies, underwent natural fission reactions within the subsurface 1.7 billion years ago, which enabled the formation, and subsequent release of fission products and actinides into the environment (Gauthier-Lafaye 2002). The natural reactors were then exhumed and weathered when in contact with oxygenated circulating groundwaters, further releasing entrained radionuclides into the environment (Gauthier-Lafaye 2002). This is similar to the emplacement of high-temperature higher activity waste into a host rock formation, and the possible mobilisation effects from contact with oxygenated groundwaters. Furthermore, hydrothermal alteration, due to the amount of heat produced by the fission reactions (up to 400 °C) created an encasing low permeability clay layer around the reactor core (Gauthier-Lafaye 2002). This clay layer can be considered analogous to an engineered bentonite buffer, but can also provide insight into radionuclide fate and transportation behaviour through argillaceous material, a possible host rock formation (Miller et al 1994), discussed further within the next section.

A similar pattern of naturally occurring Uranium ore (analogous to radioactive waste material), surrounded by a clay rich halo (analogous to the engineered bentonite clay buffer) and altered host rock (near-field) was discovered at Cigar Lake, Canada (Nuclear Decommissioning Authority 2010d). At this site, Uranium radioelements have been effectively contained within the 'near-field' for 1.3 billion years, with no radioelements detected at the surface (Nuclear Decommissioning Authority 2010d). An illustration of the similarities between Cigar Lake and a deep geological disposal facility is presented within Figure 2.12.

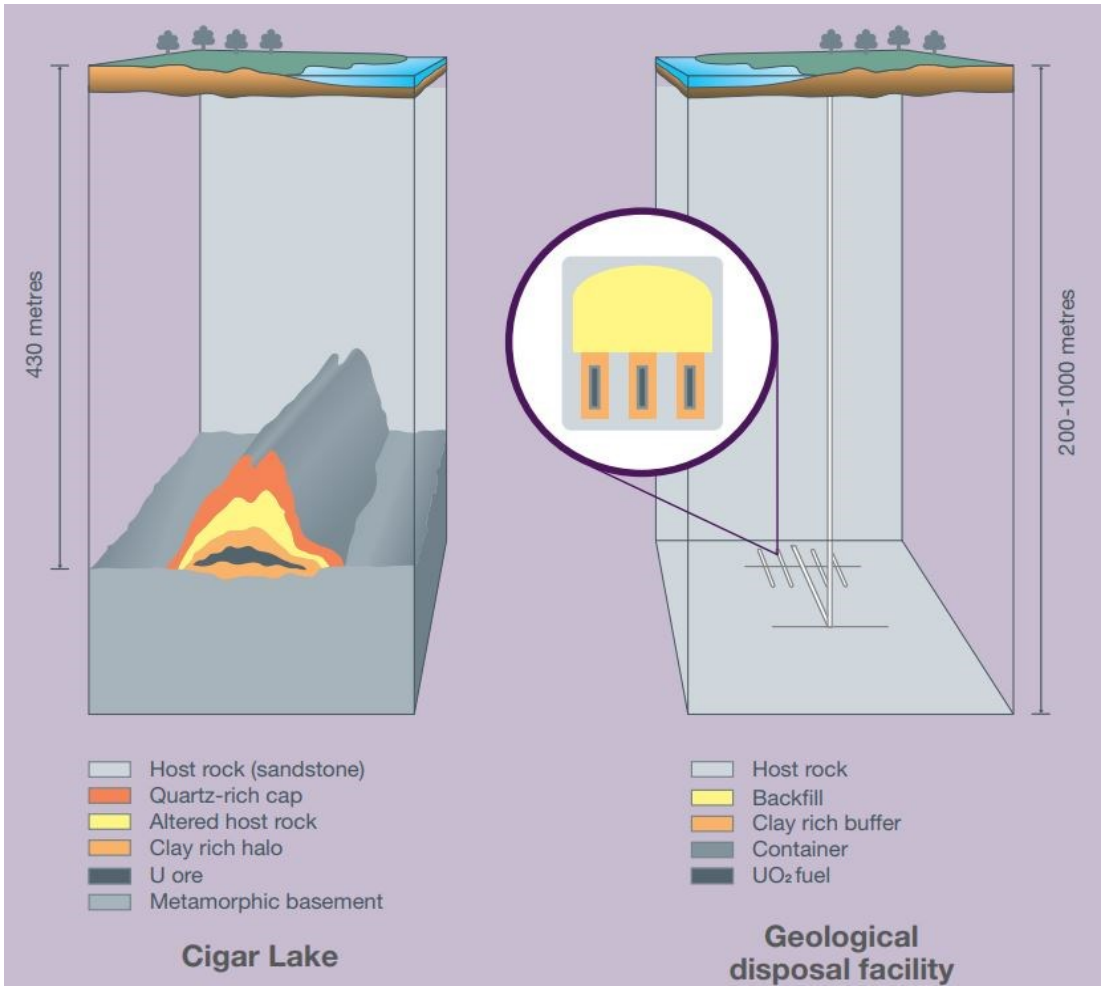

Figure 2.12: Illustration of the components of the natural Cigar Lake Uranium Ore deposit (left), and their similarities to a deep geological disposal facility (right). Image from (Nuclear Decommissioning Authority 2010d)

2.4.2 Natural analogues of host rock formations

Possible host rock formations include: fractured crystalline rock; argillaceous rocks; and evaporitic rocks (see section 2.3.1). Natural analogues have been used to investigate radionuclide fate and transportation behaviour in each of these rock types, although less research has been conducted on the latter (Chapman et al 1984, Miller et al 1994). For example, natural analogues on fractured crystalline rocks, such as at the Klipperås (Landström

& Sundblad 1986) and Palmottu (Blomqvist et al 1991) sites, indicate radionuclides, derived from igneous intrusions, associate primarily with minerals lining fracture surfaces. Furthermore Thorium was found to have higher mobility than Uranium, with both tending to associate with iron bearing mineral phases at Klipperås (Landström & Sundblad 1986), but with Uranium associating with calcite at Palmottu (Blomqvist et al 1991), highlighting changing Uranium behaviour with varying hydrogeochemical conditions.

Research undertaken on clay and argillaceous formations, most notably Loch Lomond in Scotland (Falck & Hooker 1990), and the Maderia Abyssal Plain Turbidites study (Colley & Thomson 1991) found that radionuclides migrated primarily via diffusion, with certain radionuclides e.g. Caesium and Sodium, migrating further than others e.g. Bromine, Iodine, Radium-226 and Uranium. Calculation of effective diffusion coefficients were possible under these unique hydrogeochemical conditions (Chapman et al 1984, Miller et al 1994). Diffusion coefficients can then be fed into model simulations used for site performance assessments. Furthermore, natural analogues of argillaceous formations can provide insight to radionuclide fate and transportation behaviour through the engineered bentonite clay buffer.

Finally, as previously mentioned, far fewer natural analogues have investigated radionuclide fate and transportation behaviour in evaporitic rocks (Chapman et al 1984, Miller et al 1994). Groundwater within these formations is typically in the form of isolated brine pockets, with radionuclide migration expected to be via solid state diffusion (diffusion through the rock mass) only (Miller et al 1994). This is supported by a natural analogue study undertaken by Wollenberg & Flexser (1984) who investigated salt, intruded by igneous rock, and found minimal Uranium and Thorium migration over hundreds of millions of years.

2.4.3 Relevance and limitations of natural analogues to deep geological disposal

Although natural analogues are useful in providing insight and understanding of radionuclide fate and transportation behaviour under different environment conditions, and even providing specific behavioural coefficients, no directly analogous natural analogue to a deep geological repository exists (Chapman et al 1984, Miller et al 1994). Therefore only limited process information can be extrapolated from natural analogues to a deep geological disposal setting, with care required to ensure hydrogeochemical conditions and timeframes remain applicable.

Although study of natural analogues is beyond the scope of this research, natural analogues play an important role in obtaining an insight into radionuclide fate and transportation behaviour, with much of the key process understanding (section 2.8), and complied hydrogeological datasets, applied to this research obtained from natural analogues.

2.5 International Site Selection & Natural Barrier Characteristics

Section 2.4 will discuss the approach employed for site selection and natural barrier characteristics chosen by the USA (section 2.5.1 & 2.5.2); Sweden (section 2.5.3); Finland (section 2.5.4); France (section 2.5.5); the UK (section 2.5.6); and then will finally discuss the UK approach to the natural barrier in an international context (section 2.5.6).

This section will argue that unlike Sweden or Finland whose counties are dominated by higher strength fractured crystalline basement of the Fennoscandinavian Shield, the UK has a much wider variety of far-field geological and hydrogeological settings to choose from, and that these groundwater characteristics should be explored for the purpose of deep geological disposal. This opinion will also form the basis of this research moving forward.

This section will also present information to support the idea that a national screening-out process based on high level far-field geological and hydrogeological factors, followed by volunteerism of the remaining 'potentially suitable areas' would result in a more successful site selection process within the UK than the current site selection programme.

This section is not intended to provide an exhaustive description of the disposal approach and philosophies employed by each radioactive waste producing nation, but is instead intended to highlight contrasting far-field hydrogeological characteristics and regimes, and the natural barrier disposal philosophies, in order to inform discussion for the wider public. For more information on the disposal approach employed by different nation states, the reader is referred to information published by each nation state implementer which includes the U.S. Department of Energy within the USA, Svensk Kärnbränslehantering AB (SKB) within Sweden, Posiva Oy within Finland, Agence nationale pour la gestion des déchets radioactifs (ANDRA) within France, and the Nuclear Decommissioning Authority (NDA) within the UK.

2.5.1 Waste Isolation Pilot Plant, USA

The Waste Isolation Pilot Plant (WIPP), situated in New Mexico, USA, is the only higher activity waste repository currently in operation globally, taking the USA's defence related transuranic (intermediate level-long lived) wastes since 1999 (U.S. Department of Energy 2016; Waste Isolation Pilot Plant 2018). The WIPP site was selected after a process, started in the 1950's, recommended disposal within a bedded salts (Waste Isolation Pilot Plant 2018). Site investigations commenced in 1976 (Nuclear Decommissioning Authority 2013b).

The WIPP is situated on the edge of the Delaware Basin, at a depth of *approx.* 650 m below the ground surface, within the 600 m thick Salado halite (evaporitic) formation (Figure 2.13). The Salado formation is overlain by *approx.* 100 m of interbedded anhydrites and dolomites

of the Rustler Formation, and underlain by *approx.* 400 m of interbedded anhydrites and halites of the Castile Formation (U.S. Department of Energy 2012). The Salado Halite formation has very low hydraulic conductivies and only contains isolated brine pockets (Beauheim & Holt 1990) which, due to their unconnected nature, are not considered a major concern for radionuclide transportation. The Salado forms a vertical barrier to groundwater flow (Beauheim & Holt 1990). Anhydrites within the underlying Castile, although also generally forming a vertical barrier, contain isolated pockets of pressurized, long residence, brines under confining conditions. These brine pockets are associated with gravity driven salt deformation and faulting (Beauheim & Holt 1990). Rocks within the Rustler are associated with low yielding aquifers of limited extent (Powers et al. 1978).

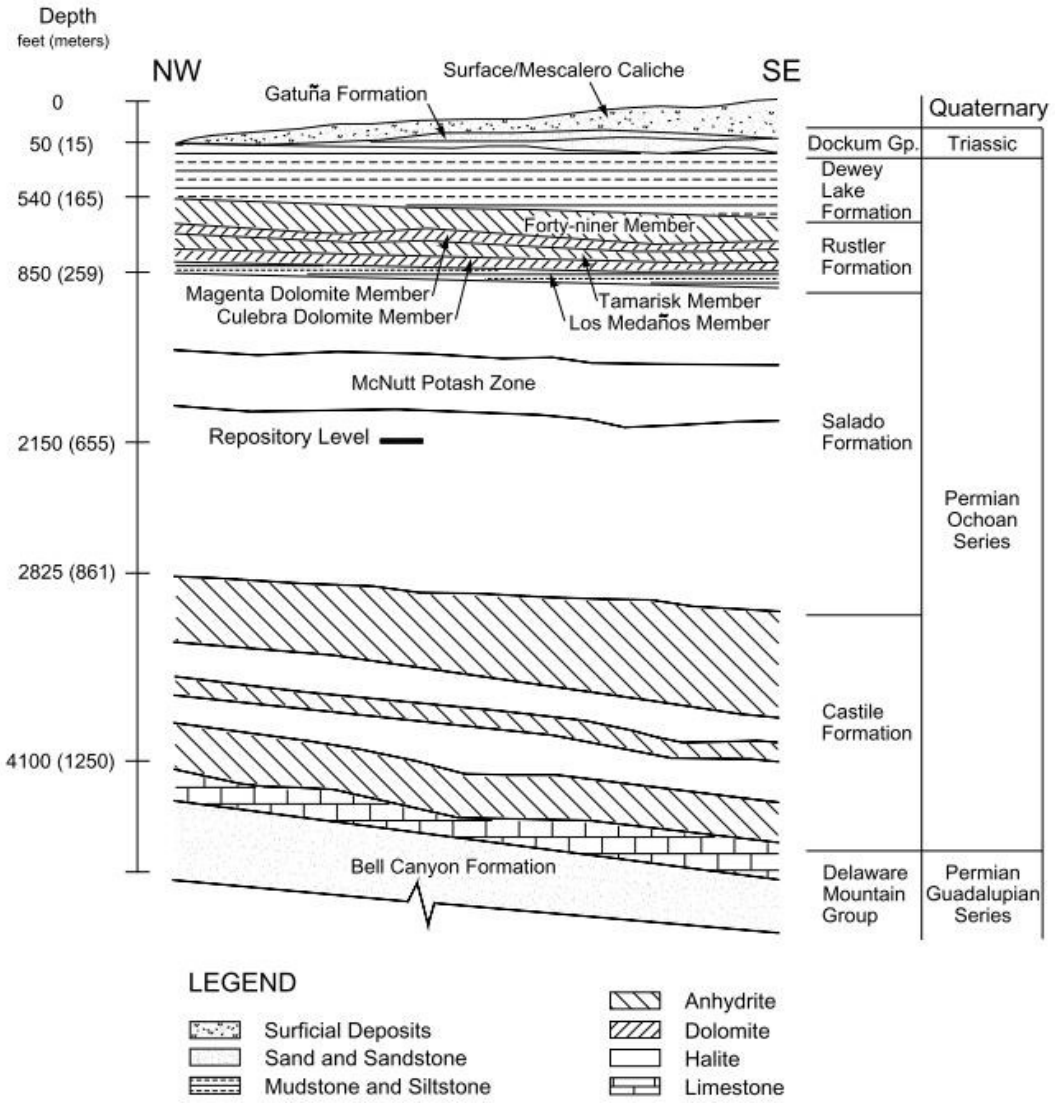

Figure 2.13: Geological sequence (not to scale) of the Waste Isolation Pilot Plant, USA (U.S. Department of Energy 2012), covering area of *approx*. 15 km in length as estimated from (Powers et al. 1978).

The WIPP site can be considered analogous to the 'Inland Basin' hydrogeological regime (Figure 2.11a) with an evaporitic host rock. This is because low permeability sedimentary layers reduce the volume and rate of vertical groundwater movement. The geosphere, and lack of effective groundwater flow vertically through the bedded halite formation, forms an integral barrier to radionuclide migration, and therefore containment of radioactive waste.

2.5.2 Yucca Mountain, USA

Yucca Mountain, located in arid southern Nevada, USA, was investigated as a potential deep geological disposal facility for the USA's higher activity waste legacy from 1978 to 2009 (Nuclear Decommissioning Authority 2013b; Rechard et al. 2014). Investigations were stopped due to public, political and legal opposition in 2009 (U.S. Department of Energy 2010).

Yucca Mountain comprises heterogeneous layers of welded and non-welded fractured volcanic tuff (derived from volcanic ash) (Bodvarsson et al. 1999). The repository was to be situated at a depth of 300 m below the surface, within the welded Topopah Spring Tuff, which contains mineral assemblages considered advantageous for radionuclide sorption (Bodvarsson et al. 1999). The welded Topopah Spring Tuff is overlain by the non-welded Paintbrush Tuff, and underlain by the Calico Hills non-welded Tuff (Bodvarsson et al. 1999) (Figure 2.14).

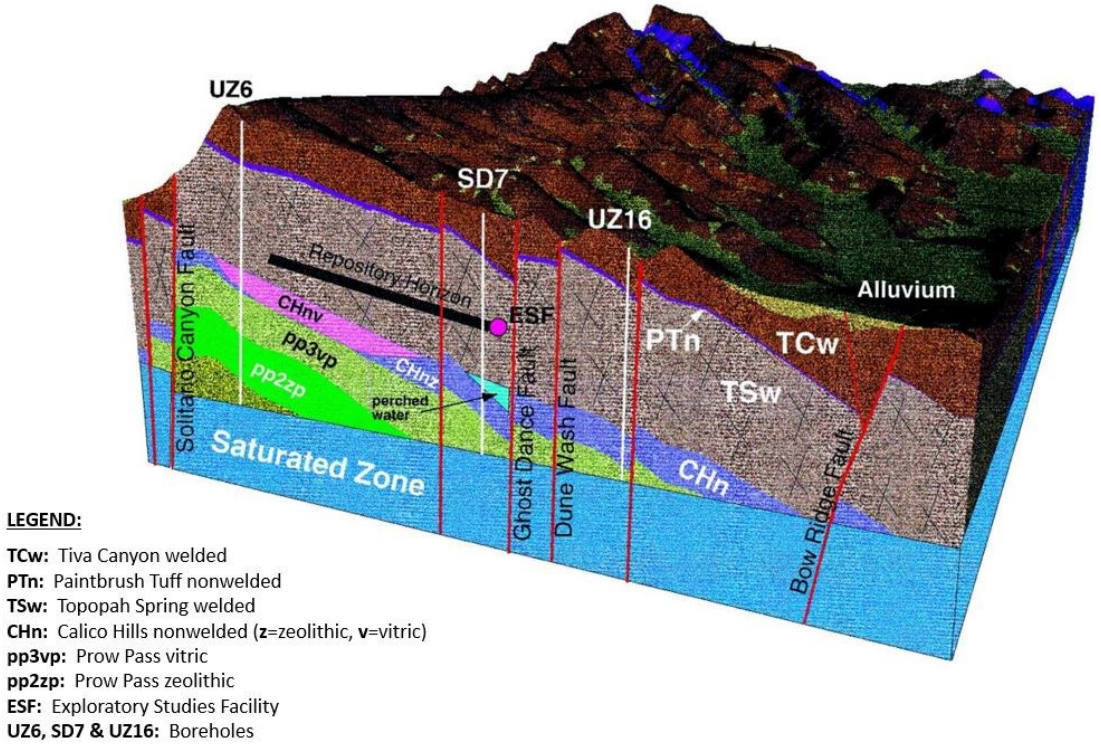

Figure 2.14: Geological cross-section of the Yucca Mountain Site, with the repository situated above the water table within unsaturated welded fractured volcanic tuffs. Image adapted from (Bodvarsson et al. 1999).

Importantly, the water table at Yucca Mountain is situated at a depth of *approx.* 600 m below the surface i.e. 300 m below the repository zone (Bodvarsson et al. 1999; Apted & Ahn 2017). This is due to very low annual rainfall rates of *approx*. 16 cm (National Research Council 1992), and even lower infiltration rates of 5 mm/year average (Bodvarsson et al. 1999). The Topopah Spring Tuff, in which the repository was to be located, is therefore unsaturated with a low volumetric moisture content of 10% (Spycher et al. 2003). Although the tuff fractures are associated with elevated permeabilities, of up to two orders of magnitude compared to the fractured tuff, the low infiltration rates result in low sub-surface groundwater flow rates.

The Yucca Mountain site is very interesting from a hydrogeological perspective as the unsaturated tuffs mean that the site cannot be compared to the hypothesised saturated hydrogeological regimes (section 2.3.7). However, Yucca Mountain still arguably illustrates beneficial groundwater characteristics as the primary transportation pathway for released radionuclides, saturated groundwater flow, has been removed. That is not to say released radionuclides cannot be transported within gravity driven percolating rainwater, however, the very low infiltration rates at the site reduces this possibility based on current climatic conditions. Much of the safety strategy for radionuclide containment and isolation at Yucca Mountain is therefore tied into the limited volume of groundwater moving through the geosphere, with extra safety functions provided by the waste packaging and surrounding engineered components (Bodvarsson et al. 1999).

A Yucca Mountain style groundwater system cannot exist within the UK as the UK experiences a greater amount of rainfall than southern Nevada (typically 60 to 300 cm/year depending on location (Meteorological Office 2017)), which means elevated sub-surface infiltration rates and higher water tables. A repository at a depth of 200-1,000 m within the UK would most likely be within the saturated zone.

2.5.3 Forsmark, Sweden

Within Sweden, a national geological screening programme was undertaken 1977 to 1985, followed by conversion to a volunteerism approach to site selection in 1992. The volunteerism approach included requirements for the site to have suitable geology (SKB 2018a; SKB 1995). Both Forsmark in Östhammar, and Laxemar in Oskarshamn were chosen for detailed investigations in 2000 and 2001 (SKB 2005a; SKB 2005b; SKB 2006; Elam & Sundqvist 2011) with Forsmark agreed in 2009 (SKB 2009). Construction is due to begin on the site in the early 2020's (SKB 2018c).

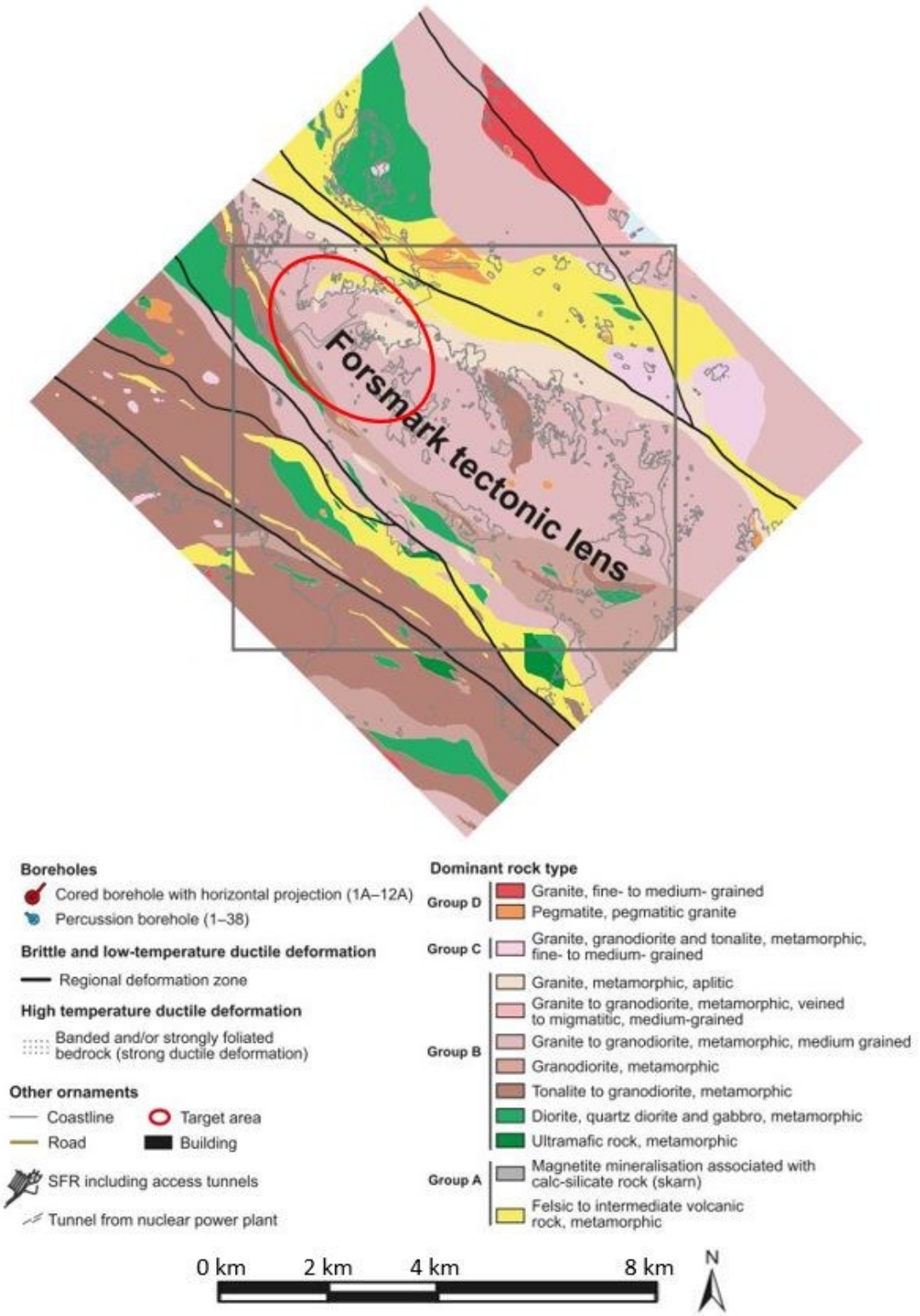

Figure 2.15: Surface geological map of the Forsmark site, situated on the coast at a depth of 500 m within granites and granodiorites. Image adapted from (Stephens 2010).

The Forsmark site is situated at a depth of *approx.* 500 m within higher strength volcanic and metamorphosed crystalline basement of the Fennoscandinavian Shield (Stephens 2010),

within a tectonic lens. The limits of the lens are delineated by a WNW-ESE to NW-SE striking deformation zone (Stephens 2010) (see Figure 2.15). Forsmark was selected over Laxmar due to: 1) *'better prospects for achieving long-term safety'*; 2) *'strong local support'*; 3) *'fewer water-conducing fractures'* (100 m spacing in Forsmark compared to 5-10 m in Laxemar); and 4) *'limited groundwater flow through the repository'* due to flat topography, and low groundwater head drive (SKB 2009). The low permeability crystalline matrix, fracture dominated flow, and flat topography, means Forsmark can be considered analogous to the hydrogeological regime 'hard rock in low relief coastal environments' (Figure 2.11d).

Interestingly, in Sweden, it is considered that *'the safety of a repository* [developed in fractured crystalline basement] *is only slightly dependent on the ability of the surrounding rock to retard and sorb leaking radionuclide materials. The primary function of the rock is* [instead] *to provide stable mechanical and chemical conditions over a long period of time so that the long-term performance of the engineered barrier is not jeopardised'* (SKB 1992; SKB 2011). This has led to the position of the natural barrier safety functions being one of indirect radionuclide containment and isolation (through preservation of the engineered barriers), rather than direct through very slow far-field radionuclide migration rates and effective sorption.

It is the opinion of the author that this philosophy has also created the engineered barrier focus of the KSB-3V containment system (section 2.2), developed by Sweden and Finland (Posiva Oy 2012), and adopted by the Nuclear Decommissioning Authority (UK).

2.5.4 Olkiluoto, Finland

Following a national screening programme starting in 1983 from which 327 100-200 km^2 unfractured tectonic blocks were identified (McEwen & Aikas 2000) (Figure 2.16), four sites were chosen for site specific investigation in 1994 (Anttila et al. 1999a; Anttila et al. 1999b; Anttila et al. 1999c; Anttila et al. 1999d).

The selection of the four sites was based on technical (geological and hydrogeology) and non-technical (transport, land ownership, population density, pre-existing geological information and ease of investigation) factors (McEwen & Aikas 2000). Of the four sites, Olkiluoto was selected for further investigation in 1999 (Posiva Oy 2003; Posiva Oy 2009a; Posiva Oy 2009b), with the site finalised in 2015 (Posiva Oy 2017) following submission of a safety case (Posiva Oy 2012). Olkiluoto is currently under construction and due to begin operations in the 2020's (Posiva Oy 2017).

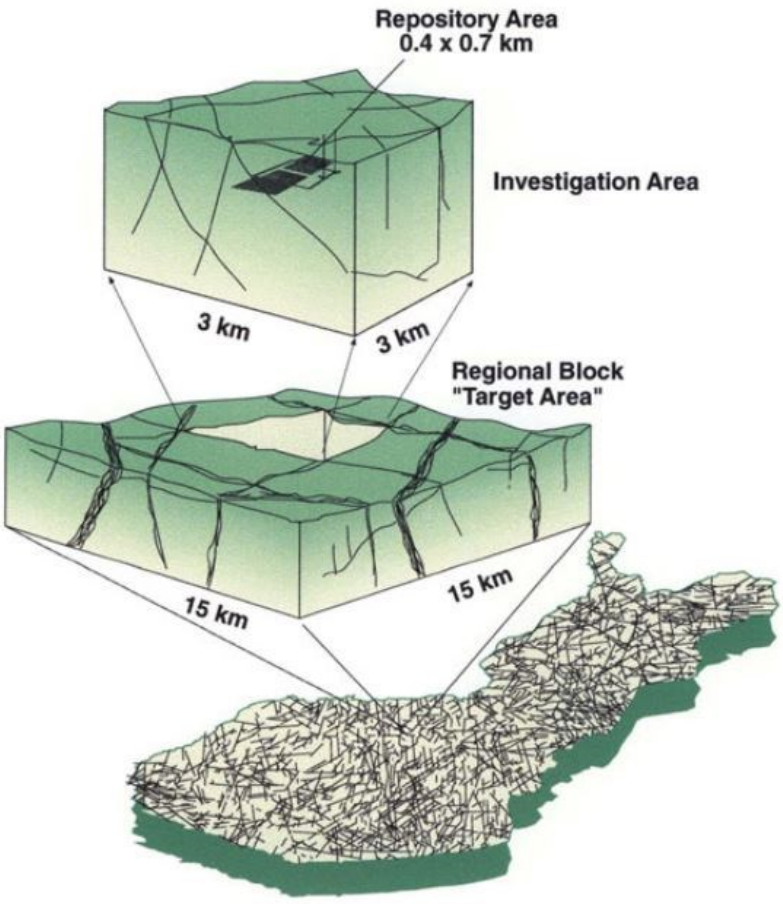

Figure 2.16: Outline of the process of site selection in Finland. Image obtained from (McEwen & Aikas 2000).

The repository at Olkiluoto is situated at a depth of 400 to 450 m (Posiva Oy 2017), within higher strength volcanic and metamorphosed rocks of the Fennoscandinavian Shield, namely Gneisses (Posiva Oy 2012) (Figure 2.15). The Olkiluoto region is affected by regional deformation, resulting in SE-dipping thrust faults and deformation zones, with NE-SW strike-slip faults also common (Posiva Oy 2012). Due to the low matrix permeability of the Gneisses, groundwater flow is fracture dominated, becoming less transmissive with depth (Posiva Oy 2012). Pressure driven groundwater flow dominates areas of topographic significance, with density driven flow being increasingly important with depth. Areas of groundwater affected by Quaternary glacial and interglacial cycles have been reported to depths of 300 m (Posiva Oy 2012) i.e. not reaching the repository horizon.

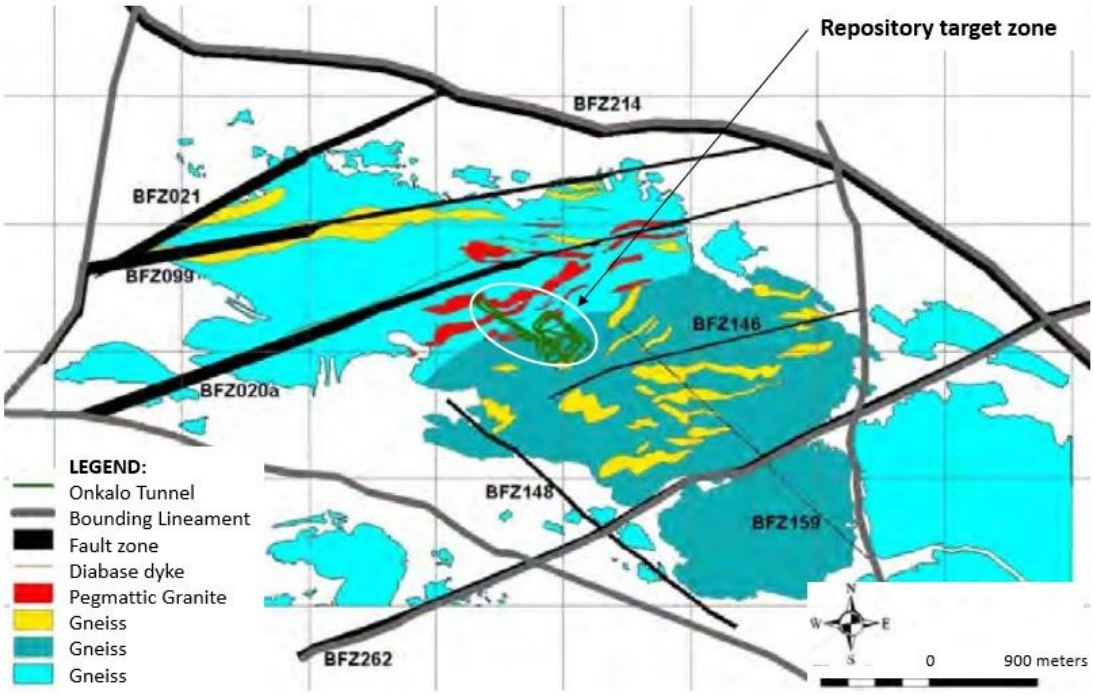

Figure 2.17: Surface geological map of Olkiluoto, Finland. The repository is situated at a depth of 400-450 m below ground level, within Gneiss of the Fennoscandinavian Shield. Image adapted from (Posiva Oy 2012).

Due to its flat topography, fracture dominated flow through higher strength rock, and coastal location, Olkiluoto, like Forsmark, can also be considered analogous to the hydrogeological regime 'hard rock in low relief coastal environments' (section 2.3.7). Finland has also opted for the KSB-3V containment system (Posiva Oy 2012) which again relies on the natural barrier indirectly containing and isolating radionuclides, rather than directly (see section 2.5.3).

2.5.5 Bure, France

Following a failed site selection process in the 1980's in which no local communities were consulted, 30 volunteered sites were identified in 1993 from which 4 locations were selected for geological screening in 1994 (Nuclear Decommissioning Authority 2013b): Gard; Vienne; Meuse; and Haute-Marne (Andra 2018b). Results from the geological screening identified both Meuse and Haute-Marne to showed geological promise due to simple geological structures (Andra 2018b). Subsequently, due to their close proximity, the two sites were combined into a single site for further investigation.

A license application was granted for development of an underground rock characterisation facility (the Meuse/Haute-Marne Centre) at a depth of 490 m, with construction beginning in 2000 (Andra 2018b). A 250 km^2 'transposition zone' around the research facility was designated and considered feasible for deep geological disposal in 2005 (Andra 2005b; Andra 2005a). A more refined 30 km^2 area, within the transposition zone, was identified for further

investigation in 2009 (Andra 2018b). The refined area was approved in 2010 (Nuclear Decommissioning Authority 2013b), with a decision on license application for repository construction due in 2019 (Andra 2018a).

The repository at Bure, if selected, will be situated at a depth of 420 to 600 m below the ground surface within the 130 to 160 m thick Callovo-Oxfordian clay, located in the east of the Paris Basin (Andra 2005b). The Callovo-Oxfordian clay is overlain by the calcareous Oxfordian limestone, and underlain by the Dogger limestone through which regional groundwater flow is dominated (Andra 2005a), although neither are considered a water resource (Andra 2005a).

The entire sequence is in a simple monoclinal structure (dipping in one direction), at a low regular angle of 1 to 1.5 degrees to the northwest (Andra 2005a) (Figure 2.18). Low matrix permeability means that solute transport through the Callovo-Oxfordian clay is diffusion dominated, with vertical permeability two orders of magnitude lower than that of horizontal permeability (Andra 2005a). Due to the high phyllosilicate minerals content of the host rock, it is considered that released radionuclides will be effectively sorbed (Andra 2005b).

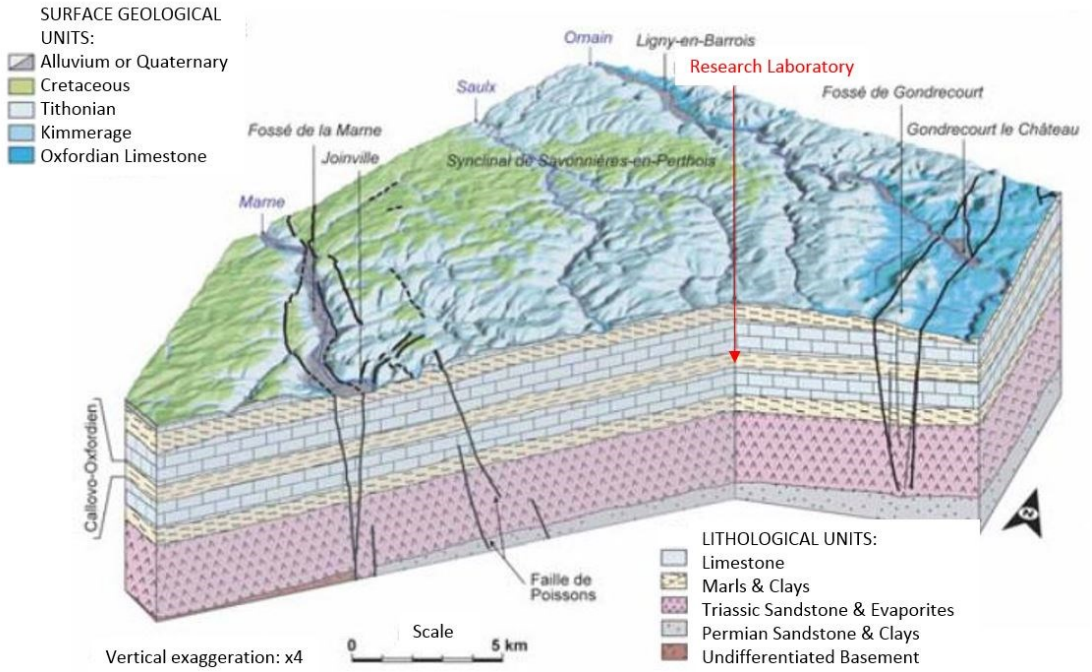

Figure 2.18: Geological cross section of the Bure site in France. The repository is located within the Callovo-Oxfordian Clay layer (Andra 2005b).

The structurally simple layered sedimentary sequence on the edge of a sedimentary basin, and the low vertical groundwater flux mean that the Bure site can be considered analogous to the hydrogeological regime 'inland basin' (Figure 2.11a).

Interestingly France state that *'the packages used in establishing the design of a deep repository in a clay environment, for example made of steel or concrete, cannot hope to have a level of durability similar to that of the half-life of a radionuclides, which can exceed hundreds of thousands of years', and that 'we will* [therefore] *rely particularly on the properties of the Callovo-Oxfordian layer in order to confine the radioactivity' (Andra 2005b).*

The role the natural barrier plays within the overall multi-barrier containment system in France is therefore different to that of either Sweden (section 2.5.3), Finland (section 2.5.4) or the opted UK approach (section 2.5.6). France places greater reliance on the natural barrier directly containing and isolating radionuclides through very slow far-field groundwater flow rates and effective chemical sorption. In contrast, Sweden, Finland and the UK place greater emphasis on the natural barrier indirectly ensuring radionuclide containment and isolation through providing the conditions necessary to preserve the integrity of the engineered barrier.

2.5.6 Sellafield, UK

Longlands Farm, located in West Cumbria (close to Sellafield, of which it will now be referred), was the focus of £400 million of drilling analyses and hydrogeological investigations in the UK for a deep geological disposal facility between 1991 and 1997 (Nirex 1997a; Nirex 1997b; Nirex 1997c; Nirex 1997d). The developer Nirex applied for permission to develop an underground rock characterisation laboratory (see section 1.2). This was rejected locally, and called in the Secretary of State for Environment, leading to a planning inquiry, the proceedings and evidence of which are detailed within (Haszeldine & Smythe 1996). Following the outcome of the public planning enquiry, exploration and appraisal investigations at Sellafield ceased (UK Parliament 1997).

In 2014 the UK re-stated their commitment to deep geological disposal (Nuclear Decommissioning Authority 2014). This was to be achieved using a volunteerism approach to site selection, in conjunction with a multi-barrier containment system, and national geological screening (Nuclear Decommissioning Authority 2014). The national geological screening programme would be undertaken in order to inform high level discussions with volunteering communities (Nuclear Decommissioning Authority 2014), rather than as part of a national scoping study. In 2016 Radioactive Waste Management (the implementers) issued a public consultation on national geological screening. The results of which have formed part of the National Geological Screening Guidance (Radioactive Waste Management 2016b). Most recently a public consultation has been undertaken on the 'National Policy Statement', and the 'Working with communities: implementing geological disposal' policy document (Nuclear Decommissioning Authority 2018).

Sellafield (Cumbria), along with Dounreay (Caithness) were originally shortlisted for consideration from an initial list of 537 sites. The reason for the Sellafield and Dounreay selection was initially reported to be based on 'technical and non-technical factors' (Nirex 2005a). However, it was later concluded to be *'strongly influenced by the non-technical'* such as *'restricted to sites that were owned by central government, or by its nuclear industry shareholder'* (Nirex 2005a). Sellafield was finally chosen over Dounreay on the consideration that *'waste transportation would be less of an issue'* (Nirex 2002; Nirex 2005a).

The Sellafield site was to be situated at a depth of *approx*. 600 m below ground level, within the 'higher strength' crystalline welded tuffs of the Borrowdale Volcanic Group. The Borrowdale Volcanic Group is characterised by low permeability matrix (Nirex 1997a; Nirex 1997b), with groundwater flow dominated along connected fault zone associated 'Potential Flowing Features' (Gutmanis et al. 1998). The Borrowdale Volcanic Group is overlain by a short section of Palaeozoic and Mesozoic sediments, which pinch out eastwards around the coast (Jackson et al. 1995). The Palaeozoic and Mesozoic sediments facilitate groundwater flow regionally, and behave as a major potable aquifer (Nirex 1997a; Nirex 1997b; Nirex 1997c; Nirex 1997d).

Sellafield has been previously described as 'a variant of basement rock beneath sedimentary cover' hydrogeological regime (Figure 2.11c). Research undertaken on the groundwater characteristics of the site by (Chaplow 1996; Black & Brightman 1996; Bath et al. 1996; Nirex 1997c; Haszeldine & McKeown 1995; Fraser Harris et al. 2015) all indicate short groundwater pathways ascending towards the surface around the coast due to a westward located dense brine formation, and strong near surface-deep groundwater coupling. None of these features are considered beneficial groundwater characteristics for long term radionuclide containment (section 2.3.6). Based on these criteria, Sellafield cannot be considered analogous to any of the idealised hydrogeological regimes (section 2.3.7).

More detail on the geology and hydrogeology of the Sellafield site, including figures, is presented in Chapter 5.

2.5.7 Discussion of UK and International Approaches

Out of the discussed international deep geological disposal sites of the Waste Isolation Pilot Plant (section 2.5.1), Yucca Mountain (section 2.5.2), Forsmark (section 2.5.3), Olkiluoto (section 2.5.4), Bure (section 2.5.5) and Sellafield (section 2.5.6), the only two that are not considered analogous to any of the idealised far-field hydrogeological regimes (section 2.3.7) are Yucca Mountain and Sellafield. Yucca Mountain is however located above the water table,

within the unsaturated zone, and due to the very low groundwater flow rates passing through the repository zone, still arguably exhibits beneficial groundwater characteristics for long term radionuclide containment. This is unlike Sellafield, which illustrates short saturated groundwater pathways ascending towards the surface.

Although the natural barrier at all discussed sites is intended to contain and isolate radionuclides for long durations, complementing the engineered barrier system (section 2.2), the mode through which this is achieved is variable. Sweden and Finland have both opted for the KSB-3V containment system, placing greater emphasis on indirect natural barrier containment and isolation through preservation of the engineered barrier facility, due in part to the poor retention properties of the far-field. In contrast, both USA and France appear to place greater emphasis on direct natural barrier containment and isolation through very low far-field flow rates and effective sorption.

The UK, by also considering the KSB-3V containment approach, appear to have, by default, chosen an indirect containment and isolation philosophy like Sweden and Finland, but without an idealised far-field hydrogeological regime to support it. This lack of emphasis on direct far-field characterisation is also supported anecdotally by the UK Radioactivity and the Environment (RATE) programme which funds three main research areas (British Geological Survey 2018); natural barrier coupled processes within the vicinity of the repository i.e. the near-field (HydroFrame), near-surface radionuclide speciation and transport (LO-RISE), and biosphere radioactivity exposure assessments (TREE), none of which explicitly cover the far-field natural barrier.

It is the opinion of the author that unlike Sweden or Finland whose counties are dominated by higher strength fractured crystalline basement of the Fennoscandinavian Shield, the UK has a much wider variety of far-field geological and hydrogeological settings to choose from, the groundwater characteristics of which should be explored. This opinion will form the basis of this research moving forward, with exploration of different UK based far-field natural barrier settings, intended to highlight the diverse range of far-field regimes available for radioactive waste containment.

Finally, the process through which deep geological disposal facilities have been selected internationally is variable, but inevitably includes some degree of technical criteria, and local community participation. The approach chosen by the UK is one of volunteerism, with subsequent exploration of the geological and hydrogeological characteristics of the site. It is the opinion of the author that a national screening-out process based on high level far-field geological and hydrogeological factors, followed by volunteerism of the remaining

'potentially suitable areas' would remove the risk of 1) unnecessary investigation of an unsuitable far-field setting, or 2) selection on an unsuitable/questionable far-field setting. Furthermore, it is considered that this would improve public confidence in the site selection process, which has been proved essential for successful site selection, such as in Sweden and France (Streffer et al. 2011).

Although an independent national geological screening programme is beyond the scope of this research, this research will provide a high level comparison of different types of far-field hydrogeological setting, cemented in site specific examples. It is considered that this will aid decision making and public understanding of what is a comparatively good, or good enough far-field setting, based on the hydrogeological principles outlined in section 2.3.6.

2.6 Potentially Suitable UK Disposal Locations

This section presents an overview of locations across the UK where the hydrogeological regimes as described in section 2.3.7 are situated, and the sites selected for analysis.

Key areas across the UK highlighted as potentially demonstrating the suitable hydrogeological regimes include: Caithness (hard rock in low relief coastal environments); the Cleveland Basin (seaward dipping and offshore sediments and/or inland basin and modified basin limb); the East England Shelf (seaward dipping and offshore sediments and/or inland basin and modified basin limb); the Southern North Sea Basin (seaward dipping and offshore sediments); the London Platform (basement rocks under sedimentary cover & inland basin and modified basin limb); the Worcester Basin (inland basin and modified basin limb); the Weald Basin (inland basin and modified basin limb); the English Channel (seaward dipping and offshore sediments); and the Irish Sea Basin (seaward dipping and offshore sediments) (Chapman et al. 1986) (see Figure 2.19).

It is interesting to note that Sellafield in West Cumbia, the only location previously investigated for a rock characterization facility in the UK (see section 2.5.6), is not highlighted as a region containing extensive potentially suitable geological and hydrogeological formations. The extension of 'potentially suitable sedimentary formations' offshore of West Cumbria beneath the Irish Sea, does however present an interesting opportunity for the UK to consider developing a deep geological disposal facility offshore, discussed in more detail in Appendix 3.

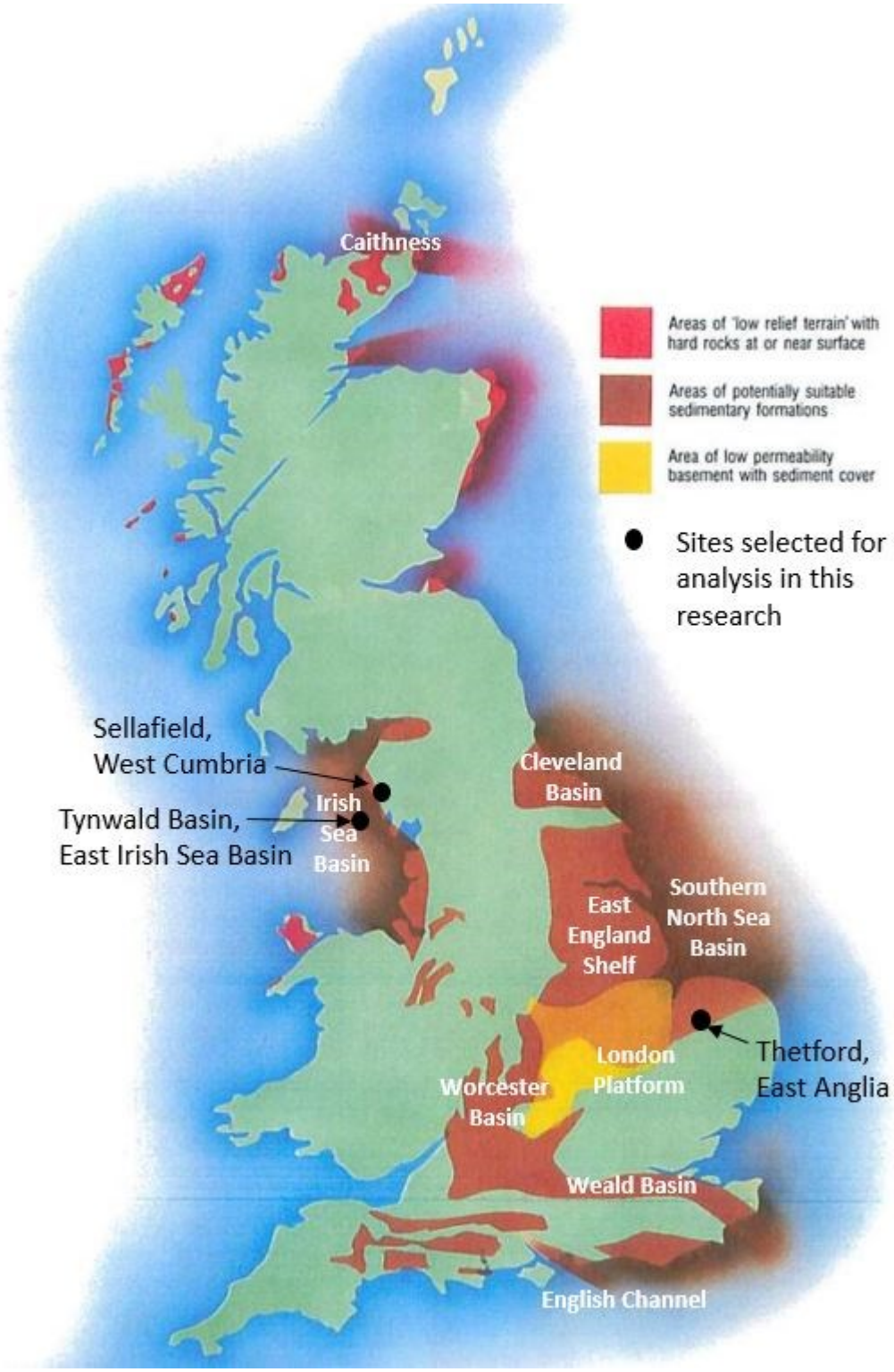

Figure 2.19: Map of areas within the UK containing potentially suitable geological and hydrogeological formations for the deep disposal of long lived intermediate level wastes, obtained from (Nirex 1987), originally adapted from (Chapman et al. 1986).

The research will compare the hydrogeological characteristics (section 2.3.6) of three contrasting far-field hydrogeological settings (section 2.3.7), for the purpose of deep geological disposal. The sites selected for comparison (see Figure 2.19) include:

1) Sellafield in West Cumbria due to historic requests for a rock characterisation facility and an abundance of detailed site specific data,

2) Thetford in East Anglia due to identified potentially suitable *'basement rock beneath sedimentary cover'* within (Chapman et al. 1986), and

3) The Tynwald Basin in the East Irish Sea Basin due to potentially suitable *'offshore sedimentary formations'* within (Chapman et al. 1986), and a previous deep brine concept study for deep geological disposal (Barnes et al. 2005) which also suggested potential suitability, and recommended further site specific research.

Settings illustrating the hydrogeological regimes '*hard rock in low relief coastal environments*' and '*inland basin and modified basin limb*' have not been selected for investigation purely due to time constraints. It is therefore recommended any future site specific research focus on these types of hydrogeological settings.

2.7 Uncertainties in Natural Barrier Performance

This section will discuss feature, event and process uncertainties surrounding natural barrier performance, including: types of uncertainty (section 2.7.1); parameter uncertainties (section 2.7.1); long timescale tectonic (section 2.7.3); climatic shifts (section 2.7.4); waste emplacement uncertainties including excavation disturbance (section 2.7.5); radiogenic heat emission (section 2.7.6); gas generation (section 2.7.7); and finally uncertainties pertaining to human interference/intrusion (section 2.7.8). This is not intended to be a full list of uncertainties, but is intended to highlight some of the key uncertainties requiring consideration for model and/or results interpretation.

2.7.1 Types of Uncertainty

Uncertainty in deep geological repository performance can be split into two main categories: 1) aleatoric uncertainty, and 2) epistemic uncertainty. Aleatoric uncertainty derives from uncertainty about the occurrence of future events, whilst epistemic uncertainty derives from incomplete knowledge about the physical properties of a system (Apted & Ahn 2017). Epistemic uncertainty is considered reducible with additional data collection and site characterisation, whilst aleatoric uncertainty is considered irreducible (Apted & Ahn 2017).

This research will consider only epistemic uncertainties, which, within the context of this research are quantifiable.

2.7.2 Parameter Uncertainties

Parameter uncertainty is epistemic, and provides a major challenge in characterising the natural barrier today and its evolution into the future (Konikow & Bredehoeft 1992). Parameter uncertainty can include material properties such as porosity and permeability, geometric uncertainties such as the location of faults and lithological boundaries, and fluid property uncertainties such as salinity or density. Uncertainties in parameter estimations arise due to data collection techniques, which naturally observe only small areas of the heterogeneous sub-surface e.g. at boreholes or via seismic surveys. Interpretations between the limited data points are thus required. For example, at Sellafield, West Cumbria where extensive site investigations have been undertaken (section 2.5.6), parameter uncertainties of porosity and permeability still range over 2 or 3 orders of magnitude for the same lithological units (Nirex 1997a). These parameters are also liable to change over long duration timescales due to geodynamic phenomena, such as tectonic and climatic changes (sections 2.7.3 & 2.7.4).

Parameter uncertainties can have a major influence on the far-field hydrogeological characteristics. This is illustrated by (Fraser Harris et al. 2015; McKeown et al. 1999; Nirex 1997d; Nirex 1997a; Nirex 1997c; Nirex 1997b), all of whom modelled the same site using parameters within a reported uncertainty range, and all of whom yielded different groundwater velocities and pathways. As such, it is important for this research to consider the parameter uncertainties at the different settings, in order to capture a range of far-field hydrogeological characteristics.

Permeability is considered the most influential parameter controlling regional groundwater movement. This is because out of the permeability, density, gravity and viscosity parameters which make up the hydraulic conductivity term (Equation A.2) of the groundwater flux equation (Equation A.1), it is the permeability which is anticipated to vary the most, up to 10 orders of magnitude (section B.1.4.1). Permeability will therefore be considered within this research as the primary material parameter uncertainty, and will be tested by running *'most-likely'*, and *'high'* permeability scenarios, detailed within section B.1.4.1.

The permeability of a sub-surface area is also however dependent on the geometry of the site i.e. the angle of the faults, or the depth of a particular lithological unit. Uncertainty in the geometry of the site arises due to the limited spatial extent of investigative techniques as outlined above. This research will use published British Geological Survey geological cross-

sections as a template for the geometry of the selected sites, as the most informed cross-sections available. This research will therefore only consider the uncertainty in permeability as a result of measurement and upscaling uncertainty, not geometry uncertainty.

2.7.3 Tectonic Changes

Longer timescale tectonic changes can be considered a result of both aleatoric and epistemic uncertainty, and can provide a source of fluid at depth through diagenetically induced changes in porosity, mineral dewatering, mechanical compaction and tectonic strain (Tsang & Niemi 2013). Changes can also occur by altering the permeability-depth characteristics of the rock mass such as through uplift and subsidence (Figueiredo et al. 2015; Rutqvist 2015; Ranjram et al. 2015; Neuzil 2003). These processes tend to operate over millions of years (McEvoy et al. 2016), and are not anticipated to have much influence on the natural barrier performance over the 1 million timescale of interest, and as such will not be considered any further.

Shorter term tectonic changes, including neotectonics, seismicity and volcanism (McEvoy et al. 2016) are aleatoric in nature, and can occur over very short timescales (seconds for an earthquake). These short term tectonic changes can affect regional groundwater flow patterns by causing disturbances to pressure heads (International Atomic Energy Agency 2011b), and by altering the permeability-depth characteristics of the rock mass (Figueiredo et al. 2015; Rutqvist 2015; Ranjram et al. 2015; Neuzil 2003). The risk posed to site performance by these shorter term tectonic events can however be limited in a UK (intraplatal) context, by avoidance of any fault zones that may be re-activated. Although an important factor for predicting site performance, these shorter term aleatoric uncertainties will not be considered within this research. Identification of fault zones that could be re-activated should however be a focus of any future detailed site specific investigation.

2.7.4 Climatic Changes

Climatic changes, such as a result of glaciation, operate over timescales of thousands of years (McEvoy et al. 2016), and are a great source of both aleatoric and epistemic uncertainty for prospective natural barrier performance (International Atomic Energy Agency 2011b). Glaciation can cause erosion and glacial rebound of the land surface changing water table elevations, and the permeability-depth relationship of the rock mass. Furthermore, regional groundwater flow patterns can be affected by glaciation through changes to recharge rates, and the temperature and chemistry of recharging groundwater (Tsang & Niemi 2013). These processes are likely to occur over timescales of repository performance, with colder climate waters (glacial waters) known to have volumetrically replaced pre-existing sub-surface water down to *approx.* 500 m depth, identified at Dounreay (Degnan et al. 2005). Such influences

have also been attributed to the high hydraulic heads presently observed within the Borrowdale Volcanic Group of West Cumbria, which are still recovering from the Late Devensian glacial retreat (Black & Barker 2015), occurring 27,000 to 15,000 years ago (Clark et al. 2012), and in the Welsh Basin, where small volumes of saline palaeowaters are still returning to the surface (Edmunds et al. 1998).

Given the likely occurrence of glaciation events, the question as to whether present day groundwater conditions are an adequate basis on which to assess long-term repository performance has been previously posed (Degnan et al. 2005). Location of a repository within a deep decoupled (Radioactive Waste Management 2016b) groundwater system could remain predictable through glaciation events. This is because these deep groundwater systems often have long groundwater residence times, and show reduced influence from past climatic (or tectonic) changes (Tsang & Niemi 2013). The near-surface parts of the system tend to respond dynamically to surface processes (Tóth 1963), dampening the effect of glaciation downwards. The depth of these deep groundwater systems is variable depending on setting and connection to the near-surface system, but typically start at a few hundred meters depth (Tóth 1963). A repository situated within one of these deep groundwater systems would offer greater confidence of long term containment on the premise of predictability, although some degree of glacially induced flushing would be anticipated.

Although this research will not explicitly consider the effects of climatic changes on the selected natural barriers due to a degree of aleatoric uncertainty, if the natural barriers exhibit the characteristics described in sections 2.3.6 & 2.3.7, they are likely to be resilient to climatic changes. Detailed site specific investigations would however be required to ascertain this.

2.7.5 Excavation Damage

Excavation of the rock mass during repository construction can lead to an excavated damaged zone (EDZ) around the repository, associated with changes to the stress state, fracture frequency, and consequential changes to rock mass permeability and flow patterns (Tsang et al. 2005). The effects of the EDZ could last for varying amounts of time depending on rock type, with the creep properties of salt rock and some clays closing induced fractures over short timescales compared to higher strength rocks (see section 2.3.1). The uncertainty surrounding the effect of the EDZ on the natural groundwater flow pattern can be reduced with enhanced data collection and research, and can thus be considered an epistemic uncertainty, although a degree of aleatoric uncertainty remains.

Although the area of the EDZ is likely to vary between host rock formations and depending on excavation technique, the area is anticipated to be relatively localized around the repository i.e. a few 10's of meters at the most (Tsang et al. 2005), and is therefore of more concern for near-field analyses than far-field analysis. As such, this research will not consider the effect of repository excavation on natural barrier characteristics any further.

2.7.6 Radiogenic Heat Emission

Radiogenic heat emission, driven by radioactive decay, and to a lesser extent heat from exothermic reactions, such as those involving hydration of cementitious material (Radioactive Waste Management 2016a), can affect the natural barrier and groundwater flow regime. This is because heat emission can cause changes to the stress field and thus of the rock mass (Min et al. 2005), or through changes in fluid properties, such as viscosity and density (Fraser Harris et al. 2015) (see section 2.3.4).

The research undertaken by (Fraser Harris et al. 2015) shows changes to the natural groundwater flow pattern up to 1 km away from the repository. Deeper saline groundwater ascended along higher permeability fault zones and as such, was shown to be influenced by the geometry and material properties of the site.

The uncertainty surrounding the effect of radiogenic heat emission on the natural groundwater flow pattern can be reduced with enhanced data collection and research, and can thus be considered an epistemic uncertainty. Furthermore, due to the role of material properties (i.e. porosity and permeability) and geometry in controlling the extent and degree to which radiogenic heat emission affects the natural groundwater characteristics, the affected area can be expected to change between disposal settings. This research will therefore investigate this uncertainty in far-field groundwater characteristics as a result of radiogenic heat emission. Maintenance of beneficial groundwater characteristics (section 2.3.6) and idealised hydrogeological regimes (section 2.3.7) through the radiogenic heat process will be considered.

Although the idealised hydrogeological regimes (section 2.3.7) were originally developed for intermediate level (none-heat producing) waste, as no research has been produced to the contrary, their characteristics and features are still considered applicable for higher level (heat producing) waste.

2.7.7 Gas Generation

Gas generation, such as from metal corrosion, microbial degradation of organic materials and radiolysis of water and organic materials (Radioactive Waste Management 2016a), can also

affect the natural barrier. This is because gas accumulation could lead to a build-up in pressure, which could fracture the engineered structure and host rock, leading to a disturbance of the pressure head gradients and groundwater flow around the repository (Sharland et al. 2008). Disposal concepts that rely heavily on the engineered barrier are more susceptible to this risk, and should be designed with higher permeability grouts that allow gases to migrate (Sharland et al. 2008).

Gas released could also affect the groundwater flow rates and direction (Metcalfe et al. 2008). This is due to complex multi-phase interactions such as from 1) the displacement of denser brine rich in dissolved gas, 2) gas blocking pore spaces to groundwater flow or 3) chemical interactions causing the precipitation of certain minerals out of solution, again blocking pore spaces and flow channels (Tsang & Niemi 2017). The uncertainty surrounding the effect of gas generation on the natural groundwater flow pattern can be reduced with enhanced data collection and research, and can thus be considered an epistemic uncertainty, although a degree of aleatoric uncertainty remains.

Although a major source of uncertainty within the prospective performance of the natural barrier at different settings, gas will not be considered within the context of this research, but should be the focus of future far-field natural barrier prospectivity scoping exercises.

2.7.8 Human Intrusion

Finally, unintended disturbances to the natural barrier could occur through inadvertent human intrusions, such as a result of mineral extraction/mining, oil and gas exploration and extraction, or groundwater exploration and extraction. This is especially true if future knowledge of the repository is lost. Human intrusion is thus a source of aleatoric uncertainty and is currently irreducible within a modelling context. Siting of a repository should avoid areas which may contain current or future resources of interest (Radioactive Waste Management 2016b). Although a major source of uncertainty, these types of aleatoric uncertainties are beyond the scope of this research, and will be considered no further.

2.7.9 Summary of Uncertainties

In summary, this research will consider the material parameter uncertainty of permeability as a result of measurement and upscaling techniques, along with the uncertainties surrounding radiogenic heat emission on far-field natural barrier characteristics and prospective performance.

This research will not consider the uncertainty of permeability on regional groundwater flow patterns as a result of geometry uncertainty, tectonic changes, climatic changes, near-field mechanical excavation disturbance, gas generation or human intrusion/disturbance.

2.8 Coupled Process Modelling to Assess Natural Barrier Prospectivity

This section will present an introduction to coupled thermal, hydraulic, mechanical and chemical processes (section 2.8.1); how they have been utilised within the study of the deep geological disposal of radioactive waste (section 2.8.2); and how coupled processes can be represented mathematically for use within numerical model simulation (section 2.8.3).

2.8.1 Coupled Processes Introduced

The movement of fluid within the sub-surface can be described through a series of interacting geological, thermal, hydraulic, mechanical and chemical processes which can be expressed mathematically, detailed within Appendix A. The term *'coupled processes'* implies that one process affects the initiation and progress of another (Stephansson et al. 2004). Coupled processes have been applied to the study of numerous geo-scientific research areas including geothermal energy, oil and gas reservoir engineering, weathering, geotechnical engineering projects, solute transportation and deep geological disposal (Stephansson et al. 2004; McDermott et al. 2006; O'Sullivan et al. 2001; Chittenden et al. 2016). A matrix illustrating sub-surface couplings between geological, thermal, hydraulic, mechanical and chemical processes is presented within Figure 2.20.

The processes are linked through a series of material properties. For example, the coupling of hydraulic and thermal processes (3,5 in Figure 2.20) affects the flow characteristics of a fluid, which are linked by temperature dependent 'density' and 'viscosity' of the fluid (section A.4.2). It is also common for geological processes to be incorporated into the model via host rock geometries and material properties (Hudson et al. 2005) (section A.4.5), which allows for unique, site specific geological model scenarios to be developed. (Hudson et al. 2005) and (Chittenden et al. 2016) however suggests that not all couplings present within a system require simulation, only those which exert the greatest influence over the problem under investigation. This also has the benefit of reducing the computational resources required for numerical simulation, especially of spatially and temporally variable coupled process.

1,1 Geology	1,2 Rock inhomogeneity and anisotropy, & fractures (geometry, etc.) affects rock properties/stresses	1,3 Rock porosity, rock mass permeability, and water-rock interaction affects water flow	1,4 Rock mineralogical composition and geometry of fractures affects hydrogeochemistry	1,5 Mineralogical composition, porosity, textural and structural anisotropy effects
2,1 Stress data affecting the geo-interptretation of facture systems and rock mass	2,2 Rock Mechanics	2,3 Spatial distribution of in situ stress and EDZ influences the hydrogeological regime	2,4 Stress changes near fractures zones affecting flow may change precipitation	2,5 Rocks & fracture zones subjected to higher stresses may be more thermally conductive
3,1 Hydrogeological tests and measures can affect the geo-interpretation of permeable features	3,2 Water pressure changes the effective stress	3,3 Hydro-Geology	3,4 The flow pattern affects dilution and mixing	3,5 The flow pattern will affect the temperature due to convection effects
4,1 Hydrogeochemistry interpretation affecting the interpretation of fracture min.rel.	4,2 Precipitation in fractures affects the fracture stiffnesses, strengths and creep properties	4,3 Effects of ground-water age, density, viscosity, and dissolution and precipitation	4,4 Hydro-geo-chemistry	4,5 No interaction
5,1 Thermal anisotropy and measurement affecting the geo-interpretation	5,2 Change in temperature can change the local stress, possibly leading to failure	5,3 Temperature gradients and thermal expansion in rock/fractures affect the water flow	5,4 Dissolution and precipitation enhanced by thermal gradients	5,5 Thermal Properties

Figure 2.20: Interaction matrix illustrating interactions between mechanisms associated with different disciplines of geology, rock mechanics, hydrogeology, hydrogeochemistry and thermal properties/processes (Hudson et al. 2005).

2.8.2 Coupled Processes within Deep Geological Disposal

The importance of understanding coupled processes for the purpose of deep geological disposal was originally brought to scientific attention by (Tsang 1991; Tsang 1987), who stated that the response of a rock mass to radioactive waste storage cannot be predicted with confidence by considering each process individually or in direct succession (Tsang 1987; Hudson et al. 2005). Since then multiple studies, most notably through international collaborations such as DECOVALEX (Development of Coupled models and their VALidation against EXperiment) and BENCHPAR (Benchmark Tests and Guidance on Coupled Processes for Performance Assessment of Nuclear Waste Repositories) have progressed international

understanding on couplings, both for the engineered and natural barrier systems (Hudson et al. 2001; Tsang et al. 2009; Hudson & Jing 2012; Jing et al. 2016; Hudson et al. 2005).

Coupled process research on the natural barrier has mainly focussed on the near-field environment (Hudson et al. 2001; Hudson et al. 2005; Rutqvist, Chijimatsu, et al. 2005; Nguyen et al. 2008; Rutqvist 2008; Kim et al. 2011; Hudson & Jing 2012; Jing et al. 2016; Bond 2016; Tsang et al. 2009; Min et al. 2005), with much less research having been undertaken over the far-field environment (section 2.3.4), such as the influence of radiogenic heat emission (section 2.7) in different far-field settings.

The basic couplings used to investigate the effect of radiogenic heat emission on far-field groundwater flow are thermal processes, due to the heat generated by the decay of the radionuclides within the waste packages, and hydraulic processes representing groundwater flow itself (3,5 and 5.3 in Figure 2.20). Geological processes are also included through site specific lithological geometries leading to geological-thermal couplings (1,5 and 5,1 in Figure 2.20), and geological-hydrogeological couplings (1, 3 and 3, 1 in Figure 2.20). Questions then arise as whether it is necessary to also include mechanical or chemical processes within this study as will now be discussed.

Coupled thermo-mechanical process modelling (2, 5 and 5,2 in Figure 2.20) undertaken by (Min et al. 2005) looked at the effect of radiogenic heat emission on the far-field stress field. The hypothetical repository site used geological data obtained from the Sellafield site. The study found only a small factor change in permeability (< 0.1) compared to baseline conditions (no heat generation), beyond an area of *approx.* 500 m from the repository (Figure 2.21).

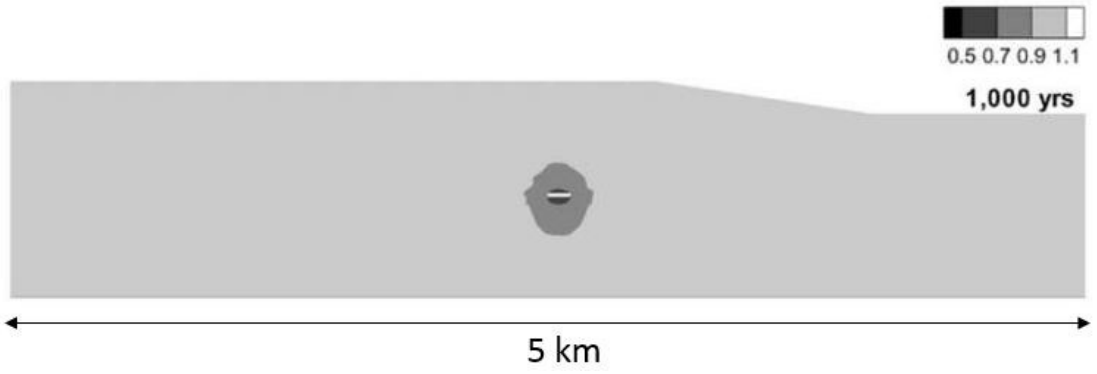

Figure 2.21: Permeability change after 1,000 years post waste emplacement due to induced thermal stress, normalised with respect to verical permeability. Image obtained from (Min et al. 2005).

As permeability is an integral component of the groundwater flow equation (section A.1.1) the effect on groundwater flow from radiogenic heat emission, as a result of mechanical processes,

can be inferred to be small. Furthermore, it has also been shown that the uncertainties generated in the upscaling of hydraulic properties, such as obtained from a single well over an entire lithological formation, introduces greater uncertainties to the modelled far-field environment than those generated from modelling thermo-mechanical couplings (Hudson et al. 2005; Andersson et al. 2005). For these reasons, mechanical processes are not considered an integral process for the problem under investigation, and will no longer be considered.

Coupled thermo-hydrogeological process modelling undertaken by (Fraser Harris et al. 2015) at Sellafield, showed large scale changes to groundwater flow patterns as a result of fluid parameter viscosity and density couplings (3,4, 3,5 & 4,3 in Figure 2.20). The inclusion of density and viscosity variations (non-reactive chemical processes) is therefore considered particularly important for variable density regional groundwater systems.

Finally, limited coupled process research has been undertaken on the effects of reactive chemical processes over the far-field environment (some of which are highlighted along row 4 and column 4 in Figure 2.20). Where this research has been undertaken, it has focussed primarily on discrete fractures or fracture networks (Bond 2016; Jing et al. 2016), with difficulties highlighted in estimating the effect of upscaling (Jing et al. 2016). Due to these uncertainties, reactive chemical processes will not be included within the first part of this research, justified as being a conservative approach i.e. radionuclides will be assumed to be transported at the same rate as groundwater. However, a subsequent retardation calculation will be undertaken to determine the scale of effect of sorption on radionuclide migration rates within different settings.

In summary, this research will: 1) consider coupled thermo-hydrogeological processes over the far-field environment of three contrasting theoretical deep geological disposal settings, including calculating the retardation factor as a result of reactive chemical processes; and 2) consider the effect of radiogenic heat emission from radioactive decay using the coupled thermo-hydrogeological model scenarios.

2.8.3 Mathematical Coupled Process Representation

The section will outline the mathematical principles underlying thermal-hydraulic-chemical coupled processes for use within this research.

Thermal processes, which represent the transport of heat, will be based on ‘Fourier’s Law’. The use of Fourier’s Law is valid for steadystate conditions; one-directional heat transport; constant temperature gradient and linear heat profile; homogenous and isotropic material; constant thermal conductivity; and constant and uniform temperature along bounding surfaces

(Cengel & Boles 2011). Hydraulic processes, which represent the flow of liquid, will be based on 'Darcy's Law'. The use of Darcy's Law is valid for a fully saturated medium; continuous, laminar and steadystate flow; when flow occurs across the entire cross-sectional area; constant hydraulic conductivity; and assumes that the relationship between velocity and hydraulic gradient are linear (Schwartz & Zhang 2003). Non-reactive chemical processes, which represent the transport of solutes, will be based on 'Fick's Law'. The use of Fick's Law is valid for continuous, laminar and steadystate solute transport; through a homogenous and isotropic medium; with no reactions; and assumes the solute transport rate is proportional to mass concentration gradient. The mathematical principles of Darcy's Law, Fourier's Law, and Fick's Law and are detailed within section A.1.1.

These mathematical principles can be developed into three-dimensional transport equations based on the principle of the conservation of energy (section A.2) for use within numerical model simulation. The three-dimensional transport equations are coupled/linked through a series of material parameters (section A.4) which enables the evolution of one process to affect another. Most notably, the transport equations are linked through the advective velocity term (section A.4.1) which is solved by the liquid flow equation, and then passed on to the heat transport and solute transport equations (section A.3). Other material properties, both solid and fluid, link the transportation equations, enabling site specific geological and hydrogeological properties to be incorporated and represented (section A.3). Full details on the mathematical principles underlying thermal-hydrogeological coupled processes is presented within Appendix A.

2.9 Natural Barrier Principles & Processes: Main Points

The key points from the literature review are as follows:

1. The natural barrier, i.e. the rock mass and groundwater, is an essential component of a multi-barrier containment system, and should be investigated as an independent barrier ensuring radionuclide containment and isolation (see section 2.2),

2. Investigation of the natural barrier across the far-field environment is essential as the regional setting determines the long term stability and predictability of the multi-barrier containment system, and also controls the characteristics of the near-field for engineered barrier preservation (see section 2.3.5),

3. Research undertaken by (Chapman et al. 1986) previously identified groundwater characteristics, along with idealised far-field hydrogeological regimes considered of

benefit to long term radionuclide containment (see sections 2.3.6 & 2.3.7), which can be used as a basis for this research,

4. Other nation states have placed greater emphasis on the role of the natural barrier in containing and isolating radionuclides than the UK, with their far-field settings mostly comparable to the idealised hydrogeological regimes hypothesised by (Chapman et al. 1986) (see section 2.4),

5. No direct comparison of the characteristics of different far-field settings within the UK has ever been undertaken, making understanding and therefore decision making as to the suitability of any individual site challenging. This is especially true as analyses of the same location (Sellafield) have historically yielded variable results (section 2.7.1), which illustrates the importance of maintaining a consistent method. A direct comparison of different far-field settings based on the same method of analysis will be provided by this research,

6. The main challenges associated with determining the characteristics of the far-field natural barrier and its prospective performance are derived from: 1) permeability uncertainties; 2) uncertainties in radiogenic heat emission (section 2.7); and 3) the role of geochemical processes in containing and isolating radioactive waste (section 2.3.2),

7. The effect on gas generation of far-field groundwater disturbance is potentially significant and although not dealt with in this research, is recommended for future far-field natural barrier investigations,

8. The UK sites selected for investigation include Sellafield in West Cumbria, the Tynwald Basin offshore within the East Irish Sea Basin, and Thetford in East Anglia, considered to represent a range of hydrogeologically contrasting far-field settings (see section 2.6), and

9. The key processes and couplings considered of importance for far-field natural barrier characteristic representation include thermal processes, hydraulic processes and chemical processes, both conservative and reactive, which will be used within the prospectivity assessments of the sites (see section 2.8).

Chapter 3 Coupled Thermo-hydrogeological Models for Natural Barrier Evaluation

Model simulation took place in two stages. Firstly coupled thermo-hydrogeological (TH) models were run using OpenGeoSys to obtain an understanding of the characteristics of the regional groundwater systems. Groundwater pathways and velocities, obtained from the TH models, were also used as a basis for radionuclide retardation calculations. Results from the TH models and natural barrier assessment are presented within Chapters 4 to 6. Secondly the TH models from the first stage were used as a basis from which radiogenic heat emission, from the emplacement of radioactive waste, were simulated. These models were analysed and reported separately in Chapter 9. The reasons for separate analysis are presented within section 8.1. A summary diagram of the modelling stages is presented in Figure 3.1.

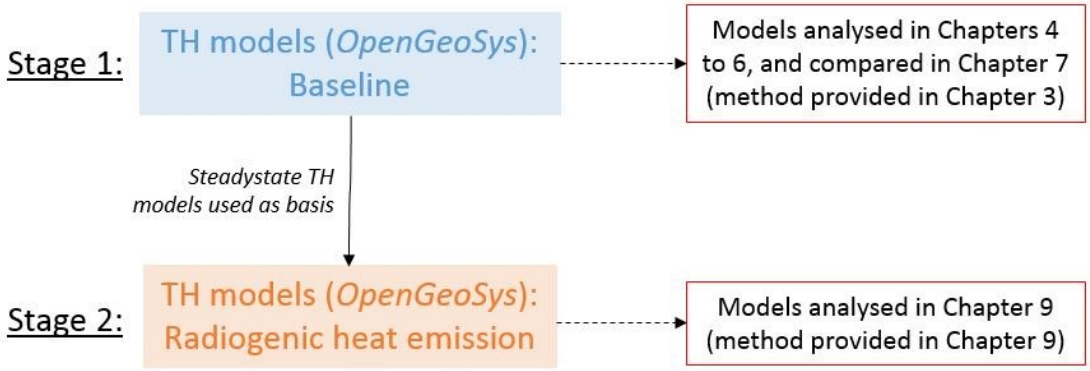

Figure 3.1: Flow chart of modelling stages undertaken within this research.

This chapter will discuss the method used to develop the TH models. This chapter will cover the philosophy of predictive modelling within the field of the deep geological disposal (section 3.1), how the predictive models were designed and constructed (section 3.2), a proposed method for model (site) analysis and comparison (section 3.3), how the proposed method was implemented (section 3.4), and finally the key assumptions and simplifications of the chosen method (section 3.5).

3.1 The Philosophy of Predictive Modelling

Models can be described as '*representations of a real system or process'* (Konikow & Bredehoeft 1992). The application of models in understanding the evolution and prospective performance of deep geological disposal facilities is particularly useful given the very long timescale involved in radionuclide containment (section 2.1), which is not possible to simulate

under standard field or laboratory conditions. Problems however arise when trying to ascertain levels of confidence in the modelled results.

Before discussing levels of confidence, it is worth talking about where the uncertainties in the model results initially come from. Uncertainties can come from inaccurate conceptualisation of the problem (the conceptual model) (see section 3.2.3), such as a misunderstanding of the key physical and chemical processes operating in the system (outlined in section 2.8), which can lead to selection of inappropriate equations (the mathematical model) (see section 3.2.4), through which the system will be represented. Uncertainties also creep in through the chosen method through which the equations are solved for (the numerical model) (see section 3.2.5), which itself provides an approximation of the mathematical model. Uncertainties can also come from model parametrisation, such as uncertainties in material properties, or boundary conditions (see section 3.2.6). (Konikow & Bredehoeft 1992) suggests the most common form of model uncertainties come from inappropriate conceptualisation, and from the data used to populate the models. The uncertainty around the material property 'permeability' will be considered within the research (see section 2.7)

A classic method to ascertain the *'validity'*, and therefore confidence in a model is through a process of *'calibration'*, whereby model results are compared to historic datasets, also known as *'history matching'* within the field of petroleum geoscience. (Konikow & Bredehoeft 1992) however argues that:

> 1) Calibration, or history matching, only provides limited assurance of model reliability, as historic data sets, within the field of groundwater modelling, are often relatively short term compared to the future timeframes under investigation,
>
> 2) That calibrated/matched solutions are none-unique, and that a match does not necessarily provide a deep understanding of the investigated system, and
>
> 3) That a match is often arbitrarily and subjectively defined by the model developer, and inevitably always leads to the question of '*is the match good enough?'*

(Konikow & Bredehoeft 1992) goes on to argue that groundwater models cannot ever be validated, only ever invalidated, and that models are actually embodiments of testable hypotheses, rather than commonly perceived predictive assessment tools, on which so much reliance for risk based decision making is made.

Within the field of deep geological disposal, (Konikow & Bredehoeft 1992) also suggests a wider problem in the final test of public support, with the terms *'validation'* and *'verification'*

used to communicate a false level of confidence in the predicted performance of a site. For example, modelling of the same Sellafield Site in West Cumbria, undertaken by (Fraser Harris et al. 2015; McKeown et al. 1999; Nirex 1997d; Nirex 1997a; Nirex 1997c; Nirex 1997b) have all yielded different results of groundwater velocities and subsequence particle travel times/distances, all of which have been *'calibrated'* an therefore supposedly *'validated'*, leading to the question of which model scenario is to be believed?

(Konikow & Bredehoeft 1992) recommends that predictive models should instead be used to organise information, and gain an understanding of a system, which includes the testing of hypotheses, ideas, and identifying sensitive parameters, which can together be used to guide and inform future investigations. Similarly (Hudson et al. 2005) also suggests that in the case of deep geological disposal, models need not predict exactly what will happen in the future, but that they only need to capture mechanisms and changes essential for understanding performance, whilst (Winograd 1990) suggests that models are good for guiding research, testing of worse case scenarios, and eliminating marginal waste disposal sites. (Konikow & Bredehoeft 1992) suggests that any test of public support for a proposed deep geological disposal facility should therefore be based on a scientific consensus, made up of individual technical and scientific judgements, and not solely on the results of predictive models which cannot be truly validated.

This research will use the philosophy of models as a tool to explore characteristics of the sub-surface system, rather than for absolute prediction. A consistent method of model construction and site analysis will be applied to different deep geological disposal settings. This will result in the same assumptions and simplifications being applied to all model scenarios, enabling direct comparison of the sites. This approach also deals with the question of which model is to be believed, in that all models are based on the same underlying assumptions and simplifications, and can therefore all be believed, or disbelieved, in equal measure.

It is this method of direct comparison between the modelled settings, applied to this research, which has never before been done in a UK context. It is believed this comparison will aid understanding of what is a comparatively '*good*' far-field setting for the general public and stakeholders.

3.2 Modelling Approach

3.2.1 Introduction

The chosen approach for predictive model development and simulation followed a recommended hydrogeological modelling methodology as described by (Anderson &

Woessner 1992), which included: statement of the problem definition; conceptual model development; mathematical model selection; numerical model selection; model construction; and a test of model confidence. These modelling stages will now be described in the context of this research.

3.2.2 Problem Definition

The full aims and hypotheses of this research are presented within section 1.3, with a wider discussion of the context of the research presented within Chapter 2.

3.2.3 Conceptual Model

The purpose of a conceptual model is to: simplify the system under investigation down to the key characteristics and processes of importance to the problem definition; allow the known information to be organised; and reduce the risk of mathematical and numerical errors later within the modelling process (Anderson & Woessner 1992).

Conceptual model development within this research was achieved through the use of published geological maps and cross sections, lithological and groundwater contour maps including salinity contours, and site specific or literature derived geological, hydrogeological, and geochemical parameters. Hydrogeological conceptual models are presented for the individual sites of Sellafield (Figure 4.5), the Tynwald Basin (Figure 5.4) and Thetford (Figure 6.4).

3.2.4 Mathematical Model

Mathematical model development involves the selection of equations considered to represent the key processes controlling the system under investigation. In the case of this research, the key processes considered of importance were liquid flow, heat transport and non-reactive mass transport (section 2.8). The equations representing these processes are detailed within Appendix A.

Liquid flow, heat transport and non-reactive mass transport are coupled through the fluid density and dynamic viscosity functions (section A.4.2), previously implemented into the OpenGeoSys code (Kolditz et al. 2012) by (Fraser-Harris 2012) (section B.1.3.1). Reactive solute transport was considered separately through a retardation calculation, but linked to the OpenGeoSys model through the advective velocity term, and particle pathway.

3.2.5 Numerical Model

The numerical model provides a method through which the chosen process equations of liquid flow, heat transport and non-reactive mass transport (see section A.3) can be solved for over the sub-surface area (domain) of interest. The process equations can be solved for either

analytically or numerically, with both methods able to provide very accurate solutions (Istok 1989).

A numerical method was chosen to solve for the process equations within this research. This was because numerical methods require less restrictive assumptions on aquifer properties, boundary conditions and initial conditions than analytical solutions do, and are better able to deal with spatially variable and time-dependent parameters (Istok 1989; McDermott et al. 2006; Konikow & Bredehoeft 1992). All of which are important features for this time dependent research. Numerical solutions do however typically require more sophisticated computational resources than analytical methods (Istok 1989). However, access to high performance computational resources (discussed later) made the use of a numerical solution possible.

The most common numerical methods are the finite difference method (FDM), the finite element method (FEM), and the finite volume method (FVM). Although the finite methods solve for the governing equations in different ways (McDermott 2015), all are able to provide very accurate results, with the final results very similar (depending on discretisation) (Istok 1989).

The FEM is considered, out of the three methods, to best handle irregular and curved boundaries, anisotropic and heterogeneous aquifer properties, sloping geometries and solute transportation (Istok 1989; Anderson & Woessner 1992). The features of which were required for the TH models.

The FEM solves by providing approximate solutions to the governing equations via a system of partial differential equations (Istok 1989). The uncertainties in results generated from the different finite method solutions, in addition to those generated by the FEM approximation, are considered less than the uncertainties in model predictions generated from inappropriate conceptualisation, or data population (Konikow & Bredehoeft 1992). Therefore, the use of the FEM is considered appropriate for the purpose of this research.

A summary of common FEM and FDM codes available for environmental simulation, along with their main programming features are presented within Table 3.1.

Table 3.1: Codes commonly used to perform environmental simulation (Bensabat 2018)

	TOUGH-ECO2N	TOUGH-ECO2M	TOUGH-FLAC	PFLOTRAN	DUMUX	PROOST	OPEN GEO-SYS	GOLDSIM	CODE_BRIGHT	FEFLOW	MODFLOW
Finite Difference	Y	Y	Y	Y	N	N	N	Y	N	N	Y
Finite Element	N	N	N	N	Y	Y	Y	N	Y	Y	N
Hydraulic	Y	Y	Y	Y	Y	Y	Y	Y	Y	Y	Y
Mechanical	N	N	Y	Y	Y	Y	Y	Y	Y	N	
Thermal	Y	Y	Y	Y	Y	Y	Y	Y	Y	Y	
Chemical	N	N	N	Y	Y	Y	Y	Y	N	Y	
Multicomponent	N	N	N	N	N	N	Y				
Two-phase[1]	Y	Y	Y	Y	Y	Y	Y	Y	Y	Y	
Three-phase[2]	N	Y	N	N	N	N	Y				
Support	N	N	N	Y	Y	N/A	N/A	Y			
Licensing	Required	Required	Required	Open Source	Open Source	N/A	Open Source	Required		Required	Open Source
Programming language	Fortran 77	Fortran 77	Fortran 77	Fortran 90 and C++	C++	C++	C++	C++			Fortran 77 and Fortran 90
User friendliness	Low	Low	Low	Good	Low		Low	Good		Good	Good
1	Two-phase: Water and CO_2 either liquid or gas. No phase change processes in the CO_2										
2	Three-phase: Water and CO_2 liquid or gas. Phase change processes in the CO_2										

The FEM open-source software 'OpenGeoSys' was selected (Table 3.1) for the TH models. This was due to its ability to solve for complex spatially and temporally variable, multi-phase and multi-physics problems (Kolditz et al. 2012). OpenGeoSys also has proven historic application to natural barrier coupled process simulation (Fraser Harris et al. 2015). The benchmark code for OpenGeoSys is presented within the OpenGeoSys Benchmark Book (Kolditz & Shao 2009).

OpenGeoSys most commonly operates by solving for liquid flow first (Equ.A.11), providing pressure heads at each node within the model. Pressure heads are then interpolated for the elements, and converted into flow velocities (Kolditz & Shao 2009). The velocities are then passed on to derive the solution of Equ.A.12 for heat transport and Equ.A.16 for mass transport (McDermott et al. 2006). OpenGeoSys also has the ability to solve for velocity directly at the nodes (rather than pressure) through the 'Fluid Momentum' method. The Fluid Momentum method is less commonly used than the aforementioned 'pressure' based method, despite the fact it is considered to cause fewer velocity discontinuities at the nodes and along element boundaries (Kolditz & Shao 2009). This is because the Fluid Momentum method requires greater computational resources and expertise (Kolditz & Shao 2009), and it was for this reason the pressure based method was employed within this research.

Numerical modelling was made possible through institutional access to high performance computational resources, namely the Edinburgh Compute and Data Facility Linux Compute Cluster (Eddie3). Eddie3 includes some 7000 cores, and up to 3 TB of memory per compute node (16 cores within a compute node) (University of Edinburgh 2018). Access to Eddie3 enabled the OpenGeoSys models to be run efficiently using parallel computing. Models were run using 4 cores, with the run scripts provided in Appendix B.3.

The FDM transport code GoldSim (Table 3.1) was selected to validate radionuclide retardation calculations. GoldSim was selected due to extensive historical use within the field of environmental risk assessments and uncertainty analysis, including that of the deep geological disposal of radioactive waste (Pulkkanen & Nordman 2010; Lee & Hwang 2009; Vopalka et al. 2006). GoldSim required less computational resources to run than OpenGeoSys.

The TH models (OpenGeoSys) were run as two-dimensional (2D) simulations in the X-Z directions, whilst the subsequent retardation calculations, including validated through Goldsim are based on one-dimension (1D) simulations/calculations. The decisions and implications for this are presented within sections B.1.1 & B.2.1 respectfully.

3.2.6 Model Construction

The key features required for numerical model construction are summarised (Figure 3.2) and include processes (PCS), equations (EQS), material medium properties (MMP), material solid properties (MSP), material fluid properties (MFP), material chemical properties (MCP). The chosen numerical method i.e. FDM, FEM or FVM, has already been introduced through the numerical model (section 3.2.5). Model geometry (GEO), mesh (MSH), boundary conditions (BC), initial conditions (IC), source term (ST) and numerical control (NUM) are also required. The meshes (MSH) developed for the TH models contained over 60,000 nodes and 118,000 elements, making them uniquely large scale and high quality, discussed further within Appendix B.1.

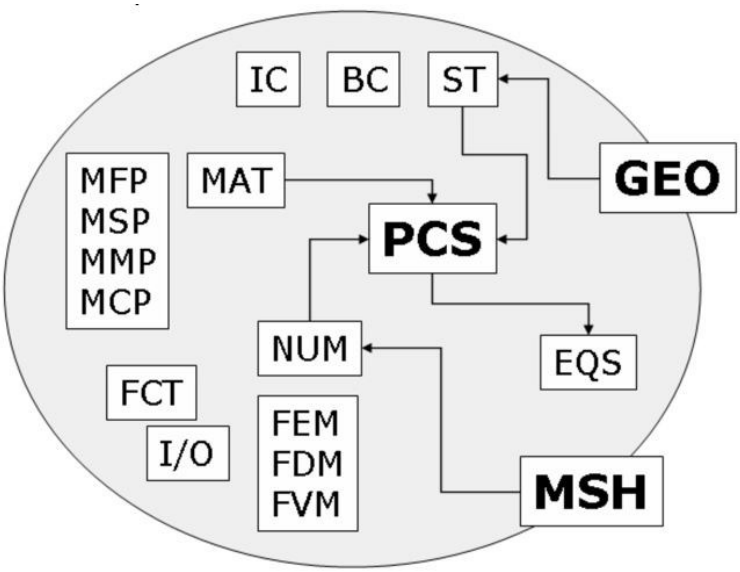

Figure 3.2: Summary diagram of features required for hydrogeological model construction and development (Kolditz et al. 2012)

The specific key features (Figure 3.2) applied to the TH models area detailed within Appendix B.1, and those of the C models used to validate the retardation calculations, are presented in Appendix B.2.

3.2.7 Ascertaining Model Confidence

The final step in the modelling methodology as described by (Anderson & Woessner 1992) is model calibration and validation, however, as discussed in section 3.1, models cannot be validated, only tested and invalidated. Some indication of accuracy in the initial conditions was however made by 'calibration/history matching' to field data, available for the Sellafield TH models. The uncertainty of none-uniqueness of the model match does however remain

(section 3.1), with the confidence in model predictions decreasing with time away from the starting point.

3.3 Proposed Method for Site Analysis and Comparison

3.3.1 Introduction

As no research has previously compared the hydrogeological characteristics of different theoretical far-field radioactive waste disposal settings, no method currently exists. This section therefore proposes a new method whereby the qualitative 'beneficial' hydrogeological characteristics, previously hypothesised by (Chapman et al. 1986) (section 2.3.6) could be turned into parameters that could be quantitatively assessed. The parameters could then be compared and scored in relation to an ideal (benchmark) far-field hydrogeological scenario.

The challenge of this method was to assess the geospatially and temporally complex hydrogeological characteristics in a simple manner, whilst still retaining a holistic perspective on long term radionuclide *containment* and *isolation*.

3.3.2 Beneficial Hydrogeological Characteristics

The beneficial hydrogeological characteristics (HC) previously hypothesised by (Chapman et al. 1986) and selected for analysis in this research (section 2.3.6) included:

HC.1 Slow far-field groundwater movement,

HC.2 Long duration and length groundwater pathways,

HC.3 Groundwater mixing downwards with older deeper waters, and

HC.4 Slow near-field groundwater movement.

3.3.3 Selected Hydrogeological Parameters

The following parameters (P) were selected as feasible outputs from a model, and were deemed representative of the above stated hydrogeological characteristics (illustrated in Figure 3.3):

P.1 (in reference to HC.1) *percentage of far-field domain (20 km length by 2 km depth area) with very slow advective velocity. Justification for the selection of the 20 by 2 km area is presented within section 3.4.1,*

P.2 (in reference to HC.2) *total length of the quasi-steadystate groundwater pathway from the top of the repository to the discharge/exit point* (the term 'quasi-steadystate' was applied as small areas of the model domain were still changing after 10,000 years. For further discussion please see section 9.2),

P.3 (in reference to HC.3) *the depth of the quasi-steadystate groundwater pathway discharge/exit point relative to the top of the repository, and*

P.4 (in reference to HC.4) *the distance the radionuclide travelled over 10,000 years once released from the top of the repository. A timescale of 10,000 years was chosen, after which time significant climatic changes could be expected to occur, and uncertainties in groundwater pathways and velocities increase substantially.*

3.3.4 Hydrogeological Parameters for the Benchmark Scenario

Comparison of parameters P.1 to P.4 against benchmark far-field hydrogeological scenario enabled a point of reference to be set from which all other sites could be considered relative to. The selected parameters (P) of the benchmark scenario are as follows (illustrated graphically in Figure 3.4):

P.1 *100% of the far-field domain (20 km length by 2 km depth area) with an advective groundwater velocity < 2.00E-10 m/s.*

P.2 a *total quasi-steadystate groundwater pathway length of >15 km from repository top to discharge/exit point, i.e. particles cannot discharge to the surface within the modelled domain*

P.3 *a quasi-steadystate groundwater pathway discharge/exit depth > 400 m below the repository top, i.e. groundwater pathway getting deeper rather than shallower*

P.4 *a radionuclide particle that has travelled a distance of <77 m over the first 10,000 years, i.e. released particles travelling at an equivalent advective velocity less than or equal to solute travel distance under diffusion. An equivalent advective velocity of 2.00E-10 m/s has been selected (see section 3.4.1).*

3.3.5 Addressing Permeability Uncertainty

P.1 to P.4 was assessed firstly in relation to a system populated with *'most-likely'* fault and lithological permeabilities, and secondly by a system populated with *'high'* fault and lithological permeabilities (see section 2.7.2). This was in order to assess the variance in hydrogeological characteristics at the three sites. Results are presented within Chapters 4 to 6 respectively.

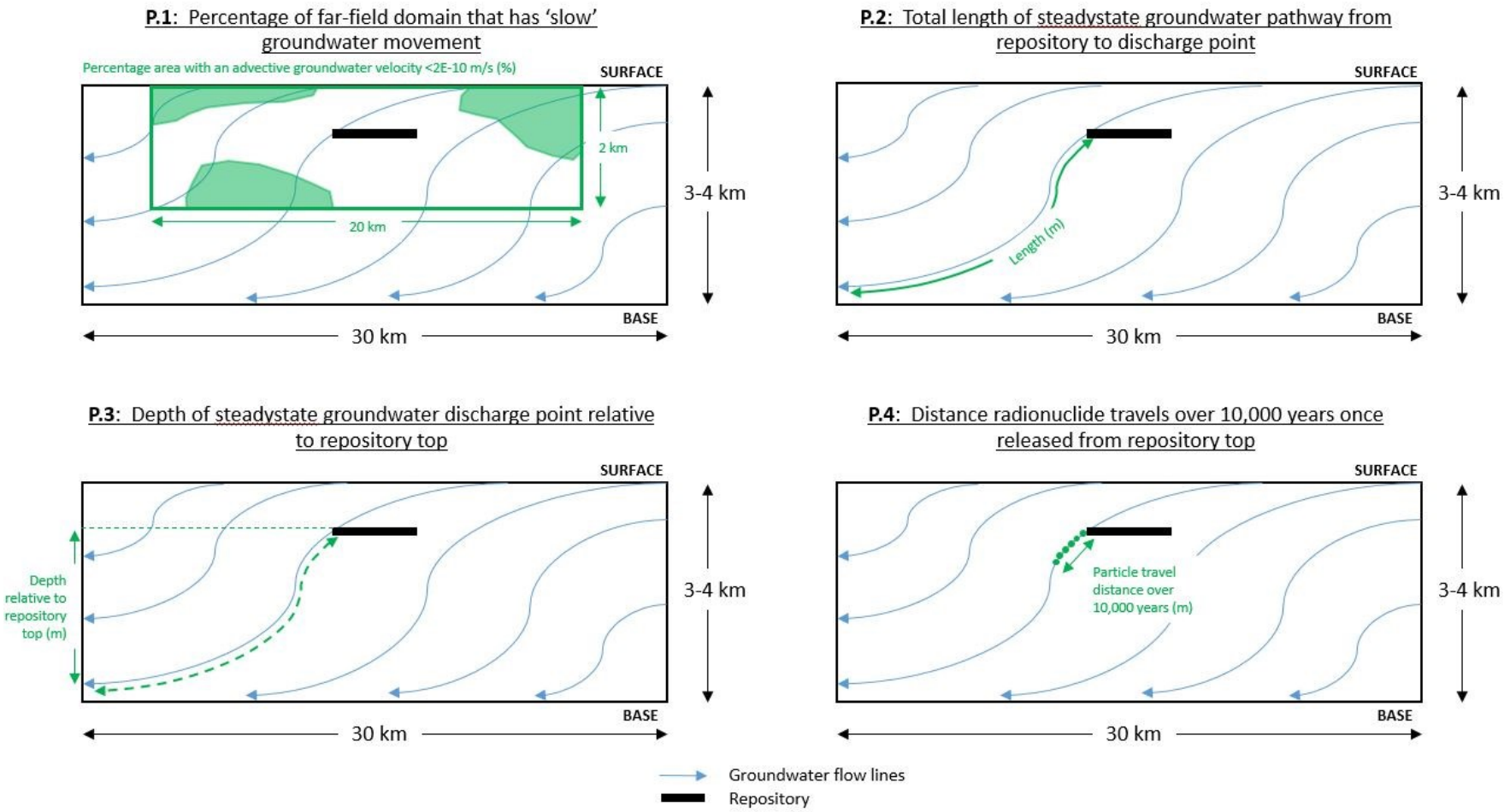

Figure 3.3: Graphical illustration of the parameters (P.1 to P.4), used to assess the hydrogeological characteristics considered of benefit for deep geological disposal within this research.

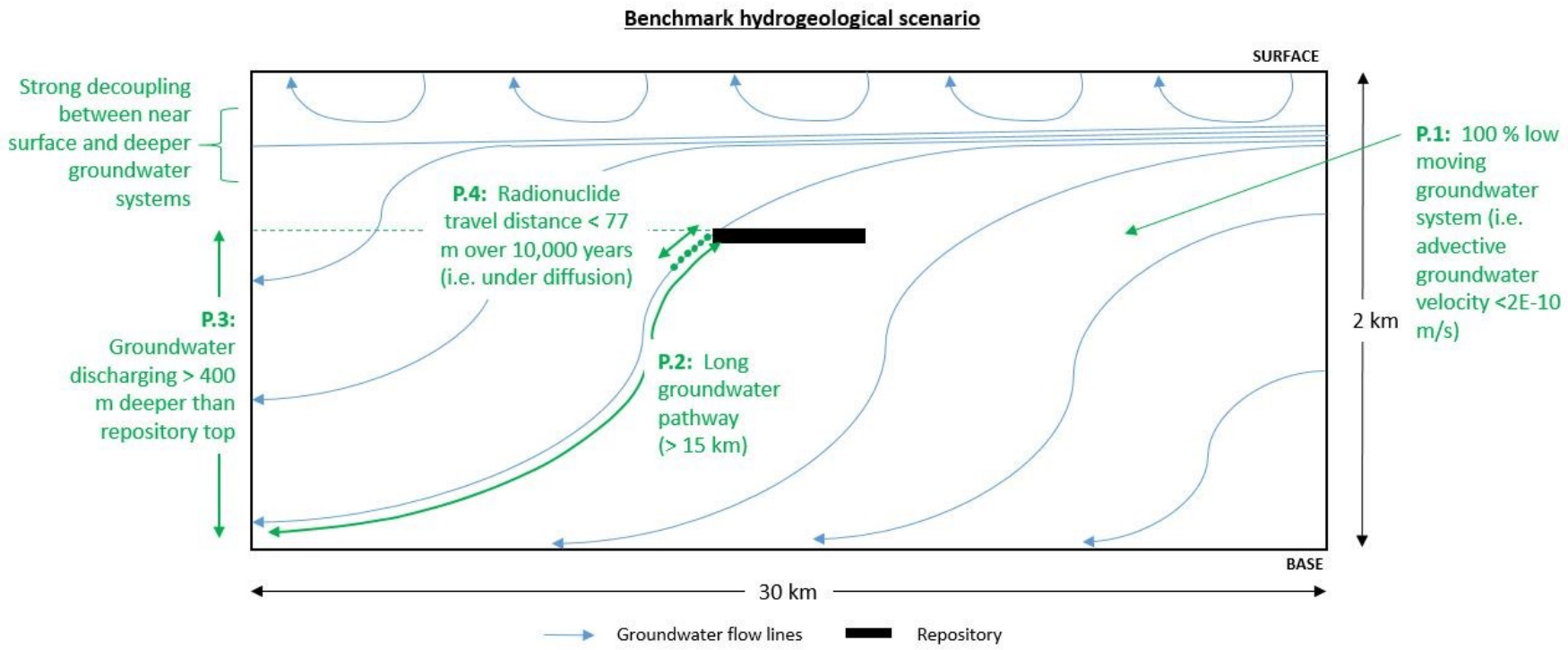

Figure 3.4: Benchmark far-field scenario with reference to selected hydrogeological parameters P.1 to P.4

3.3.6 Bar-Chart Comparison Design

Presenting values for parameters P.1 to P.4 as a series of bar charts against which the benchmark scenario achieves a sum score of '0' (see Figure 3.5), allows all sites to receive a relative score. Using this method, a worst case hydrogeological scenario has a score of '20'. The proposed method of scaling the hydrogeological parameters (P.1. to P.4) within the bar charts was as follows (and illustrated in Figure 3.5):

> **P.1** *scaled from 100% of the far-field domain having 'slow' advective velocity to 0% i.e. 100 to 83 % (score of '0'), 83 to 67% (score '1'), 67 to 50% (score '2'), 50 to 33% (score '3'), 33 to 17% (score '4'), and 17 to 0% (score of '5').*
>
> **P.2** *scaled based on a quasi-steadystate groundwater pathway exiting the model along one of the lateral boundaries (> 15 km) to one exiting towards the surface (<3 km) i.e. > 15 km (score of '0'), < 15 km (score '1'), < 12 km (score '2'), < 9 km (score '3'), < 6 km (score '4'), and finally < 3 km (score of '5').*
>
> **P.3** *scaled based on quasi-steadystate groundwater flow line extending to a depth of > 400 m below repository top, to one exiting the model domain at the surface (modelled domain will extend to > 2 km depth) i.e. > 400 m below (score of '0'), > 200 m below (score '1'), 0 to 200 m below (score '2'), 0 to 200 m above (score '3'), > 200 m above (score '4'), and finally > 400 m above (score of '5'). To ensure edge effects (see section B.1.1) do not affect the results of P.3, if the quasi-steadystate groundwater flow lines discharge to one of the lateral boundaries, the depth will be determined 1 km into the model domain.*
>
> **P.4** *scaled using a multipler of 3 starting at solutes traveling at the same rate of diffusion or less (< 77 m) over 10,000 years i.e. < 77 m (score of '0'), < 231 m (score '1'), < 693 m (score '2'), < 2,079 m (score '3'), < 6,237 m (score '4'), and finally > 6,237 m (score of '5').*

To ensure a holistic perspective is retained, any score generated was accompanied by a discussion of hydrogeological features considered of importance for the long term *containment* and *isolation* of the waste. Important features included faults, specific lithological unit, the degree of decoupling between near surface and deeper groundwater flow (section 2.3.6), and the response of the system to radiogenic heat emission (see Chapter 9).

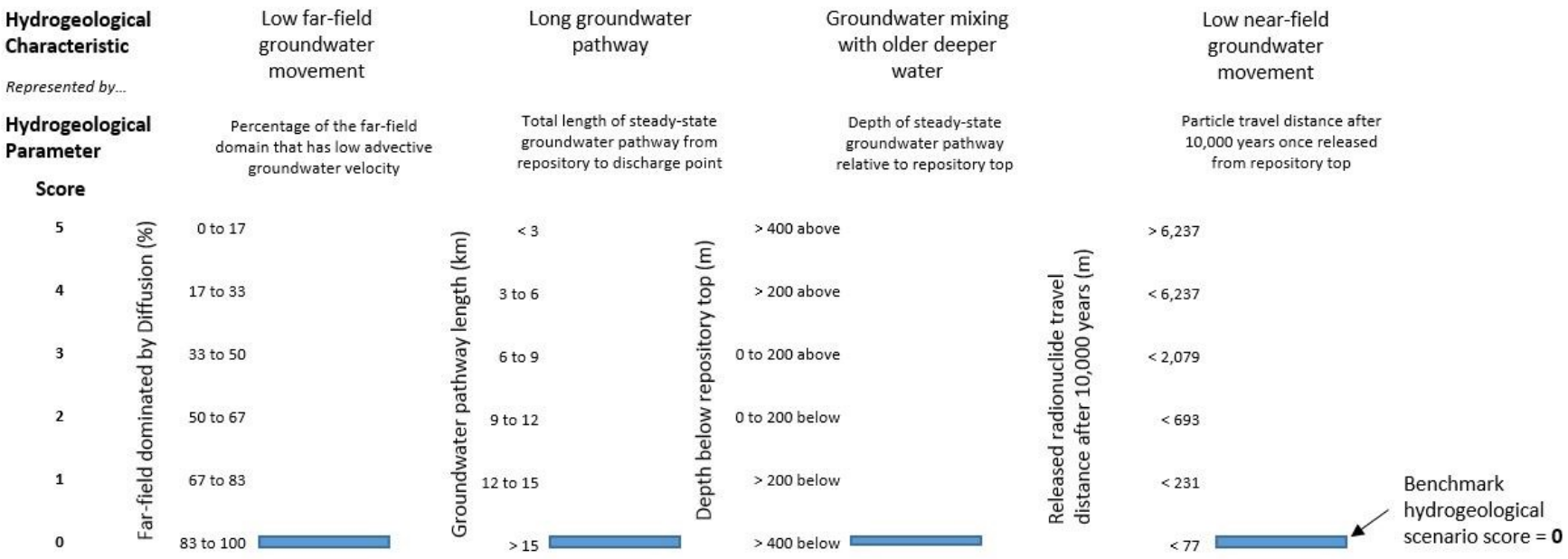

Figure 3.5: Benchmark far-field hydrogeological scenario, given a score of 0, against which the hydrogeological characteristics of other sites can be compared. Progression away from '0' becomes less beneficial for radionuclide containment and isolation.

3.3.1 Limitations of Proposed Method of Site Comparison

Although this approach enables analysis and comparison of the hydrogeological characteristics of different far-field disposal settings against a benchmark scenario, the approach assumes equal parameter (P.1 to P.4) weighting. It is therefore recommended that further research be undertaken to establish weighting factors of the selected hydrogeological parameters.

Furthermore, the proposed method does not address the *'predictability of the system'*, identified as a beneficial hydrogeological characteristic (see section 2.3.6), only the possible variance in hydrogeological characteristics as a result of scoping stage permeability uncertainty. It is believed the predictability of the system can only be adequately assessed following an advanced data collection programme. Future work should thus focus on quantification of this characteristic, and inclusion of it into the proposed scoring system.

3.4 Implementation of the Proposed Method

This section will outline the procedure used to obtain the hydrogeological parameters P.1. to P.4. (section 3.3.3) from the models.

3.4.1 Hydrogeological Parameter P.1

To determine 'slow groundwater movement' a representative groundwater velocity must be defined. Although this research aims to consider hydrogeological processes, rather than explicitly solute transportation processes, solute transport via diffusion is, to all extents and purposes, considered 'slow' within contaminant research. Therefore, if the advective groundwater velocity is less than that of the rate of solute transportation via diffusion, it is reasonable to call that advective velocity 'slow'.

Using Equ.2.4, solutes can be expected to travel no further than *approx.* 77 m over 10,000 years (the chosen assessment period) based on a conservative effective diffusion coefficient of 9.31E-09 m^2/s (see section 2.3.2.3). Solutes traveling via advecting groundwater would be required to travel at a velocity of *approx.* 2E-10 m/s to achieve the same travel distance over the same timeframe. Therefore, for the purpose of this research, an advective groundwater velocity of $\leq$ 2E-10 m/s will be considered 'slow'.

It should be noted that this method provides a simple approach to approximate 'slow' groundwater movement, however, in reality the solute transportation rate, as discussed in section 2.3.2.3, will vary as a result of solute and medium characteristics, and indeed timeframe. For example, if solutes are transported under an effective diffusion coefficient of 1.00E-12 m^2/s, solutes will be transported a distance of 0.8 m, which is the equivalent of an advective groundwater velocity of *approx.* 2.5E-12 m/s. Therefore, where diffusion is found

to be the dominant solute transport mechanism, further site specific research on radionuclide transportation pathways and rates is required.

The percentage of the regional area with 'slow groundwater movement' i.e. an advective velocity ≤ 2E-10 m/s was determined by laying a 20 by 20 m grid over the model domain, and extracting the advective groundwater velocity at the grid nodes over a 2 by 20 km area. The purpose of using a grid, rather than extracting groundwater velocities from the mesh (section B.1.2) was to avoid bias of hydrogeological features with higher mesh densities, such as faults. This data manipulation and extraction was achieved using the post-processing visualisation software 'Tecplot' (Tecplot 2018).

3.4.2 Hydrogeological Parameters P.2 & P.3

The total length of the quasi-steadystate groundwater pathway from repository top to discharge/exit point (P.2), and the depth of discharge relative to repository top (P.3) was determined by measurement of the groundwater pathway length within Tecplot.

Although these two hydrogeological parameters (P.2 & P.3) are primarily applicable when solute transport is advection driven (see Figure 2.5), it is also important they are assessed for when solutes released into the host rock formation are driven by diffusion. This is because there is natural uncertainty in subsurface geometries and sedimentology, and low permeability formations may in reality include higher permeability pathways through which released radionuclides could migrate (Figure 3.6).

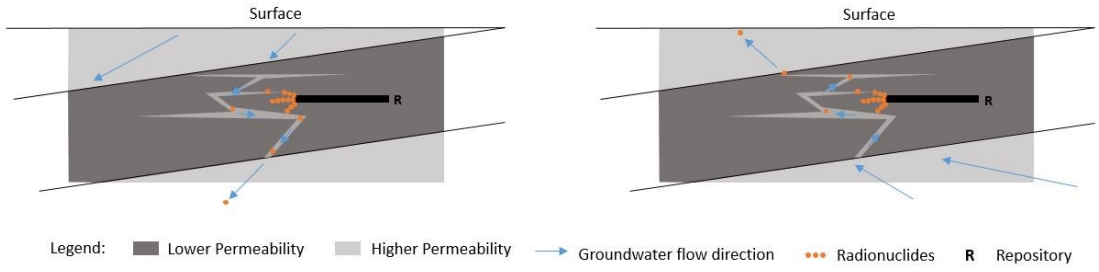

Figure 3.6: [Left] Regional groundwater system progressing deeper keeping released radionuclides contained and isolated within the subsurface environment. [Right] Regional groundwater system progressing shallower enabling released radionuclides to be discharged to the surface.

The purpose of this research is to identify far-field natural barrier settings with as many safety barrier functions as possible, despite geometric and sedimentological uncertainties, to ensure undue reliance is not placed upon the engineered barrier system alone.

3.4.3 Hydrogeological Parameter P.4

The procedure to determine the distance a released radionuclides will travel over 10,000 years was undertaken as follows:

1. particle streak-lines were generated through Tecplot using advective velocity, which enabled the pathway any (non-reactive) released particle took, and the speed at which it travelled to be tracked. Particles were released at 10 evenly spaced points along the top of the repository at set time intervals, resulting in 10 streak-lines (Figure 3.7),

2. the longest of the streak-lines, i.e. the maximum particle travel distance over the 10,000 years was selected for retardation calculations as a 'worst-case' scenario (Figure 3.7),

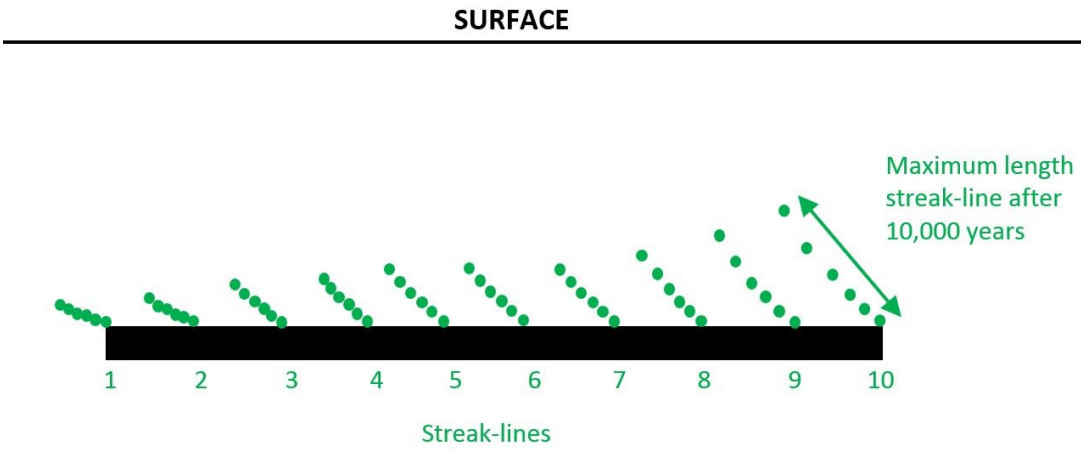

Figure 3.7: Image of streak-lines generated from 10 evenly spaced locations along the top of the theoretical repository site.

3. the retardation factor of selected radionuclides was calaculated along the 'worst-case' streak-line using Equ.A.18, accounting for radioactive decay using Equ.A.22. A list of the selected radionuclides and their respective half-lives used within the retardation calculation are presented within Table B.0.1. Applied partition coefficients (K_d) are presented within Table B.0.2.

4. Radionuclide travel distances, adjusted using the newly calculated retardation factors, are included within the bar chart method of assessment (see section 3.3.6).

Retardation factor calculations were validated using the risk assessment software 'GoldSim'. The method and values used for Goldsim modelling are detailed within Appendix B.2, with a summary of the results presented within Appendix F.

3.4.4 Summary of model scenarios

In summary six TH models were simulated, representing each of the three selected sites (Sellafield, the Tynwald Basin and Thetford), populated with 1) most likely fault and lithological permeability values, and 2) high fault and lithological permeability values.

Models were run to quasi-steadystate conditions (see section 9.2) by firstly solving for hydraulic (H) processes, and then secondly solving for coupled thermo-hydrogeological (TH) processes. Once coupled TH quasi-steadystate had been achieved, variant peak repository temperature scenarios were simulated, including a baseline scenario (none- heat producing waste scenario).

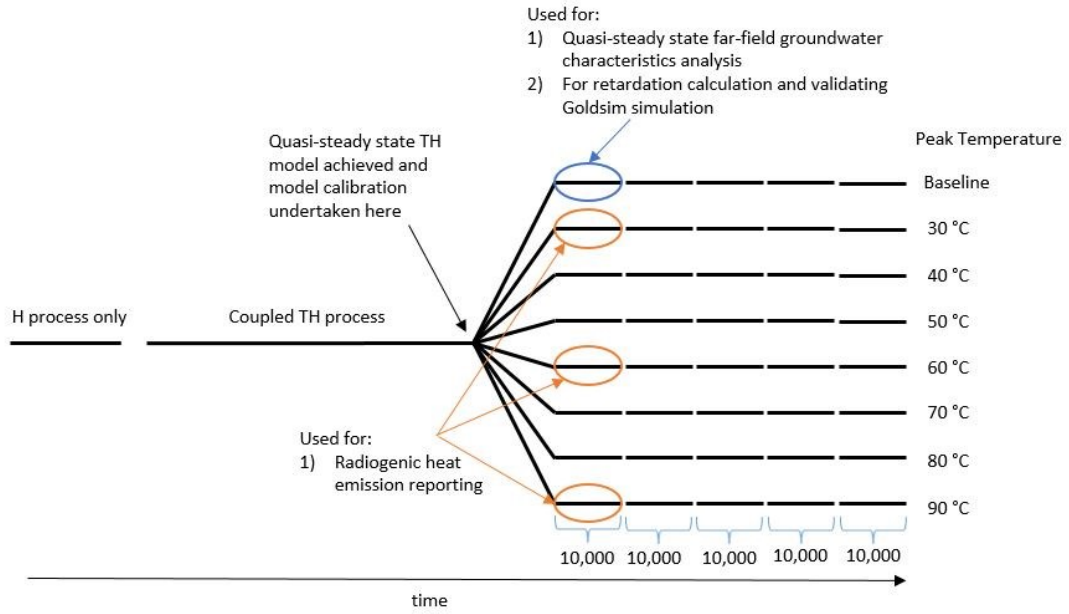

Figure 3.8: Illustration of the development and simulation of a simple model i.e. the Thetford model when populated with most-likely permeabiltiy values. This process will be undertaken 6 times, once for each of the three modelled sites, populated with either 1) most-likely or 2) high regional lithological permeabilities.

The maximum particle travel distance from each of the six baseline scenarios, represented using streak-lines (section 3.4.3), formed the basis of the reactive retardation calculations.

3.5 Assumptions & Simplifications

Although assumptions and simplifications have been highlighted and discussed throughout this chapter, and within Appendix A & B, those considered most significant for results interpretation and discussion are summarised here:

1. Modelled scenarios have assumed that the fundamental laws of heat transport (Fourier's law), mass transport (Fick's Law) and liquid flow (Darcy's Law) are correct (section A.1),

2. Modelled TH scenarios simulate groundwater flow in 2D rather than 3D (section B.1.1). This has led to an over estimation of hydraulic gradients, as pressure cannot dissipate over three dimensions. This is however considered a conservative approach for safety assessments as groundwater, and particles transported within it, will be transported faster,

3. Modelled TH scenarios do not include mechanical processes (see section 3.2.4). The consequence of not including mechanical processes is considered small based on research undertaken by (Min et al. 2005) who suggested the influence of radiogenic heat emission on TM couplings over the far-field to be minimal (section 2.8.2),

4. Modelled TH scenarios are single phase, and therefore do not consider the effects of gas within the regional groundwater system (section 2.7.7). This limitation could be significant as gas, such as the sort generated from corrosion of waste packages and microbial reactions within the repository, have the potential to facilitate faster flow, and distort natural flow patterns (Sharland et al. 2008; Metcalfe et al. 2008) (section 2.7.7),

5. Modelled TH scenarios were based on liquid flow (section A.1.1) which assumed full saturation of the model domain so that no near-surface unsaturated zone exists, and water remains connected at depth. This assumption would not be legitimate for simulation of the Yucca Mountain site for example (section 2.5.2), where the water table is situated 300 m below the proposed repository (National Research Council 1992). In Britain however, where the water table typically occurs within a few meters to tens of meters below the surface, any repository situated at a depth of 200-1,000 m below ground level would be well within the saturated zone. Furthermore, as transmissive zones have been discovered from deep petroleum and test boreholes down to 9 km depth (Tsang & Niemi 2013), model saturation to depths of 2-4 km is considered reasonable, however in reality, groundwater flow will become more 'variable' and 'compartmentalised' with depth,

6. Fractures were treated as equivalent continuous porous medium. This is considered appropriate given the macroscopic (regional) scale of the groundwater simulation (see section B.1.2),

7. The engineered barrier was not simulated. This meant that groundwater passing through the area of the repository, within the TH model, behaved as though passing through the undisturbed host rock formation. Furthermore, radionuclide retardation calculation was based on instantaneous radionuclide release. Although neither of these scenarios were realistic, with near-field groundwater likely distorted around the built facility, and the engineered barriers likely to retain radionuclides over tens or hundreds of thousands of years (Radioactive Waste Management 2016a), this research aimed to assess the natural barrier as an independent barrier to radionuclide containment and isolation (section 2.2) and as such, it is considered appropriate for the influence of the engineered barrier to have been removed as far as possible,

8. No site specific pressure, temperature or mass concentration data was available for the Thetford or Tynwald Basin models and thus material parameterisation was based on literature derived values, which is a major source of uncertainty (section 2.7.1). Furthermore, for this same reason, no initial calibration was possible for these models. It is considered that the process of calibration does not necessarily lead to model validation (section 3.1), and for that reason, the models were used to explore prospective hydrogeological characteristics and sensitivities, rather than to undertake detailed site performance safety assessments,

9. No site specific fluid density or fluid viscosity functions were available for the Thetford or Tynwald Basin models, and thus Sellafield site specific functions were applied instead (section B.1.3.1). The effect of this assumption on regional groundwater characteristics is considered less than that generated from material property uncertainty, such as intrinsic permeability (see section B.1.3.1),

10. Constant pressure head and temperatures boundaries were applied across the model domain (section B.1.6), which did not consider the flux of water through the surface as a result of rainfall, the heat flux through the surface due to the sun, or the heat flux through the base as a result of the natural geothermal gradient. The effect of this simplification on the regional groundwater characteristics is however considered less that that generated from material property uncertainty which can span 2 or 3 orders of magnitude,

11. The boundary conditions were built not to change during the model simulation (section B.1.6). In reality the wider environmental conditions could vary as a result of glaciation events or surface erosion (section 2.7.4), and boundary conditions should

also vary to reflect this. This is considered one of the major sources of uncertainty of the evolution of the groundwater characteristics over the modelled time frame,

12. Within the TH models dispersivity was set at as close as possible to 0.5 of the typical element length per hydrogeological unit to enable numerical stability (section A.3.3.3). This was done instead of application of site specific dispersivity values. Dispersivity scaling exponents have however been identified to vary between 0.40 and 0.92 in the field for a range of consolidated geological media (Schulze-Makuch 2005), which could in practice result in changes to the hydrodynamic dispersion tensor of *approx.* 0.5 of an order of magnitude. The hydrodynamic dispersion tensor was itself used to calculate P.1 (section 3.4.1). This is only however anticipated to become an issue when values for P.1, at the different sites, are similar. Finally, uncertainty in the hydrodynamic dispersion tensor is considered within that of the material parameter uncertainty (see section B.1.4.1),

13. Radionuclides within the retardation calculation were assumed to decay (Table B.0.1), with no daughter products generated (section 2.3.2). No additional radionuclide mass was added through source terms (C_s) or from reactions (Cr) (section A.3.3). Radionuclide release was assumed instantaneous, and transportation took place through chemically and physically homogeneous medium.

14. Transient groundwater conditions as a result of shorter term features, events and processes (e.g. radiogenic heat emission, gas generation and glacial flushing) were not included within site hydrogeological characteristic scoring, and finally

15. The proposed method for site analysis and comparison assumed equal selected hydrogeological parameter weighting (section 3.3.1).

Additional assumptions and simplifications specific only to the modelling of radiogenic heat emission are presented within section 8.3.3.

Chapter 4 Sellafield, West Cumbria: Model Development, Results and Discussion

4.1 History of the Sellafield Site

The history of investigations at Sellafield in West Cumbria has been outlined in section 2.5.6. Much research was undertaken on geological and hydrogeological conceptualisation of the site during the 1980's and 1990's, the main points only of which will be highlighted here. The enhanced data collection programme also enables greatest certainty of calibration and confidence in the predictive models generated.

The Sellafield cross-section extends over a distance of *approx.* 31 km from Scafell Pike in the Lake District Fells, out in a south-west orientation, past the Sellafield nuclear site which could be utilised for the required 1 km^2 secure surface facility (Nuclear Decommissioning Authority 2010a), progressing in a west-northwest orientation into the East Irish Sea Basin (Figure 4.1).

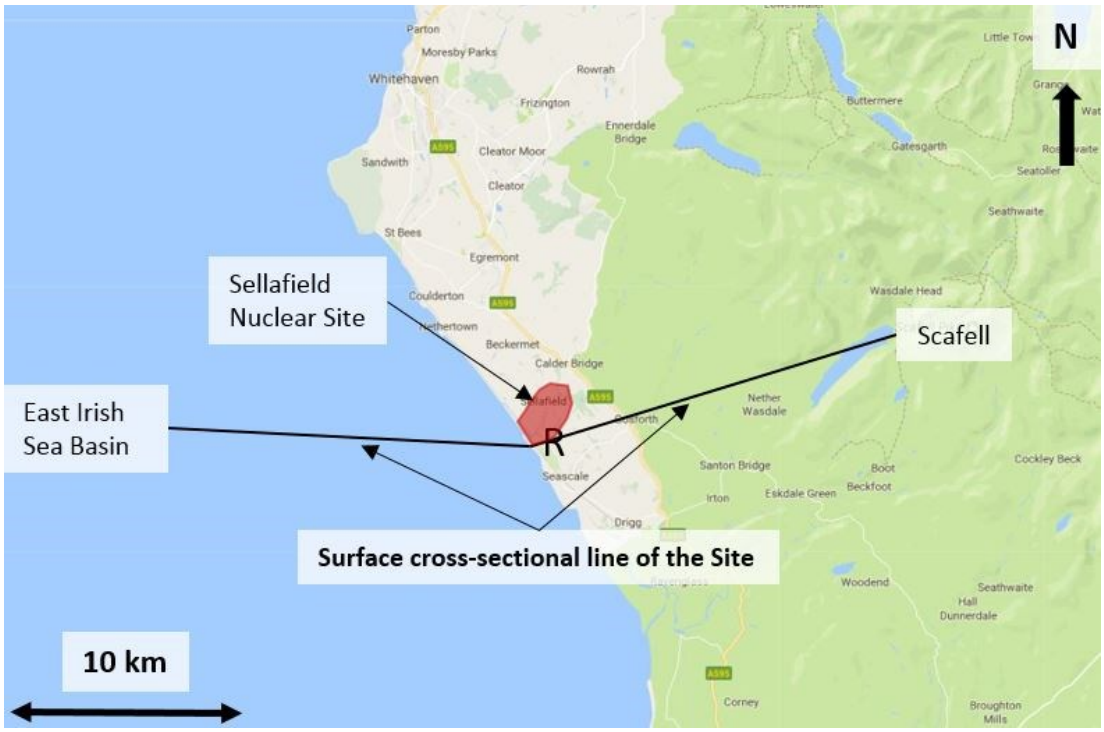

Figure 4.1: Location of the Sellafield geological cross section used as the basis for numerical model simulation (see Figure 4.5). The centre of the theoretical repository is marked with an 'R', along with the location of the secure Sellafield Nuclear Site in red.

4.2 Geological Sequence

Historic investigative drilling programmes undertaken at Sellafield occurred within an *approx.* 7 by 5 km area of the proposed rock characterisation facility, and extended to a depth of

approx. 2 km (Nirex 1997a). A northeast-southwest cross section through the vicinity of the investigated area is presented (Figure 4.2).

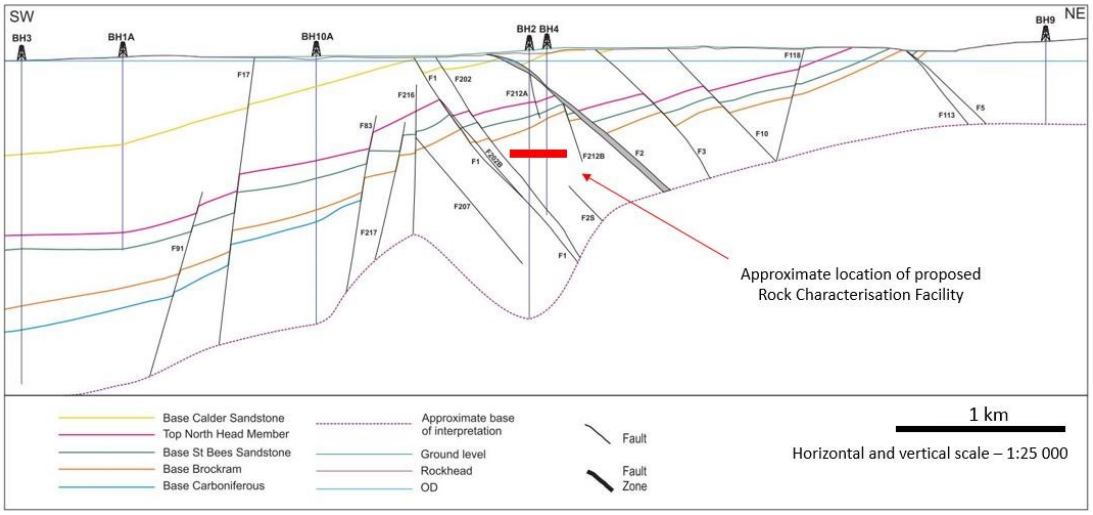

Figure 4.2: Location of boreholes 3, 10A, 2, 4 and 9 at Sellafield. Borehole data used for model boundary conditions and calibration. Image obtained from Figure 2.4(a) in (Nirex 1997a).

The geological sequence at the site comprises westward thickening lower Palaeozoic and Mesozoic sediments, namely the Carboniferous Limestone; Brockram Breccia transitioning into the St Bees Shales & Evaporites offshore; St Bees Sandstone; and the Calder Sandstone. This sequence overlies the upper Palaeozoic crystalline basement aka. the Borrowdale Volcanic Group (Michie 1996; Nirex 1997a; Chaplow 1996). The Borrowdale Volcanic Group can itself be subdivided into the Flemming Hall Formation, the Bleawath Formation and the Moorside formation (Nirex 1997a). For more information on the geology of the region, the reader is referred to (Jackson et al. 1995; Akhurst et al. 1997).

The area of interest for the purpose of this research has been extended from the originally investigated two-dimensional 7 km length section (see Figure 4.2), to a 30 km length section (Figure 4.3). The extended area stretches from the East Irish Sea Basin in the West, to the 1 km high Lake District hills and Skiddaw Group in the East. This ensures that the wider topographic features, which control far-field groundwater movement are captured (section 2.3.4).

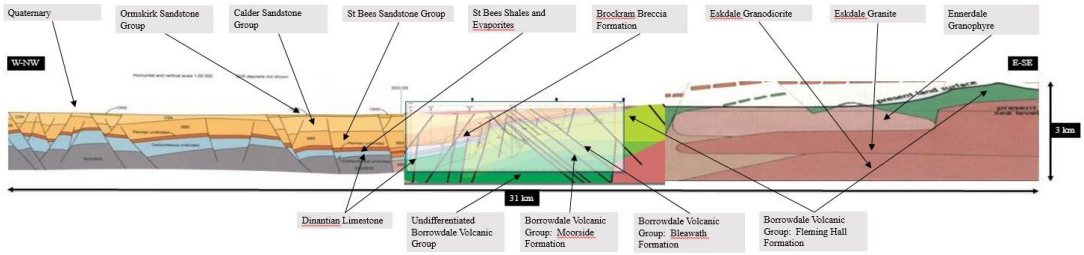

Figure 4.3: Extended geological section covering area 30 km by 2 km depth. Geological extension based on a collage of geological cross-sections provided by (British Geological Survey 1999a; Michie 1996; Nirex 1997a; Nirex 1997b). The geological disposal facility location is as proposed for the rock characterisation facility (Nirex 1997a).

4.3 Hydrogeological Conceptual Understanding

The drilling programme also identified three separate hydrogeological regimes (Black & Brightman 1996; Nirex 1997b); the Coastal Plain Regime, the Hills and Basement Regime, and the Irish Sea Brine regime (Figure 4.4), each of which will now be discussed further.

The shallowest hydrogeological regime is described as a freshwater, young, fast moving *'Coastal Plain Regime'* constrained primarily to the uppermost Sherwood Sandstone Group, St Bees Shales & Evaporites, and Brockram Breccia. The regime recharges along the coastal plain and discharges to the surface, close to the sea. The Sherwood Sandstone Group of the *Coastal Plain Regime* is designated a *'principle'*, or *'major'* potable coastal aquifer (Environment Agency 2016).

A deeper *'Hills and Basement Regime'* located primarily within the Borrowdale Volcanic Group is older and slower moving than that of the *Coastal Plain Regime*. It also has higher salinities, hypothesised to be due to both enhanced mineral interactions, and a putative saline groundwater source to the east (Bath et al. 1996). The *Hills and Basement Regime* recharges within the Lake District hills, and discharges to the *Coastal Plain Regime*, close to the coast.

The deepest regime is the *'Irish Sea Basin Regime'* classified as a dense brine formation. The *Irish Sea Basin Regime* is a dense body of salt saturated water situated primarily offshore and is reported to have very slow movement with very long residence times of > 1.5 Ma (Bath et al. 2006; Metcalfe et al. 2007). The source of its high salt content is suspected to be Permian and Triassic halite layers of the Mercia Mudstone Group and St Bees Evaporites, abundant within the East Irish Sea Basin (Bath et al. 2006; Metcalfe et al. 2007).

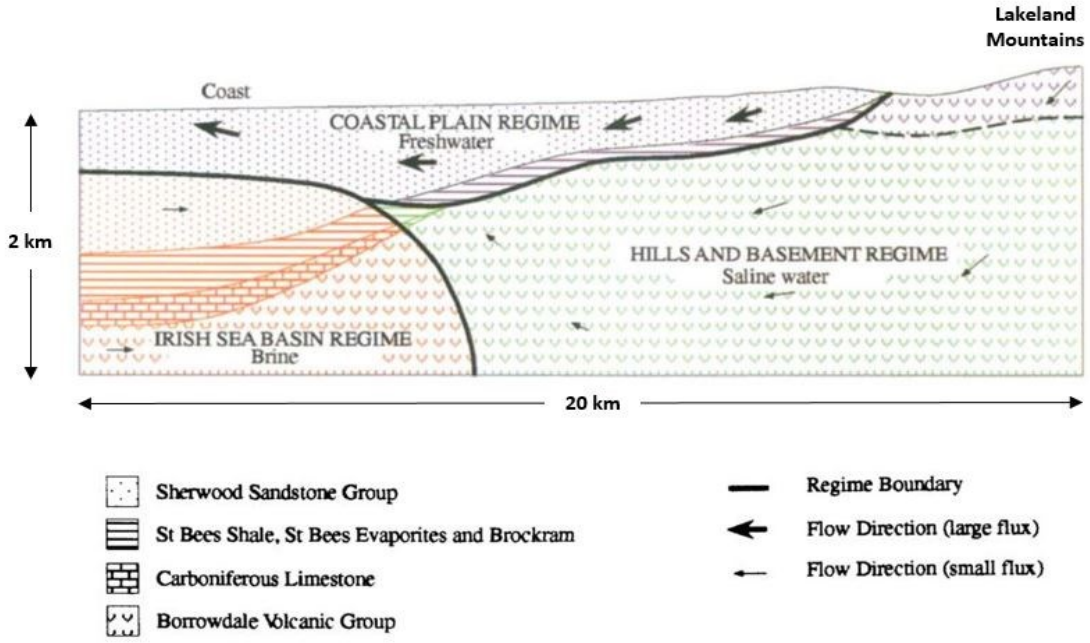

Figure 4.4: Hydrogeological conceptual model of Sellafield, West Cumbria extending *approx.* 20 km in length down to 2 km below sea level (Black & Brightman 1996).

It is hypothesised that the geological extension eastwards will result in an extension of the *Hills and Basement Regime* eastwards (see Figure 4.5). This regime will be dominated by topographically driven flow, and will discharge near to the coastline. In addition, the geological extension westwards will result in an extension of the density controlled *Irish Sea Basin Regime* westwards (see Figure 4.5), towards the offshore salt source.

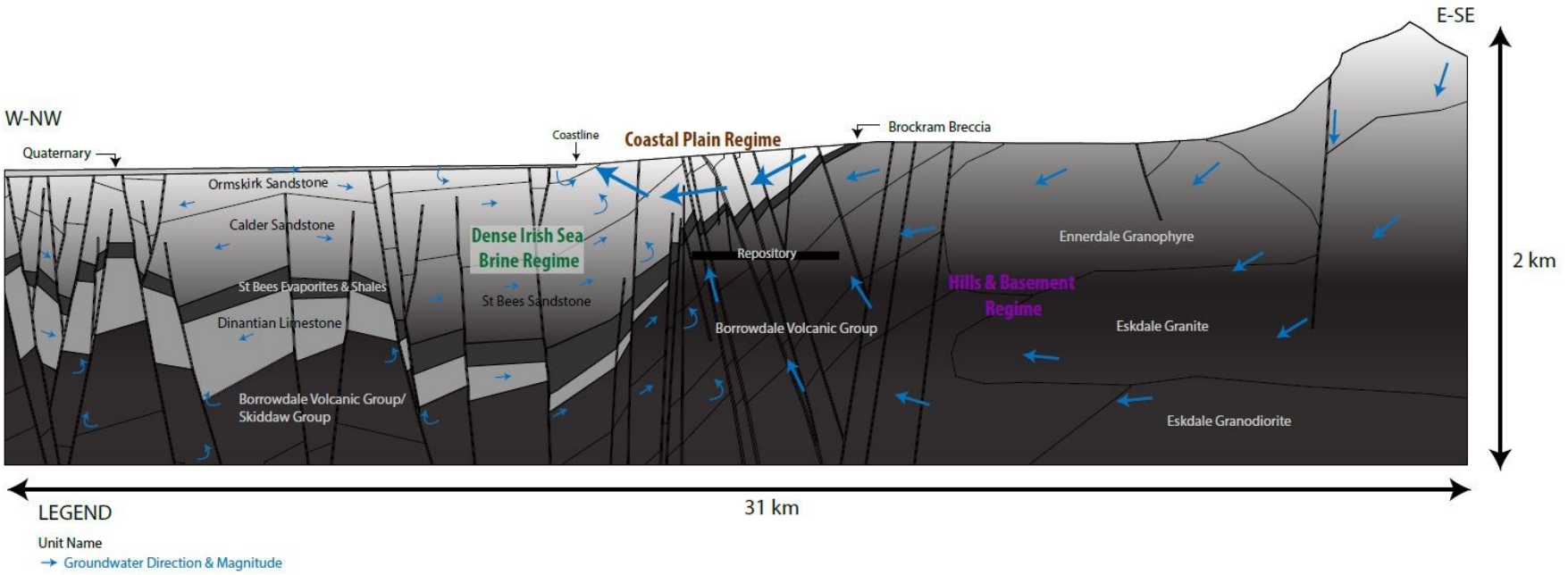

Figure 4.5: Hydrogeological conceptual model of the Sellafield site in West Cumbria including lithological units, hydrogeological regimes, and the direction and magnitude of groundwater flow, indicated by the orientation and schematic length of arrows respectively.

4.4 Model Construction & Development

4.4.1 Geometry & Mesh

The two-dimensional geometry and mesh (Figure 4.6) of the Sellafield model is based on the geological information highlighted within Figure 4.3. The mesh comprises 87,714 nodes and 173,527 elements.

4.4.2 Boundary Conditions

Pressure, mass and temperature boundary conditions have been applied as presented in Figure 4.7, and are based on site specific data where possible, including groundwater salinities obtained from boreholes (BH) 3, 10A, 2, 4 and 9A/B (Bath et al. 2006; Metcalfe et al. 2007), the locations of which are illustrated in Figure 4.2.

Temperature boundaries have been calculated based on generic surface temperatures and geothermal gradients (Downing & Gray 1986), whilst pressure boundaries have been calculated based on atmospheric pressures, and sub-surface hydrostatic pressure gradients (Engineering ToolBox 2003). The equations used for boundary condition calculation are presented within section B.1.6, and Appendix C.4.3.

4.4.3 Material Parameters

The material properties of porosity, permeability (both most-likely and high), mass dispersion, heat dispersion, storativity, bulk density, thermal capacity and thermal conductivity have been applied specifically, and uniformly, to each individual lithological unit (section C.1). Heat capacity and heat conductivity have been applied as constants across the entire modelled domain (section B.1.3.2), as has the site specific functions of fluid viscosity and density (section B.1.3.1). Faults have been represented as continuous porous mediums (see appendix section B.1.2).

4.4.4 Numerical control

Numerical control was achieved by capping the permeability range to 5 orders of magnitude (1.00E-13 and 1.00E-018 m^2) and setting mass and heat dispersivity to either 10 or 50, explained in section B.1.4.2, with the values ascribed detailed in section C.1.

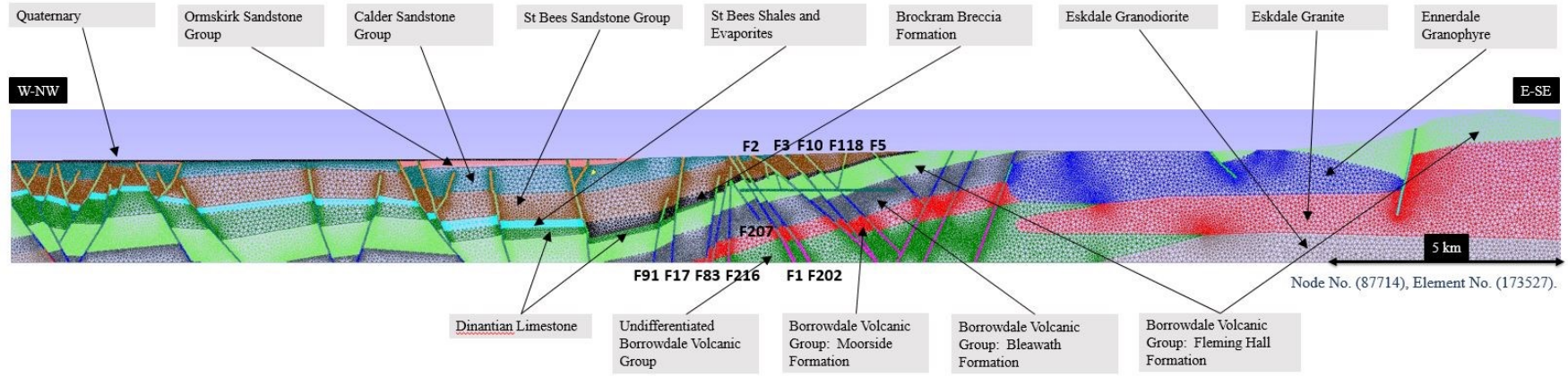

Figure 4.6: Mesh of Sellafield site encompassing a length of 31 km, and a depth of 2 km below sea level. Faults are also labelled.

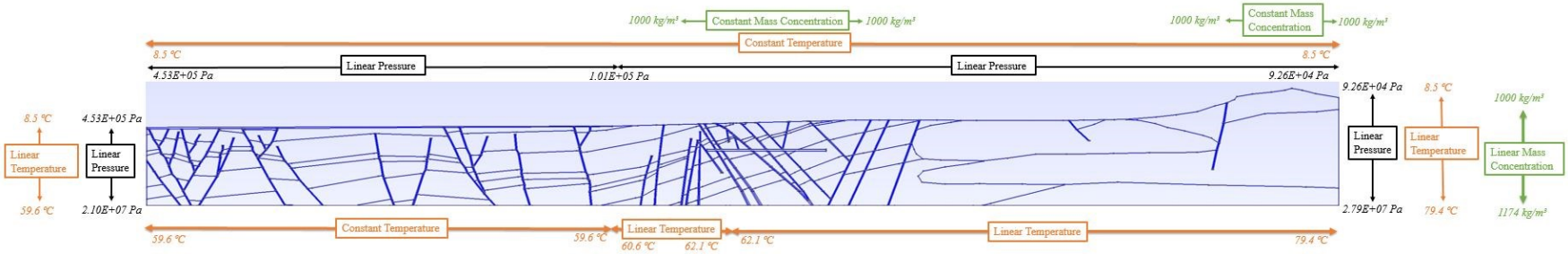

Figure 4.7: Boundary conditions applied to Sellafield model encompassing a length of 31 km, and a depth of 2 km below sea level.

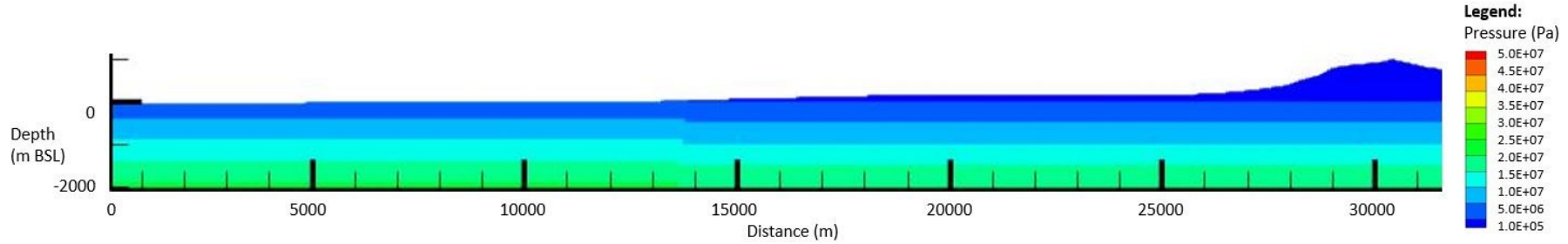

Figure 4.8: Pressure (Pa) initial conditions across the Sellafield model domain.

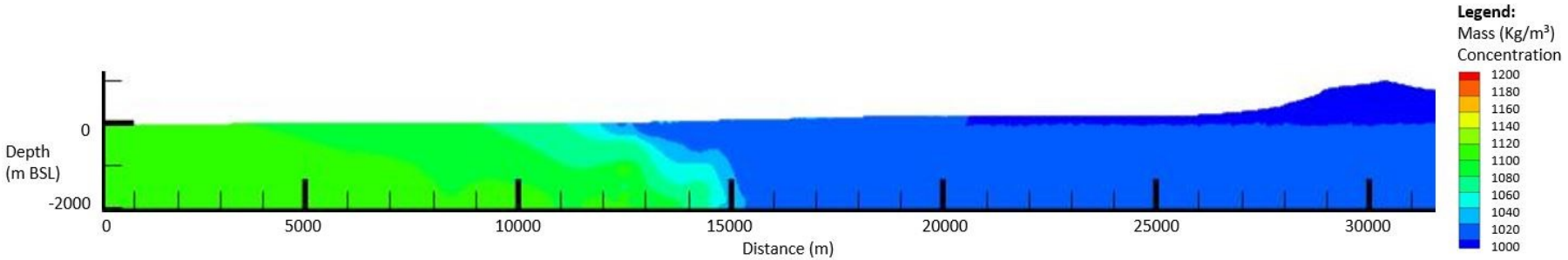

Figure 4.9: Mass concentration (kg/m^3) initial conditions across the Sellafield model domain.

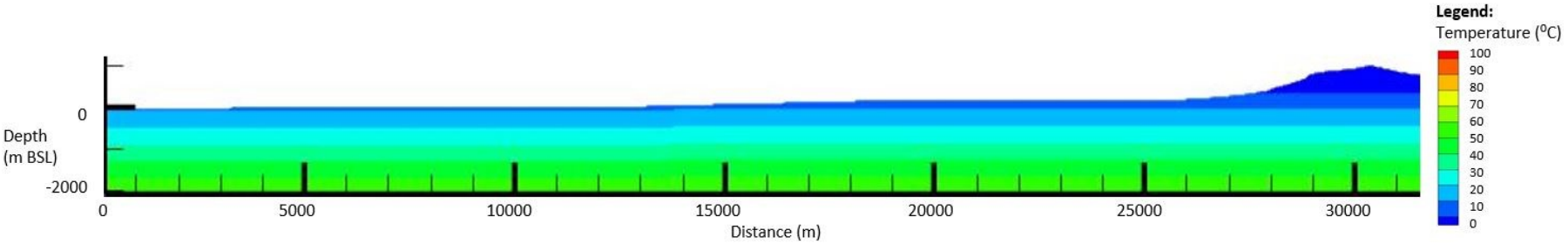

Figure 4.10: Temperature (°C) initial conditions across the Sellafield model domain.

4.4.5 Initial conditions

Initial conditions for pressure were applied based on a pressure gradient calculated using Equ.B.7 for 1) the onshore sub-surface, and 2) the offshore sub-surface (Figure 4.8).

Initial mass conditions were applied using a python script to enable a weighted mass distribution across the model domain (Figure 4.9), based on chloride values obtained for BH2, BH3, BH4, BH9A/B and BH10 (Bath et al. 2006). For example, where a chloride value of 10,000 mg/l was recorded in well 1, and 60,000 mg/l in well 2 (separated by a distance of 50 m), a chloride concentration of 30,000 mg/l was applied 20 m from well 1. This type of more advanced initial mass condition development was required to ensure an adequate mass calibration (section 4.4.6) was achieved.

Initial conditions for temperature were applied based on a typical continental gradient of 0.025 ^{o}C/m (Dowing & Gray 1986) for 1) the onshore sub-surface, and 2) the offshore sub-surface (Figure 4.10). In order to achieve quasi-steadystate conditions (see section 9.2), models were solved for hydraulics first, followed by coupled hydraulic, heat transport and mass transport. Once quasi-steadystate was reached and appropriate calibration achieved (section 4.4.6), the transient coupled hydraulic, heat transport and mass transport was simulated. The coupled TH model was made transient by the addition of a storage term. A summary log of model runs, including initial conditions at each stage is presented within section C.2.

4.4.6 Model calibration

Most-likely and high permeability models were run to quasi-steadystate conditions, and then calibrated to Sellafield field data for 1) freshwater head, 2) salinity and 3) temperature (equations and spreadsheets provided in Appendix C.3.). The accuracy of these parameter calibrations are discussed below.

Freshwater head calibration (Figure 4.11), against model pressure (Pa) output for both the high and most likely permeability scenarios, show a very good prediction for BH2 and BH4 (within *approx.* 5 m) within the upper 800 m, worsening with depth up to *approx*. 50 m freshwater head difference. If the lower portions (> 1 km) of BH2 and BH4 were connected to greater topographic drive to the east, freshwater head predictions would be anticipated to rise, closer to field measurements. In contrast however, although only a 200 m section of freshwater head field data is available for BH10, both modelled permeability scenarios show over prediction of up to *approx.* 20 m freshwater head within the upper 200 m, which is considered a significant over prediction. The reason for the over prediction could be a result of discrepancies in topographic elevation along the coastal plain, originally approximated from

geological cross-sections. Discrepancies in freshwater head calibrations could also be associated with the modelling of a 2D section with a kink, causing differences in real and modelled pressure gradients. The equation for freshwater head calibration is in section C.3.

Model predictions of salinity (Figure 4.12) show a strong calibration (within *approx.* 6 kg/m^3) against BH2 and BH4 within the upper 1 km, but with the high permeability model over predicting salinity (up to *approx.* 40 kg/m^3) with depths > 1 km. The reason for the over prediction within the high permeability model is considered a result of higher permeability lithological units and faults facilitating the transport of saline groundwater's from the *'Irish Sea Basin Brine'* towards the vicinity of the repository. The weakest mass concentration calibration is seen within BH10 (up to 60 kg/m^3), anticipated to be for the same reason. The different calibrations of BH10 do not however appear to have a significant effect on the calibration of salinity measurements within the vicinity of the repository i.e. BH2 and BH4 within the upper 1 km, which itself is strong. Furthermore, BH10 is situated within the area of the transition zone of the three identified hydrogeological regimes, which is anticipated to migrate over thousands of years, and is therefore sensitive to unknown details. The equation used for salinity calibration is in section C.3.

Finally, temperature calibration (Figure 4.13) shows a very good fit to all modelled scenarios (within *approx.* 3 °C).

In summary, although differences do exist between measured field values and model predictions, the strongest calibration for all three parameters, is seen within the vicinity of the repository (i.e. BH2 & BH4 within the upper 1 km). This is important as it is where the greatest effect from radiogenic heat emission on the groundwater characteristics will occur (detailed in Chapter 9), and therefore also requires the strongest confidence of calibration.

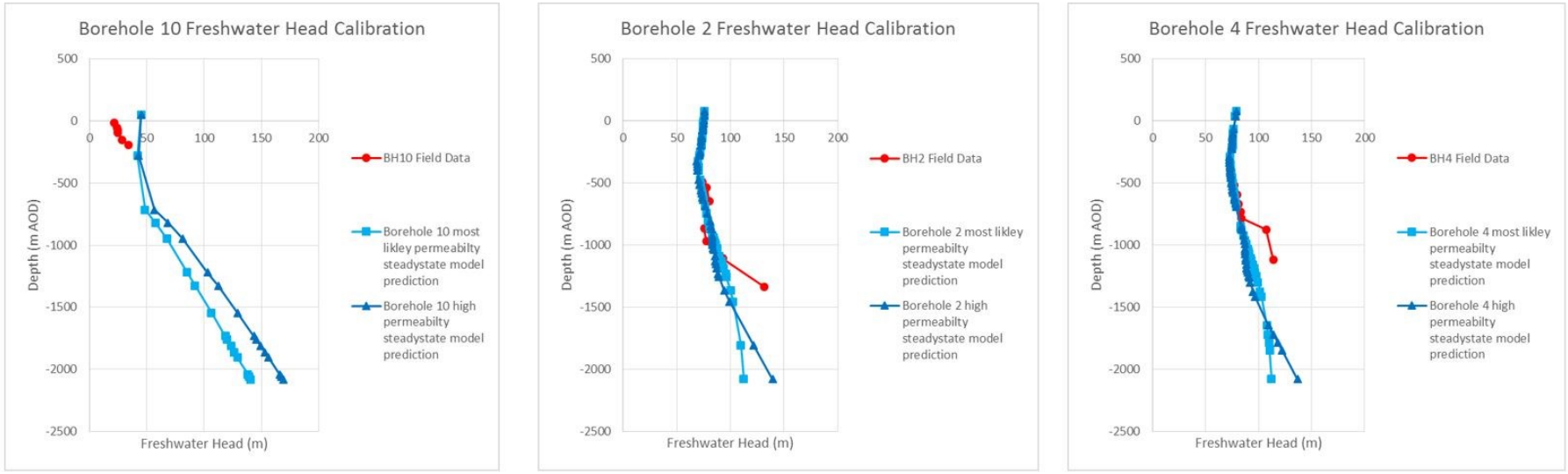

Figure 4.11: Freshwater head calibration for most likely and high permeability quasi-steadystate solutions against borehole data (BH10, BH2, BH4 and BH9A/B) from Sellafield, West Cumbria. Field data for calibration obtained from (Nirex 1997e).

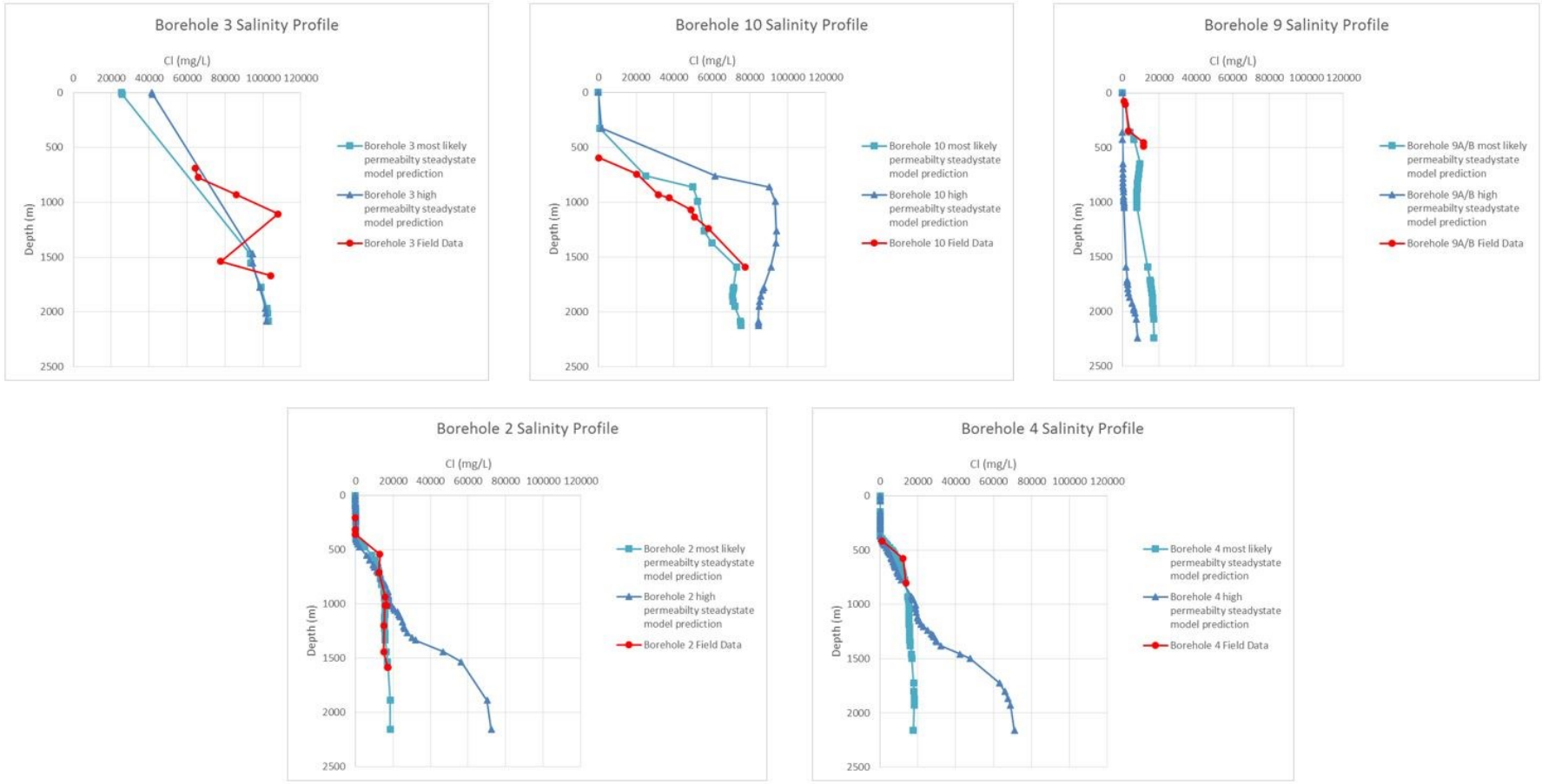

Figure 4.12: Salinity calibration for most likely and high permeability quasi-steadystate solutions against borehole data (BH3, BH10, BH2, BH4 and BH9A/B) from Sellafield, West Cumbria. Field data for calibration obtained from (Bath et al. 2006).

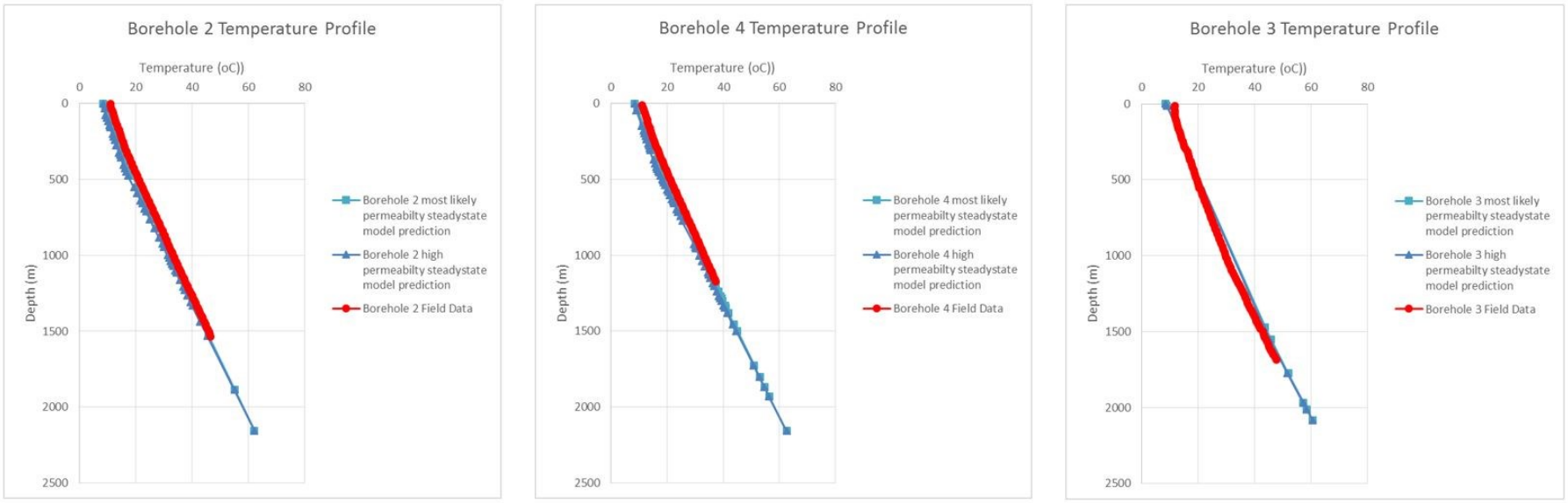

Figure 4.13: Thermal calibration for most likely and high permeability quasi-steadystate solutions against borehole data (BH3, BH2 and BH4) from Sellafield, West Cumbria. Field data for calibration obtained from (Nirex 1989b).

4.5 Results: Hydrogeological Parameters

For a description of the method used to analyse the far-field hydrogeological characteristics of the Sellafield site against the benchmark hydrogeological scenario, please see section 3.3.

4.5.1 (P.1) Far-field Groundwater Velocities

Far-field groundwater velocities range between 1.00E-12 and 1.00E-06 m/s but predominately between 1.00E-11 to 1.00E-08 m/s for the most likely permeability scenario (Figure 4.14B). 57 % of the far-field groundwater movement here can be considered 'slow', including much of the Borrowdale Volcanic Group, but with the overlying Sherwood Sandstone Group faster flowing (Figure 4.14A). Far-field groundwater velocities range between 1.00E-12 and >1.00E-06 m/s but predominately between 5.00E-11 to 5.00E-07 m/s for the high permeability scenario (Figure 4.15B). Only 20 % of the groundwater movement can be considered 'slow', with much of the Borrowdale Volcanic Group faster flowing (Figure 4.15A).

In both modelled scenarios the highest far-field groundwater velocities are observed within the near-surface Sherwood Sandstone and St Bees Sandstone Group of the *'Coastal Plain Regime'*, along the W-NW boundary, possibly due to model *'edge' effects'* (see section B.1.1) and below the Lake District hills due to the topographic drive. The lowest far-field groundwater velocities are observed between the repository and Lake District Hills, which appears to form a localised groundwater divide (section 4.6.1), and within the Borrowdale Volcanic Group offshore at depth.

4.5.2 (P.2 & P.3) Groundwater Pathway Length & Discharge Depth

In both modelled permeability scenarios, groundwater is transported up through the Borrowdale Volcanic Group's Fleming Hall Formation, towards, and into the overlying Brockram Breccia. The quasi-steadystate groundwater pathway tracks the top of the Brockram Breccia from the repository, until a location *approx.* 500 m to the west of the repository, where it ascends up through the St Bees and Calder Sandstone and discharges to the surface (Figure 4.14B & Figure 4.15B).

The groundwater pathway extends from the repository for *approx.* 2,500 m within the most likely permeability model (Figure 4.14B) and *approx.* 2,400 m within the high permeability model (Figure 4.15B) to the discharge location. Surface discharge represents the ascension of groundwater from the repository top by *approx.* 600 m within both modelled scenarios.

4.5.3 (P.4) Radionuclide travel distance over 10,000 years

Particle pathways show a maximum radionuclide travel distance of 67.5 m over 10,000 years in a system populated with most likely permeabilities (Figure 4.14C). Released particles remain within the Flemming Hall Formation. When the same pathway is simulated with sorption (Table 4.1), Cl^{36} has a retardation factor of 1 so travels an unaltered distance of 67.5 m; Tc^{99} has a retardation factor of 1.19 so travels a distance of 56.7 m; Se^{79} and U^{238} by 1.4 resulting in a distance of 48.2 m; Cs^{135} by 27.5 resulting in a distance of 2.5 m; and finally Ni^{59} with a retardation factor >200, resulting in a minimum travel distance of <1 m. Neither Am^{241}, Eu^{152} nor Sr^{90} are detected during model simulation (Table 4.1).

Particle pathways show a maximum travel distance of 602.4 m over 10,000 years in a system populated with high permeabilities (Figure 4.15C). Released particles travel up through sections of the Flemming Hall Formation, both fractured and unfractured, and enter the Brockram Breccia. When the same pathway is simulated with sorption (Table 4.1), Cl^{36} has a retardation factor of 1 so travels an unaltered distance of 602.4 m; Tc^{99} by 1.19 resulting in a distance of 506.2 m; Se^{79} by 1.32 resulting in a distance of 456.4 m; U^{238} by 1.62 resulting in a distance of 371.9 m; Cs^{135} by 28.5 resulting in a distance of 21.1 m; and finally Ni^{59} by >200 resulting in a distance of 3 m. Neither Am^{241}, Eu^{152}, nor Sr^{90} are detected during model simulation (Table 4.1).

4.5.4 Comparison against Hydrogeological Conceptual Model

In both modelled permeability scenarios, groundwater sourced from *the coastal plain* and deeper within *the hills and basement* of the Lake District hills, travels westwards ascending up through the Borrowdale Volcanic Group and discharging to the surface. This is due to the 'blocking' nature of the dense *Irish Sea Basin Brine* to the west (see Figure 9.2). These results are in line with the hypothesised conceptual model (Figure 4.5). However, unlike the hypothesised conceptual model, groundwater from *the hills and basement* of the Lake District hills discharges to the coastal plain near the base of the Lake District fells rather than just at the coastline, reducing the pressure gradient driving groundwater through the vicinity of the repository.

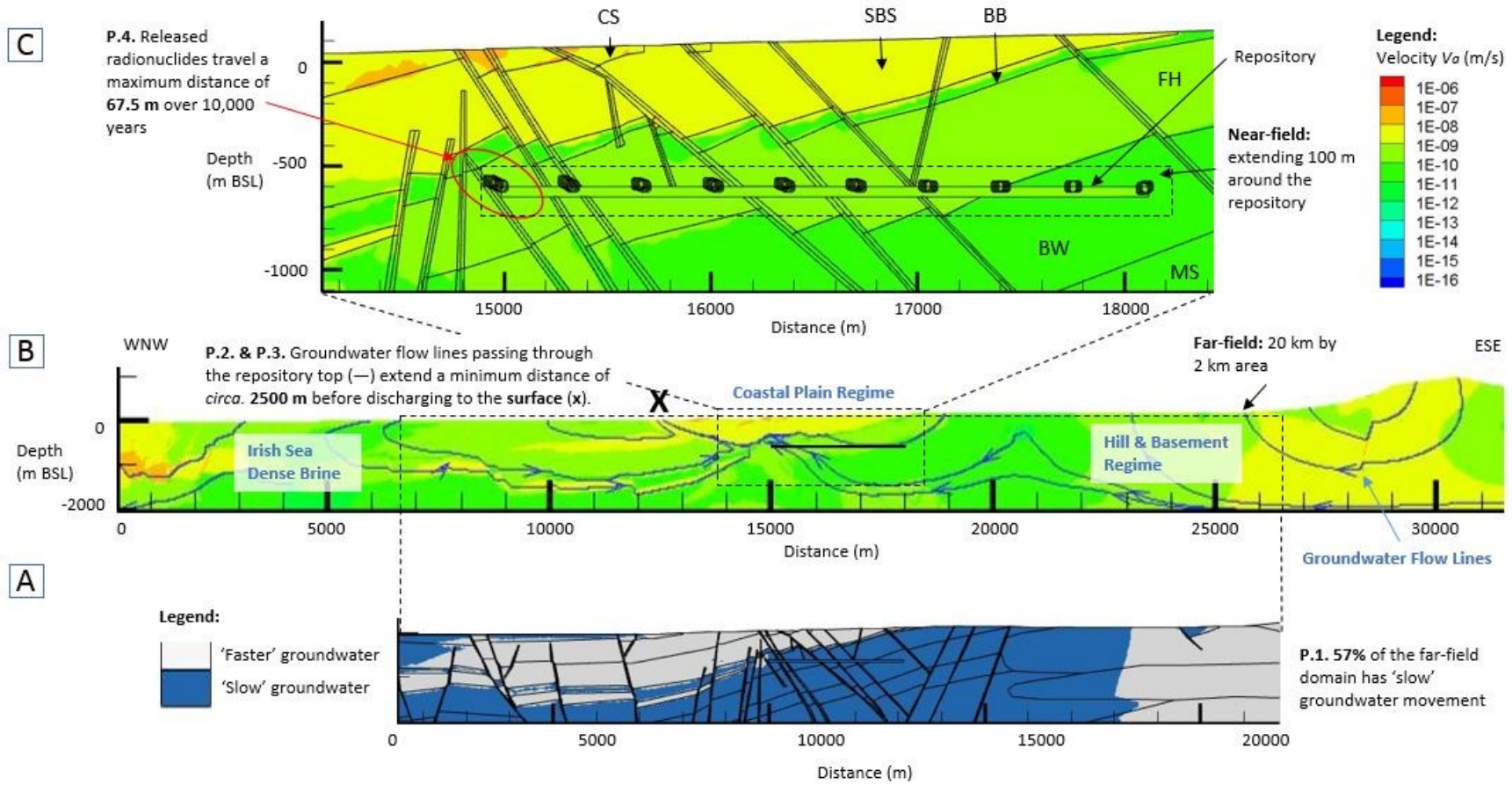

Figure 4.14: Results based on model populated with most likely permeability values. A) Areas of the far-field (20 km by 2 km) domain with 'slow' advective groundwater velocity i.e. <2.00E-10 m/s, B) Advective velocity distribution over the far-field, including groundwater flow lines and hydrogeological regimes, and C) Advective velocity distribution over the near-field, including the progression of particles released from along the top of a hypothetical repository over 10,000 years.

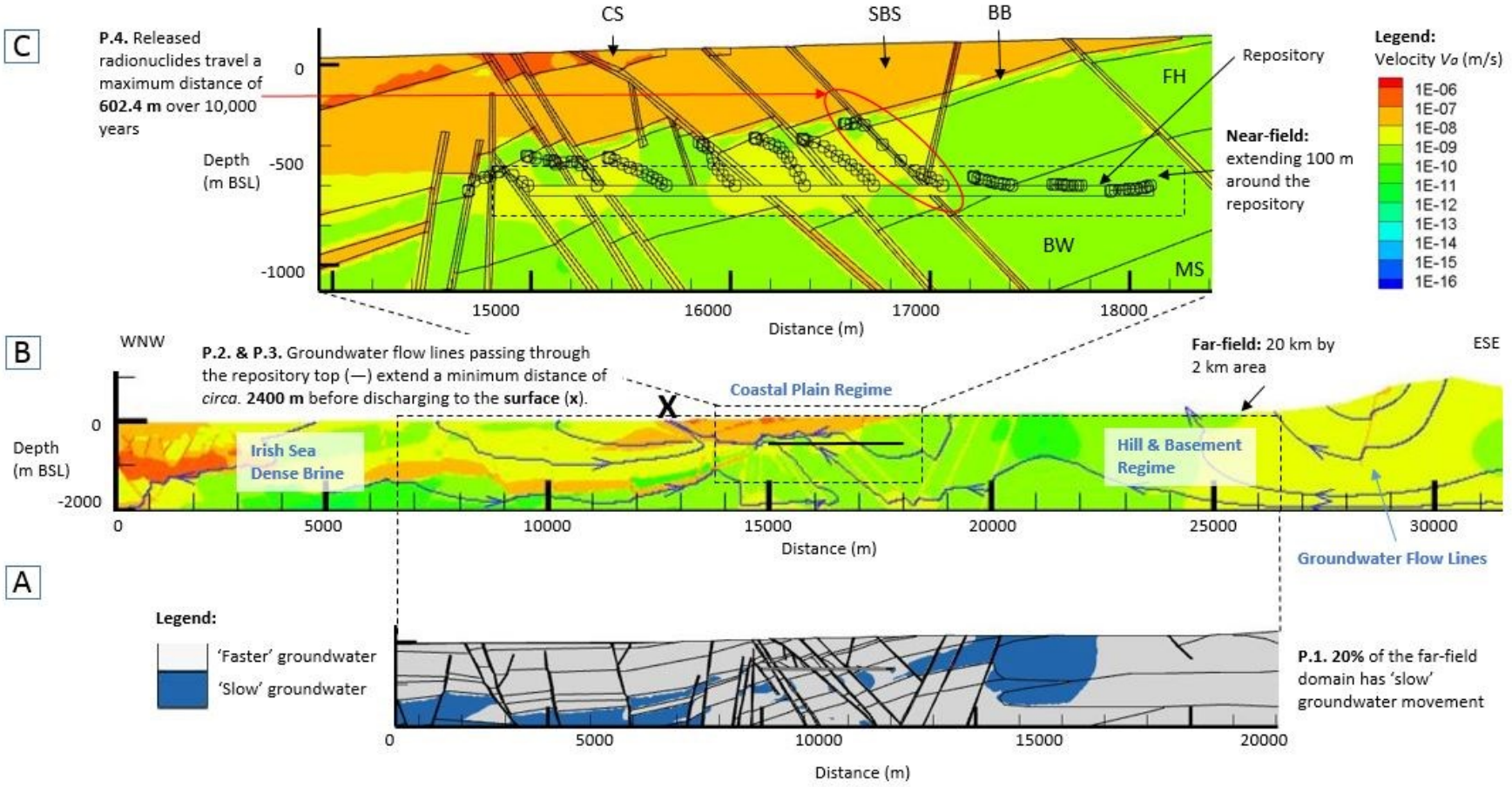

Figure 4.15: Results based on model populated with high permeability values. A) Areas of the far-field (20 km by 2 km) domain with 'slow' advective groundwater velocity i.e. <2.00E-10 m/s, B) Advective velocity distribution over the far-field, including groundwater flow lines and hydrogeological regimes, and C) Advective velocity distribution over the near-field, including the progression of particles released from along the top of a hypothetical repository over 10,000 years..

Table 4.1: Summary of retardation factors and travel distances of selected radionuclides after 10,000 years for maximum particle pathways (streak-lines) from Sellafield based on most likely and high permeability modelled scenarios.

Scenario	**Maximum Particle Travel Distance (streak-line length) (m)**	**Radionuclide**	**Am^{241}**	**Cl^{36}**	**Cs^{135}**	**Eu^{152}**	**Ni^{59}**	**Se^{79}**	**Sr^{90}**	**Tc^{99}**	**U^{238}**
		Half-life (yrs)[1]	*432.2*	*3.01E+05*	*2.3E+06*	*13.54*	*1.01E+05*	*2.95E+05*	*28.79*	*2.11E+05*	*4.47E+09*
Most-likely permeability	67.5	*Retardation Factor (R_f)*	ND (S)	1	27.5	ND (D)	>200	1.4	ND (D)	1.19	1.4
		Travel Distance (m)		67.5	2.5		<1	48.2		56.7	48.2
High permeability	602.4	*Retardation Factor (R_f)*	ND (S)	1	28.5	ND (D)	>200	1.32	ND (D)	1.19	1.62
		Travel Distance (m)		602.4	21.1		3	456.4		506.2	371.9

[1]: Radioactive half-lives obtained from (GoldSim Technology Group 2017c)
ND (D): not detected during the 2 million year model run and due to short half-lives, interpreted to have undergone radioactive decay
ND (S): not detected during the 2 million year model run, and due to very long half-lives, interpreted to have sorbed rather than decayed
When retardation factor is >200, the radionuclide travel distance has been calculated based on a retardation factor of 200.
[Retardation values validated using the GoldSim risk assessment modelling software, detailed within Appendix B.2 and F].

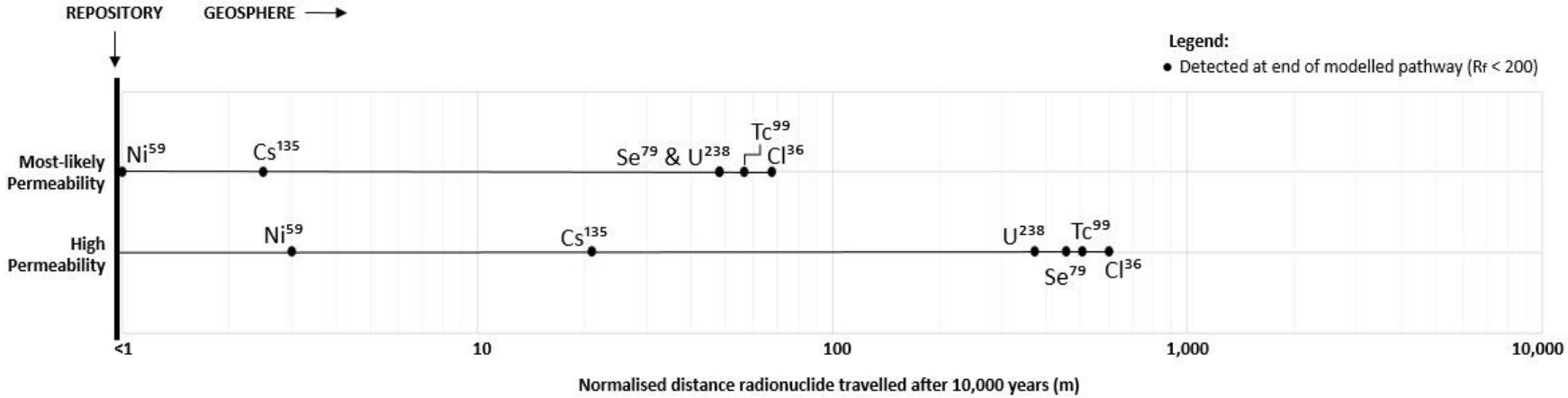

Figure 4.16: Comparison of radionuclide travel distances at Sellafield based on most-likely and high permeability particle pathway streak-lines after 10,000 years. Due to very short half-lives Eu152 and Sr90 have undergone radioactive decay and as such, are not detected at the end of the modelled pathway.

Table 4.2: Summary of results of hydrogeological parameters representing hydrogeological characteristics considered of importance for long term radioactive waste containment and isolation, generated from most likely permeability and high permeability modelled scenarios.

Hydrogeological Parameters	**Peak Repository Temperature**	**(P.1)** Areas of the far-field (20 km by 2 km) domain with 'slow' advective groundwater velocity (%)	**(P.2)** Total length of quasi-steadystate groundwater pathway from repository top to discharge point (m)	**(P.3)** Depth of quasi-steadystate groundwater pathway discharge point relative to repository top (m) where '-' represents a shallowing, and '+' represents a deepening	**(P.4)** Radionuclide travel distance over 10,000 years (m)
Most-likely permeability scenario	*Baseline*	57	2,500	-600	<1 to 67.5
High permeability scenario	*Baseline*	20	2,400	-600	3 to 602.4

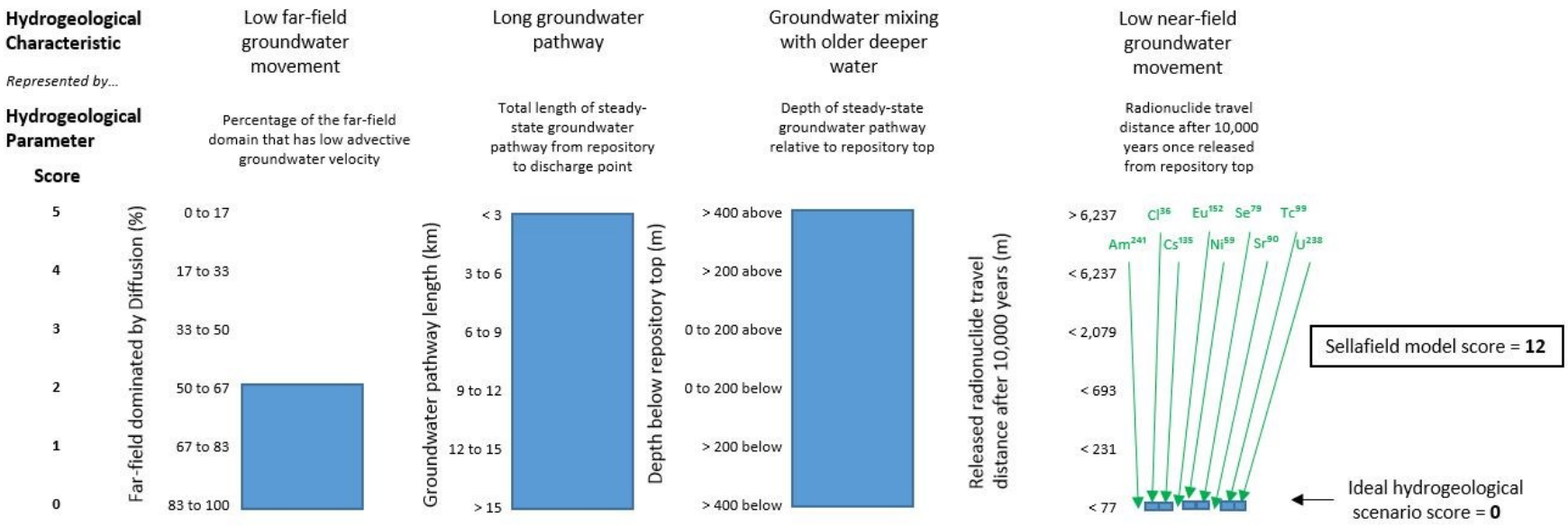

Figure 4.17: Summary chart of Sellafield hydrogeological parameters, based on most-likely permeability values, plotted and scored against 'ideal' hydrogeological parameters.

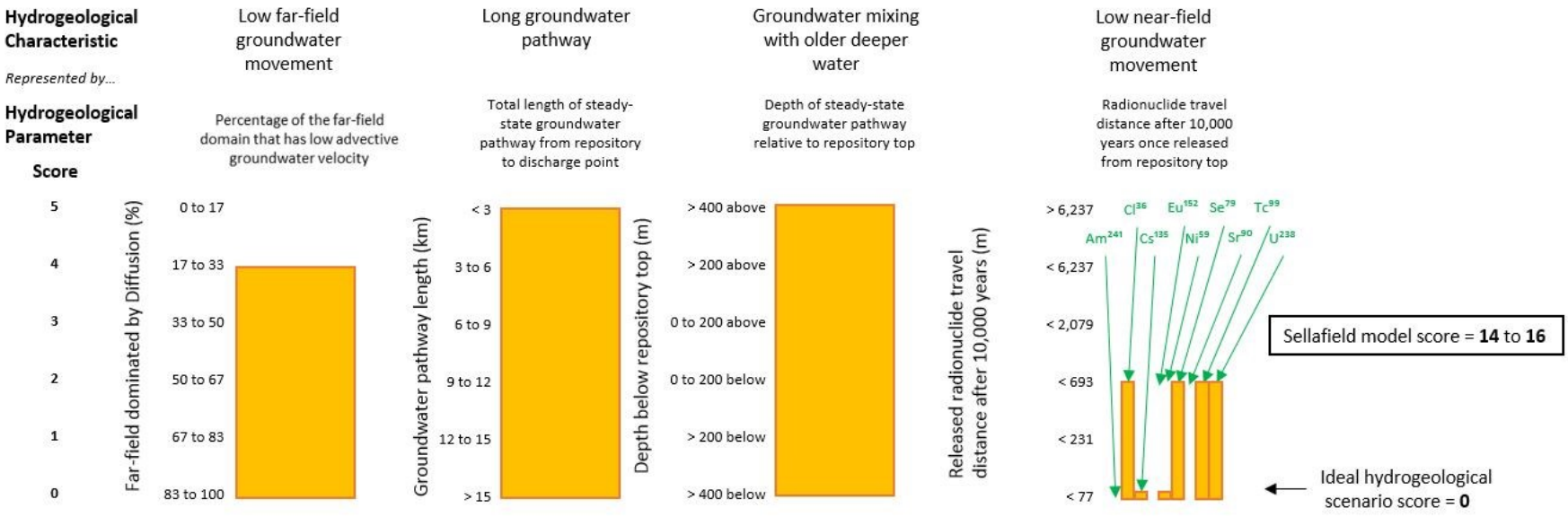

Figure 4.18: Summary chart of Sellafield hydrogeological parameters, based on high permeability values, plotted and scored against 'ideal' hydrogeological parameters.

4.6 Discussion: Hydrogeological Characteristics

4.6.1 Far-field hydrogeological characteristics

Modelling shows groundwater flow at Sellafield is at a complex intersection of three distinct groundwater systems; the C*oastal Plain Regime*, the *Hills and Basin Regime*, and the *Irish Sea Basin Regime*.

Deeper groundwater, sourced from the *Hills and Basin Regime* to the East and from the *Coastal Plain Regime*, is forced up through the vicinity of the repository. Groundwater is facilitated up along higher permeability Borrowdale Volcanic Group fracture zones, transporting released radionuclides into the overlying '*major'* Sherwood Sandstone Group aquifer. Groundwater eventually discharges to the coastline (Figure 4.14B & Figure 4.15B). Similar localised groundwater pathways have also been shown in modelling undertaken by (Fraser Harris et al. 2015; Haszeldine & McKeown 1995; McKeown et al. 1999; Nirex 1997c).

The upwards migration of groundwater within the vicinity of the repository is considered to be a result of the 'blocking' nature of the offshore dense *Irish Sea Basin Regime* (see Figure 4.4), deflecting pressure driven groundwater upwards.

Modelling shows released particles could exit the Borrowdale Volcanic Group (host rock formation) within *approx.* 7,000 years (Figure 4.15C). This prediction is based on a model scenario populated with *'high'* permeabilities for the Flemming Hall lithology and faults (3.50E-17 m^2 & 1.20E-16 m^2 respectively).

These travel times are longer than those reported by (Fraser Harris et al. 2015) who concluded particles could be released from the host rock formation within 1,300 years. This was based on Borrowdale Volcanic Group fault and lithological permeabilities of 3.80E-14 m^2 and 3.80E-15 m^2 respectively. Travel times were also longer than those reported by (Nirex 1997c), which found particles could be released from the Borrowdale Volcanic Group (host rock formation) within 2,598 years (based on calibrated reference two-dimensional model with Borrowdale Volcanic Group fault and lithological permeabilities of 1.75E-18 and 5.76E-18 m^2 respectively) (Nirex 1997b). The variation in modelled results, despite access to the same material property data set and geometric information, is stark and highlights the wider problem in assessing confidence in the performance and safety of any potential geological disposal facility from numerical model simulation alone.

The reason for the longer than previously reported travel times is suspected to be the result of the localised discharge of the upper *hills and basement regime* to the coastal plain to the east of the repository (Figure 4.14B & Figure 4.15B), reducing groundwater flux through the

repository, which was not anticipated within the hydrogeological conceptual model (section 4.2). The reason for the coastal plain discharge could be due to the selected cross-section with its higher elevation causing a steeper hydraulic gradient, and therefore deeper and narrower flow regime, as described in (Tóth 1963).

4.6.2 Effect of permeability uncertainty on the far-field hydrogeological characteristics

The modelling of the Sellafield site shows that regardless of permeability uncertainty, groundwater pathways of *the Coastal Plain Regime*, *the Hill & Basement Regime* and *the Irish Sea Basin regime* (Black & Brightman 1996) remain distinct. However, when higher permeability values are applied the control by faults on regional groundwater movement becomes more apparent (Figure 4.15B). This implies that although material parameter uncertainty does have some control on groundwater flow at Sellafield, the greatest control is from the regional topography and the presence of *the Irish Sea Basin regime* to the West. Similar conclusions as to the importance of *the Irish Sea Basin regime* in controlling the regional groundwater characteristics were drawn by (Haszeldine & McKeown 1995).

This research can therefore conclude that: 1) radionuclide travel time upwards is much more rapid (by a factor of *approx.* 10) if regional or fault permeabilities are above model average values and 2) that the regional topographic settings plays a greater role in controlling far-field groundwater characteristics than material parameter uncertainty.

4.6.3 Effects of chemical sorption on radionuclide containment and isolation

Retardation calculations at Sellafield for migrating radionuclides under variable permeability scenarios shows a large variation in retardation rates (1 to >200), and consequently a large variation in radionuclide travel distances over the first 10,000 years i.e. ranging between <1 and 67.5 m for the most likely permeability pathway, and between 3 and 602.4 m for the high permeability pathway (Table 4.1).

Interestingly U^{238} and Cs^{135} only show a slight increase in retardation along the higher permeability pathway compared to the most likely permeability pathway (Table 4.1). The increase can be attributed to the presence of the clay rich Brockram Breccia, which increases the sorption of certain migrating radionuclides. However, the thickness of the encountered Brockram Breccia is small (8.5 m) which is why the observed increase in retardation is small. Continuation of the flow path through the Brockram Breccia would be anticipated to increase the retardation of these radionuclides further.

In conclusion, the Brockram Breccia therefore not only physically perturbs groundwater flow upwards at Sellafield (see Figure 4.14B & Figure 4.15B) but also provides a function of a chemical barrier. Furthermore, due to the direction of the groundwater flow lines, the most-likely permeability model scenario would eventually also pass through the overlying Brockram Breccia, and would also be expected to undergo a degree of radionuclide retardation, as seen in the high permeability scenario.

4.6.4 Comparison of the far-field hydrogeological characteristics to the benchmark hydrogeological scenario

The comparison of the Sellafield hydrogeological parameters (within the range of known permeability uncertainty), against those of the benchmark scenario, show characteristic short pathways (< 2.5 km) ascending to the surface (- 600 m) at Sellafield. This is in comparison to beneficial long pathways (> 15 km) progressing deeper (+ 400 m). They also show areas of faster moving groundwater over the far-field domain (43 % for the most-likely permeability model and 80 % for the high permeability model). Faster flowing groundwater is found along the fault lines, and within the upper Sherwood Sandstone Group. This is in comparison to the 0 % 'faster' groundwater movement within the benchmark scenario (section 3.3.4).

Based on a method whereby an ideal far-field hydrogeological setting is given a score of '0/20', the Sellafield scenario can be ascribed a score of '12/20' when modelled with most likely permeability values (Figure 4.17), and between '14 and 16/20', depending on radionuclide, when modelled with high permeability values (Figure 4.18).

The results indicate that regardless of permeability, Sellafield does not illustrate widespread hydrogeological characteristics considered beneficial for the long term *containment* and *isolation* of radioactive waste. Sellafield is therefore a poor site from a far-field natural barrier prospectivity perspective. Furthermore, within both permeability modelled scenarios there appears little segregation between near surface and deeper groundwater flow at Sellafield, which is considered a key beneficial hydrogeological characteristic required for a deep geological disposal site (Radioactive Waste Management 2016b). These findings are in light of the extensive groundwater investigations previously undertaken in West Cumbria (section 4.1), and therefore relative material parameter certainty.

4.6.5 Comparison to Chapman 1986 Hydrogeological Regimes

Although there does exist a short geological section (*approx.* 7 km length) of basement rock beneath sedimentary cover, due to the presence of the offshore *Irish Sea Brine Regime* forcing the *Coastal Plain* and *lower Hills & Basement Regime* water up through the sedimentary

cover, creating a direct pathway from the repository to the coastline, the region cannot be considered analogous to the 'basement rock beneath sedimentary cover' hydrogeological regime previously identified as being potentially suitable to store radioactive waste (Chapman et al. 1986) (section 2.2).

4.7 Conclusion

Based on the chosen method of analysis and available site specific information, the regional setting of Sellafield cannot be deemed to exhibit widespread beneficial hydrogeological characteristics for the safe long term *containment* and *isolation* of radioactive waste, nor can it be considered analogous to any of the previously identified 'hydrogeological' regimes considered suitable for deep geological disposal (Chapman et al. 1986).

4.8 Assumptions, Limitations and Recommendations

In addition to the key modelling method limitations outlined in section 3.5, the following key limitations, specific to the Sellafield model, have also been identified:

1. The current geological template, on which the hydrogeological model is based, comprises four short, separate, superimposed cross-sections (see Figure 4.3). Further research is required to determine the 'true' continuous east-west geological section running through the Sellafield site.

2. Groundwater flow lines within the lower Hills and Basement regime is distorted and 'flattened' by the basal no-flow boundary. The Sellafield model depth should be extended as not to distort the lower hills and basement groundwater flow lines.

3. Site specific pressure, temperature, and salinity data is required within the Lake District Hills, and offshore beneath the Irish Sea to enable improved regional scale model parametrisation and calibration.

4. Improved model calibration for pressure and salinity within the high permeability scenario, at depths > 1 km within the vicinity of the repository, is required to improve confidence in modelled results.

Chapter 5 Tynwald Basin, East Irish Sea Basin: Model Development, Results and Discussion

5.1 Introduction to the Tynwald Basin Site

The Tynwald Basin has never before been investigated for the purpose of deep geological disposal, and the reasons for its selection within this research are presented within section 2.6.

The Tynwald Basin cross-section extends over a distance of *approx.* 34 km from the West Cumbrian coastline near Annaside, out in a south-west orientation beneath the Irish Sea, into the East Irish Sea Basin's Tynwald Basin (Figure 5.1).

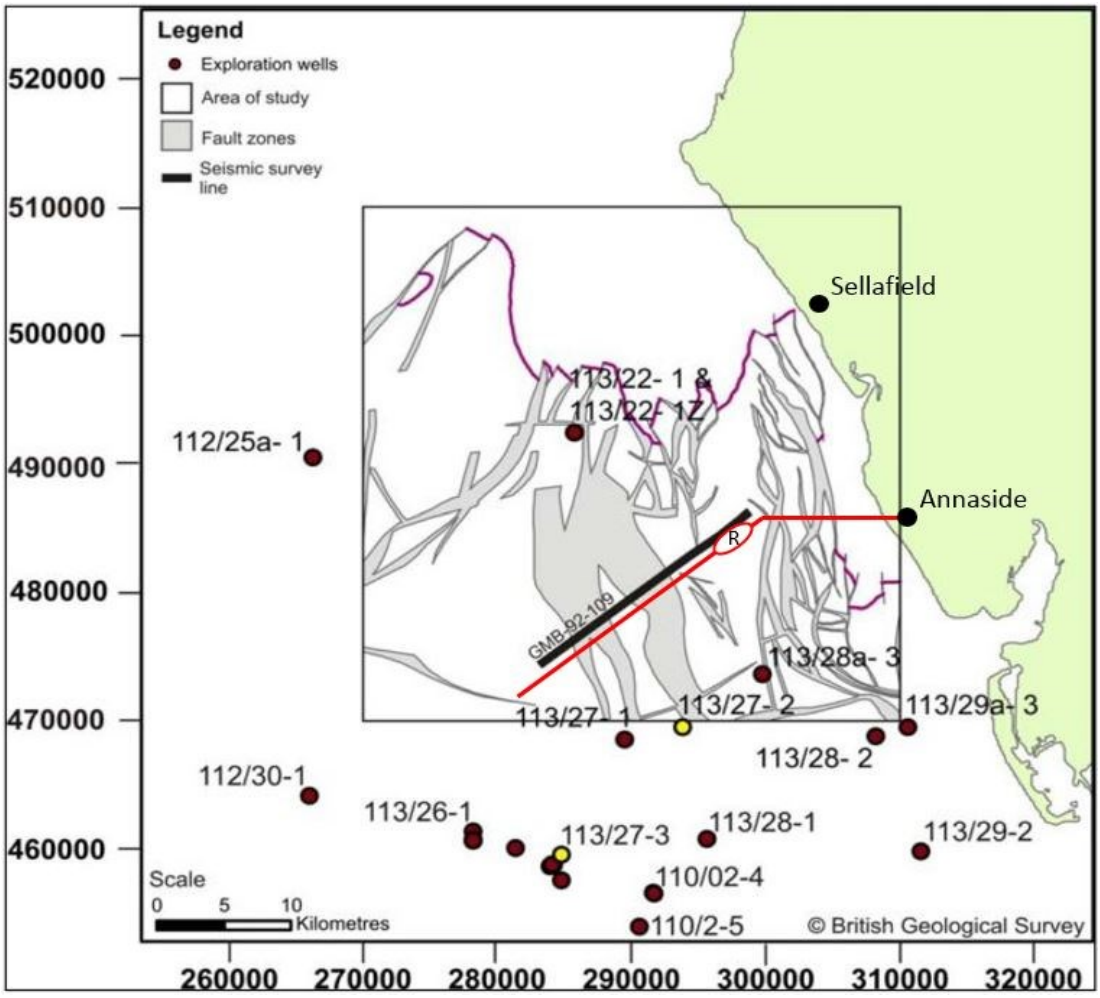

Figure 5.1: Map showing 1) the location of the theoretical repository in this research 'R'; 2) the location of the geological cross section (red line) on which the Tynwald Basin model is based (Figure 5.2) and; 3) the dense brine feasibility study area (black box), with well locations and seismic lines (Barnes et al. 2005).

The site is located *approx.* 17.5 km south-west from the onshore Sellafield Nuclear Site (Figure 5.1) which could be utilised for the required 1 km^2 secure surface facility (Nuclear Decommissioning Authority 2010a). Repository development here would require a *approx.* 20 km long sub-seabed tunnel to enable access to the repository, the technical feasibility and socio-economic implications of which were discussed within Appendix 3.

Due to the presence of important oil and gas resources within the East Irish Sea Basin (Jackson et al. 1995), such as the Lennox fields (Yaliz & Chapman 2003), Morecambe fields (Bastin et al. 2003; Cowan & Boycott-Brown 2003; Stuart & Cowan 1991) and Hamilton fields (Yaliz & Taylor 2003), the region has been extensively characterised, which presents an opportunity for improved model parameterisation. The location of these major oil and gas fields to the south of the Tynwald Basin would mean that the repository would not interfere with natural oil and gas resources.

The Tynwald Basin has itself been characterised primarily through offshore seismic reflection surveys, constrained by sporadic borehole data as compiled in (Chadwick et al. 1992; Jackson et al. 1995; Barnes et al. 2005), which will be used as a basis for geological and hydrogeological model development and analysis.

5.2 Geological Sequence

The Tynwald Basin is one of a number of permo-triassic syn-depositional basins located within the Caledonide aged northwest trending Clyde Belt (Jackson & Mulholland 1993; Jackson et al. 1987). The Tynwald Basin is characterised by a Caledonide aged crystalline basement, overlain by a thick mid-Palaeozoic to Quaternary sedimentary sequence (Jackson et al. 1995), in which the theoretical repository will be situated, at a depth of 360 m within the Mercia Mudstone Group (Figure 5.2).

5.2.1 Quaternary Sequence

The Quaternary (1.67 Ma to present) deposits of the Tynwald Basin can be broadly described as *thick, continuous glacio-marine sediments* (Nirex 1997f), with three depositional phases having been identified relating to pre, syn (during), and post Devensian glaciation deposition (Nirex 1997f; Akhurst et al. 1997).

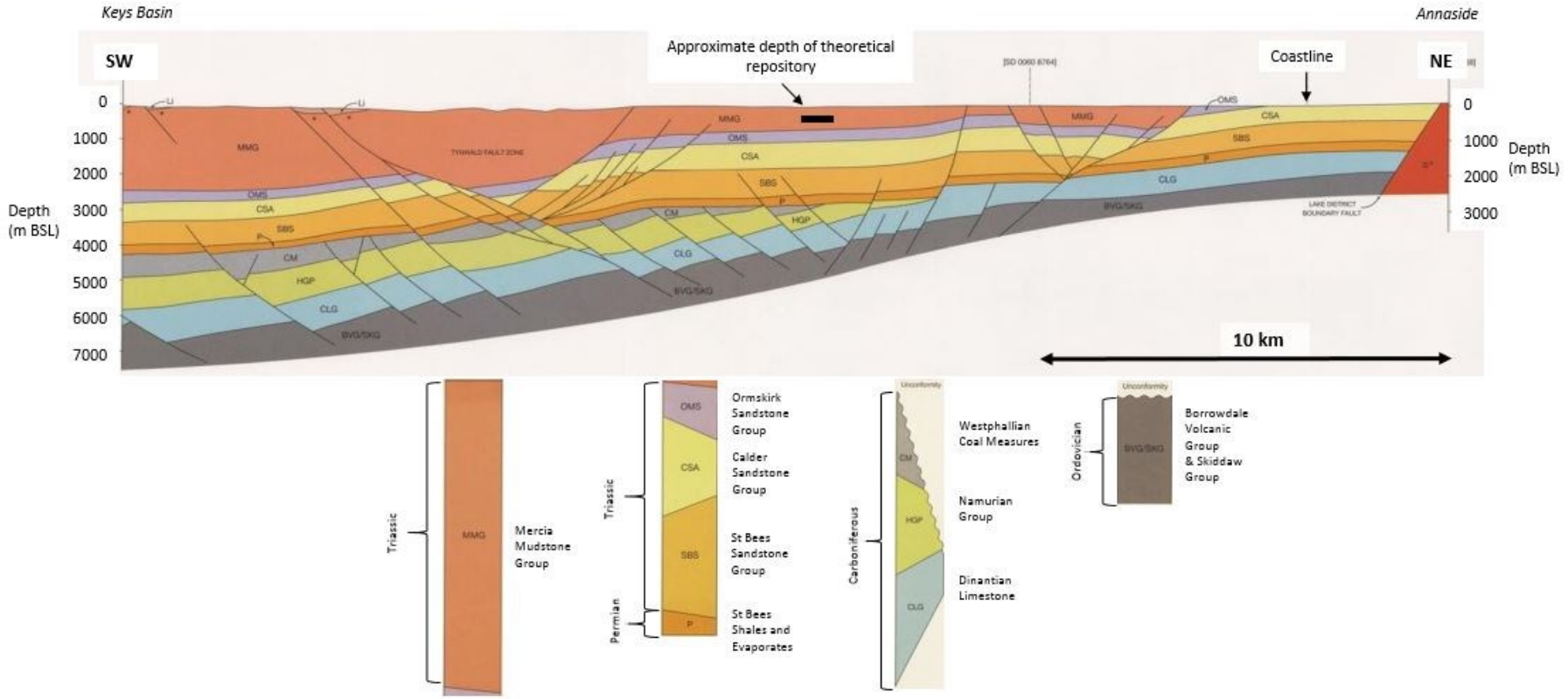

Figure 5.2: Geological 2D cross-section of the Coastal Plain and East Irish Sea Basin (British Geological Survey 1997).

A syn-depositional fault has been identified within the quaternary sediments of the northern splays of the Tynwald Fault Zone (Nirex 1997f), which is considered of importance for radionuclide containment as the presence of near-surface faults could provide a pathway for migrating radionuclides. The syn-depositional fault is interpreted to have occurred within the past 15 ka (post-Devensian Glaciation), and although it is not considered a result of Quaternary fault re-activation, it could be a result of underlying progressive salt withdrawal (Nirex 1997f), which has implications for near-surface lithological stability and therefore radionuclide containment. Further research must be undertaken to determine the cause and extent of offshore quaternary syn-depositional faulting.

The Quaternary deposits unconformably overlie the Triassic Strata. The Triassic strata appears unaltered by recent glaciation events (Nirex 1997f), and by proxy, can therefore be inferred to remain unaltered by near-future glaciation events if no information is provided to the contrary.

5.2.2 Permian-Triassic Sequence

The Triassic deposits, in which the theoretical repository will be situated, comprise *interbedded halite, dolomite, anhydrite, mudstone, siltstone and sandstone* of the Mercia Mudstone Group (237 to 210 Ma) (Jackson et al. 1997; Jackson et al. 1987; Warrington 1997; Wilson 1990), reaching a total thickness of > 2 km locally within the Tynwald Basin Fault Zone.

Thinning of the Mercia Mudstone Group eastwards is considered a mixture of stratigraphic thinning, and post-depositional erosion (Barnes et al. 2005; Chadwick et al. 1994). Relative thicknesses of the Dowbridge Mudstone to Elswick Mudstone (units of the Mercia Mudstone Group) have been interpreted from the generalised vertical section for the East Irish Sea Basin in (Jackson et al. 1987). Relative thicknesses of the Preesall Halite to Stanah Member have been interpreted based on average lithological thicknesses across boreholes 113/22-1 (Schlumberger 2016) and 113/27-3 (Barnes et al. 2005). These boreholes were chosen due to their similar lower Mercia Mudstone Stratigraphy. Finally, erosion down to the Preesall Halite has been interpreted eastwards based on aerial extent interpretations of the main halite units of the Mercia Mudstone Group, provided by (Barnes et al. 2005). The location of boreholes and seismic lines used within this study were presented within Figure 5.1.

A summary of the interpreted Mercia Mudstone units, their main lithologies and relative thicknesses are presented within Table 5.1 and Figure 5.3 for use within the numerical model.

Table 5.1: Description of the Mercia Mudstone Group members interpreted across the Tynwald Basin.

Member	Lithological Description (Jackson et al. 1997)	Interpreted Classification (Barnes et al. 2005; Jackson et al. 1997)	Percentage lithological contribution to MMG when full sequence present
Elswick Mudstone	*Red brown mudstones*	*Mudstone*	*8.4*
Worton Halite	*Clean massive halite with mudstone partings*	*Clean Massive Halite*	*8.4*
Dowbridge Mudstone	*Structure less, red silty mudstone with siltstone packets*	*Mudstone*	*8.4*
Preesall Halite	*Clean massive halite with mudstone partings (generally 1-3 m)*	*Clean Massive Halite*	*10.5*
Cleveley Mudstone	*thick, lithologically varied, mudstone and siltstone unit which contains a high percentage of halite*	*Bedded Halite*	*17.3*
Mythop Halite	*Halite layers separated by laterally persistent silty mudstone intercalations*	*Bedded Halite*	*16.6*
Blackpool Mudstone	*Uniform red structureless mudstones*	*Mudstone*	*14.3*
Rossall Halite	*Layers of clean halite, separated by widespread mudstone intercalations that become progressively thinner upwards*	*Bedded Halite*	*6.8*
Ansdell Mudstone	*Red with subordinate green silty mudstone with a single thin (3 m) near-median halite*	*Mudstone*	*3.0*
Flyde Halite & Stanah Member	*Halite layers with mudstone partings becoming thicker and more numerous towards the top of the sequence*	*Bedded Halite*	*6.3*

Halokinetic structures, including salt diapirs and pillow salts, have also been identified within the Mercia Mudstone Group of the East Irish Sea Basin (Jackson et al. 1987), which has implications for radionuclide containment and isolation due to structural lithological

instability. Although the halokinetic structures are mainly found within the deeper keys basin, due to thickness of layers, and depth of burial (Jackson et al. 1987), a possible halokinetic feature has also been identified within the Mercia Mudstone Group of the Tynwald Basin from Seismic Line GMB-92-109 (Barnes et al. 2005) (see Figure 5.2). It is suggested however that this structure may be a seismic velocity push-down artifact from an overlying Quaternary in-filled channel, and that more research should be undertaken to determine the presence and cause of the Quaternary in-fill channel, along with the presence of any further halokinetic features within Mercia Mudstone Group of the Tynwald Basin (Barnes et al. 2005).

The Mercia Mudstone Group is underlain by *fine to medium sub-feldspathic arenite* (Ormskirk Sandstone), *coarser Aeolian and sub-ordinate fluvial sandstone* (Calder Sandstone), and *sub-feldspathic arentite with mudstone and siltstone interbeds* (St Bee's Sandstone Formation), of the Sherwood Sandstone Group (250 to 237 Ma).

The Triassic sequence is conformably underlain by Permian *marginal marine and evaporitic deposits* (St Bees Evaporite and Shale) (260 to 250 Ma) (Jackson et al. 1995), which grade into *alluvial fan breccio-conglomerates* (Brockram Breccia) and the *cleaner, finer-grained deposits* (Collyhurst Sandstone) near the coast (Akhurst et al. 1997).

5.2.3 Ordovician-Carboniferous Sequence

The Permian sequence unconformably overlies *interbedded sandstone, siltstone, mudstone and seat earth* (clay or fine grained sediment underlying a coal seam, often containing fossil roots and soil structures) *and coal* (Westphallian Coal Measures) (315 to 305 Ma), *Sandstone, siltstone, argillaceous limestone and coal* (Namurian Group) (325 to 315 Ma), and *limestones separated by mudstones and sandstones* (Dinantian Limestone) (355 to 325 Ma) (Jackson et al. 1995; Barclay et al. 1994). This carboniferous sequence unconformably overlies an Ordovician Sequence.

The Ordovician sequence of the East Irish Sea Basin comprises *low metamorphic grade basaltic, andesitic, dacitic and rhyolitic lavas, sills and pyroclastic rocks, and volcanoclastic sedimentary rocks* (Borrowdale Volcanic Group) (458 to 449 Ma), and *cleaved turbiditic sandstones, siltstones and mudstone* (Skiddaw Group) (485 to 458 Ma) (Jackson et al. 1995). However, due to lack of site specific boreholes, the boundaries between the two within the Tynwald Basin are presently unknown.

Illustration of the geological cross section (Figure 5.2) and interpretation of lithological units and thicknesses for this research (Figure 5.3) are presented.

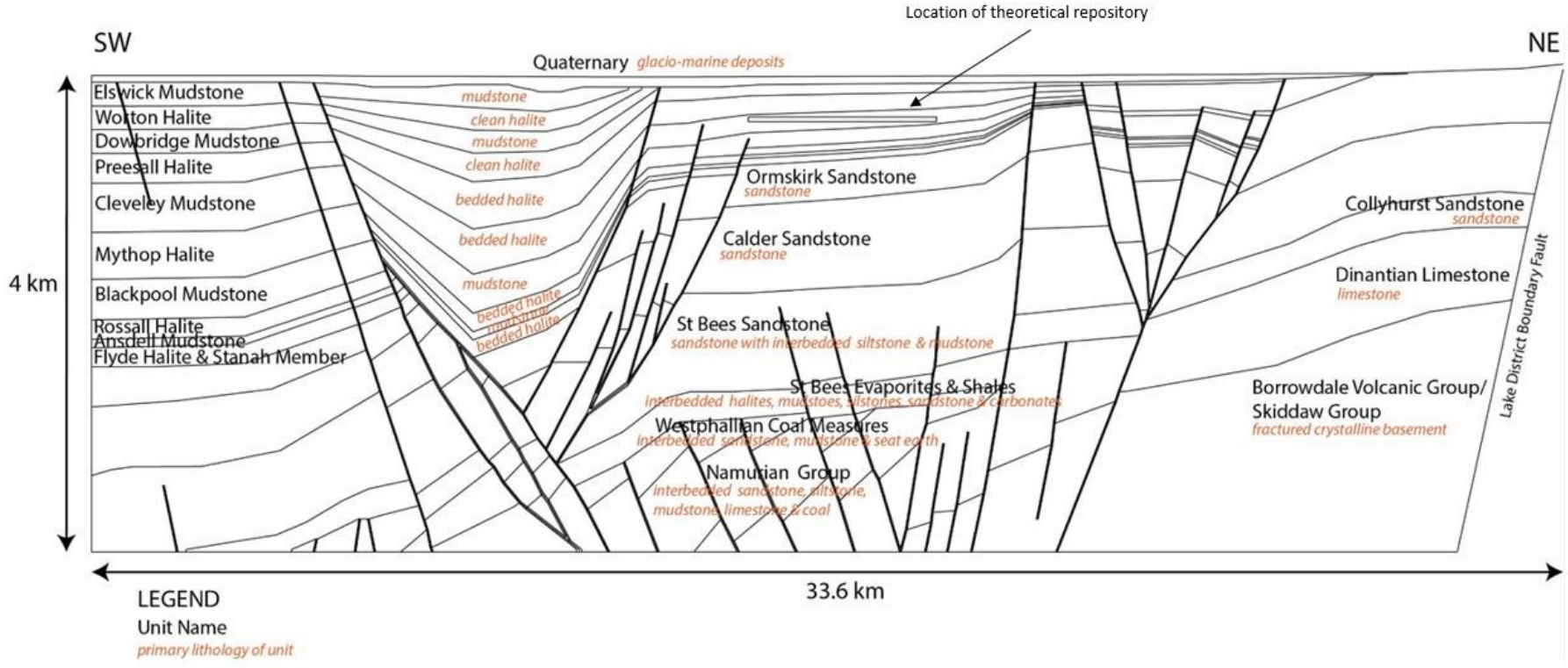

Figure 5.3: Interpretation of geological units, primary lithology and approximate thicknesses beneath the Site based on geological cross section provided in (British Geological Survey 1999b) for Swaffham, and lithological information provided in (Lee et al. 2015).

5.3 Hydrogeological Conceptual Understanding

5.3.1 Quaternary Sequence

Groundwater flow within the Quaternary sequence is considered to be facilitated laterally along higher permeability layers. The Quaternary sequence will therefore be classified as one hydrogeological unit.

5.3.2 Permian to Triassic Sequence

Groundwater flow through the Triassic Mercia Mudstone Sequence is hypothesised to be very slow. This interpretation is based on permeability values taken from the upper and middle onshore Mercia Mudstone Group by (Armitage et al. 2013; Armitage et al. 2015). Research undertaken by (Armitage et al. 2013; Armitage et al. 2015) was for the use of the Mercia Mudstone Group as a potential carbon capture and storage caprock (with the underlying Sherwood Sandstone Group as the reservoir), highlighting the competition for sub-surface spaces. Vertical groundwater movement is thus considered restricted due to the laterally extensive low permeability units. In addition, faults are not anticipated to play a significant role in facilitating groundwater movement within the Mercia Mudstone Group due to the creep nature of the halite rich lithological layers, closing up fractures under hydrostatic pressure (Cosenza et al. 1999; Houben et al. 2013; Liu et al. 2015), and the possible smear effect from the clay rich units reducing fracture permeability.

Groundwater flow within the underlying Ormskirk Sandstone, Calder Sandstone and St Bees Sandstone units are hypothesised to be of greater volumetric significance than that of the Mercia Mudstone Group, but still with very low flow rates, potentially perturbed along sub-vertically orientated faults.

Groundwater samples obtained from oil and gas wells, drilled into the Ormskirk Sandstone and St Bees Sandstone within the Irish Sea Basin, have been reported to have a high percentage of chloride (Table D.0.3) (Barnes et al. 2005; Yaliz & McKim 2003; Yaliz & Taylor 2003; Yaliz & Chapman 2003; Cowan & Boycott-Brown 2003; Bastin et al. 2003). The source of this salt is purported to be halite rich layers of the Mercia Mudstone and possible St Bees Shales & Evaporates (Bath et al. 1996). The presence of dense brines offshore, as previously identified within the near-shore Irish sea Basin Regime at Sellafield (Black & Brightman 1996), along with little topographic head difference (sea surface), suggest possible density driven flow. Groundwater residence times in excess of 2 million years have been reported for the Irish Sea Basin Regime at Sellafield (Bath et al. 2006). Thermally driven flow may also become important with depth.

A small section of meteorically derived fresh water, driven by an onshore topographic pressure gradient is also anticipated, forming a fresh-saline-brine groundwater transition zone along the coastline, similar to that observed at Sellafield (Black & Brightman 1996).

The following hydrogeological units have been derived for the Permian-Triassic Sequence based on lithological units considered to behave in a similar far-field hydrogeological manner: the Elswick Mudstone; Worton Halite; Dowbridge Mudstone; Preesall Halite; Cleveley Mudstone; Mythop Halite; Blackpool Mudstone; Rossall Halite; Ansdell Mudstone; Flyde Halite; Ormskirk & Calder Sandstone Undifferentiated; Ormskirk & Calder Sandstone Faulted; St Bees Sandstone Undifferentiated; St Bees Sandstone Faulted; and the Permian.

Groundwater within the Permian to Triassic Sequence is anticipated to be fully saturated with respect to chloride due to the halite rich Mercia Mudstone Group layers, with corresponding long groundwater residence times (see section 5.3.1). Groundwater here is hypothesised to be density driven, with thermally driven flow also becoming important with depth.

5.3.3 Carboniferous to Ordovician Sequence

Groundwater flow within the Carboniferous Westphallian Coal Measures, Namurian Group, Dinantian Limestone and underlying Ordovician Sequence is considered primarily fracture dominated, with very slow groundwater movement occurring through the low permeability matrix, as indicated by site specific investigations historically undertaken at Sellafield on the Borrowdale Volcanic Group (Nirex 1997a; Nirex 1997b). As no lithological differentiation can currently be determined between the Borrowdale Volcanic Group and Skiddaw Group offshore, the two formation will be combined into one hydrogeological unit.

The following hydrogeological units have thus been derived for the Ordovician-Carboniferous Sequence based on lithological units considered to behave in a similar far-field hydrogeological manner: Westphallian Coal Measures Undifferentiated; Westphallian Coal Measures Faulted; Namurian Undifferentiated; Namurian Faulted; Dinantian Limestone Undifferentiated; Dinantinan Limestone Faulted; the Borrowdale Volcanic Group & Skiddaw Group Undifferentiated; and the Borrowdale Volcanic Group & Skiddaw Group Faulted.

Groundwater within the Carboniferous to Ordovician Sequence is also anticipated to contain a high percentage of chloride, derived from the overlying Permian-Triassic sequence. Density may therefore play an important role in characterising regional flow, with thermally driven flow also being important with depth.

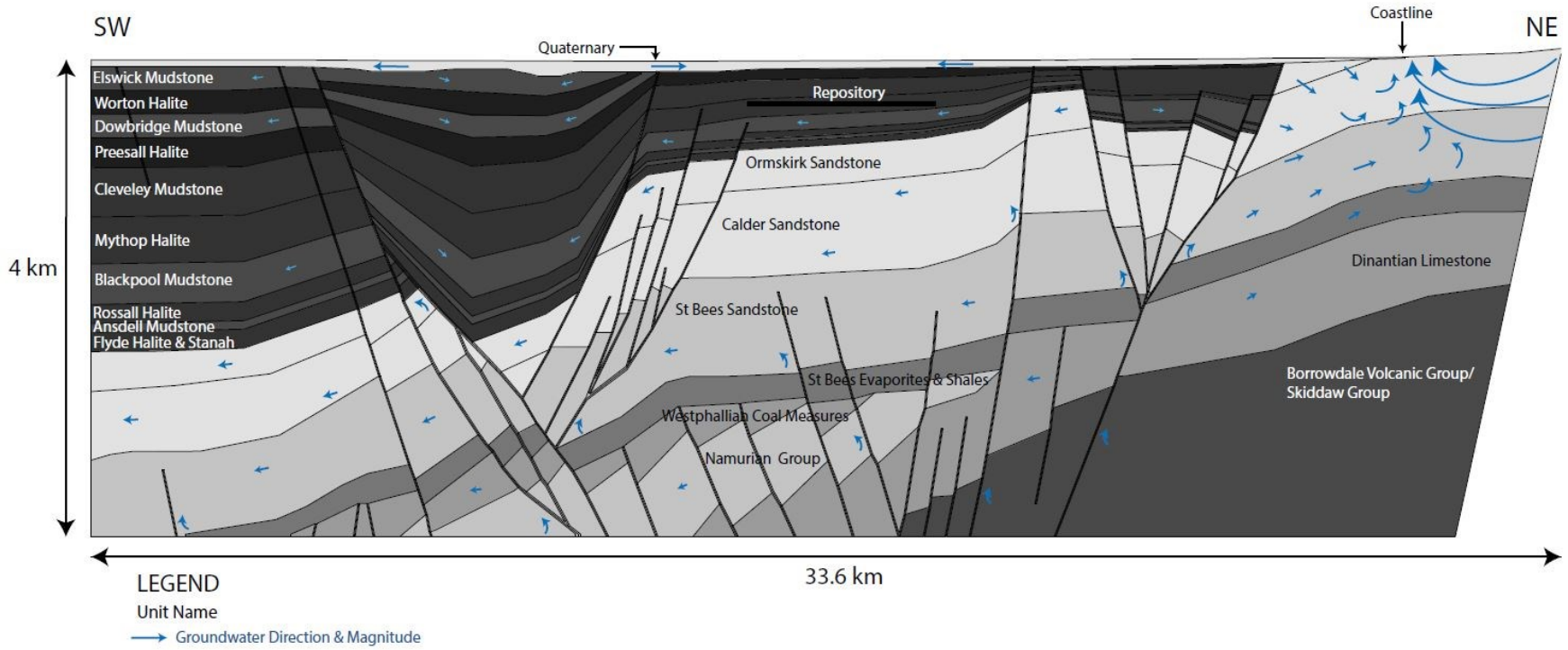

Figure 5.4: Hydrogeological conceptual model of the Tynwald Basin Site including the main hydrogeological units, predominate pathways, and the direction and magnitude of groundwater flow indicated by the orientation and schematic length of arrows respectively.

5.4 Model Construction & Development

5.4.1 Geometry & Mesh

The two-dimensional geometry and mesh (Figure 5.5) of the Tynwald Basin model, based on the information highlighted in section 5.3, comprises 130,362 nodes and 258,920 elements.

5.4.2 Boundary Conditions

Pressure, mass and temperature boundary conditions have been applied as presented in Figure 5.6. A constant mass concentration boundary of 1000 kg/m^3 has been applied along the onshore surface based on infiltration of fresh meteoric water, whilst a constant mass concentration has been applied along the southwest boundary, progressing from fully saturated dense brine next to the Mercia Mudstone Group (1200 kg/m^3, down to a high concentration of chloride (1174 kg/m3) within the underlying Sherwood and St Bees Sandstone based on average chloride concentration provided from Irish Sea Oil and Gas wells (section D.3).

Temperature boundaries have been calculated based on generic surface temperatures and geothermal gradients (Downing & Gray 1986), whilst pressure boundaries have been calculated based on atmospheric pressures, and sub-surface hydrostatic pressure gradients. The equations used for boundary condition calculation are presented within section B.1.6.

5.4.3 Material Parameters

The material parameters of porosity, permeability (both most likely and high), mass dispersion, heat dispersion, storativity, bulk density, thermal capacity and thermal conductivity have been applied specifically, and uniformably to each individual lithological unit (section D.1). Heat capacity and heat conductivity have been applied as constants across the entire modelled domain (section B.1.3.2), as has the site specific functions of fluid viscosity and density (section B.1.3.1), and finally faults have been represented as continuous porous mediums (section B.1.2).

5.4.1 Numerical control

Numerical control was achieved by capping the permeability range to 5 orders of magnitude (1.00E-13 and 1.00E-018 m^2) and setting mass and heat dispersivity to either 10 or 50, explained in section B.1.4.2, with the values ascribed detailed in section D.1.

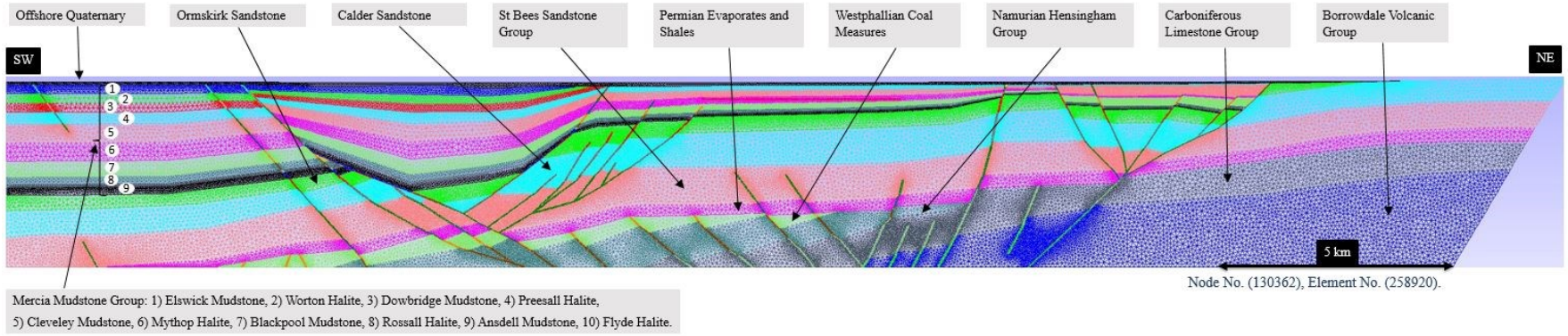

Figure 5.5: 2D triangular element mesh of Tynwald Basin site

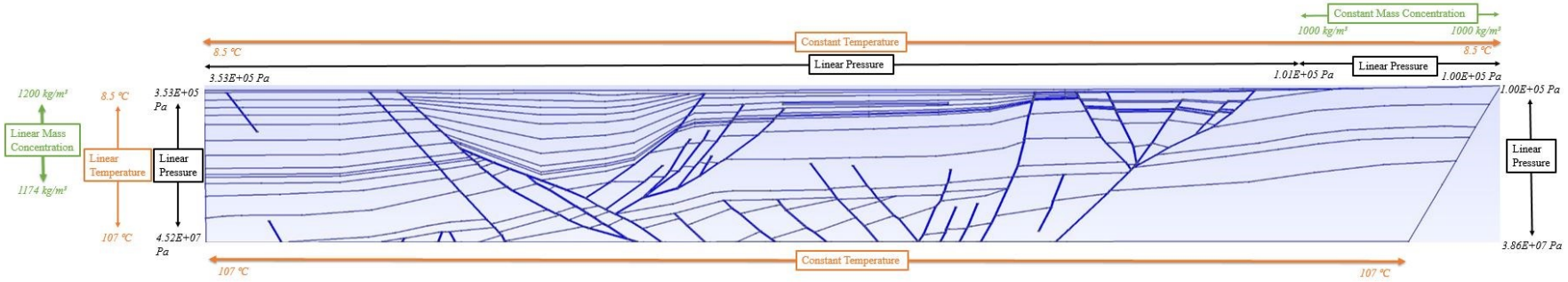

Figure 5.6: Boundary conditions applied to the Tynwald Basin model.

5.4.1 Initial conditions

Initial conditions for pressure (Figure 5.7) were applied based on a pressure gradient calculated using Equ.B.7 for the entire model domain (see section D.2).

Initial mass conditions (Figure 5.8) were developed by application of a linear mass concentration gradient for the offshore quaternary (based on a typical seawater mass density of 1,019.4 kg/m^3), and constant mass densities of 1,200 kg/m^3 for the Mercia Mudstone Group, and 1,174 kg/m^3 for the remainder of the model domain. These values are based on average chloride concentrations obtained for offshore Sherwood Sandstone and St Bees Sandstone Formations (see Table D.0.3), and the assumption of full salt saturation within the Mercia Mudstone Group. The top northeast corner of the applied mass distribution was then adjusted to enable simulation of a coastal fresh-water interface. The freshwater interface was applied using a python script to enable a weighted mass distribution (see section D.2) based on chloride values obtained for BH10 from Sellafield (Bath et al. 2006). BH10 was selected as analogous due to exposure of Ormskirk/Calder Sandstone at the surface. This type of more advanced initial mass condition development was required to enable an appropriate initial condition to be achieved.

Initial conditions for temperature (Figure 5.9) were applied based on a typical continental gradient of 0.025 °C/m (Dowing & Gray 1986) for 1) the onshore sub-surface, and 2) the offshore sub-surface (see section D.2).

In order to achieve quasi-steadystate conditions (see section 9.2), models were first solved for hydraulics, followed by coupled hydraulic, heat transport and mass transport. Once quasi-steadystate was reached, transient coupled hydraulic, heat transport and mass transport were simulated. The coupled TH model was made transient by the addition of a storage term. A summary log of model runs, including initial conditions is presented within section D.2.

5.4.2 Model calibration

No calibration was possible for the Tynwald Basin models due to an absence of site specific data. The purpose of these models is however to guide further far-field hydrogeological research, rather than to undertake an absolute risk assessment of the quality of a site for deep geological disposal, as discussed within section 3.1. Therefore, these models are considered appropriate for the objectives of this research.

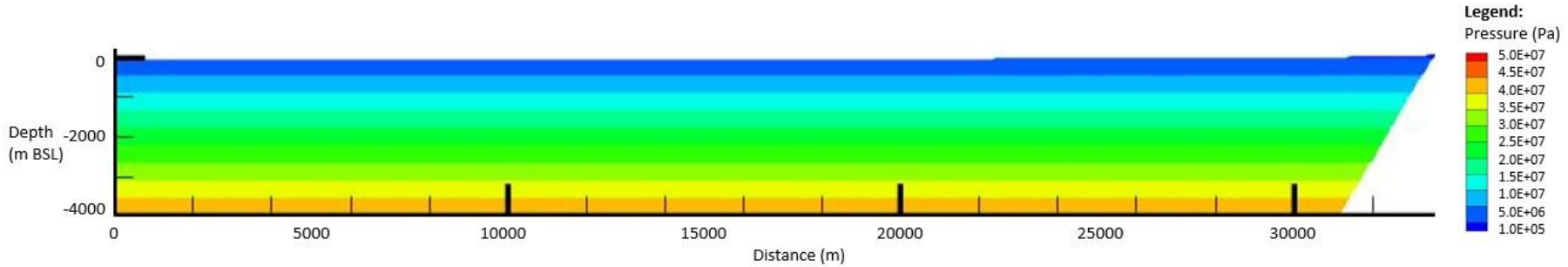

Figure 5.7: Pressure (Pa) initial conditions across the Tynwald Basin model domain.

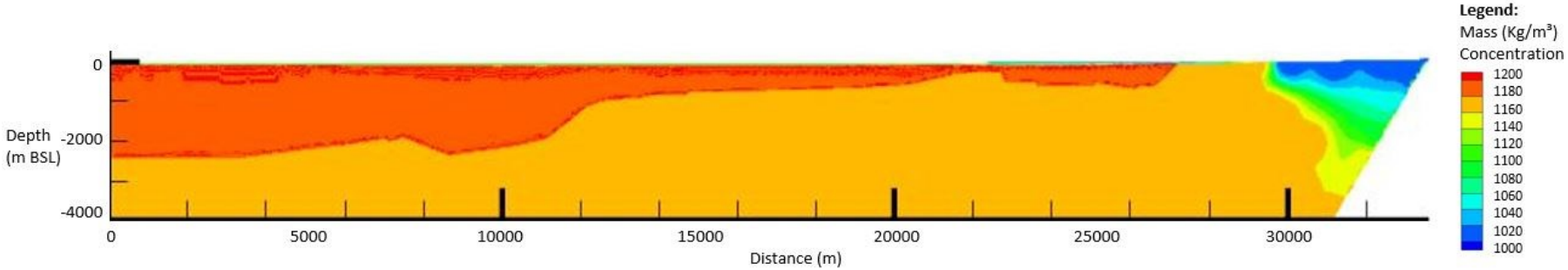

Figure 5.8: Mass Concentration (Kg/m³) initial conditions across the Tynwald Basin model domain.

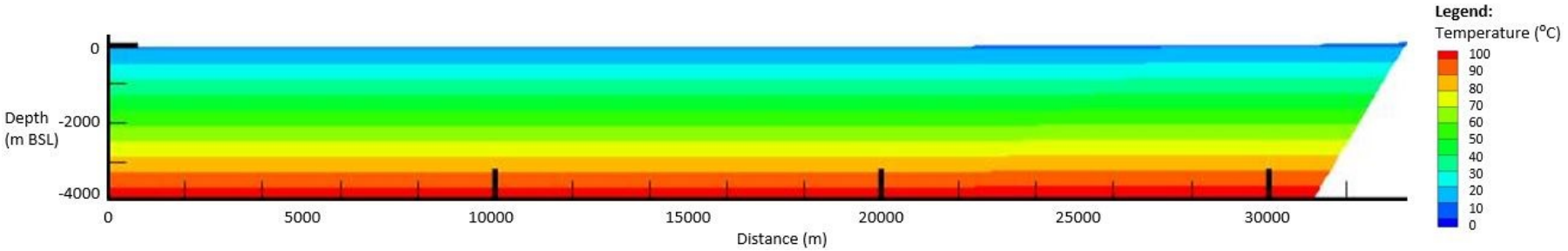

Figure 5.9: Temperature (°C) initial conditions across the Tynwald Basin model domain.

5.5 Results: Hydrogeological Parameters

For a description of the method used to analyse the far-field hydrogeological characteristics of the Tynwald Basin site against the benchmark hydrogeological scenario, please see section 3.3.

5.5.1 (P.1) Far-field Groundwater Velocities

Far-field groundwater velocities range between 5.00E-13 and 1.00E-07 m/s but predominately between 1.00E-12 to 1.00E-07 m/s for the most likely permeability scenario (Figure 5.10B). 66 % of this groundwater system has 'slow' groundwater movement, including the Mercia Mudstone Group where the repository is situated (Figure 5.10A). Far-field groundwater velocities range between 5.00E-12 and >1.00E-06 m/s but predominately between 1.00E-11 to 1.00E-06 m/s for the high permeability scenario (Figure 5.11B). 39 % of this groundwater system has 'slow' groundwater movement, again including the Mercia Mudstone Group where the repository is situated (Figure 5.11A). The underlying Sherwood Sandstone Group is faster flowing (Figure 5.11A).

The lowest far-field groundwater velocities are observed across the Mercia Mudstone Group in which the theoretical repository is situated, while the highest far-field velocities are observed within the Dinantian Limestone (Figure 5.10B & Figure 5.11B), situated towards the northeast boundary.

5.5.2 (P.2 & P.3) Groundwater Pathway Length & Discharge Depth

The groundwater pathway in both permeability modelled scenarios progresses down from the repository through the Mercia Mudstone Group layers, into the underlying Sherwood Sandstone Group (Figure 5.10B & Figure 5.11B). The groundwater flow lines track the Sherwood Sandstone Group until *approx.* 7 km northeast of the repository, at which point they drop down through the Permian into the Dinantian Limestone. The groundwater discharges to the northeast boundary at a distance of *approx.* 14,000 m from the repository.

The groundwater has a total pathway length of *approx.* 13,900 m in the most likely permeability modelled scenario, exiting the model at a depth of-1,908 m. This equates to a deepening relative to the repository top of 1,508 m (Figure 5.10B). The groundwater has a total pathway length of *approx.* 13,700 m in the high permeability modelled scenario, exiting the model at a depth of -1,697 m. This equates to a deepening relative to repository top of 1,337 m (Figure 5.11B).

5.5.3 (P.4) Radionuclide travel distance over 10,000 years

Particle pathways show that with most-likely lithological and fault permeabilities radionuclides travel 0.74 m i.e. < 1 m over the first 10,000 years (Figure 5.10C). Released particles remain within the Mythop Halite. In a system populated with high lithological and fault permeabilities, released particles travel a maximum distance of 14.5 m (Figure 5.11C), also remaining within the Mythop Halite.

The retardation factor of selected radionuclides was calculated for the maximum particle pathway of the two permeability model scenarios. No radionuclides were retarded (R_f=1) and consequently all radionuclides traveling along the most-likely permeability model scenario pathway travelled a distance of < 1 m over 10,00 years, and those traveling along the high permeability model pathway travelled a distance of 14.5 m (Table 5.2).

5.5.4 Comparison against Hydrogeological Conceptual Model

Both modelled scenarios (Figure 5.10B & Figure 5.11B) show very slow groundwater movement down through the Mercia Mudstone Group. The vertical groundwater movement downwards was not hypothesised by the conceptual model (Figure 5.4), rather lateral movement along the higher permeability Mercia Mudstone Group units. The vertical movement is considered most likely to be a result of density driven flow, however, other explanations cannot be ruled out, discussed further in section 5.6.

Furthermore, model results (Figure 5.10B & Figure 5.11B) show groundwater movement to be southwest to northeast within the Sherwood Sandstone Group, rather than the hypothesised northeast to southwest flow direction (Figure 5.4). The southwest to northeast flow is considered a result of the hydraulic connection from the seabed to the onshore Lake District Boundary Fault, and because of the offshore southwest pressure boundary, causing pressure driven rather than density driven flow. This is also considered the reason why groundwater flow within this unit is faster flowing within the high permeability model, rather than the hypothesised very slow moving groundwater system.

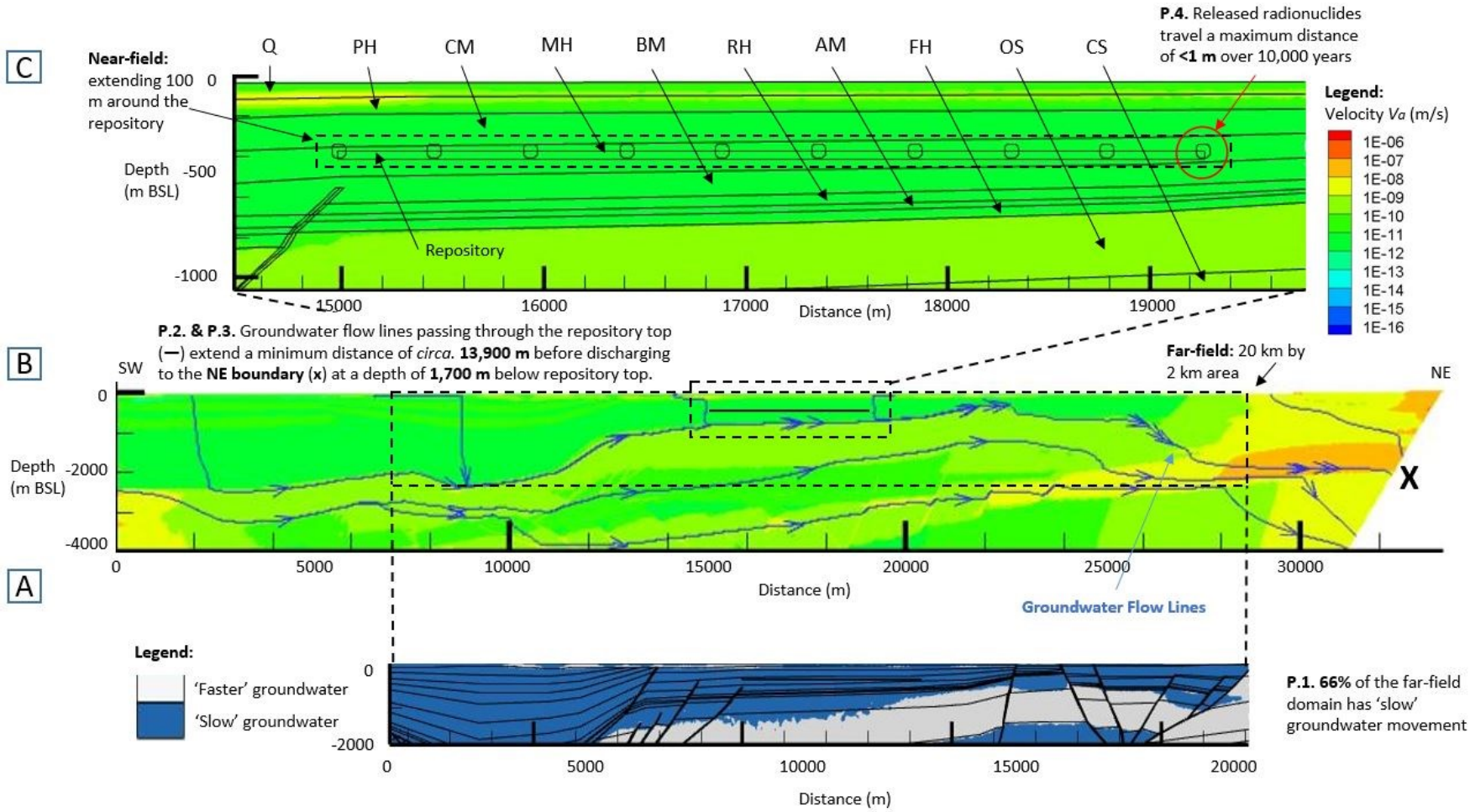

Figure 5.10: Results based on model populated with most likely permeability values. A) Areas of the far-field (20 km by 2 km) domain with 'slow' advective groundwater velocity i.e. <2.00E-10 m/s, B) Advective velocity distribution over the far-field, including groundwater flow lines and hydrogeological regimes, and C) Advective velocity distribution over the near-field, including the progression of particles released from along the top of a hypothetical repository over 10,000 years.

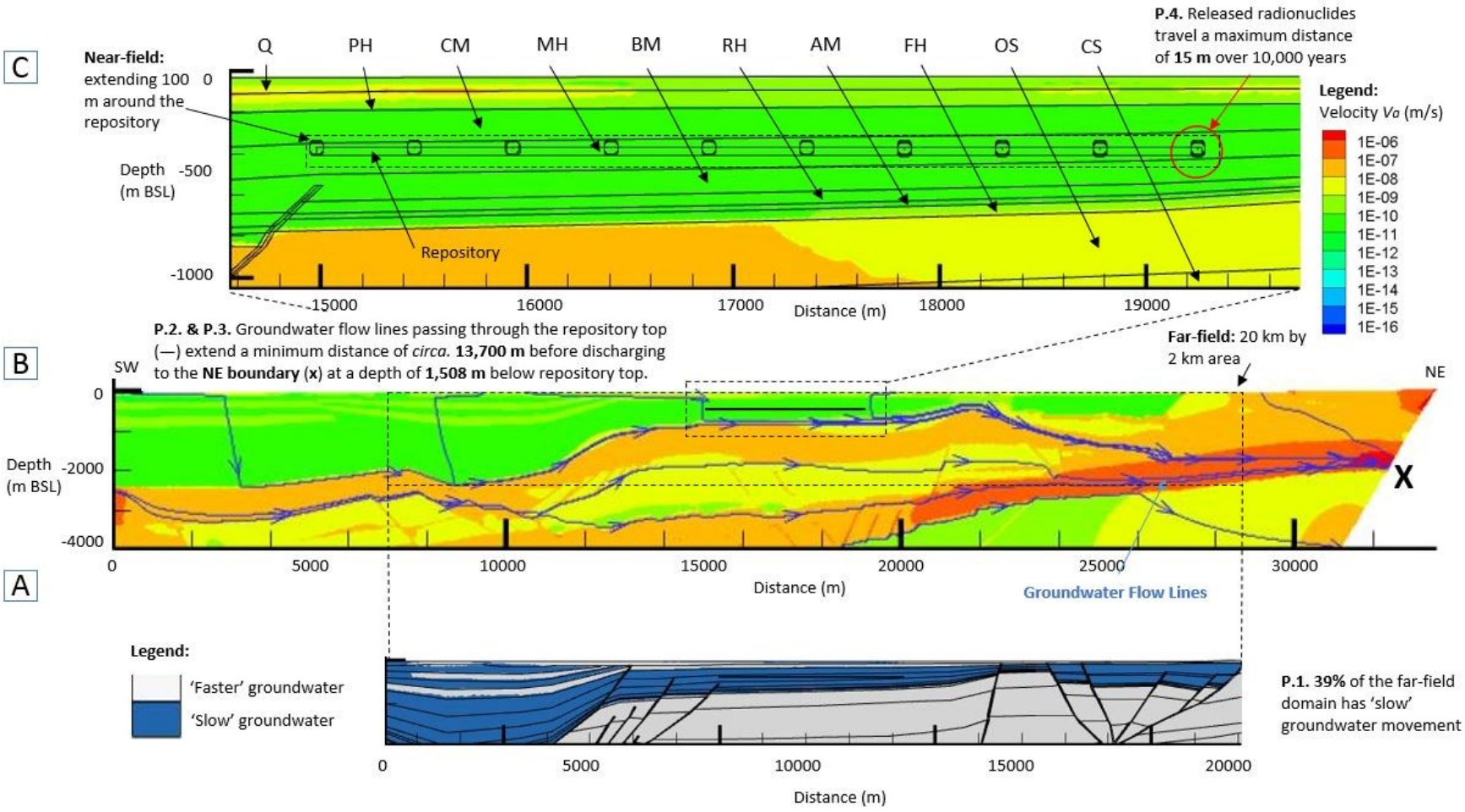

Figure 5.11: Results based on model populated with high permeability values. A) Areas of the far-field (20 km by 2 km) domain with 'slow' advective groundwater velocity i.e. <2.00E-10 m/s, B) Advective velocity distribution over the far-field, including groundwater flow lines and hydrogeological regimes, and C) Advective velocity distribution over the near-field, including the progression of particles released from along the top of a hypothetical repository over 10,000 years.

Table 5.2: Summary of retardation factors and travel distances of selected radionuclides after 10,000 years for maximum particle pathways (streak-lines) from the Tynwald Basin based on most likely and high permeability modelled scenarios.

Scenario	**Maximum Particle Travel Distance (streak-line length) (m)**	**Radionuclide**	**Am^{241}**	**Cl^{36}**	**Cs^{135}**	**Eu^{152}**	**Ni^{59}**	**Se^{79}**	**Sr^{90}**	**Tc^{99}**	**U^{238}**
		Half-life (yrs)[1]	*432.2*	*3.01E+05*	*2.3E+06*	*13.54*	*1.01E+05*	*2.95E+05*	*28.79*	*2.11E+05*	*4.47E+09*
Most-likely permeability	0.74	*Retardation Factor (R_f)*	1	1	1	ND(D)	1	1	ND(D)	1	1
		Travel Distance (m)	< 1	< 1	< 1		< 1	< 1		< 1	< 1
High permeability	14.5	*Retardation Factor (R_f)*	1	1	1	ND(D)	1	1	ND(D)	1	1
		Travel Distance (m)	14.5	14.5	14.5		14.5	14.5		14.5	14.5

[1]: Radioactive half-lives obtained from (GoldSim Technology Group 2017c)
ND (D): not detected during the 2 million year model run and due to short half-lives, interpreted to have undergone radioactive decay
[Retardation values validated using the GoldSim risk assessment modelling software, detailed within Appendix B.2 and F].

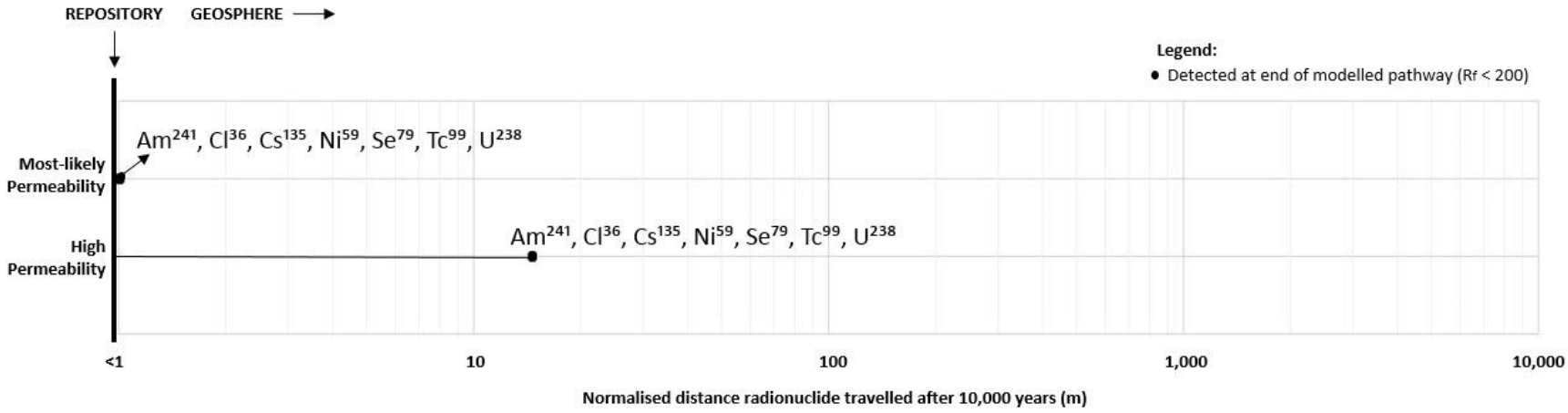

Figure 5.12: Comparison of radionuclide travel distances within the Tynwald Basin based on most-likely and high permeability particle pathway streak-lines after 10,000 years. Due to very short half-lives Eu^{152} and Sr^{90} have undergone radioactive decay and as such, are not detected at the end of the modelled pathway

Table 5.3: Summary of results of hydrogeological parameters representing hydrogeological characteristics considered of importance for long term radioactive waste containment and isolation, generated from most likely permeability and high permeability modelled scenarios.

Hydrogeological Parameters	**Peak Repository Temperature**	**(P.1)** Percentage of the far-field (20 km by 2 km) domain with 'slow' advective groundwater velocity (%)	**(P.2)** Total length of quasi-steadystate groundwater pathway from repository top to discharge point (m)	**(P.3)** Depth of quasi-steadystate groundwater pathway discharge point relative to repository top (m) where '-' represents a shallowing, and '+' represents a deepening	**(P.4)** Radionuclide travel distance over 10,000 years (m)
Most-likely permeability scenario	*Baseline*	66	13,900	+1,508	<1
High permeability scenario	*Baseline*	39	13,700	+1,337	14.45

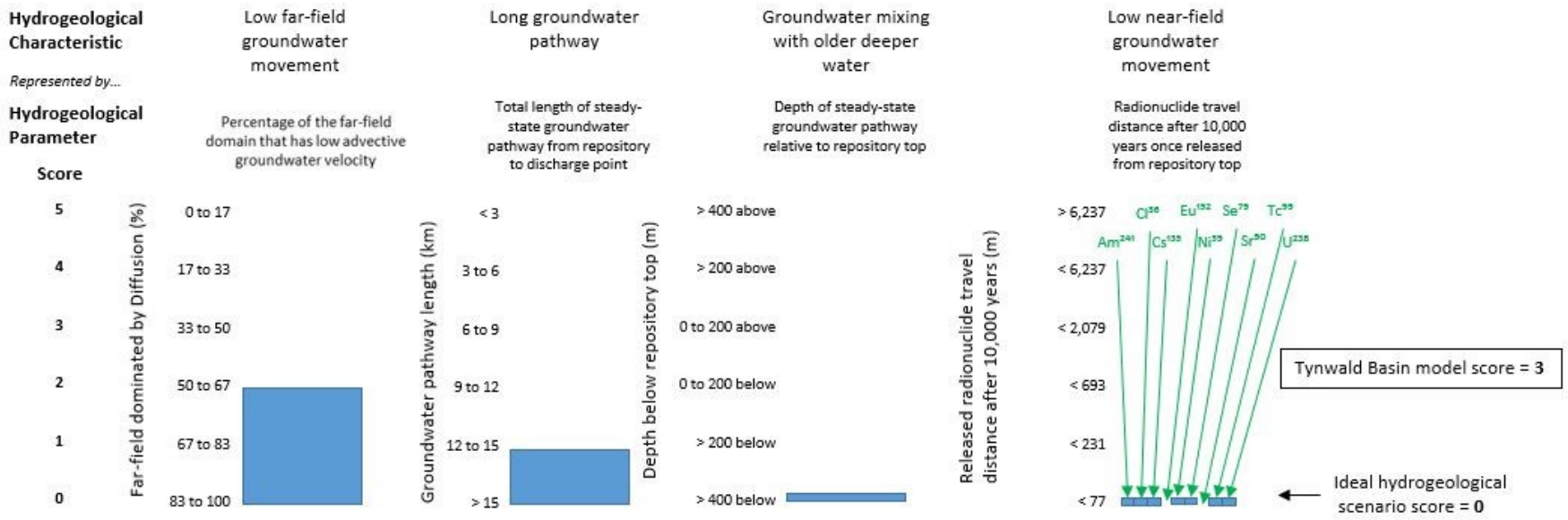

Figure 5.13: Summary chart of Tynwald Basin hydrogeological parameters, based on most-likely permeability values, plotted and scored against 'ideal' hydrogeological parameters.

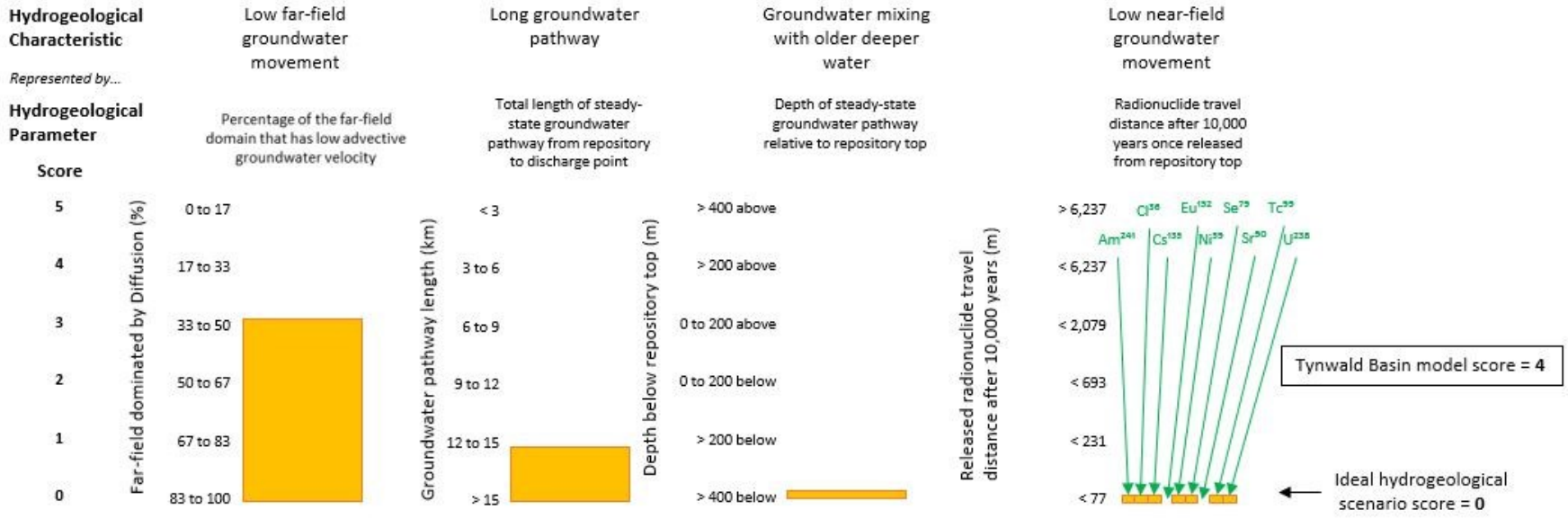

Figure 5.14: Summary chart of Tynwald Basin hydrogeological parameters, based on high permeability values, plotted and scored against 'ideal' hydrogeological parameters.

5.6 Discussion: Hydrogeological Characteristics

5.6.1 Comparison to Chapman 1986 Hydrogeological Regimes

The Tynwald basin models, regardless of permeability, shows very similar regional scale hydrogeological characteristics and groundwater movement. This indicates a small level of likely variance in groundwater characteristics, despite a comparatively large amount of lithological and fault permeability uncertainty. Groundwater movement is very slow and progresses downwards through the Mercia Mudstone Group into the underlying faster flowing Triassic-Permian sedimentary sequence (Figure 5.10B & Figure 5.11B). Regional groundwater flow through the lower Triassic-Permian sedimentary sequence is southwest to northeast orientated, with groundwater discharging to the surface near to the coast-line, forming a freshwater-brine groundwater interface along the coastline. Southeast flow is considered to be due to the pressure applied to the offshore boundary, and the hydraulic connection onshore.

The regional flow characteristics most closely resemble that of (Chapman et al. 1986) *'seaward dipping and offshore sediments'* hydrogeological regime, with groundwater flow dominated horizontally along higher permeability units and with vertical groundwater movement limited due to laterally extensive low permeability units (Figure 2.11b). The Tynwald Basin models do however differ from the *'seaward dipping and offshore sediments'* analogy in the respect that the repository is not situated within a sequence of interbedded higher permeability-lower permeability layers along which groundwater is facilitated, rather the Mercia Mudstone Group, in which the repository is situated, forms a single large low permeability unit, with the higher permeability Sherwood Sandstone Group situated below it.

The vertical groundwater movement down through the Mercia Mudstone Group was not originally hypothesised (section 5.3), and is considered most likely to be a result of the extreme density difference (*approx.* 25 kg/m^3) between the Halite rich Mercia Mudstone Group, and the underlying Sherwood Sandstone Group, causing vertical density driven flow rather than horizontal pressure driven flow. An alternative theory that cannot however be excluded is that the liquid flow equation, based on Darcian Flow (section A.3.1), provides an inappropriate mathematical solution to such low permeability units, and the observed groundwater behaviour is instead a result of an inaccurate solution of the initial conditions. Examples of non-Darcian flow phenomena include osmosis and ultrafiltration, although application to regional scale coupled groundwater flow is considered problematic, and controversial (Neuzil 1986).

The density difference theory will be given precedence in this research due to the long duration timescales over which this pattern is observed (50,000 years). It is recommended further research is undertaken to characterise the processes controlling groundwater movement through the Mercia Mudstone Group.

5.6.2 Effects of chemical sorption on radionuclide containment and isolation

The Tynwald Basin shows no effective chemical retardation as a result of sorption based on the 10,000 year streak-lines generated under variable permeability scenarios. This is because the pathways do not extend beyond the salt rich Mythop Halite, which, due it its naturally high groundwater ion content and competition for sorption sites, is hypothesised not to permit effective sorption.

Beyond the Mythop Halite released radionuclides would pass through a number of clay rich Mercia Mudstone Group layers. This would be anticipated to effectively sorb radionuclides further reducing radionuclide concentration within groundwater. This is considered to be especially important for long-lived radionuclides such as U^{238}.

5.6.3 Comparison to idealised hydrogeological regimes & benchmark scenario

Although the Tynwald Basin cannot be considered a direct analogy to the *'seaward dipping and offshore sediments' regime* (Figure 2.11b), it can be argued that this scenario still achieves the desired 'hydrogeological characteristics'. This is because it exhibits long and deepening groundwater pathways, and very low far-field groundwater velocities (see section 3.3.2). This same pattern of flow is seen in both permeability scenarios which suggests a small level of likely variance in the regional groundwater characteristics.

Based on a method whereby an ideal far-field hydrogeological setting is given a score of '0/20', the Tynwald Basin scenario can therefore be ascribed a score of '3/20' based on most-likely permeability values (Figure 5.13), and '4/20' based on high permeability values (Figure 5.14). As such, based on current regional scale uncertainties in permeability, the Tynwald Basin can be considered to exhibit potentially beneficial hydrogeological characteristics for long term *containment* and *isolation* of radioactive waste, regardless of ineffective near-field chemical processes.

5.6.4 Important Hydrogeological Features

The key features ensuring radionuclide containment and isolation within the Tynwald Basin can be summerised as: 1) the low permeability Mercia Mudstone Group, and its ability to perturb vertical radionuclide migration; and 2) the progression of groundwater downwards

through the Mercia Mudstone Group (where the repository is situated) into the underlying Sherwood Sandstone Group.

Further research therefore should be undertaken to determine: 1) the permeability of the individual Mercia Mudstone Group layers; 2) the groundwater densities across the entire regional system, which appear to have a major influence on regional groundwater movement; and 3) the offshore pressure boundary which appears to be driving groundwater movement within the Triassic sequence towards the coastline.

5.7 Conclusion

Based on current regional scale lithological and fault permeability uncertainties, the Tynwald Basin site exhibits potentially beneficial hydrogeological characteristics for the safe long term *containment* and *isolation* of radioactive waste, despite not being directly analogous to the *'seaward dipping and offshore sediments'* hydrogeological regime, and thus warrants further investigation. More research is required to characterise the permeability and the processes driving groundwater through the Mercia Mudstone Group, and regional groundwater densities, considered to control regional groundwater movement.

5.8 Assumptions, Limitations and Recommendations

In addition to the key modelling method limitations outlined in section 3.5, the following key limitations, specific to the Tynwald Basin model, have also been identified:

1. Interpretation of Mercia Mudstone Group lithological layers was based on sporadic borehole data, the locations of which were outside of the chosen 2D cross-section. Further research should therefore be undertaken to determine the exact Mercia Mudstone Group sequence through the Tynwald Basin and Tynwald Basin Fault zone.

2. No halokinetic features or salt disturbances assumed. Further research required to determine the occurrence of halokinetic features within the vicinity of site.

3. Material medium properties and material solid properties applied to hydrogeological units based on interpretation of 'primary' lithological constituent only.

4. Site specific pressure, temperature and salinity data required to improve model parameterisation, boundary conditions and calibration, including the influence of the Lake District Boundary Fault and southwest boundary as a boundary conditions.

5. Improved initial conditions required across Mercia Mudstone Group in light of site specific data to ensure an appropriate solution is found, with mass initial condition considered particularly important.

Chapter 6 Thetford, East Anglia: Model Development, Results & Discussion

6.1 Introduction to the Thetford Site

The Thetford site has never before been investigated for the purpose of deep geological disposal, and the reasons for its selection for this research are presented within section 2.6.

The Thetford Site extends over a distance of *approx.* 29 km from West Dereham in the west-northwest, to near Rockland All Saints in the east-southeast. The Site crosses the Stanford Military Base which could be utilised for the required 1 km^2 secure surface facility (Nuclear Decommissioning Authority 2010a).

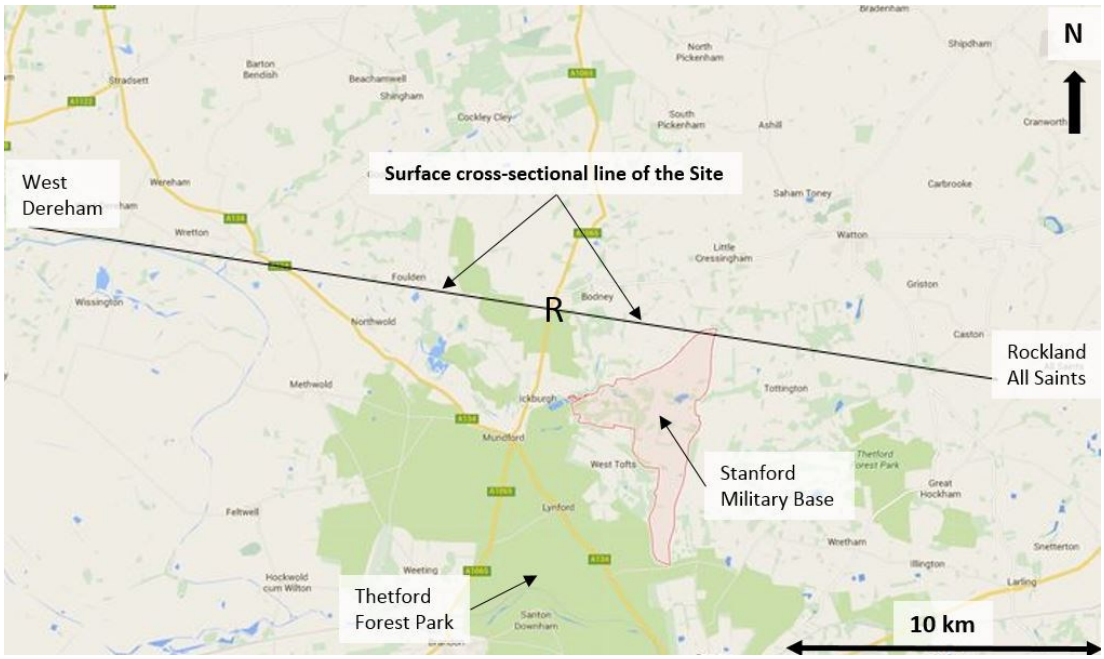

Figure 6.1: Location of the geological cross section used as the basis for numerical model simulation (see Figure 6.3). The centre of the theoretical repository is marked with an 'R', along with the secure Stanford Military base.

Although a limited number of deep boreholes exist within this area (Lee et al. 2015), a number of shallower boreholes do exist, These are for investigation of the Chalk Formation which is classified as a '*major*' or '*principle*' aquifer (Environment Agency 2016; Ander et al. 2004), and for the Sandringham Sands Formation, from which a significant potable water supply is obtained (Lee et al. 2015). These near surface wells will enable greater characterisation of the near-surface sedimentary sequence (Lee et al. 2015) (next section), but the aquifers also presents a potential groundwater receptor for migrating radionuclides if not assessed properly.

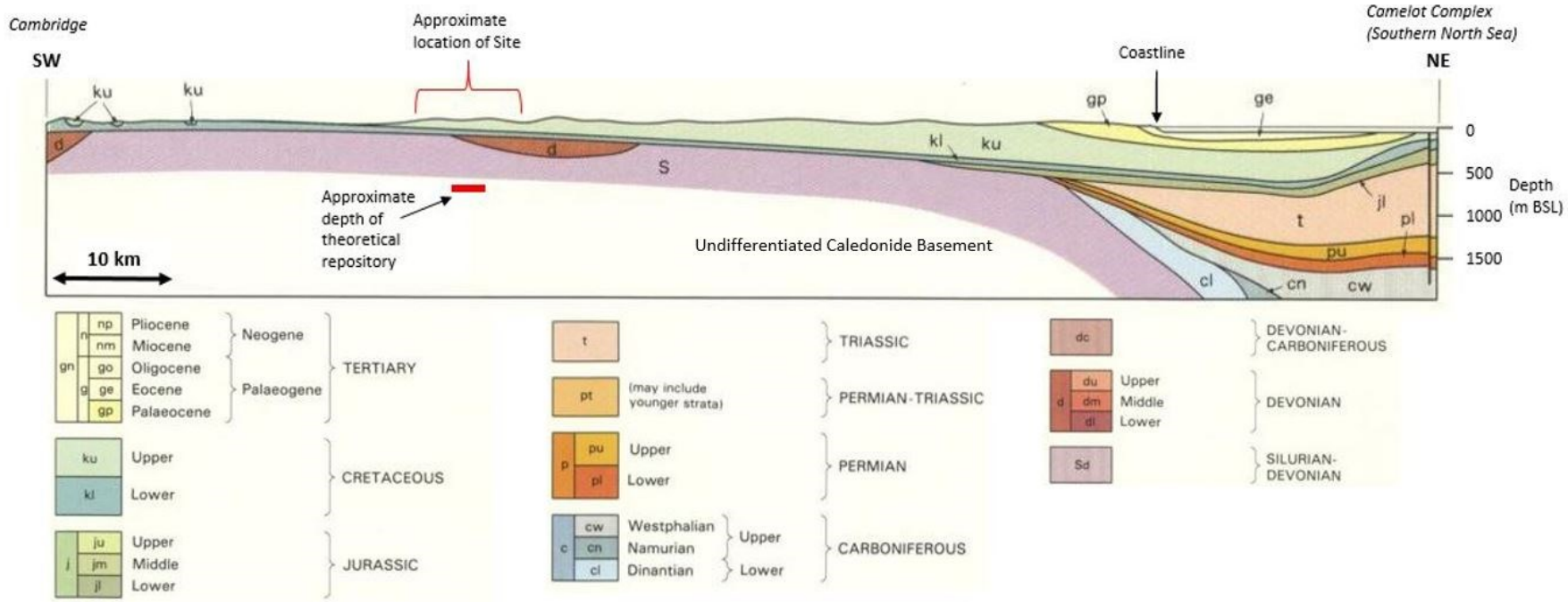

Figure 6.2: Regional geological cross section stretching from Cambridge in the southwest to the Camelot Complex in the Southern North Sea to the northeast (British Geological Survey 1991). The approximate location of the Site is marked with a red line.

6.2 Geological Sequence

The geology of East Anglia is characterised by seaward thickening Cenozoic and Mesozoic sedimentary layers, underlain by lower Palaeozoic and Precambrian Caledonide basement (British Geological Survey 1991). The theoretical repository will be situated at a depth of *approx.* 600 m below ground level (Figure 6.2), within the Caledonide Basement.

6.2.1 Cenozoic & Mesozoic Sedimentary Sequence

The Lowestoft Glacigenic Subgroup, described as a *Chalky diamicton,* deposited during the Anglian Glaciation (0.45 Ma) is the main Quaternary aged deposit of the region. The Lowestoft Glacigenic Subgroup is restricted to the eastern portion of the Site (Lee et al. 2015).

The Lowestoft Subgroup unconformably overlies late cretaceous (100.5 to 66 Ma) *thicker pure white chalk* (White Chalk) and *mud rich grey chalk* (Grey Chalk), and early Cretaceous (145 to 100.5 Ma) *marine mudstone* (Gault Clay Formation)*, ferruginous, pebbly sandstone* (Carstone Formation), and *glauconitic sandstone with mudstone and phosphatic pebbles* (Sandringham Sands Formation) (Lee et al. 2015) (Figure 6.3).

The cretaceous sequence overlies Jurassic aged (201.3 to 145 Ma) *marine mudstone, with fine-grained sandstone, silty sandstone and limestone* (Ancholme Group)*, intercalated shallow limestone and mudstone* (Great Oolite), *marine and nonmarine sandstone, siltstone, mudstone and limestone* (Inferior Oolite), and *thick mudstone with thin limestone, sandstone and ironstone horizons* (Lias Group) (Lee et al. 2015). The Jurassic sequence pinches out southeastwards around the Site (Figure 6.3).

The Jurassic sequence overlies the Triassic aged Mercia Mudstone-Penarth Group, interpreted to be dominated by *interbedded mudstone, siltstone and fine-grained sandstone* (Lee et al. 2015). The Triassic sequence unconformably overlies the Caledonide Basement (Figure 6.3).

6.2.2 Caledonide Basement

The regional Caledonide Basement is interpreted to be *hard fissile shales, sandstones and siltstones that are tectonically cleaved* (Lee et al. 2015). The Caledonide Basement directly beneath the site is of Silurian age, and contains a high percentage of mudstone (Woodcock & Pharaoh 1993). Although no deep boreholes exist within the area the Caledonide Basement can be interpreted to extend to depths of > 2 km. This interpretation is based on analogies with other Silurian basement sequences including: the Welsh Basin; Windermere Group; East England Shelf (all of which extend to between 2 and 6 km depth) (British Geological Survey 1991; Pharaoh et al. 1987; Dimberline et al. 1990; Kneller et al. 1994); and to an extent the Ordovician Borrowdale Volcanic Group (Akhurst et al. 1997).

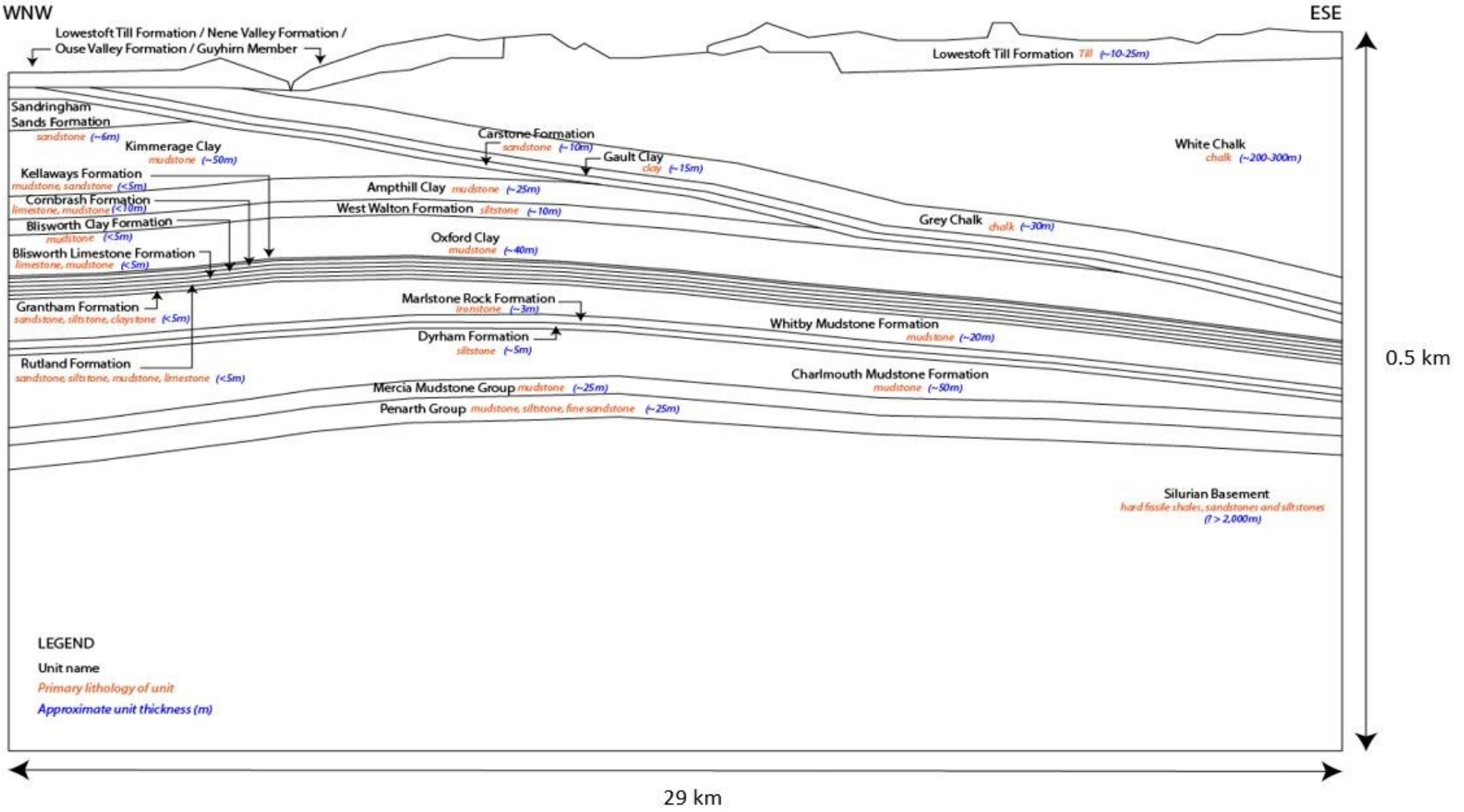

Figure 6.3: Interpretation of geological units, primary lithology and approximate thicknesses beneath the Site based on geological cross section provided in (British Geological Survey 1999b) for Swaffham, and lithological information provided in (Lee et al. 2015).

6.3 Hydrogeological Conceptual Understanding

6.3.1 Cenozoic & Mesozoic Sedimentary Sequence

Groundwater flow within the Cenozoic and Mesozoic sedimentary sequence is considered to be dominated horizontally along higher permeability units, such as the Jurassic Great and Inferior Limestone, or fractures within the dual porosity cretaceous Chalk (Ander et al. 2004). Abundant flow around near-surface topographic recharge and discharge points is also anticipated. Vertical groundwater movement is considered restricted due to laterally extensive low permeability units such as the Gault Clay.

The Cenozoic and Mesozoic sedimentary sequence, based on lithological units considered to behave in a similar far-field hydrogeological manner, are as follows; the Lowestoft Till Formation, the cretaceous Chalk, the Ancholme Group and Gault Clay, the great and inferior Oolite, and the Lias Group & Mercia Mudstone Penarth Group.

Groundwater within the sedimentary sequence is considered to be fresh to brackish meteoric derived depending on the unit, with chloride concentrations reaching up to 50 mg/l (British Geological Survey 1976) within the Chalk. Groundwater within this sequence is considered to be pressure driven with relatively short residence times of days near the surface, increasing down to a purposed 10,000 years with depth (Ander et al. 2004).

6.3.2 Caledonide Basement

Groundwater flow within the Caledonide Basement is considered primarily fracture dominated, with slow groundwater movement through the low permeability indurated (hard) matrix. The fracture frequency and therefore abundance of flow is considered greater within the upper Silurian Basement, than the lower. This is due to a period of later Variscan aged (*circa.* 290 ma) sub-aerial erosion (Lee et al. 2015). As such, two hydrogeological units have been identified within the Caledonide Basement for use within the models 1) the Upper Silurian Basement, and 2) the Lower Silurian Basement.

Based on analogies to other Silurian aged basements (section 6.2.2), namely the Welsh Basin, groundwater can be considered brackish to saline, with recharge from the overlying sedimentary sequence, and some possible Pleistocene (> 10,000 ma) aged groundwater entrapment (Edmunds et al. 1998). Groundwater is considered pressure driven, although density and/or thermal drive may become important with depth. Residence times are anticipated in excess of 10,000 years i.e longer than residence times of the shallower sedimentary sequence (see section 6.3.1), supported by ^{14}C isotopic evidence from the Welsh Basin, suggesting groundwater of late Pleistocene age (Edmunds et al. 1998).

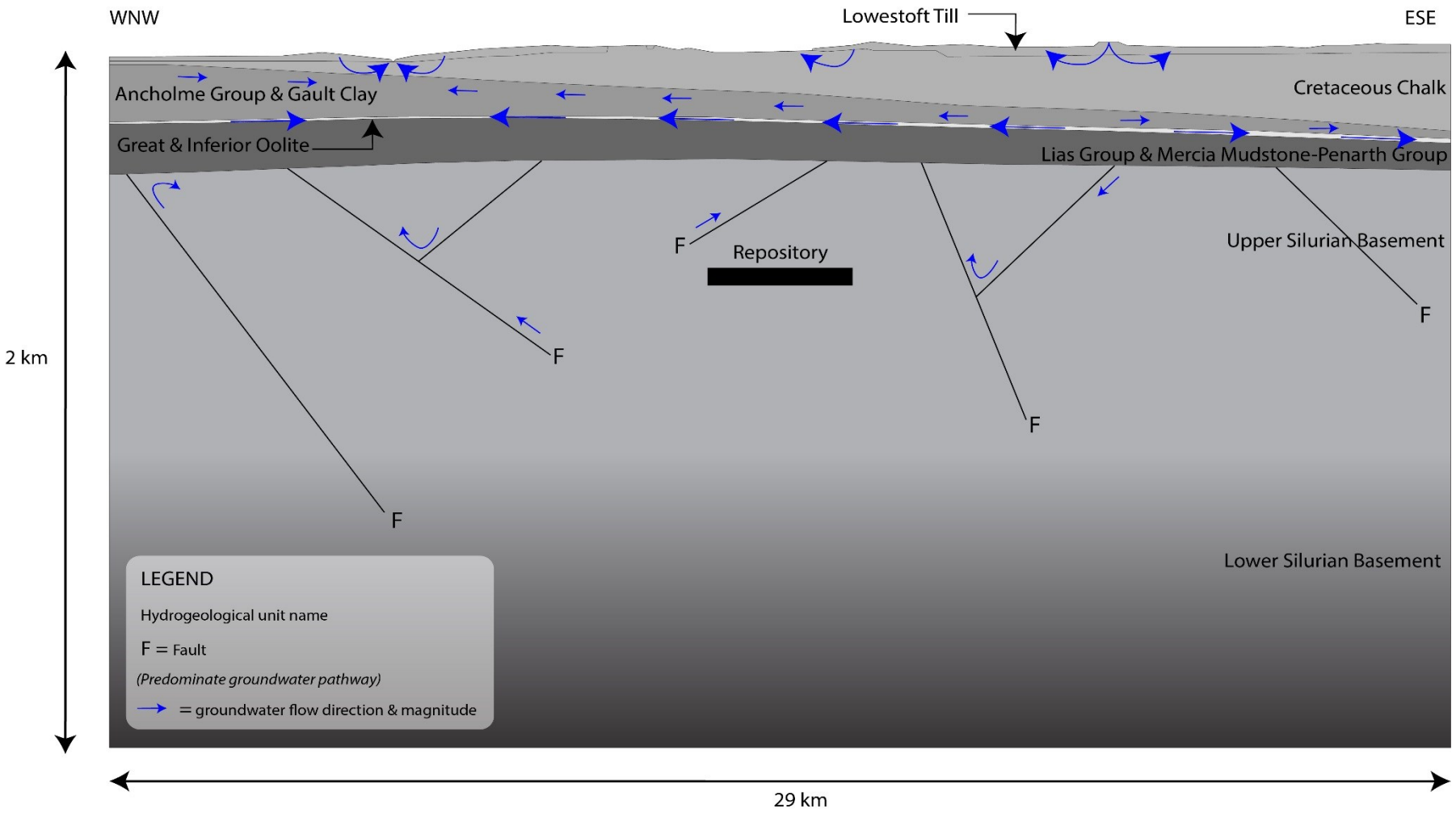

Figure 6.4: Hydrogeological conceptual model of the Thetford Site including the main hydrogeological units, predominate pathways, and the direction and magnitude of groundwater flow

6.4 Model Construction & Development

6.4.1 Geometry & Mesh

The two-dimensional geometry and mesh (Figure 6.5) of the Thetford model is based on the information highlighted in section 6.3, and comprises 60,084 nodes and 117,461 elements.

6.4.2 Boundary Conditions

Pressure, mass and temperature boundary conditions have been applied as presented in Figure 6.6. A linear mass concentration of 1000 kg/m^3 progressing down to 1017.4 kg/m^3 at the base of the East-Southeast boundary has been applied. This basal value is based on the chloride concentration recorded at the base of Borehole 2 (1586 m depth), situated within the 'Hills and Basement Regime' of West Cumbria (see section 4.4 & 6.2.2). The Hills and Basement has been used as an analogy due to their Caledonian aged alteration, fracture dominated flow, and saline-brackish waters, without an apparent lithological salt source.

Temperature boundaries have been calculated based on generic surface temperatures and geothermal gradients (Downing & Gray 1986). Pressure boundaries have been calculated based on atmospheric pressures, and sub-surface hydrostatic pressure gradients. The equations used for boundary condition calculation are presented within section B.1.6.

6.4.3 Material Parameters

The material parameters of porosity, permeability (both most-likely and high), mass dispersion, heat dispersion, storativity, bulk density, thermal capacity and thermal conductivity have been applied specifically, and uniformably, to each lithological unit (section E.1). Heat capacity and heat conductivity have been applied as constants (section B.1.3.2), as has the fluid viscosity and density functions (section B.1.3.1).

As the nature of the fracture network within the Silurian basement is presently unknown, a permeability of faulted crystalline rock will be applied to the entire basement, which conservatively assumed released radionuclides will travel along fractures, unconstrained by direction.

6.4.1 Numerical control

Numerical control was achieved by capping the permeability range to 5 orders of magnitude (1.00E-13 and 1.00E-018 m^2) and setting mass and heat dispersivity to either 10 or 50, explained in section B.1.4.2, with the values ascribed detailed in section E.1.

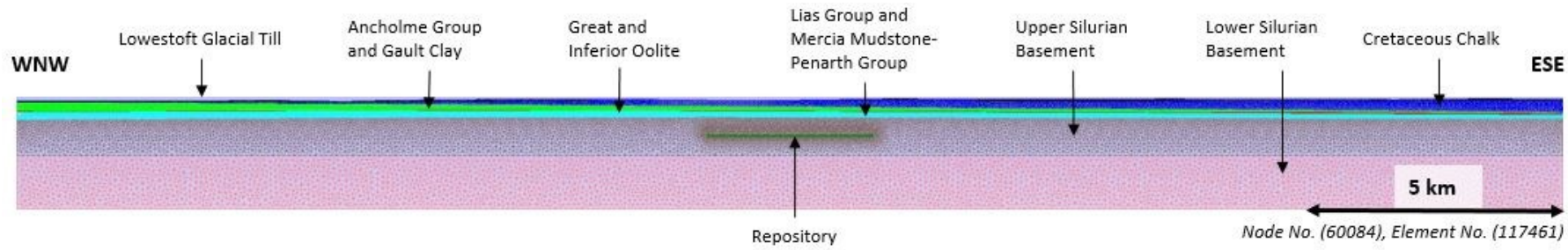

Figure 6.5: Mesh of Thetford site

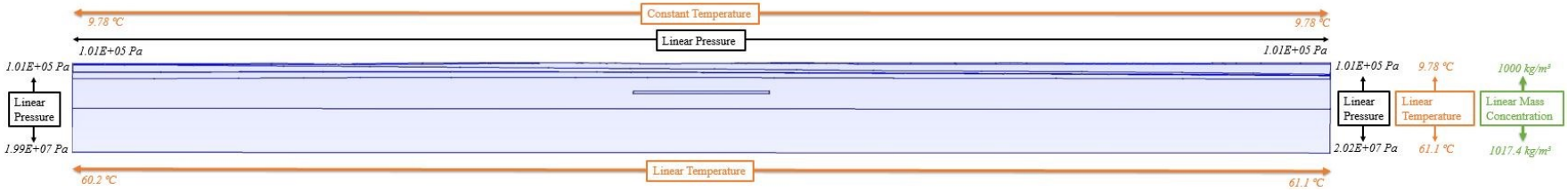

Figure 6.6: Boundary conditions applied to Thetford model

6.4.1 Initial conditions

Initial conditions for pressure (Figure 6.7) were applied based on a pressure gradient calculated using Equ.B.7.

The initial mass concentration for the sedimentary cover (Figure 6.8) is based on a linear gradient from freshwater at the surface (1000 kg/m^3), down to a mass concentration of 1003.3 kg/m^3 at -312.5 m depth, using a 3,300 mg/l chloride value from 347 m depth within BH9A at Sellafield (Bath et al. 2006). This chloride value is considered suitable to use due to the similar depth and location within a fresh-brackish groundwater system, as previously reported for the Chalk by (British Geological Survey 1976). The initial mass concentration for the basement (Figure 6.8) extends down to 1017.4 kg/m^3, using a 17,400 mg/l chloride value from 1586 m depth within BH2 at Sellafield (Bath et al. 2006). Again, this chloride value is considered suitable to use due to the similar depth and location within a saline groundwater system (see section 4.2). However, further work would be required to obtain site specific salinity values.

Initial conditions for temperature (Figure 6.9) were applied based on a typical continental gradient of 0.025 °C/m (Dowing & Gray 1986). Applied initial conditions for mass were specified for 1) the sedimentary cover, and 2) the Caledonide Basement.

In order to achieve quasi-steadystate conditions (see section 9.2), models were solved for hydraulics first, followed by coupled hydraulic, heat transport and mass transport. Once quasi-steadystate was reached, transient coupled hydraulic, heat transport and mass transport were simulated. The coupled TH model was made transient by the addition of a storage term. A summary log of model runs, including initial conditions is presented within section E.2.

6.4.2 Model calibration

No calibration was possible for the Thetford models due to an absence of site specific data. The purpose of these models is however to guide further far-field hydrogeological research rather than to undertake an absolute risk assessment of the quality of a site for deep geological disposal, as discussed within section 3.1. Therefore, these models are considered appropriate for the objectives of this research.

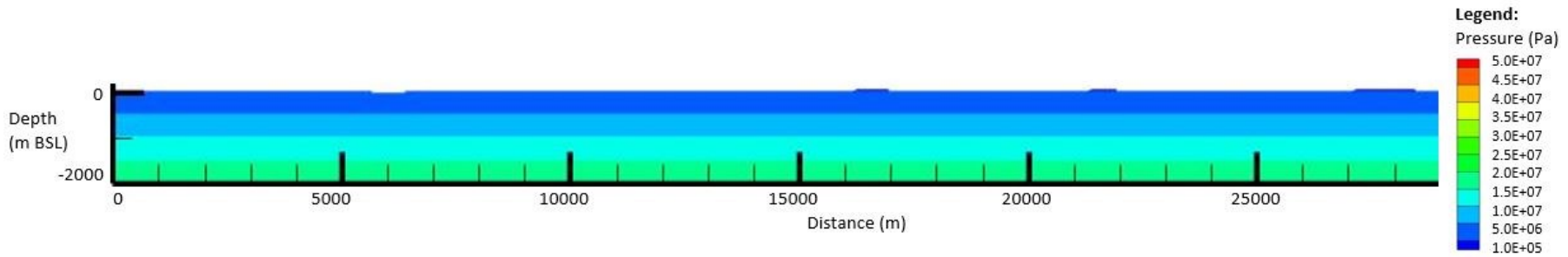

Figure 6.7: Pressure (Pa) initial conditions across the Thetford model domain.

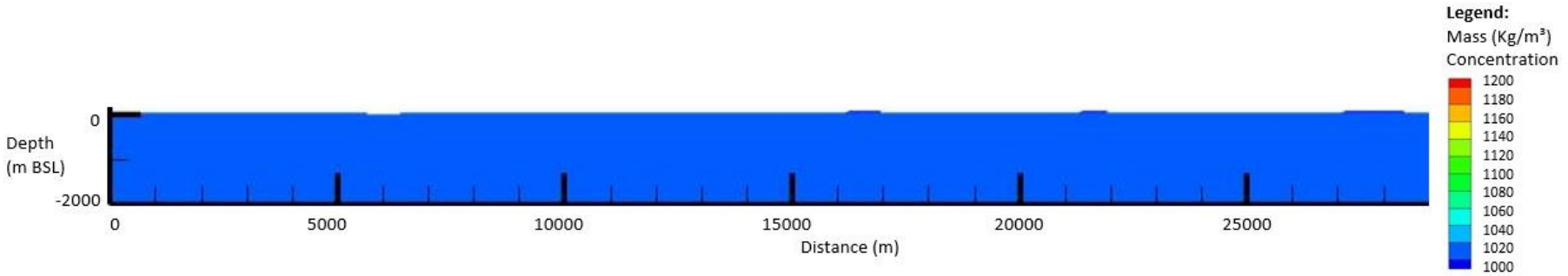

Figure 6.8: Mass Concentration (Kg/m³) initial conditions across the Thetford model domain.

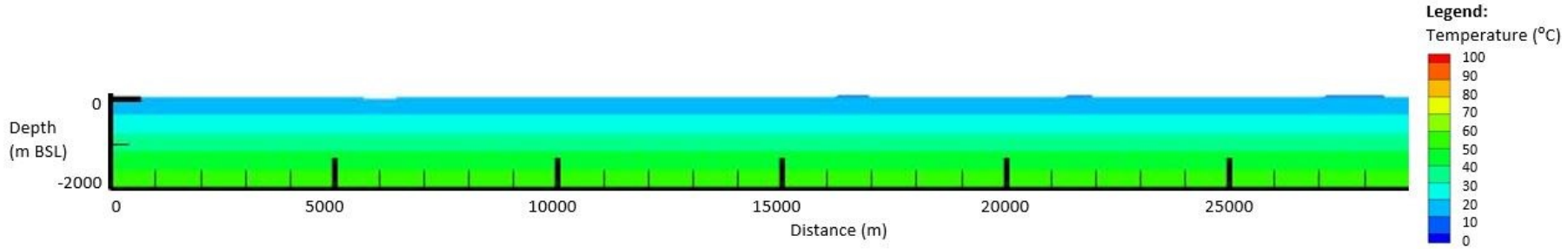

Figure 6.9: Temperature (°C) initial conditions across the Thetford model domain.

6.5 Results: Hydrogeological Parameters

For a description of the method used to analyse the far-field hydrogeological characteristics of the Thetford site against the benchmark hydrogeological scenario, see section 3.3.

6.5.1 (P.1) Far-field Groundwater Velocities

Far-field groundwater velocities range between 5.00E-13 and 5.00E-08 m/s but predominately between 1.00E-12 to 1.00E-08 m/s for the most likely permeability scenario (Figure 6.10B). 56 % of this groundwater system has 'slow' groundwater movement, including the lower Silurian Basement and the Lias Group & Mercia Mudstone Group (Figure 6.10A). Far-field groundwater velocities range between 1.00E-12 and 1.00E-06 m/s but predominately between 1.00E-11 to 1.00E-07 m/s for the high permeability scenario (Figure 6.11B). 47 % of this groundwater system is 'slow' moving, including the lower Silurian Basement but not the Lias Group & Mercia Mudstone Group (Figure 6.11A).

In both modelled scenarios, the lowest far-field groundwater velocities are observed within the Lias Group & Mercia Mudstone Penarth Group, and within the Lower Silurian Basement (Figure 6.10B & Figure 6.11B). The highest far-field velocities are found within portions of the overlying sedimentary cover sequence, such as the Cretaceous Chalk and the Great and Inferior Oolite, and also within the Upper Silurian Basement (Figure 6.10B & Figure 6.11B).

6.5.2 (P.2 & P.3) Groundwater Pathway Length & Discharge Depth

The groundwater pathway within the most likely permeability scenario progresses within the Upper Silurian Basement, for a distance of *approx.* 12,900 m, before exiting the model at a depth of *approx*. -750 m along the WNW boundary, which equates to a deepening of 150 m relative to repository top (Figure 6.10B).

The groundwater pathway within the high permeability model has in contrast two distinct pathways. The first, which is similar to the most likely permeability scenario, progresses within the Upper Silurian Basement, for a distance of *approx.* 13,000 m, before exiting the model at a depth of -783 m along the WNW boundary, and equates to a deepening of 183 m relative to repository top (Figure 6.11B). The second progresses up through the Upper Silurian Basement into, and through, the overlying sedimentary sequence for a distance of *approx.* 3,100 m, before exiting the model at the surface. This equates to a shallowing of 630 m relative to the repository top (Figure 6.11B). It is the results from this second pathway that will be used for comparison against the benchmark hydrogeological scenario, as it is considered the 'worst-case' scenario due to the surface discharge and progression through the major potable Chalk aquifer.

6.5.3 (P.4) Radionuclide travel distance over 10,000 years

Released particles travel a maximum distance of 375 m over 10,000 years in a system populated with most likely permeability values (Figure 6.10C). When the same pathway is simulated with sorption (Table 6.1), Cl^{36} has a retardation factor of 1 so travels an unaltered distance of 375 m; Tc^{99} is retarded by 1.2 which equates to a distance of 312.5 m; both Se^{79} and U^{238} are retarded by 1.32 which results in a distance of 284.1 m; Cs^{135} is retarded by a factor of 27.7 which results in a distance of 13.5 m; and finally Ni^{59} is retarded by a factor >200 which results in a travel distance of <1.9 m. Neither Am^{241}, Eu^{152}, nor Sr^{90} are detected during model simulation (Table 6.1).

The radionuclide travel distance is slightly more complicated for the high permeability scenario, with two distinct pathways identified. Radionuclides travelling along the first pathway (pathway 1) travel a maximum distance of 5,574 m. Those travelling along the second (pathway 2) travel a maximum distance of 3,118 m (Figure 6.11C).

When pathway 1 was simulated with sorption (Table 6.1), Cl^{36} showed a retardation factor of 1 so travels an unaltered distance of 5574 m; Tc^{99} by 1.21 which results in a travel distance of 4606.6 m; both Se^{79} and U^{238} by 1.28 which results in distances of 4354.7 m; Cs^{135} by 27.8 which results in a distance of 200.5 m; and finally Ni^{59} by >200 which results in a travel distance of <27.9 m. Neither Am^{241}, Eu^{152} nor Sr^{90} are detected during model simulation (Table 6.1).

When pathway 2 was simulated with sorption (Table 6.1), Cl^{36} showed a retardation factor of 1 so travels an unaltered distance of 3118 m; Tc^{99} by 1.18 with a travel distance of 2642.4 m; Se^{79} by 1.2 resulting in a distance of 2598.3 m; U^{238} 2.83 resulting in a distance of 1101.8 m; Cs^{135} by 38.5 resulting in a distance of 81 m; and finally Ni^{59} by >200 which results in a normalised travel distance of 15.6 m. Neither Am^{241}, Eu^{152}, nor Sr^{90} are detected during model simulation (Table 6.1).

6.5.4 Comparison against Hydrogeological Conceptual Model

The most likely permeability scenario (Figure 6.10B) shows pressure driven ESE to WNW groundwater flow, with strong hydraulic decoupling (little flow) between the overlying sedimentary sequence, and the Silurian basement, as anticipated with the conceptual model (section 6.3). The high permeability scenario (Figure 6.11B) however, although also showing east-southeast to west-southwest pressure driven flow, shows a strong hydraulic coupling between the sedimentary cover and that of the basement, not anticipated within the conceptual model (section 6.3), and not desirable from a radionuclide containment perspective.

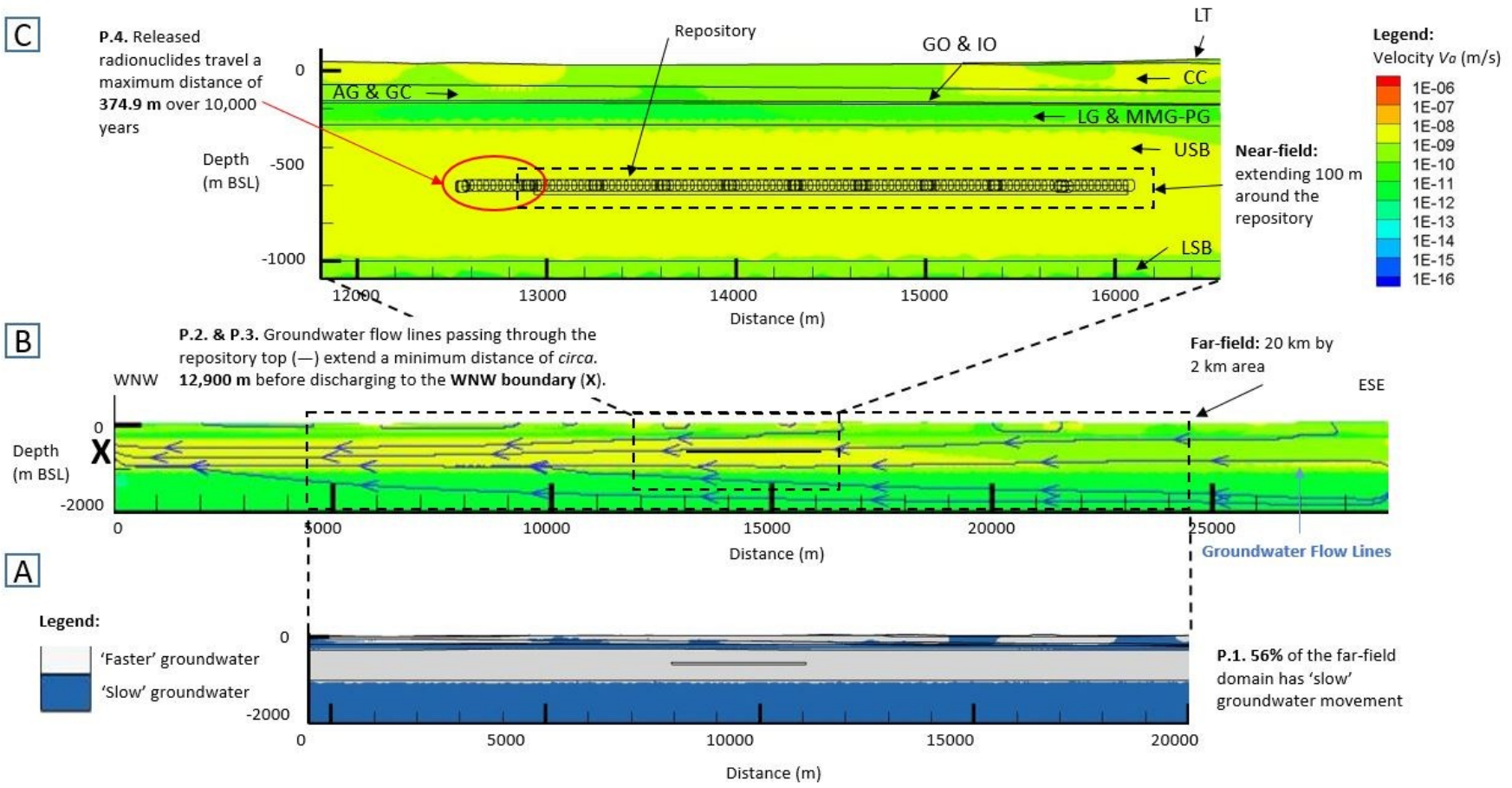

Figure 6.10: Results based on model populated with most likely permeability values. A) Areas of the far-field (20 km by 2 km) domain with 'slow' advective groundwater velocity i.e. <2.00E-10 m/s, B) Advective velocity distribution over the far-field, including groundwater flow lines and hydrogeological regimes, and C) Advective velocity distribution over the near-field, including the progression of particles released from along the top of a hypothetical repository over 10,000 years.

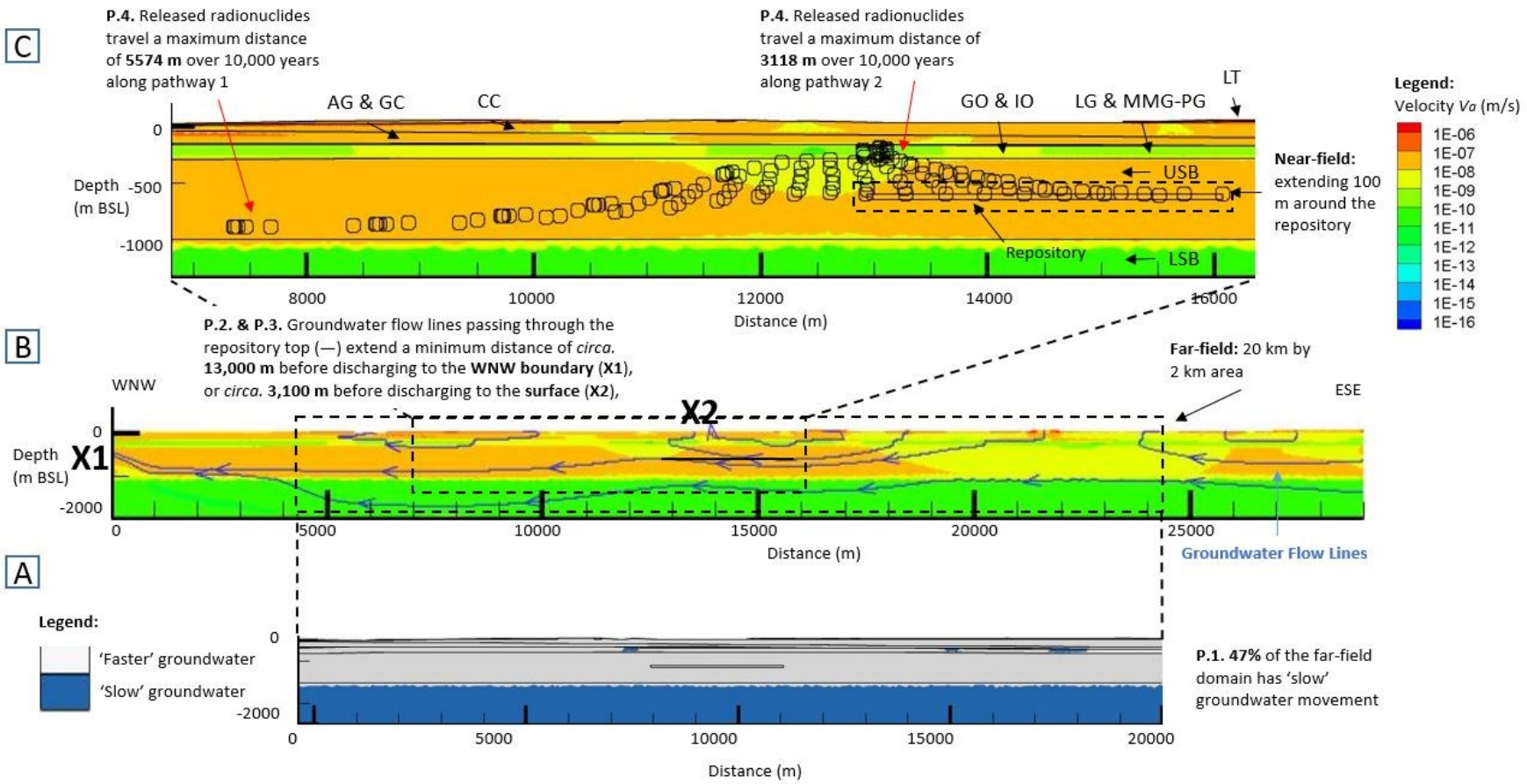

Figure 6.11: Results based on model populated with high permeability values. A) Areas of the far-field (20 km by 2 km) domain with 'slow' advective groundwater velocity i.e. <2.00E-10 m/s, B) Advective velocity distribution over the far-field, including groundwater flow lines and hydrogeological regimes, and C) Advective velocity distribution over the near-field, including the progression of particles released from along the top of a hypothetical repository over 10,000 years.

Table 6.1: Summary of retardation factors and travel distances of selected radionuclides after 10,000 years for maximum particle pathways (streak-lines) from Thetford based on most likely and high permeability modelled scenarios.

Scenario	**Maximum Particle Travel Distance (streak-line length) (m)**	**Radionuclide**	**Am^{241}**	**Cl^{36}**	**Cs^{135}**	**Eu^{152}**	**Ni^{59}**	**Se^{79}**	**Sr^{90}**	**Tc^{99}**	**U^{238}**
		Half-life (yrs)[1]	*432.2*	*3.01E+05*	*2.3E+06*	*13.54*	*1.01E+05*	*2.95E+05*	*28.79*	*2.11E+05*	*4.47E+09*
Most-likely permeability	375	*Retardation Factor (R_f)*	ND(S)	1	27.7	ND(D)	>200	1.32	ND(D)	1.2	1.32
		Travel Distance (m)		375	13.5		1.9	284.1		312.5	284.1
High permeability (pathway 1)	5574	*Retardation Factor (R_f)*	ND(S)	1	27.8	ND(D)	>200	1.28	ND(D)	1.21	1.28
		Travel Distance (m)		5574	200.5		27.9	4354.7		4606.6	4354.7
High permeability (pathway 2)	3118	*Retardation Factor (R_f)*	ND(S)	1	38.5	ND(D)	>200	1.2	ND(D)	1.18	2.83
		Travel Distance (m)		3118	81		15.6	2598.3		2642.4	1101.8

[1]: Radioactive half-lives obtained from (GoldSim Technology Group 2017c)
ND (D): not detected during the 2 million year model run and due to short half-lives, interpreted to have undergone radioactive decay
ND (S): not detected during the 2 million year model run, and due to very long half-lives, interpreted to have sorped rather than decayed
When retardation factor is >200, the radionuclide travel distance has been calculated based on a retardation factor of 200.
[Retardation values validated using the GoldSim risk assessment modelling software, detailed within Appendix B.2 and F].

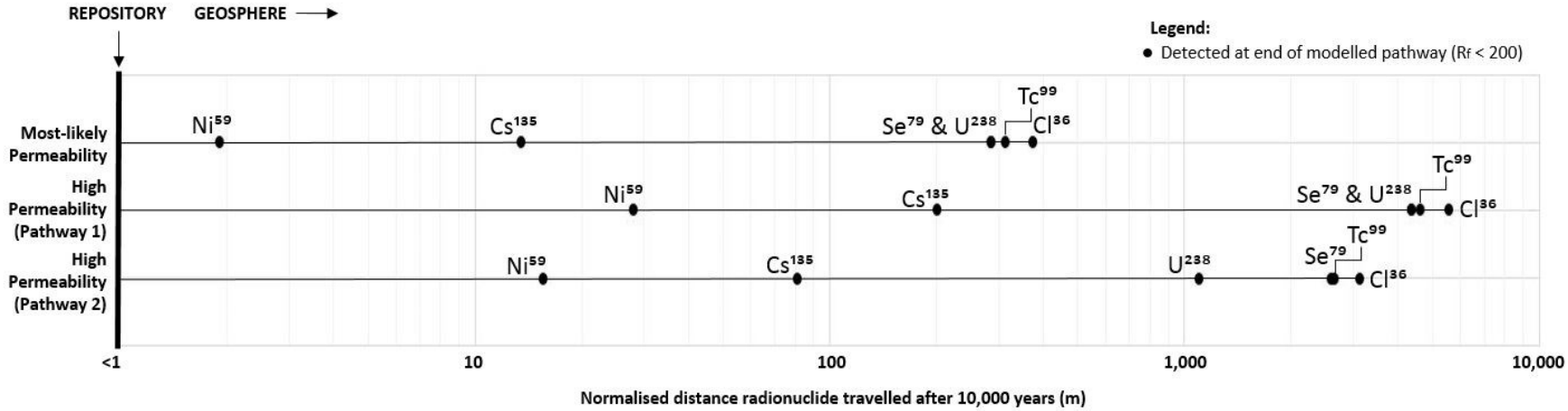

Figure 6.12: Comparison of radionuclide travel distances at Thetford based on most-likely and high permeability particle pathway streak-lines after 10,000 years. Due to very short half-lives Am241, Eu152 and Sr90 have undergone radioactive decay and as such, are not detected at the end of the modelled pathway

Table 6.2: Summary of results of hydrogeological parameters representing hydrogeological characteristics considered of importance for long term radioactive waste containment and isolation, generated from most likely permeability and high permeability modelled scenarios.

Hydrogeological Parameters	**Peak Repository Temperature**	**Pathway**	**(P.1)** Percentage of the far-field (20 km by 2 km) domain with 'slow' advective groundwater velocity (%)	**(P.2)** Total length of quasi-steadystate groundwater pathway from repository top to discharge point (m)	**(P.3)** Depth of quasi-steadystate groundwater pathway discharge point relative to repository top (m) where '-' represents a shallowing, and '+' represents a deepening	**(P.4)** Radionuclide travel distance over 10,000 years (m) (variable depending on radionuclide)
Most-likely permeability scenario	*Baseline*	1	56	12,900	+150	<1.9 to 375
High permeability scenario	*Baseline*	1	47	13,000	+183	<27.9 to 5,574
		2		3,100	-630	<15.6 to 3,118

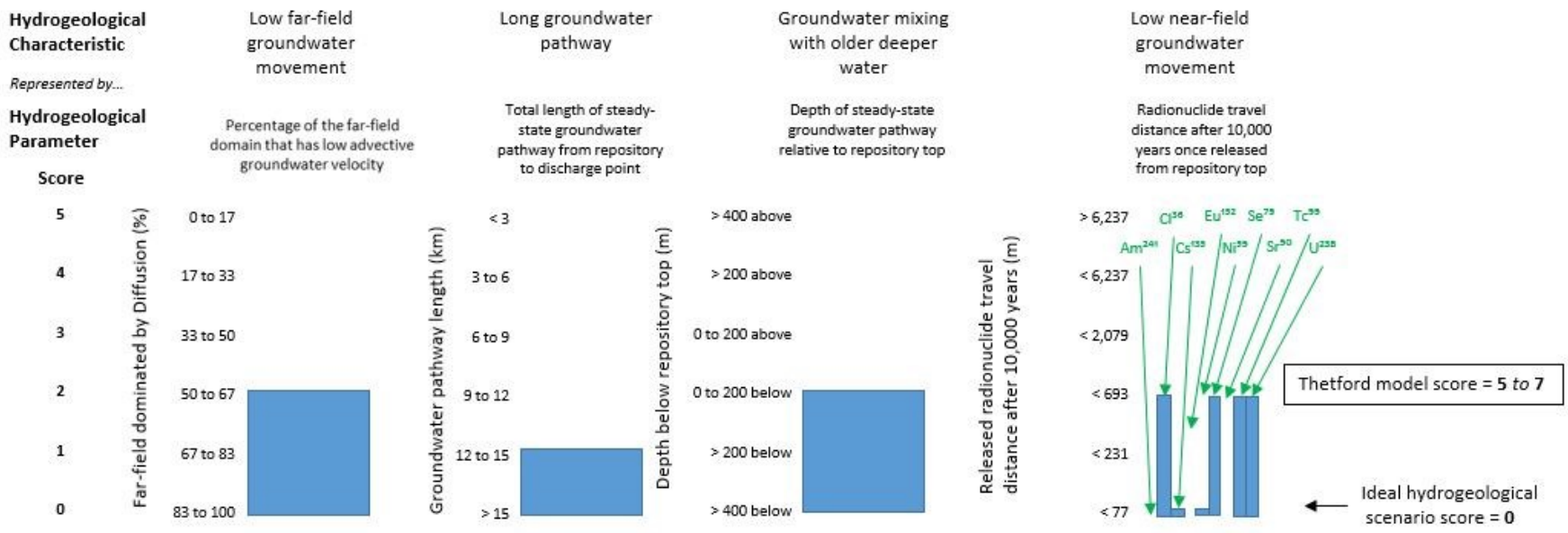

Figure 6.13: Summary chart of Thetford hydrogeological parameters based on most-likely permeability values plotted and scored against 'ideal' hydrogeological parameters.

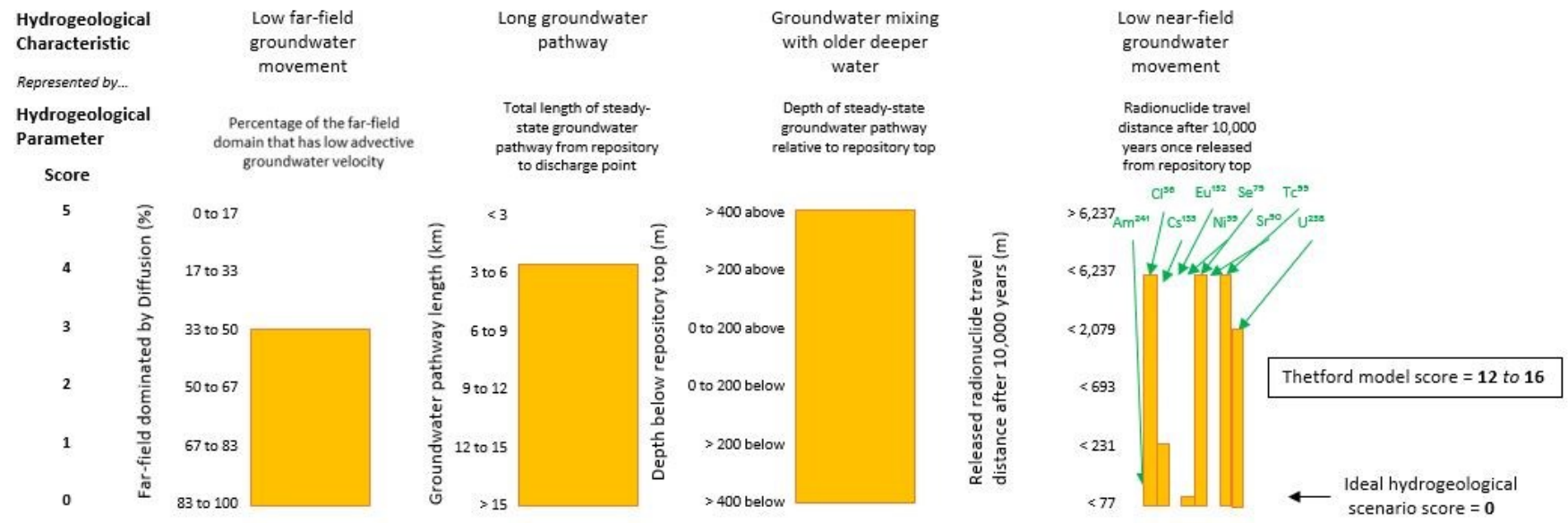

Figure 6.14: Summary chart of Thetford hydrogeological parameters based on high permeability values plotted and scored against 'ideal' hydrogeological parameter

6.6 Discussion: Hydrogeological Characteristics

6.6.1 Far-field hydrogeological characteristics under variable permeability scenarios

Modelling of the Thetford site shows that the uncertainty in permeability has a big effect on the regional groundwater characteristics, and thus, based on the current uncertainty range, the sites' suitability to host a deep geological disposal facility cannot be determined.

Under most likely permeability conditions, the site can be considered analogous to '*basement beneath sedimentary cover'* type hydrogeological regime (Figure 2.11c). This is because flow is dominated horizontally along higher permeability units, with strong decoupling between near-surface and deeper flow. However, under higher permeability conditions, groundwater readily moves between the near-surface sedimentary sequence and the deeper Silurian basement, creating a direct pathway up to the surface for released radionuclides to migrate along. Groundwater here exits the host rock formation in *approx.* 6,000 years and thus cannot be considered analogous to the hypothesised hydrogeological regime. These findings also highlight the point that 'most-likely' permeabilities cannot be used in isolation to test the suitability of a site.

The defence of the Thetford site is arguably therefore tied into the vertical permeability of the overlying sedimentary cover sequence, and its ability to prevent vertical radionuclide migration. Similar functions can be observed in the cap-rocks of oil and gas reservoirs, and carbon capture and storage sites. Focused site specific research is therefore required to determine the vertical permeability range of the lower lithological units of the overlying sedimentary sequence.

As the Lower Silurian Basement also expresses much lower groundwater velocities than that of the Upper Silurian basement, where the theoretical repository is currently situated, repository development deeper within the Silurian Basement, >1 km depth, may also prove beneficial for *containment* and *isolation*. Further site specific research is therefore recommended to determine the permeability-depth relationship of Silurian Basement, with particular focus on characterisation of the Silurian Basement fracture network required.

6.6.2 Effects of chemical sorption on radionuclide containment and isolation

Simulation of sorption at Thetford for migrating radionuclides under variable permeability scenarios shows a large variation in retardation rates (1 to >200), and consequently a large variation in normalised radionuclide travel distances over the first 10,000 years i.e. ranging

between <1.9 and 375 m for the most likely permeability pathway, and <15.6 to 3,118 m for pathway 2 of the high permeability pathway (Table 7.2).

Although the most likely permeability model and pathway 1 of the high permeability model show similar radionuclide breakthrough and retardation characteristics (Table 6.1), retardation is markedly greater for Cs^{135} and U^{238} along pathway 2 of the high permeability model. This is interpreted to be a result of the overlying Lias Group & Mercia Mudstone-Penarth Group through which Pathway 2 of the high permeability model passes. The high clay content of the Lias Group & Mercia Mudstone-Penarth Group is considered to effectively sorb certain migrating radionuclides, and as such, not only has the potential to provide an effective physical barrier to groundwater flow (see section 6.6.1), but can also provide an important chemical barrier to radionuclide migration.

6.6.3 Comparison to beneficial hydrogeological characteristics and the benchmark hydrogeological scenario

Comparison of the Thetford site against the benchmark far-field hydrogeological scenario (section 3.3.4) can be ascribed a score of between '5 and 7/20', depending on the radionuclide, when modelled with most likely permeability values (Figure 6.13), and between '12 and 16/20', depending on the radionuclide, when modelled with high permeability values (Figure 6.14).

As the total scores of the most likely and high permeability models do not overlap, regional permeability values can be considered to have a larger impact on the suitability of a site to *contain* and *isolate* radionuclides than that of the chemical characteristics based on the selected method of assessment.

Furthermore, if permeabilities were similar to most-likely permeability values, Thetford could exhibit beneficial hydrogeological characteristics for long term radionuclide *containment* and *isolation* characterised by: 1) long groundwater pathways; 2) groundwater pathways progressing deeper; and 3) slow groundwater movement through the overlying sedimentary sequence, causing decoupling of shallower and deeper groundwater flow (section 2.3.6). If permeability values were however similar to the high permeability values applied, the site could not be considered to exhibit beneficial hydrogeological characteristics. This is due to: 1) short pathways; 2) pathways ascending up towards the surface; and 3) faster flowing water through the overlying sedimentary layers, causing a direct pathway between shallow and deep groundwater, despite effective chemical sorption. Site specific research is therefore recommended to refine the vertical permeability range of the overlying sedimentary sequence.

6.7 Conclusion

Based on the current uncertainty in regional scale permeability at the Site, the far-field hydrogeological suitability of the Thetford Site to host a deep geological disposal facility cannot be determined. However, if the regional scale permeability ranges are found to be most similar to the 'most-likely' permeability scenario, the Thetford site has potential to be analogous to a *'basement rock beneath sedimentary cover'* type hydrogeological regime. In this case the Thetford site could be considered to exhibit beneficial characteristics to host a deep geological disposal facility.

More research is therefore required to more clearly constrain permeability ranges at the Thetford site, especially the vertical permeability ranges of the overlying sedimentary sequence, which would play a key role in preventing vertical radionuclide migration.

6.8 Assumptions, Limitations and Recommendations

In addition to the key modelling method limitations outlined in section 3.5, the following key limitations, specific to the Thetford model, have also been identified:

1. Interpretation of the lithological sequence at the site is based on boreholes located outside of the 2D cross-section, or on analogous formations. Further research is therefore required to more clearly constrain the lithological sequence and thicknesses of units at the site, and the dominant groundwater flow direction across the region.

2. Material medium properties and material solid properties applied to hydrogeological units based on interpretation of 'primary' lithological constituent only.

3. Average horizontal and vertical permeabilities calculated for Ancholme Group & Gault Clay, and the Lias Group & Mercia Mudstone-Penarth Group based on interpreted primary lithology per sub-unit only.

4. Site specific pressure, temperature and salinity data required to improve model parameterisation, boundary conditions and calibration.

5. Fractures were not explicitly modelled within the Silurian Basement (section 6.4.3) and as such, fracture characterisation of the basement, with particular emphasis on the permeability-depth relationship should be determined and applied to the model.

Chapter 7 Comparison of the Prospective Far-Field Hydrogeological Characteristics of the Assessed Sites

Determination and assessment of the far-field hydrogeological characteristics of Sellafield, the Tynwald Basin and Thetford, against the benchmark hydrogeological scenario, are detailed within Chapters 4 to 6 respectively. This chapter presents a summary of those findings, and compares the prospective far-field hydrogeological characteristics of the three settings.

Consideration of the far-field groundwater characteristics reveals that the Tynwald Basin has the greatest promise for long term radionuclide containment and isolation out of the three modelled sites, regardless of permeability uncertainty (Figure 7.2 and Figure 7.3), and in despite of its lack of effective chemical retardation potential (Figure 7.1). The Tynwald Basin has scores of '3/20' and '4/20' for most-likely and high permeability scenarios respectively (where '0/20' represents an *ideal* hydrogeological scenario). Permeability only changes the overall score by 1 points i.e. 5 % and is thus relatively predictable. Although the Tynwald Basin cannot be considered directly analogous to the *'seaward dipping and offshore sediments*' hydrogeological regime (section 2.3.7), the Tynwald Basin can be considered to show promising groundwater characteristics for long term radionuclide containment and isolation. This is due to its very slow local and regional groundwater movement, and long and deepening groundwater pathways. The groundwater density across the regional setting due to dissolved salts, in addition to the low permeability of the Mercia Mudstone Group and low hydraulic gradient, are considered major controls on the regional groundwater movement here. The regional density profile and Mercia Mudstone Group permeability should be the focus of any future Tynwald Basin studies.

Thetford also shows promise with a score of '5-7/20' when modelled with most-likely regional lithological permeabilites, and is considered analogous to *'basement rock beneath sedimentary cover'* hydrogeological regime (section 2.3.7). However, when modelled with higher permeability values, the score increases to '12-16/20' and is no longer analogous to any of the hypothesised hydrogeological regimes (section 2.3.7), and thus cannot be considered to express beneficial far-field groundwater characteristics for radionuclide containment. The current permeability uncertainty at Thetford has a major influence on the groundwater characteristics (11/20 points i.e. 55 %), and work should be undertaken to reduce this uncertainty, especially as the site shows promise. Particular focus should be paid to the vertical

permeability of the overlying sedimentary sequence which has a major control on the regional groundwater characteristics and prospective site performance by controlling the coupling between near-surface and deep groundwater flow (section 2.3.6), and effectively sorbing certain migrating radionuclides (Figure 7.1).

Finally Sellafield is also moderately predictable in its far-field groundwater characteristics, with scores of ’12/20’ and ’14-16/20’ respectively (a change of 4/20 points i.e. 20 %). However, the setting cannot be considered to exhibit wide ranging beneficial groundwater for radionuclide containment and isolation due to vertically ascending water and rapid return rates, despite some chemical sorption potential provided by the overlying Brockram Breccia. Furthermore, this research confirms previous investigations undertaken at Sellafield e.g. (Fraser Harris et al. 2015), which show that despite Sellafield having a geological section of ‘basement rock beneath sedimentary cover’, the regional setting cannot be considered analogous to the hydrogeological regime *‘basement rock beneath sedimentary cover’* (section 2.3.7). This is due to blocking nature of the Dense Irish Sea Brine Formation, facilitating groundwater flow up towards the surface, coupling the deep and near groundwater systems.

In summary: 1) the Tynwald Basin shows the greatest prospectivity out of the three sites performing between 3.5 and 4 times better than Sellafield, and between 1.7 and 4 times better than Thetford (Figure 7.3); 2) the natural barrier performance of Thetford cannot at present be determined due to parameter uncertainty, although if permeability is closest to most-likely modelled values, the site could performance up to 2.4 times better than Sellafield; and 3) the role of chemical processes over physical processes in controlling radionuclide travel distances is setting dependent, with chemical processes playing a greater role at Sellafield and Thetford (R_f = 1 to 200) than that of the Tynwald Basin (R_f = 1).

These findings are significant as they illustrate that: 1) the UK possess a range of variable quality far-field barriers for the safe long term disposal of radioactive waste; 2) the far-field quality of a site should not be determined based on a single/central metric, but a variety; and 3) a simple method of site comparison is possible under steadystate groundwater conditions.

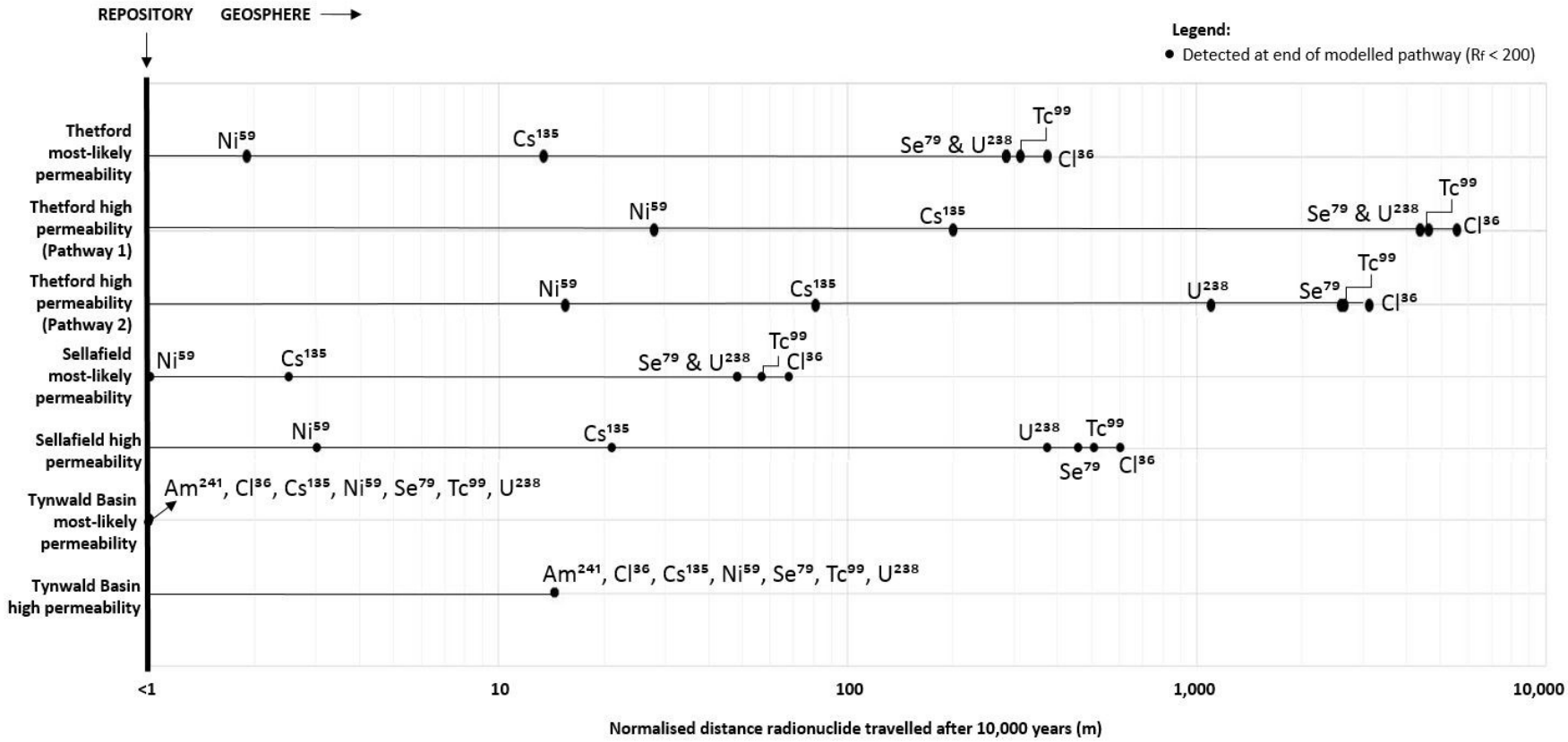

Figure 7.1: Comparison chart of normalised radionuclide travel distances over 10,000 years based on groundwater particle pathways (streak-lines) generated for each modelled site under variable permeability conditions.

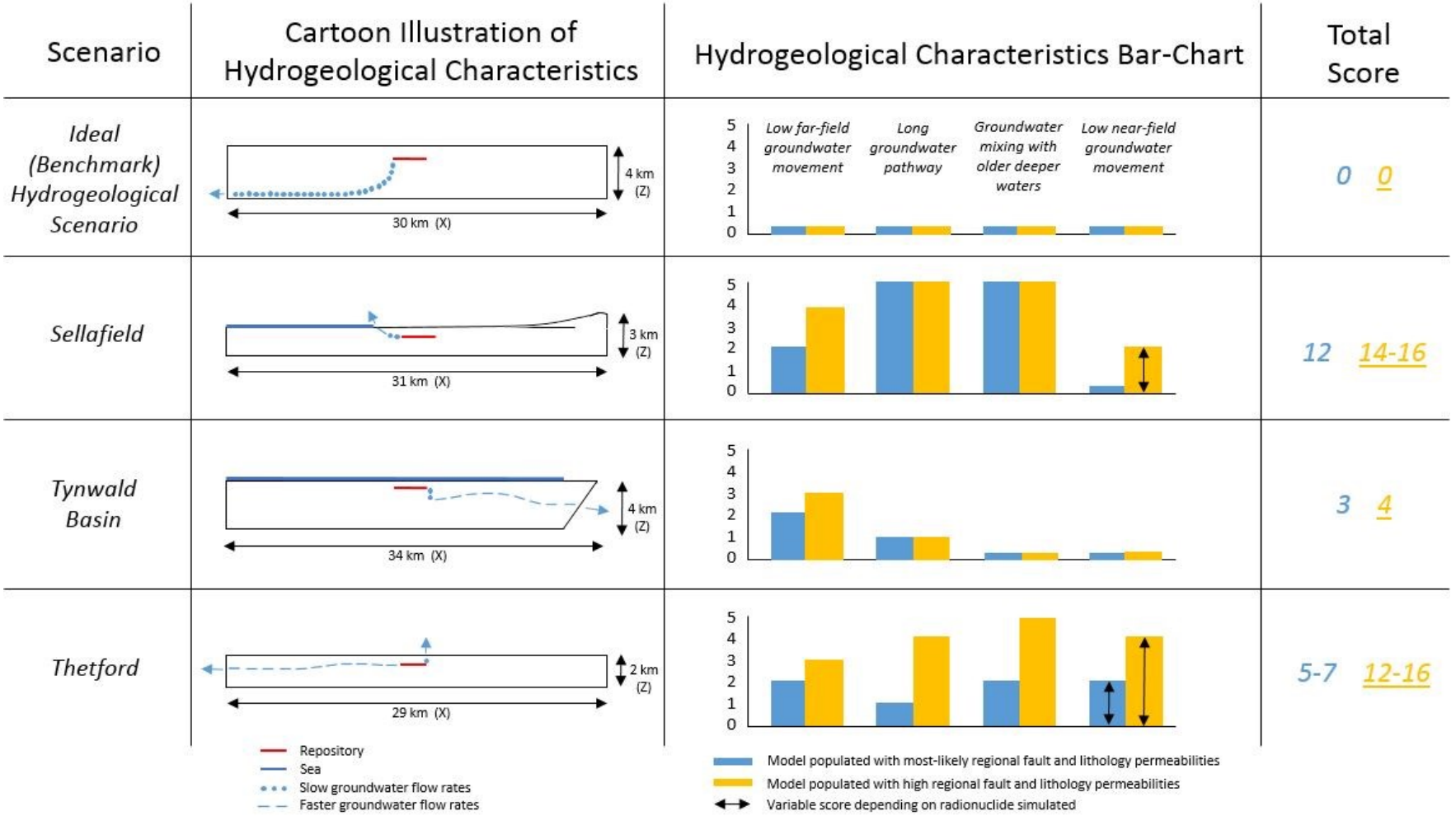

Figure 7.2: Summary comparison chart illustrating the hydrogeological characteristics and total scores of the three modelled sites (Sellafield, Tynwald Basin and Thetford) against a benchmark far-field hydrogeological scenario.

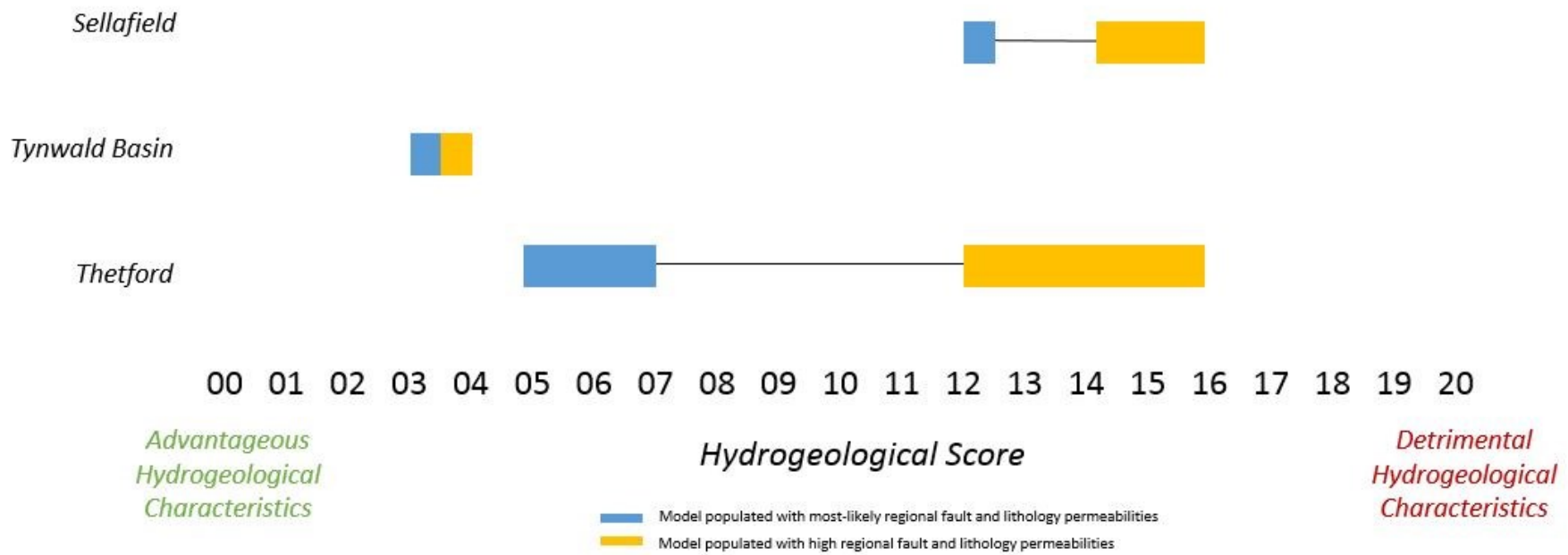

Figure 7.3: Summary chart illustrating the position of the hydrogeological scores of the three sites against each other. The Tynwald Basin can be seen to exhibit the most advantageous far-field hydrogeological characteristics for long term radionuclide containment and isolation.

Chapter 8 The Change in Far-Field Groundwater Characteristics as a Result of Higher Activity Waste Emplacement: Defining the Near-Field and Far-Field

8.1 Context

The context for this chapter was introduced within sections 2.3.4 and 2.7.6. The reason that the effect of heat was not considered as part of the regional groundwater comparison (summarised in Chapter 8) is due to the dynamic transient behaviour of radiogenic heat emission and decay, against which quantification of static groundwater velocities, pathway lengths and discharge depths were found to be challenging. Analysis of the effect of radiogenic heat emission on the far-field groundwater flow pattern and characteristics has therefore been considered separately.

8.2 Aim & Hypotheses

The aim of this chapter is to explore the physical extent to which radiogenic heat emission, from emplaced higher activity radioactive waste, disturbs the natural groundwater characteristics at three different UK settings. The hypothesis addressed in this chapter is hypotheses 2 from section 1.3.3 as follows:

2. Does the regional geological and hydrogeological setting control the effect of radiogenic heat emission on natural groundwater flow patterns?

8.3 Method

8.3.1 General Approach

This chapter will build on the coupled TH models previously developed for the sites of Sellafield, the Tynwald Basin and Thetford, reported in Chapters 5 to 7.

Most likely and high permeability models developed for the three sites were also run for 10,000 years with radiogenic heat emission and decay, reaching a peak repository temperature of 90 °C, although only the results of the 30, 60 and 90 °C models are reported within this chapter (Figure 3.8). Modelled scenarios did not reach 100 °C in line with canister designs to ensure fundamental physical and chemical changes are not induced within the surrounding engineering barrier. This is in order to maintain the required safety functions (see section 1.1.4).

Results have been presented as the relative (factor) change in advective groundwater velocity compared to baseline (no radiogenic heat emission) for increasing peak repository temperatures, across the far-field domain. The factor change approach was chosen as it enables changes to low permeability formations to be captured, identifying those areas most sensitive to radiogenic heat emission. The relative factor change has been presented for 100, 1,000 and 10,000 years after waste emplacement. Results are reported only when above 5% of the baseline velocity, and when values are geospatially significant i.e. do not occur at a single node.

The change in the maximum distance a particle has migrated from the repository over 10,000 years with increasing peak repository temperature has been reported and determined using '*streak-lines'* (section 3.4.3). However, where travel distance remains below 1 m the increase has not been reported as these values are considered small in the scheme of possible particle travel distances.

To ensure the full effect of radiogenic heat emission and decay on the groundwater system is captured, particles were released after 1, 2, 3, 10, 30, 100, 300 and 1,000 years, after which particles were released every 1,000 years, up until 10,000 years.

8.3.2 Radiogenic Heat Emission Representation

The uncertainty in peak repository temperature over time comes from the heat generated by the decay of radionuclides within the higher activity waste packages. The waste packages will express different *'heat decay curves'* depending on the canister design and the waste composition (McGinnes 2002). As these waste-canister packages are emplaced within the repository, the repository too will express a characteristics heat decay curve, which must be defined for this research.

A 'typical' heat decay rate curve (W/canister) has been fitted to predefined radiogenic heat output from a three-dimensional steel 'BE-6' style canister (Johnson & King 2003) for spent fuel respectively (McGinnes 2002). The heat decay curve assumes emplacement 40 years after removal from the reactor (Figure 8.1) (McGinnes 2002). The function fitting the 'typical' decay curve is presented within Equ.8.1.

$$y = h_0 e^{-1\times10^{-10}t} \qquad (8.1)$$

Where y is the heat decay rate (W/canister/s), t is time (s) and h_0 is the initial starting heat, and is 2000 W/canister in the case of the 'typical' decay curve.

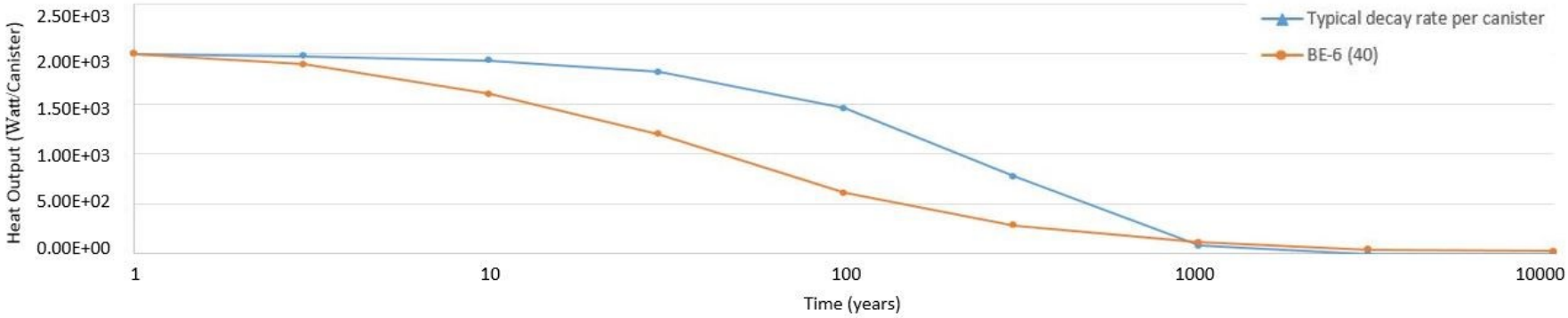

Figure 8.1: Graph presenting a 'typical' decay curve fitted to a predefined radiogenic decay curve for canister style BE-6, which assumes emplacement 40 years after removal from the reactor (McGinnes 2002).

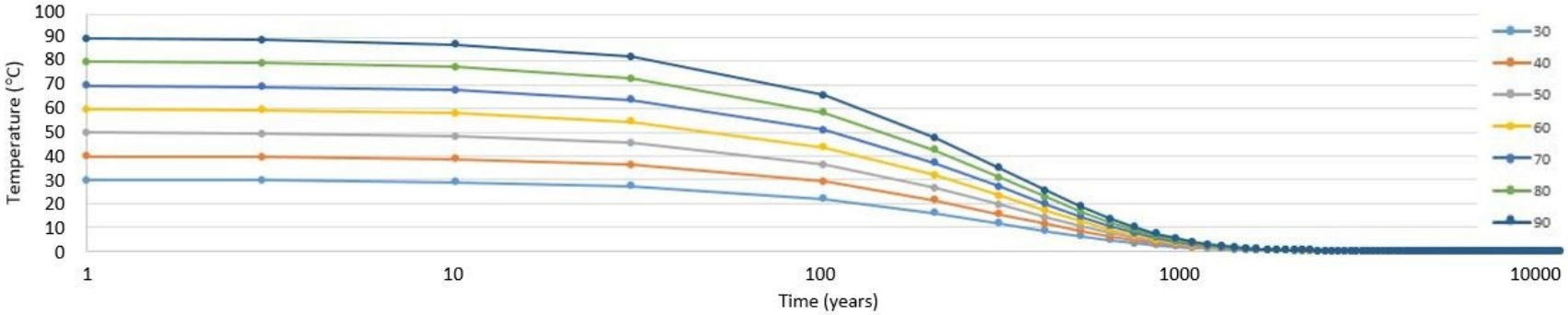

Figure 8.2: Temperature decay curves for incremental initial starting temperatures based on the 'typical' heat decay curve function.

The decay curve presented in Figure 8.1 is based on a three-dimensional canister (X, Y, Z) whilst model simulation will be undertaken in two-dimensions only (X, Z). Application of three-dimensional heat output to a two-dimensional section would result in an over estimation of heat generated across the cross-sectional area. Furthermore, the two-dimensional model could only disperse the heat in two dimensions, rather than the required three-dimensions, causing further unrepresentative heat build-up and a consequential uncontrolled rise in temperature, exceeding the 100 °C limit. As such, heat was instead represented as a temperature boundary condition along the centre of the repository, thus controlling the amount of heat emitted.

Heat E_h is the total amount of kinetic energy transferred from a system with units of (J), with temperature T a measure of the average kinetic energy of that system with units of (K). Heat and temperature are thus proportional, and are related through the heat capacity c (J/kg K), and mass m (kg) of the system (Equ.8.2).

$$E_h = c \times m \times \Delta T \quad (8.2)$$

A decrease in temperature therefore results in a proportional decrease in heat. A constant heat capacity and bulk density have been applied to the repository area, which ensures that the temperature decay curve proportionally represents the heat decay curve.

The difference between modelling radiogenic heat emission with a heat decay curve and a temperature decay curve is considered within the uncertainty associated with the final canister design, waste composition, and the number and layout of canisters within the repository. It is for this reason that a number of different temperatures decay curves were simulated, based on the 'typical' heat decay function (Equ.8.1), with peak repository temperatures ranging between 30 and 90 °C (Figure 8.2).

It should be noted that although Figure 8.2 shows decay down to 0°C, the final target temperature will actually be a value representing the average temperature along the repository prior to waste emplacement. The ambient temperature for the repository was obtained from the most likely and high permeability baseline models simulated for the three sites, detailed within Chapters 5 to 7 (see Table 8.1). For example, if prior to waste emplacement, the temperature along the repository ranges from 20.4°c to 22.6°c, the temperature decay curves for that particular site reduce down towards a final average temperature of 21.5 °C. The decay rate was defined by the decay function (Equ.8.2).

Table 8.1: Summary of model simulations run, along with the ambient repository temperatures, towards which the peak repository temperature decayed.

Site	Permeability	Average ambient repository temperature (°C), from the baseline (no heat emission) scenarios	Peak repository temperature (°C)		
			30	60	90
Sellafield	Most likely	25.34	✓	✓	✓
	High	24.56	✓	✓	✓
Tynwald Basin	Most likely	17.59	✓	✓	✓
	High	19.89	✓	✓	✓
Thetford	Most likely	29.77	✓	✓	✓
	High	29.66	✓	✓	✓

8.3.3 Assumptions & Simplifications

These assumptions and simplifications are in addition to those stated for the TH models (section 3.5), and pertain explicitly to radiogenic heat emission simulation:

1. Three-dimensional heat decay curve represented by two-dimensional temperature curve. The uncertainty between modelling heat and temperature on the regional groundwater characteristics are considered within the range of uncertainty generated from final waste package composition and distribution within the repository,
2. Temperature changes are assumed to be even across the repository, however, in reality, heat producing waste (HLW & SF) is likely to be located separate from none heat producing waste (ILW), with temperature changes variable over the repository,
3. Peak repository temperature assumed not to exceed 90 °C on the outside of the canisters as per the design criteria, to limit damage to the engineered barrier facility, through mineralogical changes (see section 1.1.4),
4. Repository temperature assumed to return to baseline temperature i.e. pre radiogenic heat emission over 10,000 years, with no residual heat remaining.
5. Radionuclides release from the top of the repository however, in models where pathways decend, travel distances will be limited by radiogenic heat emission.

8.4 Results

8.4.1 Sellafield, West Cumbria

8.4.1.1 Most-likely fault and lithological permeabilities

Simulations of increasing peak repository temperatures at Sellafield when populated with most-likely fault and lithological permeabilities (Figure 8.3) show increases in the advective velocity up to a factor of 1.15 for a peak repository temperature of 30 °C, 1.55 for 60 °C and 2.15 for 90 °C. The greatest velocity increases are associated with fault zones F1 and F202.

Groundwater velocity increases (Figure 8.3) are observed up to 1,400 m away from the repository with a peak repository temperature of 90 °C after 1,000 years. No change to groundwater velocities are seen after 10,000 years in any of the peak temperature scenarios. An asymmetry in the area of increased groundwater velocity can also be observed (Figure 8.3), extending downwards and to the west-northwest of the repository. Furthermore, although a slight inflection in groundwater flow lines can be observed around the repository as a result of heat emission, no major change in the wider groundwater flow pattern occurs.

The increase in advective groundwater velocity corresponds to a relative increase in the maximum particle travel distance away from the repository compared to baseline (67.5 m) of 1.5 % for to 30 °C scenario 3.6 % for the 60 °C scenario and 6.1 % for the 90 °C scenario (Figure 8.5 & Table 8.2). The furthest travelled particles are associated with streakline #1.

8.4.1.2 High fault and lithological permeabilities

Increasing peak repository temperatures at Sellafield when populated with high fault and lithological permeabilities (Figure 8.4) show factor increases in advective velocity of 1.08 for a peak repository temperature of 30 °C, 1.45 for 60 °C, and 1.90 for 90 °C. Again the greatest increases are associated with fault zones F1 and F202, with F2 also becoming influential.

Increases in groundwater velocity are observed extending to the base of the model down fault lines F1, F202, and F2, laterally 3.4 km to the east-southeast, and upwards into the overlying Sherwood Sandstone Group, with peak repository temperatures of 60 and 90 °C (Figure 8.4). Although a slight inflection in groundwater flow lines can be observed around the repository as a result of radiogenic heat emission, no major change in the wider groundwater flow pattern occurs.

The increase in advective groundwater velocity does not correspond to a relative increase in maximum particle travel distance, with all model scenarios achieving a maximum particle distance of 307 m away from the repository (Figure 8.5 & Table 8.2). The particles achieving the 307 m distance are associated with streakline #7.

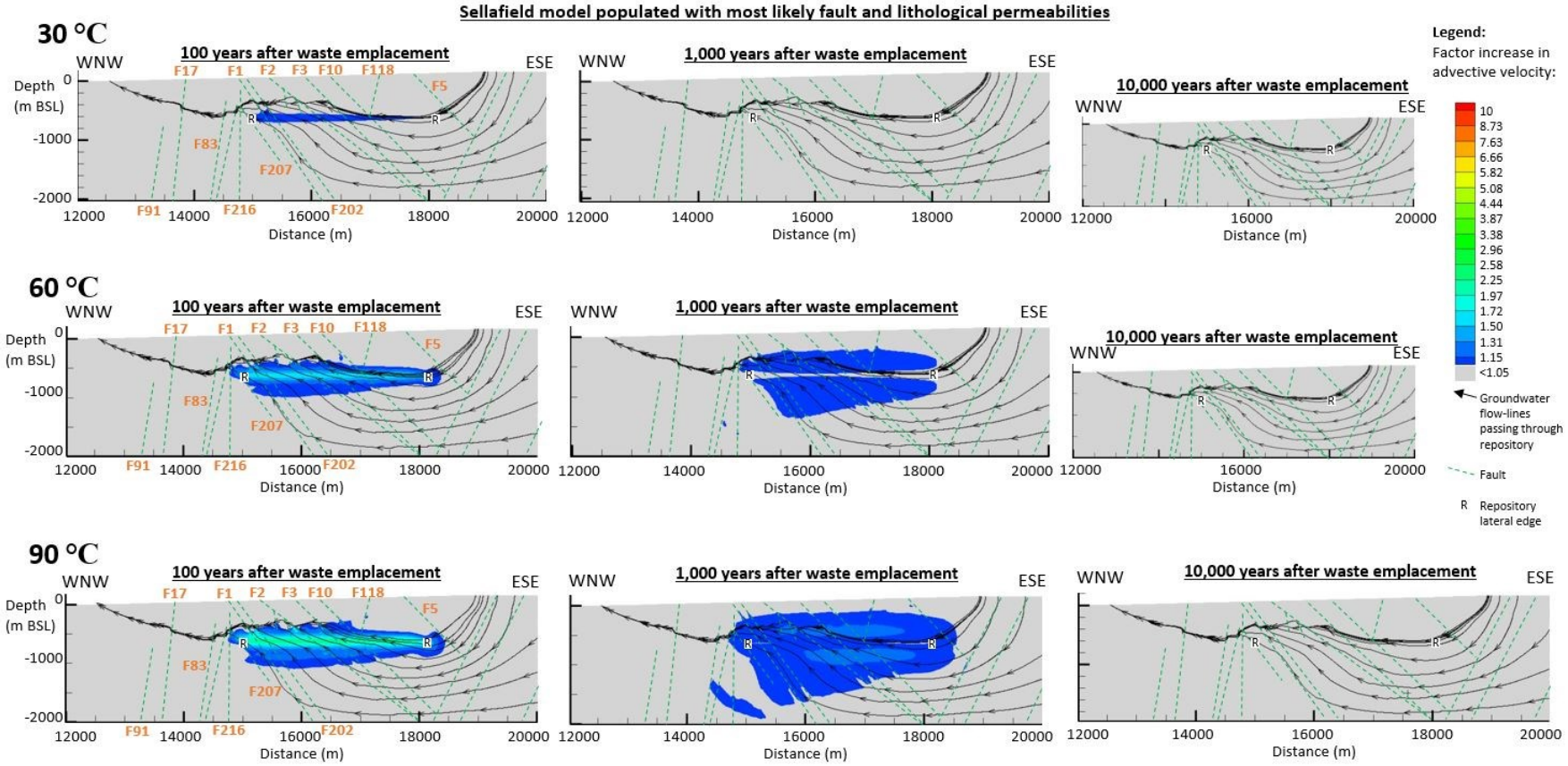

Figure 8.3: Factor increase in advective groundwater velocity compared to baseline (no heat emission) for the Sellafield model populated with most likely fault and lithological permeabilities for peak repository temperatures of 30, 60 and 90 °C after 100, 1,000 and 10,000 years. The two 'R's' delineate the repository lateral boundaries.

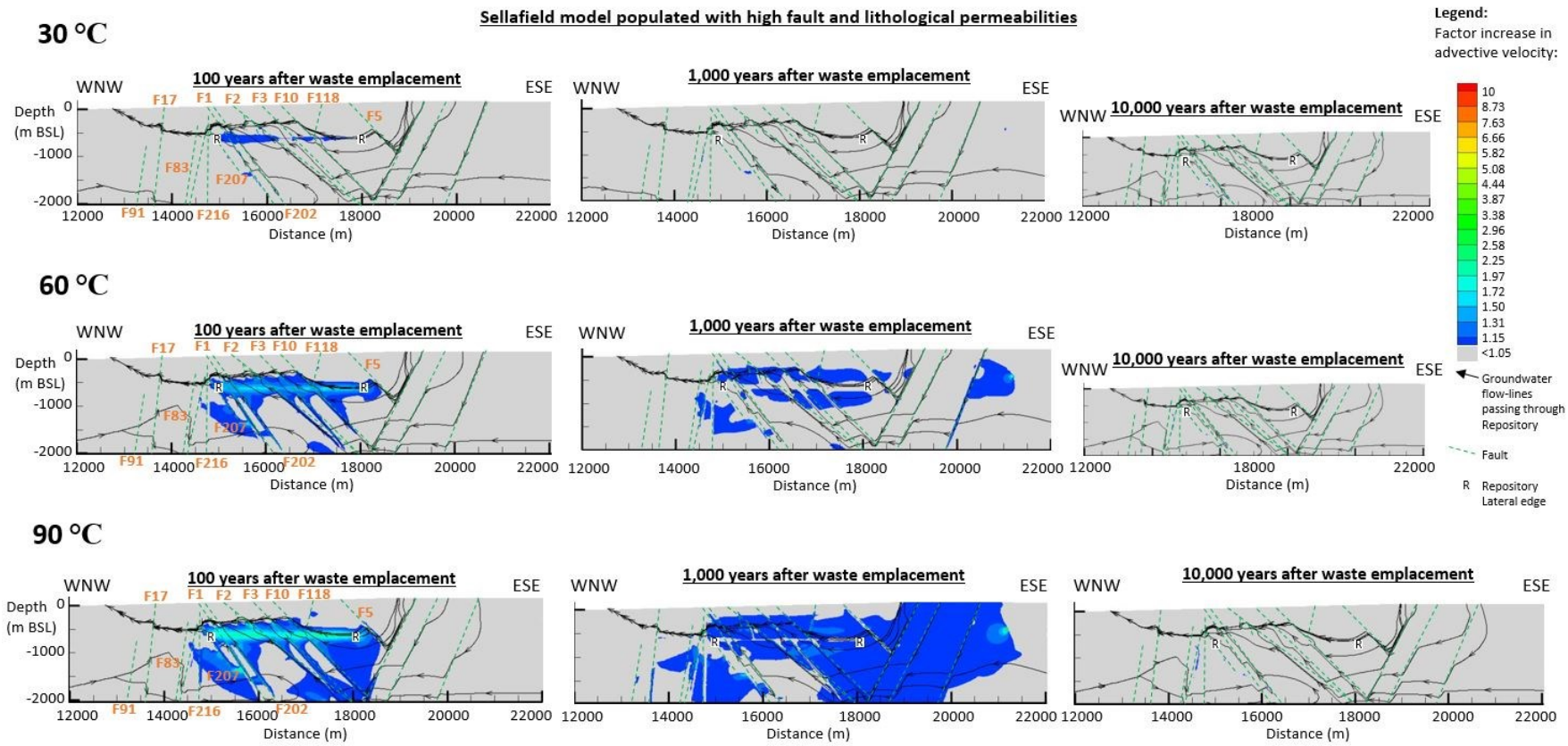

Figure 8.4: Factor increase in advective groundwater velocity compared to baseline (no heat emission) for the Sellafield model populated with high fault and lithological permeabilities for peak repository temperatures of 30, 60 and 90 °C after 100, 1,000 and 10,000 years. The two 'R's' delineate the repository lateral boundaries.

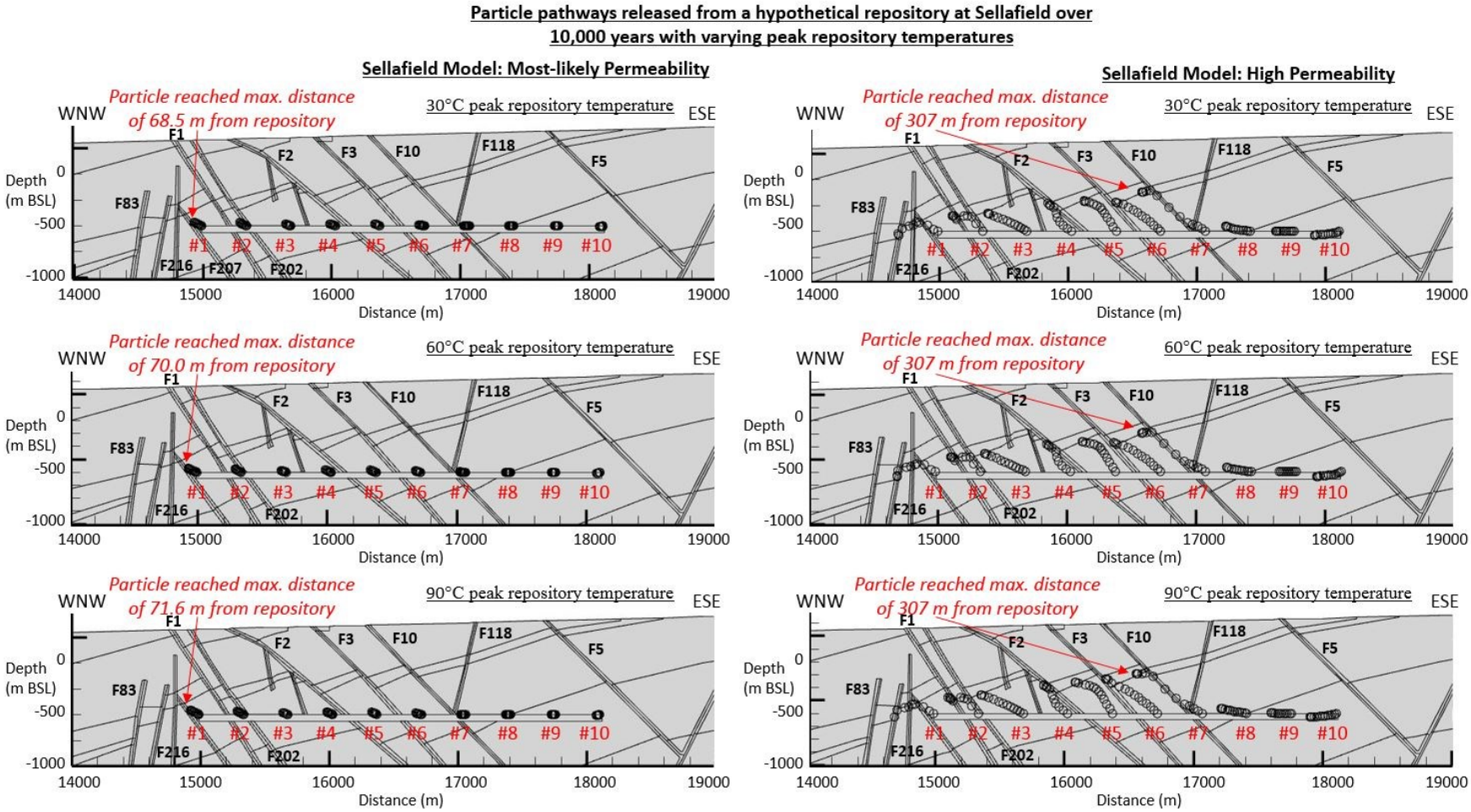

Figure 8.5: Particle pathways released from 10 evenly spaced points along the top of the theoretical repository site for the Sellafield model, populated with both most likely and high permeabilities, and peak repository temperatures of 30, 60 and 90 °C respectively.

8.4.2 Tynwald Basin, East Irish Sea Basin

8.4.2.1 Most likely fault and lithological permeabilities

Increasing peak repository temperatures within the Tynwald Basin when populated with most-likely fault and lithological permeabilities (Figure 8.6) show a factor increase in advective velocity of 1.06 around the repository for a peak repository temperature of 30 °C, and 1.11 for 60 and 90 °C. Factor increases of 1.20, 1.60 and 2.10 are also observed within the underlying Sherwood Sandstone Group for the 30, 60 and 90 °C modelled scenarios respectively.

The area of increased groundwater velocity is constrained to a 150 m area around the repository over the first 100 years, extending down into the underlying Sherwood Sandstone Group over 1,000 years (Figure 8.6). A secondary deeper area of increased groundwater velocity, up to a factor of 1.17, is observed, associated with the St Bees Shales & Evaporites after 10,000 years. No change in groundwater flow lines as a result of increasing peak repository temperature have been observed.

Despite the increases in advective velocity, maximum particle travel distance remains < 1 m away from the repository (Figure 8.8 & Table 8.2).

8.4.2.2 High fault and lithological permeabilities

Increasing peak repository temperatures within the Tynwald Basin when populated with high fault and lithological permeabilities (Figure 8.7) show factor increases in advective velocity up to 1.08 for a peak repository temperature of 30 °C, 1.25 for 60 °C and 1.40 for 90 °C.

The area of increased groundwater velocity is primarily constrained to the Mercia Mudstone Group, within 300 m of the repository site, but with some increase also observed within the underlying Sherwood Sandstone Group after 1,000 years (Figure 8.7). A secondary deeper area of increased groundwater velocity is observed, associated with the St Bees Shales & Evaporites, after 10,000 years, although less extensive than observed within the most-likely permeability scenario (section 8.4.2.1). No change in groundwater flow lines as a result of increasing peak repository temperature have been observed.

The increase in advective velocity corresponds to a relative increase in the maximum particle travel distance away from the repository compared to baseline (14.4 m) of 0.2 % for to 30 °C scenario; 1.3 % for the 60 °C scenario; and 2.3 % for the 90 °C scenario (Figure 8.8 & Table 8.2). The furthest travelled particles are associated with streakline #10.

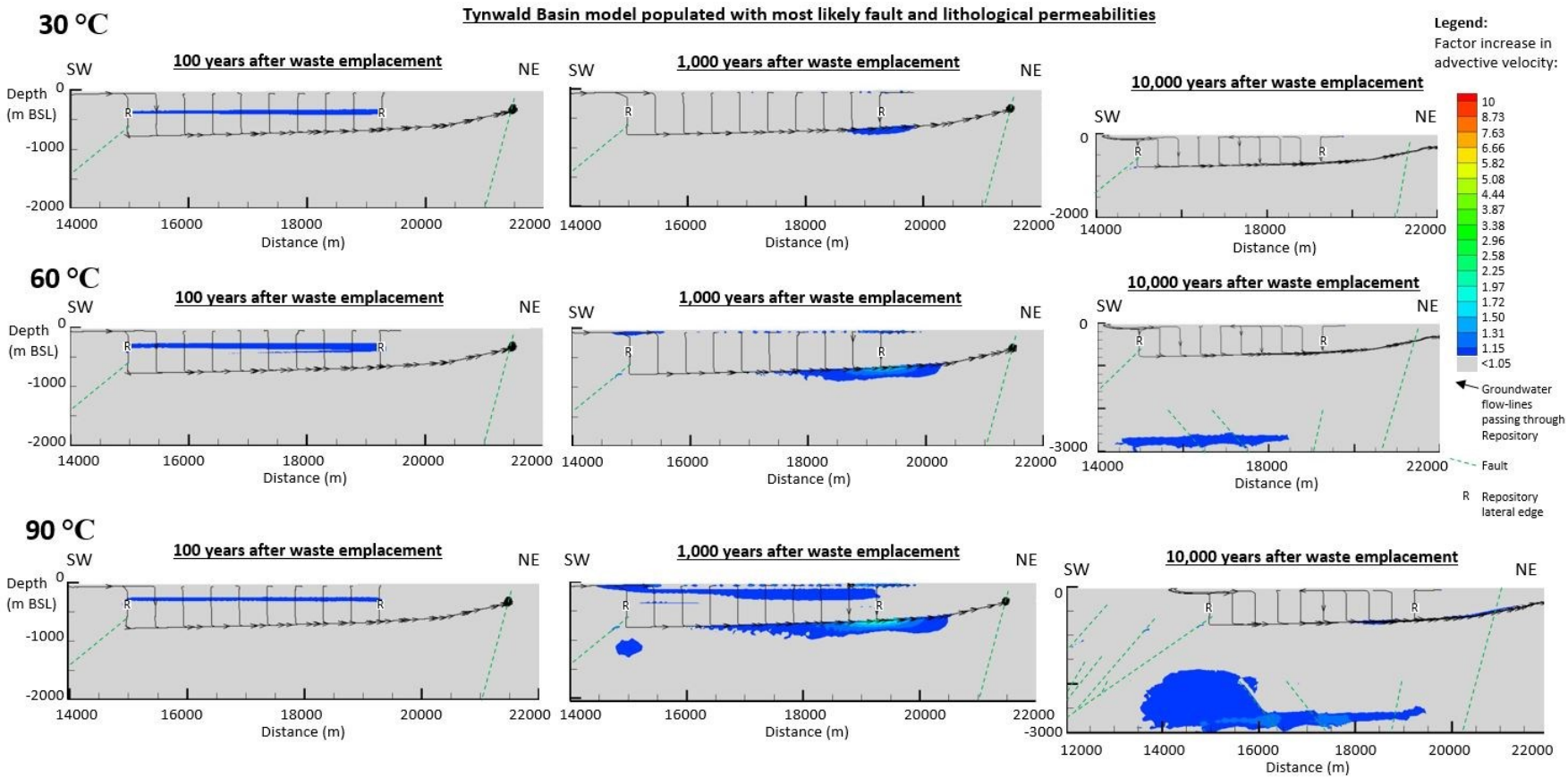

Figure 8.6: Factor increase in advective groundwater velocity compared to baseline (no heat emission) for the Tynwald Basin model populated with most likely fault and lithological permeabilities for peak repository temperatures of 30, 60 and 90 °C after 100, 1,000 and 10,000 years. The two 'R's' delineate the repository lateral boundaries.

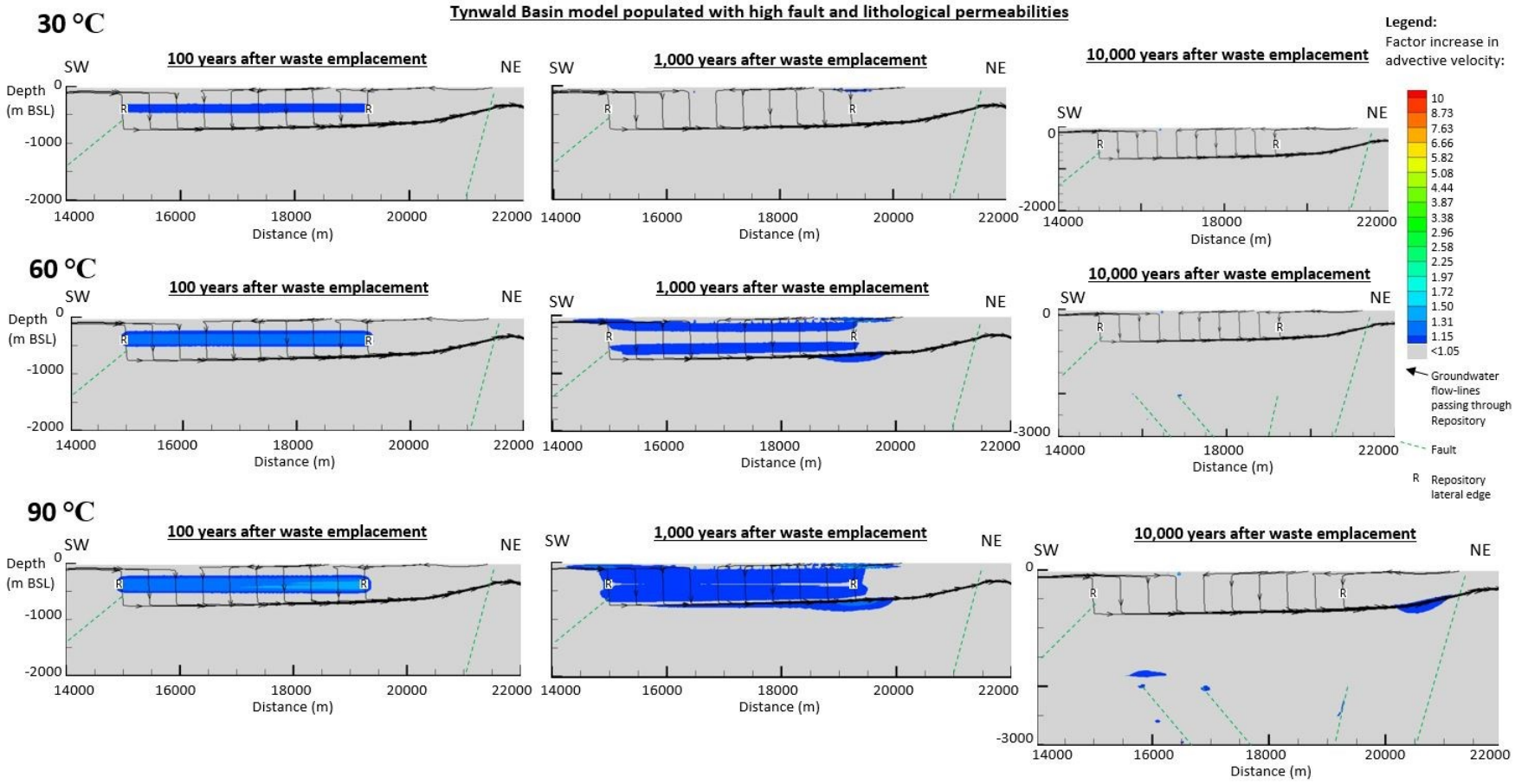

Figure 8.7: Factor increase in advective groundwater velocity compared to baseline (no heat emission) for the Tynwald Basin model populated with high fault and lithological permeabilities for peak repository temperatures of 30, 60 and 90 °C after 100, 1,000 and 10,000 years. The two 'R's' delineate the repository lateral boundaries.

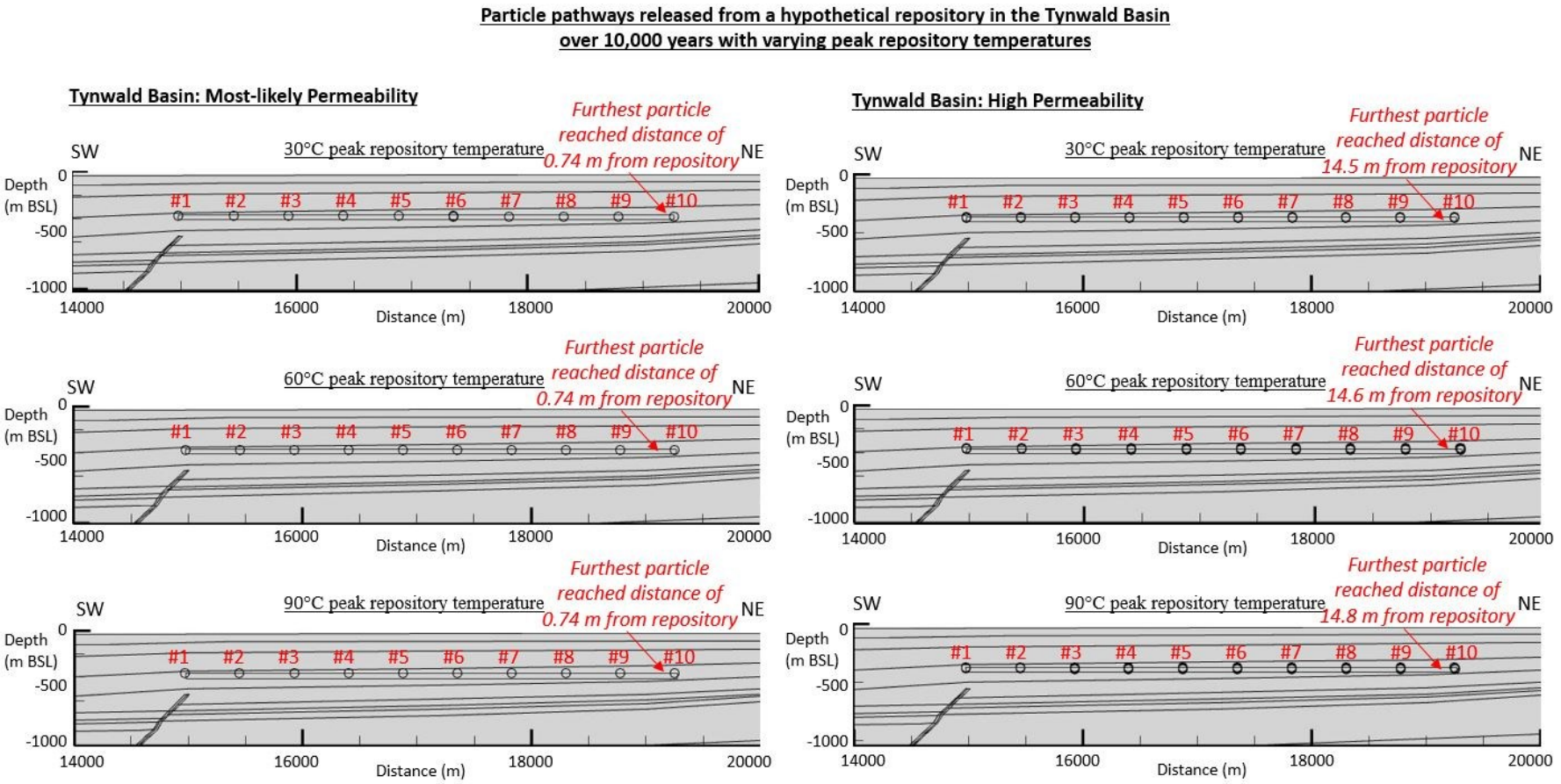

Figure 8.8: Particle pathways released from 10 evenly spaced points along the top of the theoretical repository site for the Tynwald Basin model, populated with both most likely and high permeabilities, and peak repository temperatures of 30, 60 and 90 °C respectively.

8.4.3 Thetford, East Anglia

8.4.3.1 Most likely lithological permeabilities

Increasing peak repository temperatures when populated with most-likely lithological permeabilities (Figure 8.9) show factor increases in advective velocity of 3.70 for the 60 °C scenario, and 8.20 for the 90 °C scenario. The greatest factor increases in advective velocity are associated with the ends of the repository, and the top of the Lower Silurian Basement. No change to the groundwater velocity is observed with the 30 °C model scenario.

The area of increased groundwater velocity extends out a maximum distance of 4.1 km east-southeast from the repository, 2 km west-northwest, down to the base of the model, and upwards 600 m through the overlying sedimentary sequence to the surface (Figure 8.9). Baseline conditions do however return within 10,000 years at Thetford.

Radiogenic heat emission creates groundwater convection cells at the edge of the repository (Figure 8.9). These convection cells pull groundwater down from the overlying sedimentary sequence as close as 320 m from the repository (90 °C scenario), to as far as 6.2 km away (60 °C scenario). The convection cells also pull groundwater up from the Lower Silurian Basement up to the repository horizon (Figure 8.9).

The increase in advective velocity corresponds to a relative increase in the maximum particle travel distance away from the repository compared to baseline (375 m) of 0 % for the 30 °C scenario; 4.5 % for the 60 °C scenario; and 12.7 % for the 90 °C scenario (Figure 8.11 & Table 8.2). The furthest travelled particles are associated with streakline #1.

8.4.3.2 High lithological permeabilities

Increasing peak repository temperatures when populated with high lithological permeabilities (Figure 8.10) show factor increases in advective velocity of 3.10 for the 60 °C scenario, and 7.20 for the 90 °C scenario. The greatest factor increases in advective velocity are associated with the ends of the repository, and the top of the Lower Silurian Basement. Again, no change to the groundwater velocity is observed with the 30 °C model scenario.

The area of increased groundwater velocity extends out a maximum distance of 7 km east-southeast from the repository (90 °C scenario), 2 km west-northwest, down to the base of the model, and upwards 600 m through the overlying sedimentary sequence to the surface (Figure 8.10). Small patches of elevated groundwater velocities are still observed after 10,000 years.

Radiogenic heat emission causes the development of convection cells which shorten the groundwater pathway between the repository and the surface, and increases the amount of groundwater ascending towards the surface (pathway 2) over the first 100 years. This is

instead of groundwater continuing westwards along the Upper Silurian Basement (pathway 1) (Figure 8.10).

The increase in advective velocity with increasing peak repository temperature has a variable effect on the maximum distance particles travel away from the repository. Particles travelling along pathway 1 decreased from baseline (5579 m) by 0.4 % within the 30 °C scenario; increase by 6.2 % for the 60 °C scenario; and increase by 0.5 % for the 90 °C scenario. Particles travelling along pathway 2 decreased from baseline (414 m) by 2.7 % within the 30 °C scenario, but increased by > 52.3 % for the 60 °C and 90 °C scenarios in which particles were discharged to the surface. The maximum particle travel distance along pathway 1 are associated with streakline #1, while those travelling along pathway 2 are associated with streakline #10 (Figure 8.11 & Table 8.2).

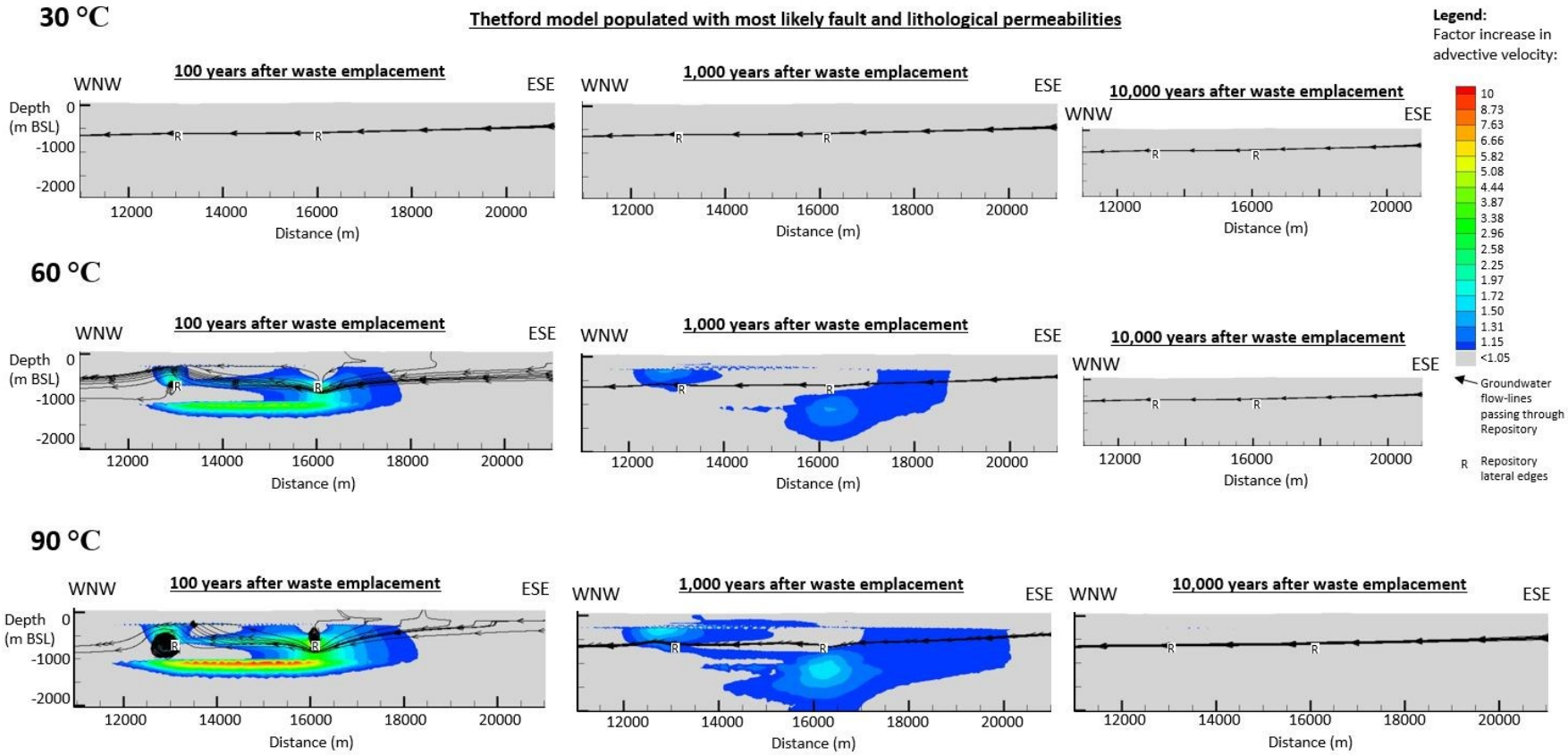

Figure 8.9: Factor increase in advective groundwater velocity compared to baseline (no heat emission) for the Thetford model populated with most likely fault and lithological permeabilities for peak repository temperatures of 30, 60 and 90 °C after 100, 1,000 and 10,000 years. The two 'R's' delineate the repository lateral boundaries.

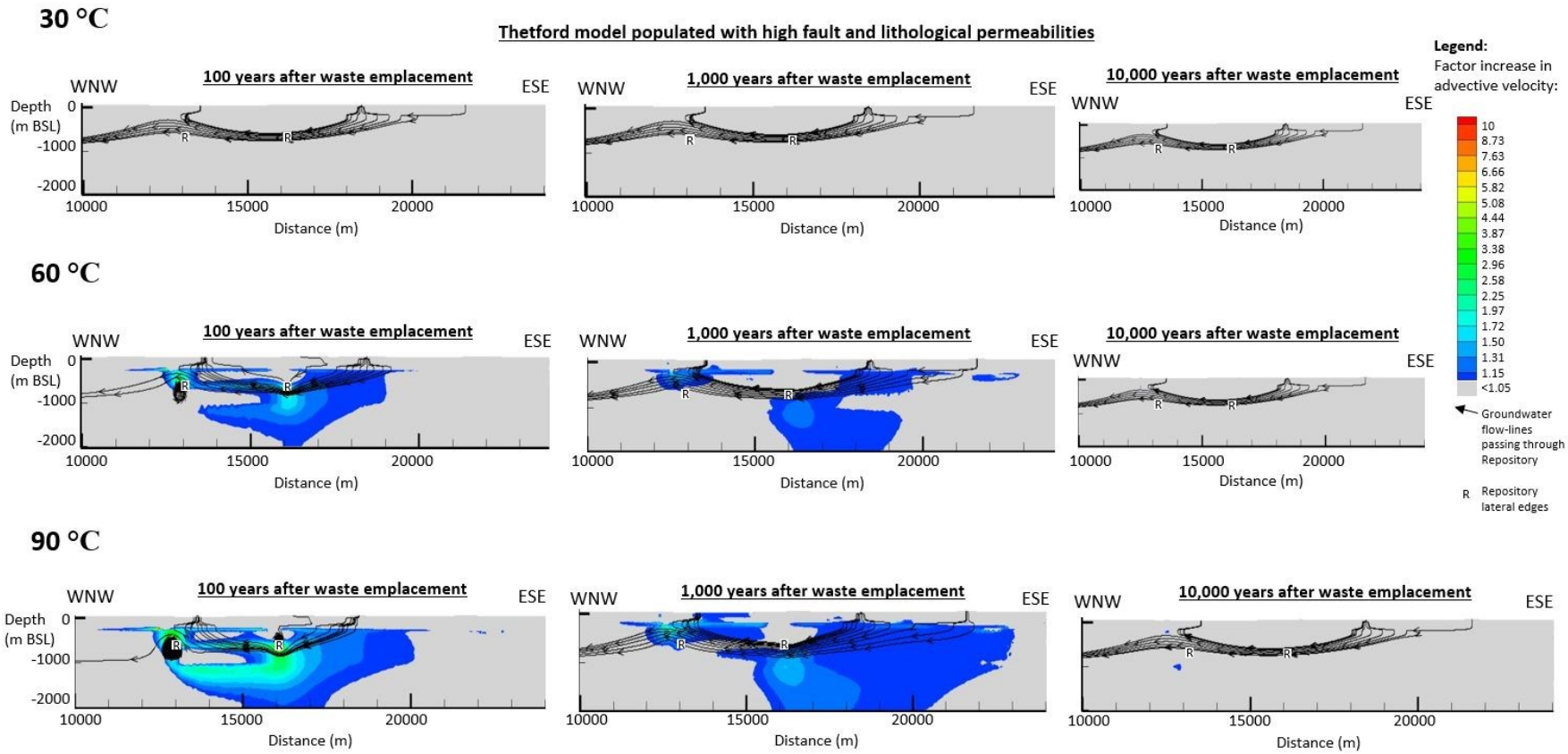

Figure 8.10: Factor increase in advective groundwater velocity compared to baseline (no heat emission) for the Thetford model populated with high fault and lithological permeabilities for peak repository temperatures of 30, 60 and 90 °C after 100, 1,000 and 10,000 years. The two 'R's' delineate the repository lateral boundaries.

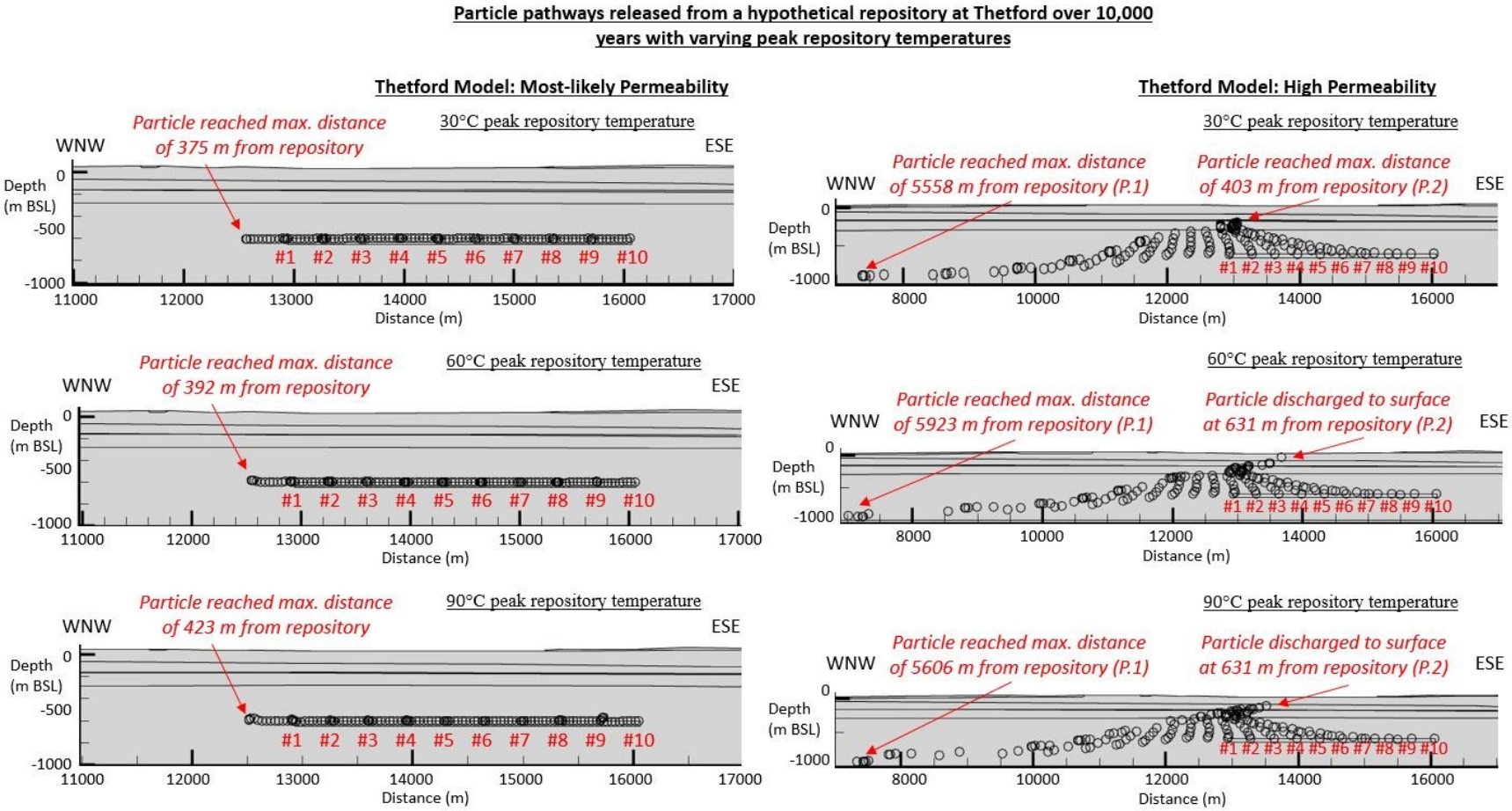

Figure 8.11: Particle pathways released from 10 evenly spaced points along the top of the theoretical repository site for the Thetford model, populated with both most likely and high permeabilities, and peak repository temperatures of 30, 60 and 90 °C respectively.

Table 8.2: Summary table of maximum particle travel distances over 10,000 years for the three selected sites (Sellafield, the Tynwald Basin, and Thetford) based on both most-likely and high fault and lithological permeabilities, and increasing peak repository temperatures of 30, 60 and 90 °C.

Location	Permeability	Pathway	Peak Repository Temperature (°C)			
			B	30	60	90
			Maximum particle distance from repository after 10,000 years (m) *(percentage change compared to baseline)*			
Sellafield, West Cumbria	*Most-likely*	*1*	67.5 m	68.5 m *(1.5 %)*	70.0 m *(3.6 %)*	71.6 m *(6.1 %)*
	High	*1*	307 m	307 m *(-0.1 %)*	307 m *(0 %)*	307 m *(0 %)*
Tynwald Basin, East Irish Sea Basin	*Most-likely*	*1*	< 1 m	< 1 m *(insig.)*	< 1 m *(insig.)*	< 1 m *(insig.)*
	High	*1*	14.4 m	14.5 m *(0.2 %)*	14.6 m *(1.3 %)*	14.8 m *(2.3 %)*
Thetford, East Anglia	*Most-likely*	*1*	375 m	375 m *(0 %)*	392 m *(4.5 %)*	423 m *(12.7 %)*
	High	*1*	5579 m	5558 m *(-0.4 %)*	5923 m *(6.2 %)*	5606 *(0.5 %)*
		2	414 m	403 m *(-2.7 %)*	>631* *(>52.3 %)*	>631* *(>52.3 %)*

***** Released particle discharged to the surface within 10,000 years.
Insig. Total particle travel distance < 1 m. Percentage increase considered insignificant.

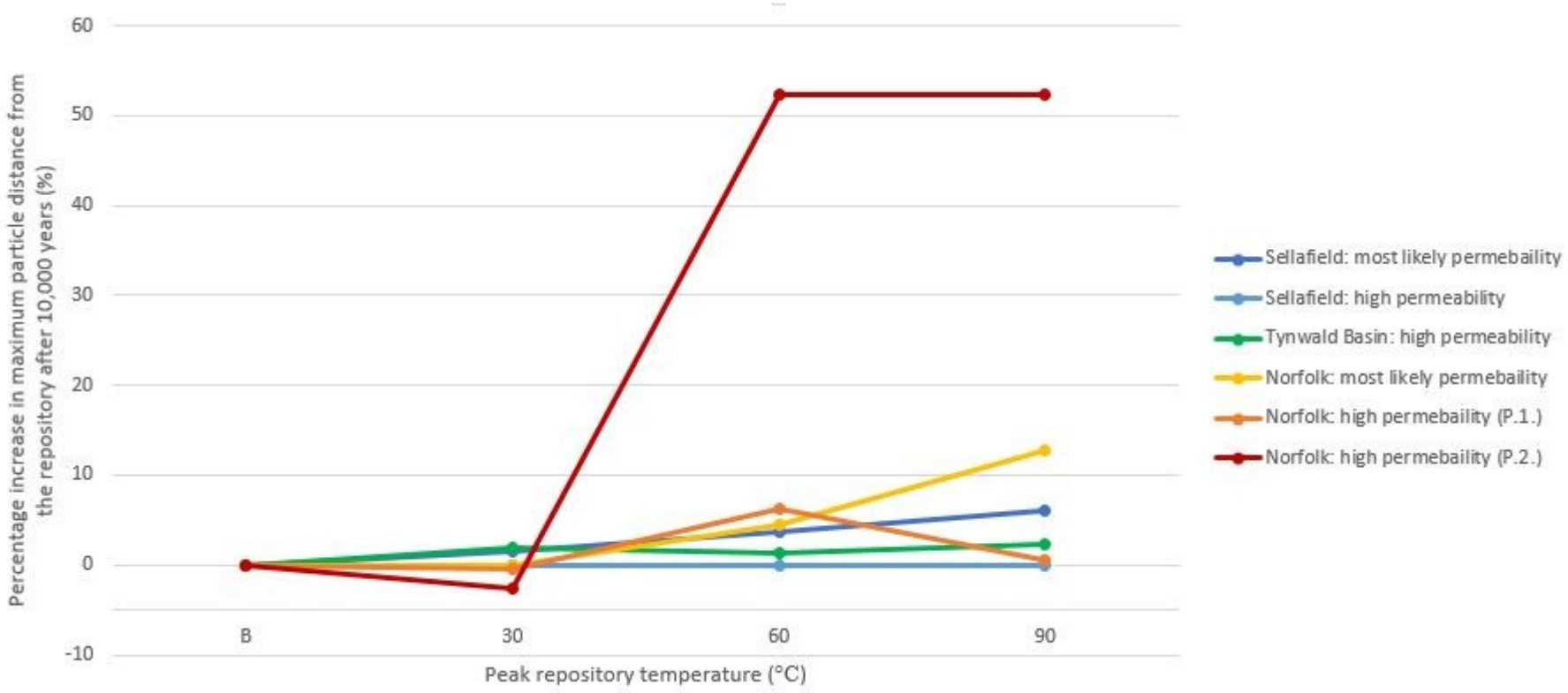

Figure 8.12: Graph showing the percentage increase in the maximum particle distance from the repository after 10,000 years, compared to baseline, with increasing peak repository temperatures of 30. 60 and 90 °C. Results for the Tynwald basin when populated with most likely permeability values has not been reported as all particle travel distances are < 1 m so percentage increases are considered insignificant.

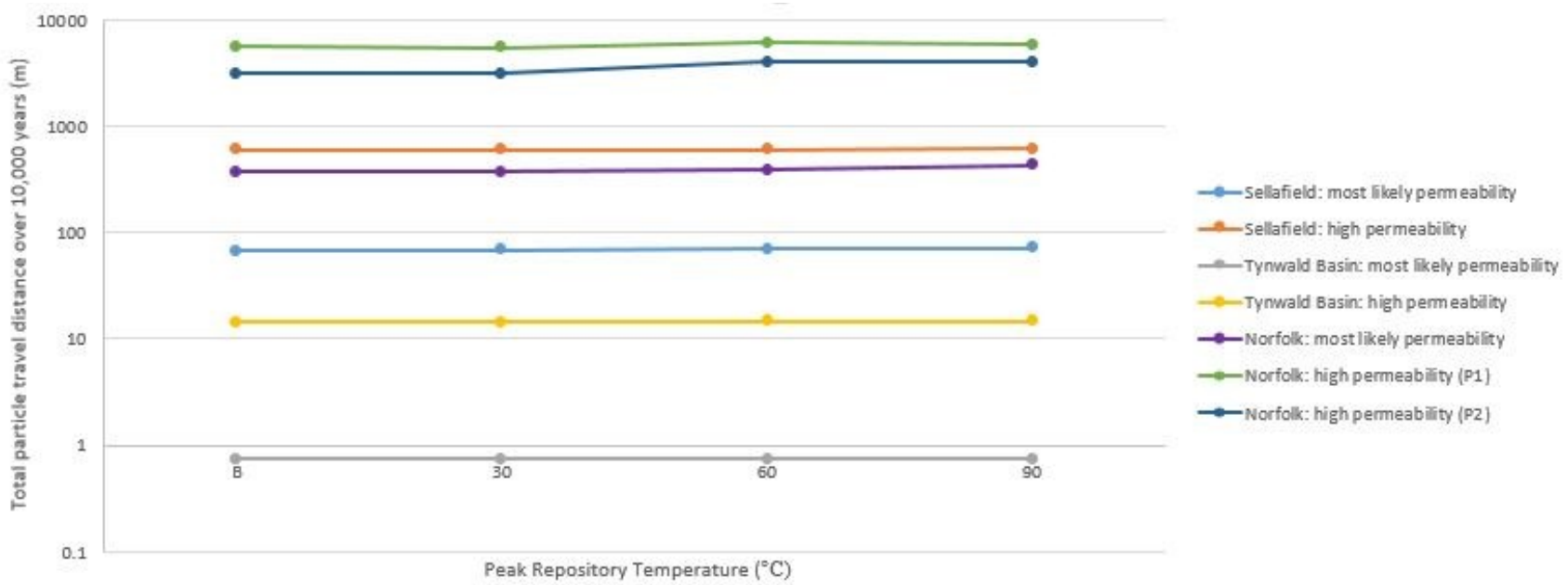

Figure 8.13: Total particle travel distance for the Sellafield, Tynwald Basin and Thetford models, populated with both most likely and high permeabilities, and peak repository temperatures of 30, 60 and 90 °C.

8.5 Discussion

8.5.1 The control of the far-field setting on groundwater disturbance as a result of radiogenic heat emission

The Thetford site shows the greatest potential out of the three sites to be affected by radiogenic heat emission with: 1) groundwater velocity increases by a factor of 8.2; 2) the development of large scale convection currents at the end of the repository in both permeability scenarios; 3) natural groundwater flow patterns affected as far away as 7 km from the repository; and 4) increases in particle travel distance due to radiogenic heat emission of > 52 %, higher than any other site (Figure 8.12). This results in surface radionuclide discharge within 10,000 years.

In comparison both Sellafield and the Tynwald Basin showed less of a response with: 1) groundwater velocity increases remaining below a factor of 2.15 in both models; 2) no groundwater convection cell development, although disturbances to the natural groundwater pattern were observed at Sellafield; 3) the area of groundwater affected by radiogenic heat emission was laterally constrained to *approx.* 3 km within the Sellafield model, and *approx.* 1 km within the Tynwald Basin model; and 4) increases in particle travel distances relative to a no-radiogenic heat emission scenario did not exceed 6% in either scenario (Figure 8.12).

The development of the heat driven groundwater convection cells within the Thetford models is considered a result of modelling the fractured crystalline basement as a continuous porous medium due to lack of site specific fracture information (see section 6.4.3). In reality, fractures would facilitate groundwater flow, and therefore heat transport in a linear fashion, reducing the likelihood of convection cell development, as seen at Sellafield (see section 8.4.1). Furthermore, the elevated groundwater velocity seen along the top of Lower Silurian Basement is not anticipated to be as stark in reality due to the gradational decrease in permeability with depth of the Silurian Basement, rather than the instant decrease implemented in the model (see section 6.4.1). Finally, the lack of change in groundwater flow patterns and velocities within the 30 °C model is because the additional 0.5 °C contributed by the repository to the natural background water temperature of 29.5 °C does not add enough heat into the system to affect the natural groundwater characteristics.

The influence of radiogenic heat emission at the Sellafield site is laterally constrained to the hydrogeological '*Coastal Plain Regime*', itself controlled by the dense brine formation to the west, and the topographic elevation to the east (see section 4.6.1). Heat is facilitated by groundwater along the faults (F1, F202 and F2), increasing groundwater velocity, but preventing the development of convection cells, as seen within the Thetford model. Although

elevated groundwater velocities extend up along the faults into the overlying Sherwood Sandstone Group, the maximum particle travel distance over 10,000 years becomes capped by the low permeability Brockram Breccia. Finally, the heat carried by upwelling warmer waters is sapped away by the cooler, meteoric derived *'coastal plain regime'* (section 4.6.1), capping the influence of radiogenic heat emission on groundwater velocity vertically.

No discernible change in groundwater flow lines due to radiogenic heat emission was observed within the Mercia Mudstone Group of the Tynwald Basin. This is considered a result of the dominating effect of the groundwater density difference driving groundwater down, though the Mercia Mudstone Group, into the less saline underlying Sherwood Sandstone Group (section 5.6.1). Furthermore, in addition to the immediate vicinity of the repository, increases in groundwater velocity were observed in both the overlying Quaternary sediments, and underlying Sherwood Sandstone Group (Figure 8.6 & Figure 8.7) after 1,000 years. This is considered a result of the slow transfer of heat through the low permeability Mercia Mudstone Group. This suggests that within some groundwater settings the longer term influence on groundwater velocities, as a result of radiogenic heat emission, might not be associated with water within the host rock formation but with groundwater in surrounding formations. This could lead to the risk of heat pollution of potentially useful groundwater resources. Finally, the reason for the elevated groundwater velocities, observed at depth within and around the Permian St Bees Shales & Evaporites is at present unclear, but is considered more likely to be a result of numerical instability (see Chapter 10 for further discussion), triggered by radiogenic heat emission, rather than a *'real-life'* coupled response, although either is possible.

These results from the three sites highlight that the response of a location to radiogenic heat emission is entirely setting dependent, determined by site specific geological and hydrogeological characteristics. It can therefore be concluded that certain natural barrier settings have greater prospectivity for radiogenic heat emission resilience than others.

Interestingly however, despite the dramatic variations in total particle travel distance with increasing peak repository temperature (> 52 %), these effects do not change the comparative particle travel distance across the three sites. The greatest particle travel distance is still associated with pathway 1 of the high permeability Thetford model, and the smallest with the Tynwald Basin models (Figure 8.13). This therefore illustrates other geological and hydrogeological features, such as low local and regional groundwater velocities, are more influential in determining total particle travel distances over 10,000 years than radiogenic heat emission.

8.5.2 Defining the Near-Field and Far-Field

Modelling radiogenic heat emission, represented by elevated peak repository temperatures, shows theoretical disturbances to the natural groundwater flow patterns up to 7 km away from the repository (Thetford). Groundwater (within the Thetford model) was pulled down from the overlying sedimentary sequence, which could inadvertently affect useful groundwater resources and/or dependencies at distance from a theoretical repository. The area defined as the near-field i.e. the area significantly affected by waste emplacement, therefore has the potential to extend over a much greater distance than is commonly utilised within site performance research or risk assessments (see section 2.3.4).

Furthermore, changes to groundwater velocity as a result of radiogenic heat emission are still possible 10,000 years post waste emplacement, such as at Sellafield and within the Tynwald Basin. Complexities also arise in that the affected area may no longer be associated with the host rock formation, such as within the Tynwald Basin where the affected area has migrated to the underlying Sherwood Sandstone Group or overlying Quaternary sequence over this timescale.

It is interesting therefore to note that the defined 'near-field' and 'far-field' is inevitably entirely site dependent, controlled by the geological and hydrogeological characteristics of the individual setting. For example, at Sellafield, the affected area is limited to the *'coastal plain regime'*, itself controlled by the topography of the Lake District, and the dense offshore brine. Or at Thetford, where the overlying sedimentary sequence can act to dampen the influence of radiogenic heat emission on near-surface groundwater velocities.

It is therefore recommended that the application of the term 'near-field' (section 2.3.4) should be reconsidered in light of spatial and temporal variations.

8.5.3 Significance of radiogenic heat emission compared to permeability uncertainty

Although increases in groundwater velocity have been observed due to radiogenic heat emission (discussed in section 8.5.1), the change in groundwater velocity as a result of radiogenic heat emission is still broadly however less than the change to groundwater velocity produced by regional permeability uncertainty (see Figure 8.14).

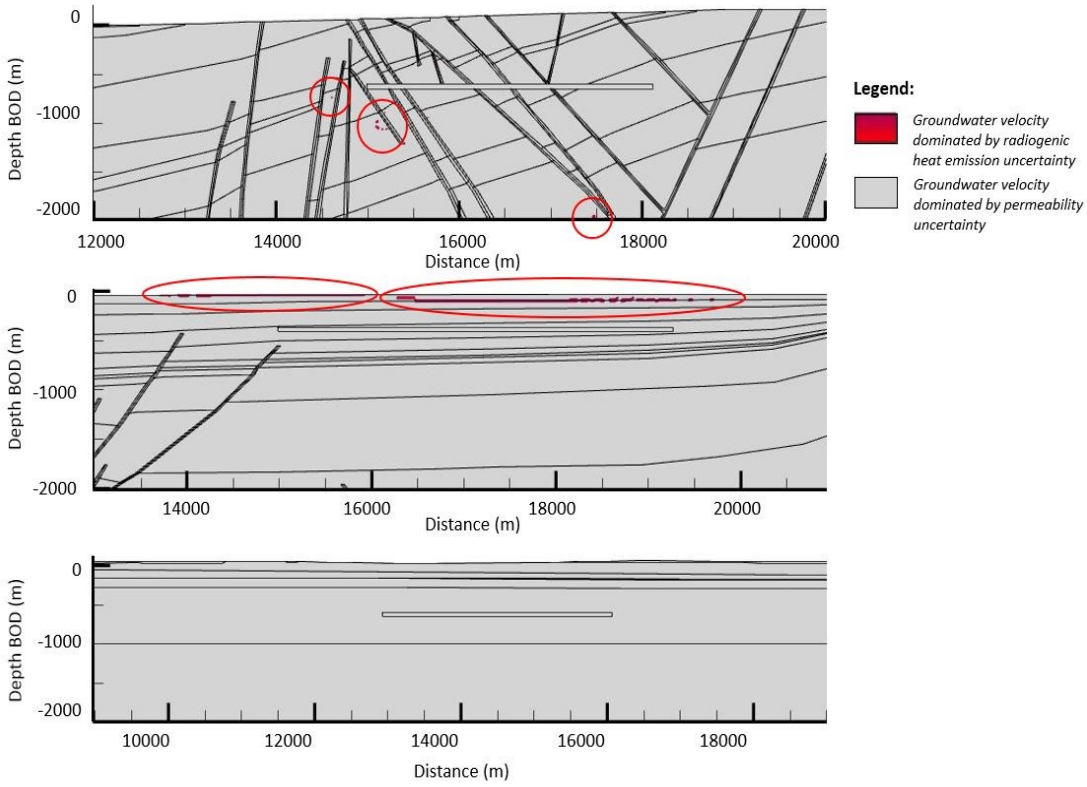

Figure 8.14: Illustration showing the areas in which groundwater velocity is dominated by radiogenic heat emission uncertainty (red) and areas in which groundwater velocity is dominated by permeability uncertainty (grey): [Top] Sellafield, [Middle] the Tynwald Basin and [Bottom] Thetford.

Figure 8.14 was determined by comparing the change in groundwater velocity as a result of 1) increased repository temperature and 2) increased permeability, from the most-likely permeability baseline (no radiogenic heat emission) scenario (see Figure 8.15).

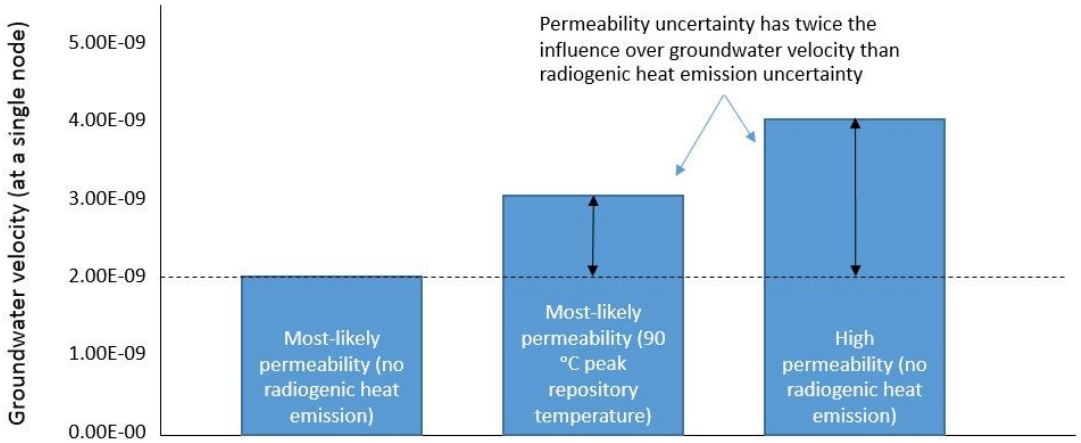

Figure 8.15: Method of assessment to determine whether radiogenic heat emission uncertainty, or permeability uncertainty has a greater influence on groundwater velocity at the three selected sites. Calculations were undertaken at each node, and percentages presented for the entire domain of each of the three simulated sites.

Results indicate that permeability is a more influential uncertainty than radiogenic heat emission on determining groundwater velocities across 99.9 % of the Sellafield model domain, 99.3 % of the Tynwald Basin model domain, and 100 % of the Thetford model domain (see Figure 8.14).

It can therefore be concluded that permeability is a greater source of advective velocity uncertainty than radiogenic heat emission. Radiogenic heat emission can thus be ignored for the purpose of far-field deep geological prospectivity assessments. However, radiogenic heat emission can not only affect the advective groundwater velocity, but can also affect the groundwater flow direction. Therefore simulation of the effect of radiogenic heat emission on groundwater behaviour, on a site by site basis, is still important, especially when permeability uncertainties have been reduced.

8.6 Conclusion, Significance & Recommendations

The effect of radiogenic heat emission on the natural groundwater flow pattern is dependent on the unique site specific geological and hydrogeological characteristics, with changes to the natural groundwater flow pattern observed up to 7 km away from the theoretical repository site at Thetford, but only 3 km at Sellafield and 1 km within the Tynwald Basin. These findings are significant as they show the area defined as the near-field i.e. *the area significantly affected by waste emplacement*, is entirely setting dependent, and can theoretically extend many kilometers away from the repository site, not just the few tens of meters as typically assessed. This is important because it highlights the potential risk posed to sensitive groundwater dependencies/resources, either through changes to water supply or temperature driven chemical and/or microbial alteration, over the far-field domain. It is therefore recommended that the 'near-field' be defined on a site-by-site basis to encompass its geo-spatial and temporal extent.

Finally, permeability uncertainty has been found to have a greater control over groundwater velocity than radiogenic heat emission at an early stage of site assessment. Simulation of transient groundwater conditions as a result of radiogenic heat emission is therefore not necessary as part of an initial hydrogeological prospectivity assessment. However, assessment of the effect of radiogenic heat emission would be required once permeability uncertainty has been reduced to determine the geospatial and temporal extent of the 'near-field'.

Chapter 9 Discussion of the Challenges of Far-Field Groundwater Flow Simulation: Implications for Natural Barrier Assessment

This chapter will outline some of the challenges faced with far-field groundwater flow modelling, and their implications for future far-field groundwater investigations. Discussion includes achieving numerical stability (section 9.1), and quasi-steadystate conditions (small on-going numerical changes associated with the solution over long timescales) (section 9.2).

9.1 Numerical Stability

Coupled process modelling is necessary when trying to understand regional groundwater systems, as interactions and dependencies are complicated and numerous, and difficult to characterise without numerical assistance. Problems can however occur due to the range of permeabilities encountered across a typical regional groundwater system, over 10 orders of magnitude (see section B.1.4.1), leading to a wide range of groundwater velocities which require to be solved for in a numerically stable fashion.

Mathematical relationships exist to determine the numerical stability of a solution. Of importance to this research is the Courant Stability Criterion (Equ.9.1), where v_a is the advective velocity of the groundwater (m/s), t is time (s) and x is the element length, and the Neumann Stability Criterion (Equ.9.2), where D is the Hydrodynamic Dispersion tensor (m^2/s). The Courant Criterion represents the distance an advecting front travels across an element within a timestep. The Neumann Criterion represents the amount of diffusion/dispersion occurring within an element per timestep.

$$Courant = \frac{|v_a\ |\Delta t}{\Delta x} \leq 1 \qquad (9.1)$$

$$Neumann = \frac{D\Delta t}{\Delta x^2} \leq 0.5 \qquad (9.2)$$

The model should be designed so that the Courant Criterion is equal to or less than 1 (to ensure that the advecting groundwater front does not jump cleanly across the element), and that the Neumann Criterion is between 0.001 and 0.5 (controlling the amount of dispersion within the element).

The Peclet Number (P_e) (section A.3.3.3) can also be used to determine stability as it represents the Courant, divided by the Neumann Stability Criterion. The Peclet Number should be ideally

twice the size of the Courant Number (Equ.9.3), and equal to, or less than 2 (section B.1.4.2) for a perfect numerical relationship (McDermott 2015).

$$Courant \leq \frac{1}{2} P_e \qquad (9.3)$$

The problems of the extremes of groundwater velocities within a regional system are exacerbated by the fact that these extremes are often associated with geometrically thin hydrogeological units, such as faults along which rapid groundwater flow occurs, or thin mudstone units, acting as barriers to flow.

These thin units require higher mesh densities i.e. smaller element sizes (Δx) to ensure a full element is represented within the material group of interest (see section B.1.2). Element lengths range from *approx.* 5 m to 100 m within this research. This range of element size and velocities (v_a) therefore leads to challenges in selecting an appropriate unit of time to qualify the Courant (Equ.9.1) and Neumann (Equ.9.2) criterion. This is because only one value of time (t) can be applied across the entire model domain at any one moment in time, using the chosen method. Consequently, where one time-step might be suitable for one part of the system to solve numerically, it may be inappropriate for another.

One option is to distort the geometric width of the thin hydrogeological features, as was undertaken within this research with discrete faults represented as 50 m wide fault damage zones (see section B.1.2) in order to increase element size. However, parameters must be adjusted to be representative, with the risk of the control of the thin features on regional groundwater movement being artificially dampened or enhanced, leading to unrepresentative flow patterns. To improve stability within this research groundwater velocities were also limited to *approx.* 6 orders of magnitude by limiting permeability to 5 orders of magnitude (1.00E-013 to 1.00E-018 m^2), conservatively making the lowest permeabilities higher.

Another option is to employ an alternative numerical method. This research used a 'Galerkin' Finite Element Method, which solves for pressure at the nodes, then calculates the groundwater velocity from approximated pressure and permeability fields (Istok 1989). Due to over-simplifications, the Galerkin Finite Element Method is known to produce velocity 'discrepancies' at nodes and along element boundaries (Mose et al. 1994; Cordes & Kinzelback 1992; Yeh 1981), which can lead to the build up of numerical errors and instability.

Alternative numerical methods include the 'Fluid Momentum' Finite Element Method, which solves directly for velocity at the nodes (Yeh 1981), and the 'Mixed Hybrid' Finite Element Method, which solves for the pressure at the nodes and element-to-element fluxes

simultaneously (Mose et al. 1994). Both are considered to produce fewer velocity discrepancies, but the 'Fluid Momentum' Method is the only other method available for implementation within OpenGeoSys (Kolditz & Shao 2009), requiring greater computational resources than the Galerkin method applied. Finally, numerical stability can also be improved through post-processing, such as described by (Cordes & Kinzelback 1992), however this approach is not applicable to transient models, required for this research.

Although modelled scenarios within this research were broadly stable, small areas of time dependent numerical instability were still observed, such as along a fault within the Tynwald Basin's most-likely fault and lithological permeability model (see Figure 9.1).

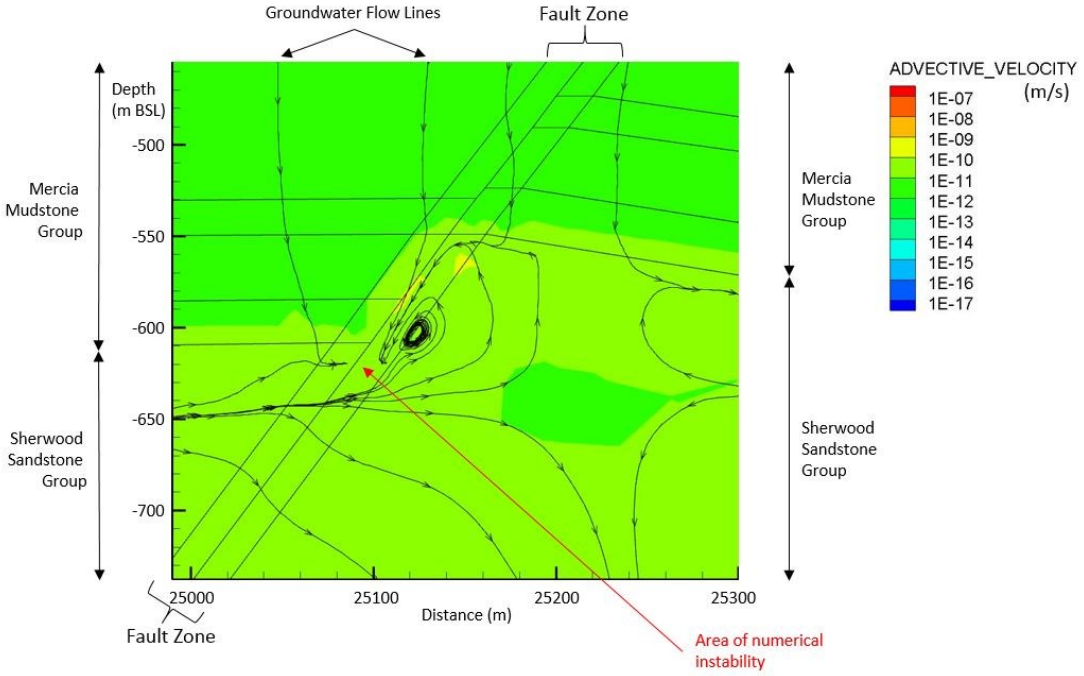

Figure 9.1: Illustration of small area of numerical instability, located along a fault-line within the Tynwald Basin model when populated with most-likely fault and lithological permeabilities.

Despite these small areas of numerical instability, it was still possible to capture the regional groundwater characteristics of the modelled settings (see Figure 5.10B), and was thus considered an adequate solution for the purposes of this research.

It is however recommended that further research be undertaken to improve regional groundwater modelling stability, such as through the development of geospatially dependent time-stepping, envisaged through adaptation of current parallel computing techniques, or implementation of the Fluid Momentum' Finite Element Method when undertaking this type of regional scale groundwater flow modelling, especially important for geological disposal.

9.2 Quasi-Steadystate Conditions

Although groundwater models were run for very long timescales, small changes to the numerical solution were still being observed in some parts of the regional groundwater system, such as along the brine-saline-freshwater interface at Sellafield (see Figure 9.2).

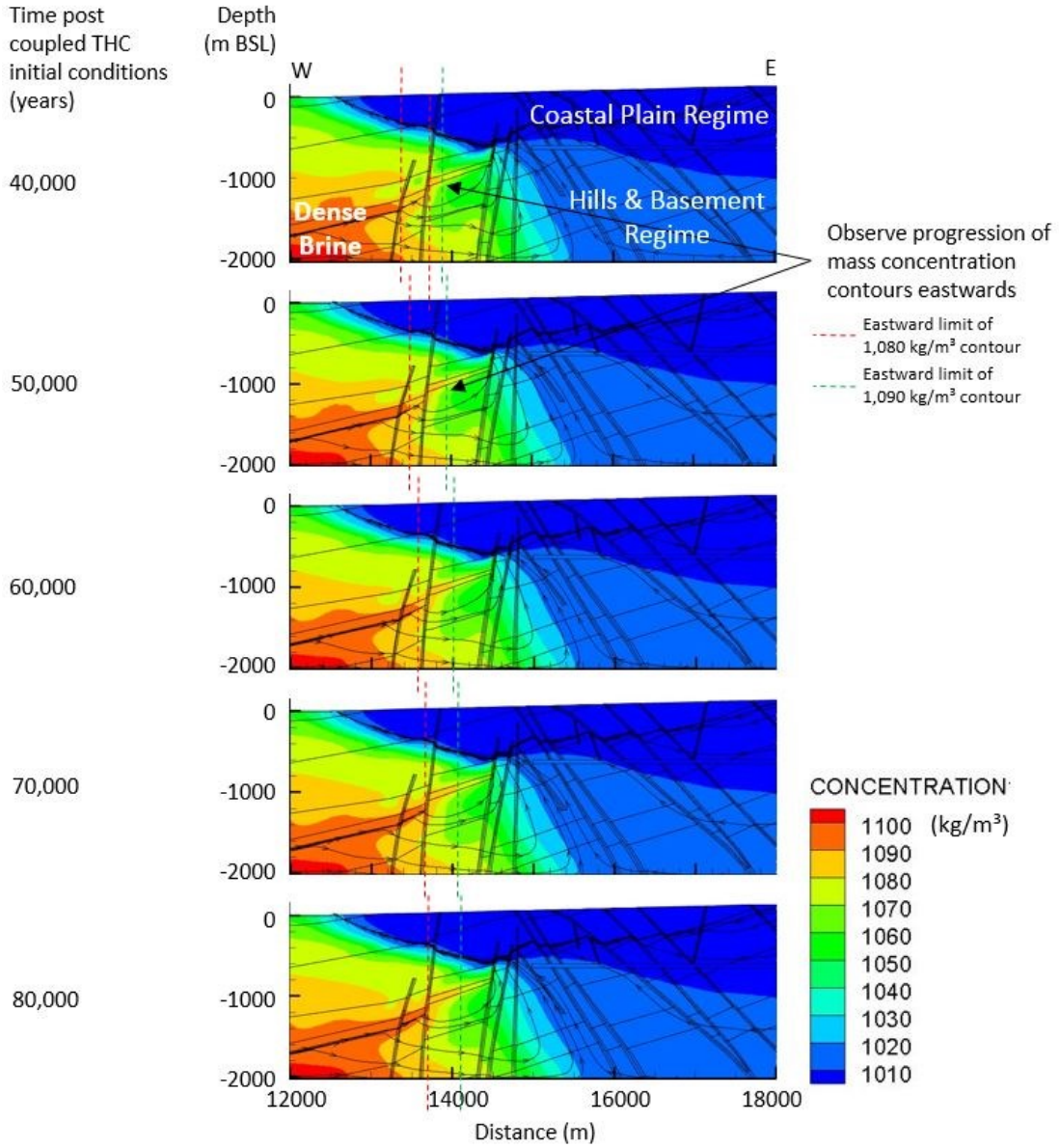

Figure 9.2: Illustration of the small numerical changes associated with the saline-freshwater transition zone still occurring over 40,000 years post coupled TH initial conditions within the Sellafield model when simulated with most-likely fault and lithological permeabilities.

It is for this reason that the term 'quasi-steadystate' conditions has been applied to this research, rather than 'steadystate'.

These results are interesting for two different reasons. Firstly it illustrates the very slow response of certain parts of the regional groundwater system to changes in external conditions, such as would be caused by climatic (e.g. glacial) or tectonic changes (McEvoy et al. 2016). These ongoing numerical changes are occurring over glacial-interglacial timescales (the last glacial retreat finished *approx.*15,000 years ago), suggesting that parts of the regional groundwater system are unlikely to ever achieve a truly 'steady-state' condition, as climatic changes, such as glaciation events, would change the boundary conditions.

This leads to the wider question then of the appropriateness of representing a regional groundwater system as steadystate, especially given the 1 million years performance timescale of concern for deep geological disposal. The use of quasi-steadystate conditions were considered appropriate for the purposes of this research, which was to capture the regional, present day groundwater flow characteristics, which did not 'significantly' change over the modelled timeframe. The quasi-steadystate conditions from which radiogenic heat emission was simulated (discussed in Chapter 9) was also considered acceptable for the purposes of this research due to the shorter process timescales (< 10,000 years) which could be approximated as steadystate.

Secondly, these findings highlight the problem of 1) initial condition application given the ever changing groundwater system (where to start) (Tsang & Niemi 2013), and 2) how to solve for these conditions as time step lengths are restricted (see section 9.1). Very slow response parts of the regional system, such as low permeability units (Neuzil 1986), would require running for very long durations to achieve absolute steadystate condition. This is considered computationally expensive and ultimately unrealistic given likely climatic influences as previously discussed.

Further research is therefore required on how to appropriately represent regional groundwater evolution, factoring in very low response groundwater units, and the nature and appropriateness of the starting conditions.

9.3 Summary

Far-field groundwater simulation is possible using pre-existing numerical methods, however, further research is required to; 1) improve numerical stability when modelling systems with variable geometric thicknesses, and therefore element sizes, but fixed time-steps; 2) the treatment of very low permeability units in achieving steadystate conditions; and 3) the applicability of modelling steadystate conditions for parts of the groundwater system that are unlikely to achieve steadystate conditions over repository performance timeframes.

Chapter 10 Conclusions

10.1 Overview

This research has investigated the hydrogeological suitability of three selected UK settings to host a theoretical deep geological disposal facility.

This was achieved by identifying groundwater characteristics considered of benefit for long term radionuclide containment and isolation, and then assessing these characteristics across three UK specific far-field settings. The settings selected for analysis included Sellafield in West Cumbria, the Tynwald Basin in the East Irish Sea Basin, and Thetford in East Anglia. The chosen method of assessment was coupled process numerical simulation using the OpenGeoSys simulation softwares. The quality of the groundwater characteristics at the individual sites were then scored in relation to a benchmark hydrogeological scenario, enabling direct comparison between the prospective hydrogeological performances of the natural barrier at the three locations in consideration of permeability uncertainty.

The overarching findings from this research are that: 1) the Tynwald Basin performs between 3.5 and 4 times better than Sellafield, and between 1.7 and 4 times better than Thetford, and thus this research can conclude that due to natural geological and hydrogeological variability, some locations offer substantially better radionuclide containment and isolation potential than others; 2) the effect of radiogenic heat emission on the natural groundwater flow pattern is dependent in the site specific geological and hydrogeological characteristics, and therefore so is the area defined as the 'near-field'; and 3) a simple method of site comparison is possible for regional groundwater system under steadystate conditions.

The major contribution of this research is that it enables, for the first time, a direct comparison between the characteristics, and the quality, of different UK based far-field settings to contain and isolate radioactive waste. It is hoped that this will achieve two things; firstly, that it will widen the discussion as to the role the regional groundwater setting should play in final deep geological disposal facility site selection, and secondly, to aid understanding for the public and stakeholders as to what is a comparatively *'good'*, or *'good enough'* far-field setting.

What this research is not intended to do is to provide an absolute safety assessment of the selected sites to host a deep geological disposal facility, but is instead intended to guide further UK based research on natural barrier performance within different regional settings.

10.2 Key Findings, Conclusions and Significance/Implications

The key findings, conclusions and implications of this research will now be outlined.

10.2.1 Hypothesis 1

Do the regional geological and hydrogeological characteristics of some locations offer greater long term radionuclide containment and isolation potential than others?

Key Findings:

1. The prospective natural barrier performance is the greatest at the Tynwald Basin. Results indicate performance between 3.5 and 4 times better than Sellafield, and between 1.7 and 4 times better than Thetford.

2. The prospective natural barrier performance of Thetford cannot at present be determined due to parameter uncertainty, although if permeability is closest to central/middle modelled values, the performance could be up to 2.4 times better than Sellafield.

3. The role of chemical processes over physical processes in controlling radionuclide travel distances is setting dependent, with chemical processes playing a greater role at Sellafield and Thetford (Rf = 1 to 200) than that of the Tynwald Basin (Rf = 1).

Conclusion:

Different locations exhibit different far-field geological and hydrogeological characteristics, and therefore variable prospectivity for long-term radioactive waste containment and isolation.

Significance/Implications:

These findings highlight a range of variable quality far-field natural barrier settings available both onshore and offshore the UK, which should be explored as part of the on-going site selection programme. Improved performance of the natural barrier will uphold the multi-barrier safety principle, by not placing undue reliance on the engineered barriers.

Furthermore, assessment of possible offshore deep geological disposal locations, in addition to possible economic costs, legal and social opposition is imperative. This is especially true as the Nuclear Decommissioning Authority have recently extend the search area for a deep geological disposal facility up to 20 km offshore of the UK.

10.2.2 Hypothesis 2

Does the regional geological and hydrogeological setting control the effect of radiogenic heat emission on natural groundwater flow patterns?

Key Findings:

1. Radiogenic heat emission at Thetford causes the development of groundwater convection cells, pulling water down from the over lying sedimentary sequence over 7 km away, and increasing groundwater velocities by up to a factor of 8.2.
2. The area affected by radiogenic heat emission at Sellafield is constrained to the 'Coastal Plain' hydrogeological regime, with the transfer of heat controlled by faults. Groundwater velocity increases do not exceed a factor of 2.15.
3. The area affected by radiogenic heat emission within the Tynwald Basin is constrained primarily to the Mercia Mudstone Group (host rock formation) and underlying Sherwood Sandstone Group. Groundwater velocity increases do not exceed 2.15.
4. Increases in groundwater velocity, compared to baseline, are still visible after 10,000 years post waste emplacement within the Sellafield and Tynwald Basin models.
5. Permeability uncertainty considered a greater control on groundwater velocity than peak repository temperature uncertainty.

Conclusion:

The effect of radiogenic heat emission on the natural groundwater flow pattern is dependent in the unique site specific geological and hydrogeological characteristics, and therefore so is the area defined as the 'near-field'.

Significance/Implications:

These findings are significant as they show the area defined as the near-field is entirely setting dependent, and can theoretically extend many kilometers away from the repository site. This highlights the potential risk posed to sensitive groundwater dependencies/resources over the regional setting, not currently assessed. It is recommended that any future site performance research undertaken on the 'near-field' quantifies its spatial and temporal extent, or re-defines it to encompass these variabilities.

This research also highlights the overarching importance of the regional groundwater setting in controlling the influence of radiogenic heat emission, and on radionuclide travel distances.

10.2.3 Hypothesis 3

Is a simple method of far-field natural barrier comparison possible, despite complex and detailed regional geological and hydrogeological characteristics?

Key Findings:

1. Direct comparison between the steadystate groundwater characteristics of three different sites was possible by conversion of qualitative groundwater characteristics into quantifiable parameters, which were then assessed through numerical models.

2. Although application of the current groundwater parameters (section 2.3.6) cannot be easily applied to transient groundwater characteristics, permeability uncertainty has a greater influence on groundwater velocities than radiogenic heat emission. Quasi-steadystate assessment is therefore appropriate for an initial prospectivity assessment.

3. Regional scale groundwater simulation requires advanced computational resources (cores and memory), computational techniques (parallel computing) and meshing techniques (large detailed meshes i.e. > 60,000 nodes and 118,000 elements).

4. Small areas of time-step, element size and permeability dependent numerical instability present when modelling regional scale hydrogeological systems.

5. Challenges associated with achieving truly steadystate initial conditions (solution still changing after 50,000 years) due to the presence of very low permeability units.

Conclusion:

A simple method of site comparison is possible using current modelling techniques when the regional groundwater system can be approximated to steadystate.

Significance/Implications:

It is considered that a simple method of direct comparison between the far-field characteristics of different settings will aid understanding as to what is a relatively *'good'* disposal location, and will improve public confidence in the site selection procedure, proven essential for a successful programme. Furthermore, research highlights the importance of a hollistic site assessment method, not simply based on a single metric or central parameter value.

Further method development is required to 1) improve numerical stability over regional domain with variable geometries; 2) achieve steadystate conditions in low permeability units; and 3) consider the applicability of steadystate models for long-term dynamic systems.

10.3 Recommendations & Future Work

1. High level comparison of far-field natural barrier characteristics should be undertaken, across the UK, to identify areas with strong natural barrier prospectivity using a consistent simple method of model development and site analysis.

2. Further research and data collection should be undertaken at Thetford as it shows containment potential, with particular focus on constraining the vertical permeability of the Lias Group, and on fracture characterisation within the Silurian Basement.

3. Further research and data collection should be undertaken within the Tynwald Bain as it shows the greatest containment potential. Particular focus should be placed on characterisation of the regional groundwater densities, suspected to play a major role in controlling regional flow patterns, and on the Mercia Mudstone permeabilities.

4. Research should be undertaken on how to improve regional scale groundwater modelling capabilities including; 1) numerically stable representation of thin hydrogeological units, envisaged through application of unit dependent time stepping; 2) the treatment of very low permeability units in achieving steadystate conditions, such as through machine learning; and 3) the applicability of modelling steadystate conditions for on-going and changing groundwater systems.

5. Processes uncertainties, including gas generation, glaciation and climate change on regional groundwater characteristics, should also be explored within different settings.

6. Research should be undertaken to weight the hydrogeological parameters chosen to represent the hydrogeological characteristics considered of benefit for deep geological disposal, as this could alter the relative overall scores assigned to the individual sites. .

7. The area and timeframe beyond which waste emplacement should no longer affect the natural groundwater behaviour should be considered for regulatory purposes.

10.4 Summary

This research has successfully investigated the hydrogeological suitability of three selected UK settings to host a theoretical deep geological facility, and has highlighted the importance of characterisation of the far-field natural barrier setting in ensuring long term radionuclide *containment* and *isolation*.

References

A

Acuña Duhart, E.I. (2010) 'Multiple Period Mine Ventilation and Fan Selection Optimization', PhD Thesis, Laurentian University, Ontario, Canada.

Akhurst, M.C., Chadwick, R.A., Holliday, D.W., McCormac, M., McMillian, A.A., Millward, D., Young, B., Ambrose, K., Auton, C.A., Barclay, W.J., Barnes, R.P., Beddoe-Stephens, B., James, J.W.C., Johnson, H., Jones, N.S., Gover, B.W., Hawkins, M.P., Kimbell, G.S., MacPherson, K.A.T., Milodowski, A.E., Riley, N.J., Robins, N.S., Stone, P. and Wingfield, R.T.R. (1997) 'Geology of the west Cumbria District', *Memoir of the British Geological Survey,* Sheets 28, 37 and 47 (England and Wales), Keyworth, Nottingham.

Allen, D.J., Brewerton, L.J., Coleby, M.M., Gibbs, B.R., Lewis, M.A., MacDonald, A.M, Wagstaff, S.J. and Williams, A.T. (1997), 'The physical properties of major aquifers in England and Wales', *British Geological Survey Technical Report* WD/97/34, pp. 312. Environment Agency R&D Publication 8.

Anagnostou, G. (2014) 'Some Critical Aspects of Subaqueous Tunnelling', *Muir Wood Lecture 2014*, published by *The International Tunnelling and Underground Space Association*, May 2014.

Ander, E.L., Shand, P., Griffiths, K.J., Lawrence, A.R., Hart, P. and Pawley, J. (2004) 'Baseline Report Series 13: The Great Ouse Chalk Aquifer, East Anglia' British Geological Survey, Commissioned Report No. CR/04/236N.

Anderson, M.P. and Woessner, W.W. (1992) 'Applied Groundwater Modelling: Simulation of Flow and Advective Transport', Academic Press Inc., San Diego, California.

Andersson, J., Staub, I. and Knight, L. (2005) 'DECOVALEX III/BENCHPAR PROJECTS: Approaches to Upscaling Thermo-Hydro-Mechanical Processes in a Fractured Rock Mass and its Significance for Large-Scale Repository Performance Assessment - Summary of Findings', Report of BMT2/WP3, SKI Report No. 2005:27, Stockholm, Sweden.

Andra (2018a) 'Cigéo' webpage, Accessed January 2018, Available at <https://www.andra.fr/cigeo>

Andra (2018b) 'Cigéo Project', Accessed January 2018, Available at <https://www.andra.fr/download/andra-international-en/document/editions/568bva.pdf>

Andra (2005a) 'Dossier 2005 Argile: Synthesis - Evaluation of the feasibility of a geological repository in an argillaceous formation – Meuse/Haute-Marne site', Report Series, Châtenay-Malabry, France.

Andra (2005b) 'Dossier 2005 Argile: Tome - Safety evaluation of a geological repository', Report Series, Châtenay-Malabry, France.

AngloGoldAshanti (2017) 'AngloGoldAshanti' home webpage, Accessed December 2017, Available at <http://www.anglogoldashanti.com/>

Anttila, P., Ahokas, H., Front, K., Hinkkanen, H., Johansson, E., Paulamäki, S., Riekkola, R., Saari, J., Saksa, P., Snellman, M., Wikström, L. and Öhberg, A. (1999a) 'Final disposal of

spent nuclear fuel in Finnish bedrock - Hästholmen site report', Report code POSIVA 99-08, Helsinki, Finland.

Anttila, P., Ahokas, H., Front, K., Heikkinen, E., Hinkkanen, H., Johansson, E., Paulamäki, S., Riekkola, R., Saari, J., Saksa, P., Snellman, M., Wikström, L. and Öhberg, A. (1999b) 'Final disposal of spent nuclear fuel in Finnish bedrock - Kivetty site report', Report code POSIVA 99-09, Helsinki, Finland.

Anttila, P., Ahokas, H., Front, K., Hinkkanen, H., Johansson, E., Paulamäki, S., Riekkola, R., Saari, J., Saksa, P., Snellman, M., Wikström, L. and Öhberg, A. (1999c) 'Final disposal of spent nuclear fuel in Finnish bedrock - Olkiluoto site report', Report code POSIVA 99-10, Helsinki, Finland.

Anttila, P., Ahokas, H., Front, K., Hinkkanen, H., Johansson, E., Paulamäki, S., Riekkola, R., Saari, J., Saksa, P., Snellman, M., Wikström, L. and Öhberg, A. (1999d) 'Final disposal of spent nuclear fuel in Finnish bedrock - Romuvaara site report', Report code POSIVA 99-11, Helsinki, Finland.

Apted, M.J. and Ahn, J. (2017) 'Geological Repository Systems for Safe Disposal of Spent Nuclear Fuels and Radioactive Waste', 2nd edn, Woodhead Publishing Series in Energy, Duxford, United Kingdom.

Armitage, P.J., Worden, R.H., Faulkner, D.R., Aplin, A.C., Butcher, A.R. and Espie, A.A. (2013) 'Mercia Mudstone Formation caprock to carbon capture and storage sites: petrology and petrophysical characteristics' in *Journal of the Geological Society, London,* vol. 170, pp. 119-132. doi: 10.1144/jgs2012-049. Available at <http://jgs.lyellcollection.org/content/170/1/119>

Armitage, P.J., Worden, R.H., Faulkner, D.R., Butcher, A.R. and Espie, A.A. (2015) 'Permeability of the Mercia Mudstone: suitability as caprock to carbon capture and storage sites' *Geofluids,* vol. 16, pp. 26-42. doi: 10.1111/gfl.12134. Available at <http://doi.wiley.com/10.1111/gfl.12134>

Atkins, P. (2001) 'The Elements of Physical Chemistry: With Applications in Biology', 3rd edn, Chapter 16, Published in the UK by Oxford University Press. Available at https://www.chem.uwec.edu/chem406_f06/pages/lecture_notes/lect05/Atkins-Ch16_big.pdf

B

Bala, A. (2014) 'Sub-Seabed Burial of Nuclear Waste: If the Disposal Method Could Succeed Technically, Could It Also Succeed Legally?' *Boston College Environmental Affairs Law Review*, vol. 41, Issue 2, pp.455–486. Available at <http://lawdigitalcommons.bc.edu/ealr/vol41/iss2/6>

Banks, D., Withers, J.G., Cashmore, G. and Dimelow, C. (2013) 'An overview of the results of 61 in situ thermal response tests in the UK', *Quarterly Journal of Engineering Geology and Hydrogeology*, vol. 46, 2013, pp. 281–291. Available at < http://qjegh.lyellcollection.org/content/46/3/281>

Barclay, W.J., Riley, N.J. and Strong, G.E. (1994) 'The Dinantian rocks of the Sellafield area, west Cumbria', *Proceedings of the Yorkshire Geological Society*, vol. 50, Part 1, pp.37–49. Available at <http://pygs.lyellcollection.org.ezproxy.is.ed.ac.uk/content/50/1/37>

Barnes, R.P., Chadwick, R.A., Darling, W.G., Gale, I.N., Kirby, G.A. and Kirk, K.L. (2005) 'Contribution to Nirex review of a Deep Brine Repository Concept', *British Geological Survey, Commissioned Report,* CR/05/230N. Available at <http://nora.nerc.ac.uk/11333/>

Bastin, J.C., Boycott-Brown, T., Sims, A. and Woodhouse, R. (2003) 'The South Morecambe Gas Field, Blocks 110/2a, 110/3a, 110/7a and 110/8a, East Irish Sea', *United Kingdom Oil and Gas Fields, Commemorative Millennium Volume.* Geological Society, London, Memoir, vol. 20, pp.107–120. Available at <http://mem.lyellcollection.org.ezproxy.is.ed.ac.uk/content/20/1/107>

Bath, A.H., Richards, H., Metcalfe, R., McCartney, R., Degnan, P. and Littleboy, A. (2006) 'Geochemical indicators of deep groundwater movements at Sellafield, UK', *Journal of Geochemical Exploration*, vol. 90, pp. 24–44. Available at <https://www.sciencedirect.com/science/article/pii/S0375674205002281>

Bath, A.H., McCartney, R., Richards, H., Metcalfe, R.and Crawford, M.B. (1996) 'Groundwater chemistry in the Sellafield area: a preliminary interpretation', *Quarterly Journal of Engineering Geology,* vol. 29, pp.30-57. Available at <http://qjegh.lyellcollection.org/content/29/Supplement_1/S39>

Batu, V. (1998) 'Aquifer Hydraulics: A comprehensive Guide to Hydrogeologic Data Analysis', John Wiley & Sons Inc.

Beale, H. and Taylor, S.J. (1989) 'Deep Repository Design - Offshore Concepts', *Advances in underwater technology ocean science and offshore engineering*, Graham & Trotman, London, pp. 305–316.

Beauheim, R.L. and Holt, R.M. (1990) 'Hydrogeology of the WIPP Site', Accessed 2017, Available at <http://www.wipp.energy.gov/library/Information_Repository_A/Supplemental_Information/Beauheim and Holt 1990.pdf>

Bein, A. and Arad, A. (1992) 'Formation of saline groundwaters in the Baltic region through freezing of seawater during glacial periods', *Journal of Hydrology*, vol. 140, pp.75–87, Elsevier Science Publishers B.V., Amsterdam.

Bensabat, J. (2018) 'Panacea Deliverable: Predicting and monitoring the long-term behaviour of CO_2 injection in deep geological formations'. ***Unpublished***.

Berry, J.A., Baker, A.J., Bond, K.A., Cowper, M.M., Jefferies, N.L. and Linklater, C.M. (1999) 'The role of sorption onto rocks of the Borrowdale Volcanic Group in providing chemical containment for a potential repository at Sellafield'. From Metcalfe, R. and Rochelle, C.A. (ed.) (1999) 'Chemical Containment of Waste in the Geosphere', *Geological Society, London, Special Publications,* vol. 157, pp. 101-116. Available at <http://sp.lyellcollection.org/cgi/doi/10.1144/GSL.SP.1999.157.01.08>

Best, M.G (2002) 'Igneous and Metamorphic Petrology', 2nd edn, Wiley-Blackwell. ISBN: 978-1-4051-0588-0.

Bjørlykke, K. (1993) 'Fluid flow in sedimentary basins', *Sedimentary Geology*, vol. 86, pp.137–158. Available at <https://www.sciencedirect.com/science/article/pii/003707389390137T>

Bjørlykke, K. (1994) 'Fluid-flow processes and diagenesis in sedimentary basins'. From Parnell, J. (ed.) (1994) 'Geofluids: Origin, Migration and Evolution of Fluids in Sedimentary Basins', *Geological Society Special Publication,* No. 78, pp 127-140. Available at < http://sp.lyellcollection.org/content/78/1/127>

Bjørlykke, K. and Høeg, K. (1997) 'Effects of burial diagenesis on stresses, compaction and fluid flow in sedimentary basins', *Marine and Petroleum Geology*, vol. 14, no. 3, pp.267–276. Available at <https://www.sciencedirect.com/science/article/pii/S0264817296000517>

Black, J.H. and Barker, J.A. (2015) 'the puzzle of high heads beneath the West Cumbrian coast, UK: a possible solution', *Hydrogeology Journal*, vol. 24, pp.439–457, DOI 10.1007/s10040-015-1340-4. Available at <http://link.springer.com/10.1007/s10040-015-1340-4>

Black, J.H. and Brightman, M.A. (1996) 'Conceptual model of the hydrology of Sellafield', *Quarterly Journal of Engineering Geology*, vol. 29, pp. 83–93. Available at <http://qjegh.lyellcollection.org/content/29/Supplement_1/S83>

Blomqvist, R., Jaakkola, T., Niini, H. and Ahonen, L. (1991) 'The Palmottu Analogue Project: Progress Report 1990', *Geological Survery of Finland, Nuclear Waste Disposal Research,* Report YST-73. Available at <http://tupa.gtk.fi/julkaisu/ydinjate/yst_073.pdf>

Bodvarsson, G.S., Boyle, W., Patterson, R. and Williams, D. (1999) 'Overview of scientific investigations at Yucca Mountain - the potential repository for high-level nuclear waste', *Journal of Contaminant Hydrology*, vol. 38, Issues 1-3, pp. 3–24. Available at <https://www.sciencedirect.com/science/article/pii/S0169772299000091>

Bond, A. (2016) 'DECOVALEX-2015 project Task C1 final report', KTH Architecture and the Built Environment, Stockholm, Sweden. Available at <http://decovalex.org/resources.html>

Boulby (2017) 'Boulby Underground Laboratory' webpage, Accessed 2017, Available at <www.boulby.stfc.ac.uk>

British Geological Survey (1976) 'Hydrogeological Map of North East Anglia: Sheet 1 Regional Hydrological Characteristics and Explanatory Notes', Accessed 2016, Available at <http://www.largeimages.bgs.ac.uk/iip/mapsportal.html?id=1003972>

British Geological Survey (1991) 'Geology of the United Kingdom, Ireland and the Adjacent Continental Shelf (South Sheet)'. *British Geological Survey*, 1:1 000 000, small scale (non-series) maps. Accessed September 2016, Available at <http://www.largeimages.bgs.ac.uk/iip/mapsportal.html?id=1004594>

British Geological Survey (1997) 'Bootle', England and Wales Sheet 47. Solid and Drift Geology. 1:50 000 Series. Available at <http://www.largeimages.bgs.ac.uk/iip/mapsportal.html?id=1001526>

British Geological Survey (1999a) 'Gosforth', England and Wales Sheet 37, Solid Geology, 1:50 000 Series. Available at <http://www.largeimages.bgs.ac.uk/iip/mapsportal.html?id=1001517>

British Geological Survey (1999b) 'Swaffham', England and Wales Sheet 160. Solid and Drift Geology. 1:50 000 Series. Available at <http://www.largeimages.bgs.ac.uk/iip/mapsportal.html?id=1001651>

British Geological Survey (2018) 'Radioactivity and the Environment' webpage, Accessed 2018, Available at <http://www.bgs.ac.uk/rate/>

C

Cai, Z. and Ofterdinger, U. (2014) 'Numerical assessment of potential impacts of hydraulically fractured Bowland Shale on overlying aquifers', *Water Resources Research*, vol. 50, pp.6236–6259. Available at <https://agupubs.onlinelibrary.wiley.com/doi/abs/10.1002/2013WR014943>

Cao, X., Hu, L., Wang, J, and Wang, J. (2017) 'Regional Groundwater Flow Assessment in a Prospective High-Level Radioactive Waste Repository of China', *Water*, vol. 9, issue 551. doi: 10.3390/w9070551. Available at <http://www.mdpi.com/2073-4441/9/7/551>

Cengel, Y.A. and Boles, M.A. (2011) 'Energy, Energy Transfer, and General Energy Analysis', from 'Thermodynamics: An Engineering Approach', 7th edn., McGraw-Hill. ISBN: 978-007-131111-3.

Chadwick, R.A., Evans, D.J., Wingfield, R.T.R., Hulbert, A.G. and Holliday, D.W. (1992) 'An Interpretation of Regional Seismic Reflection Data Offshore Sellafield', British Geological Survey Technical Report No. WA/91/56C Version 2, Nirex Report No. 270.

Chadwick, R.A., Kirby, G.A. and Baily, H.E. (1994) 'The post-Triassic structural evolution of north-west England and adjacent parts of the East Irish Sea', *Proceedings of the Yorkshire Geological Society*, vol. 50, part 1, pp.91–102. Available at <http://pygs.lyellcollection.org/content/50/1/91>

Chambers, A.V. and Williams, S.J. (2010) 'The Basis for Cumulative Distribution Functions Used in the Groundwater Pathway Calculations of the Nirex Generic Post-closure Performance Assessment'. Available at <https://tools.nda.gov.uk/publication/the-basis-for-cumulative-distribution-functions-used-in-the-groundwater-pathway-calculations-of-the-nirex-generic-post-closure-performance-assessment/>

Chaplow, R. (1996) 'The geology and hydrogeology of Sellafield: an overview', *Quarterly Journal of Engineering Geology and Hydrogeology*, vol. 29, pp. S1–S12. Available at <http://qjegh.lyellcollection.org/content/29/Supplement_1/S1>

Chapman, N.A., McEwen, T.J. and Beale, H. (1986) 'Geological Environments for Deep Disposal of Intermediate Level Wastes in the United Kingdom', pp.311–328, from 'Siting, Design and Construction of Underground Repositories for Radioactive Wastes', Proceedings of a Symposium, Hannover, 3-7 March 1986. International Atomic Energy Agency, Vienna. Available at <http://www.geos.ed.ac.uk/homes/rsh/Chapman_McEwen_Beale_BGS_1986_geol_environments_deep_disposal_ILW_UK_IAEA-SM-289-37_Vienna_1986.pdf>

Chapman, N.A., McKinley, I.T. and Smellie, J.A.T. (1984) 'The potential of natural analogues in assessing systems for deep disposal of high-level radioactive waste', SKB Technical Report

TR 84-16, Stockholm, Sweden. Available at <http://skb.se/upload/publications/pdf/TR84-16webb.pdf>

Chittenden, N., McDermott, C.I., Bond, A., Wilson, J. and Norris, S. (2016) 'Evaluating the importance of different coupled thermal, hydraulic, mechanical and chemical process simulations during fluid flow experiments in fractured novaculite and fractured granite', *Environmental Earth Sciences*, vol. 75, pp. 1–18, doi: 10.1007/s12665-016-5938-1.

Clark, C.D., Hughes, A.L.C., Greenwood, S.L., Jordan, C. and Petter Sejrup, H. (2012) 'Pattern and timing of retreat of the last British-Irish Ice Sheet', *Quaternary Science Reviews*, vol. 44, pp. 112–146, doi: 10.1016/j.quascirev.2010.07.019. Available at <http://dx.doi.org/10.1016/j.quascirev.2010.07.019>

Coli, M. and Pinzani, A. (2014) 'Tunnelling and Hydrogeological Issues: A Short Review of the Current State of the Art', *Rock Mechanics and Rock Engineering*, vol. 47, issue 3, pp. 839–851, doi: 10.1007/s00603-012-0319-x. Available at <https://link.springer.com/article/10.1007/s00603-012-0319-x>

Colley, S. and Thomson, J. (1991) 'Migration of uranium daughter radionuclides in natural sediments, *Institue of Oceanographic Sciences Deacon Laboratory,* Report No. 276. Available at <http://nora.nerc.ac.uk/id/eprint/115295/1/15295-01.pdf >

Copeland Borough Council (2013) 'Executive decision regarding the WC MRWS process' letter, 11th February 2013. Available at <http://www.westcumbriamrws.org.uk/all_documents.asp>

Cordes, C. and Kinzelbach, W. (1992) 'Continuous Groundwater Velocity Fields and Path Lines in Linear, Bilinear, and Trilinear Finite Elements', *Water Resources Research,* vol. 28, No. 11, pp. 2903-2911. Available at <https://agupubs.onlinelibrary.wiley.com/doi/pdf/10.1029/92WR01686>

Corkhill, C.L., Cassingham, N.J, Heath, P.G. and Hyatt, N.C. (2013) 'Dissolution of UK High-Level Waste Glass Under Simulated Hyperalkaline Conditions of a Colocated Geological Disposal Facility', *International Journal of Applied Glass Science*, vol. 4, issue 4, pp. 341–356, doi: 10.1111/ijag.12042. Available at <https://onlinelibrary.wiley.com/doi/abs/10.1111/ijag.12042>

Cosenza, P., Ghoreychi, M., Bazargan-Sabet, B. and de Marsily, G. (1999) 'In situ rock salt permeability measurement for long term safety assessment of storage', *International Journal of Rock Mechanics and Mining Sciences*, vol. 36, pp. 509–526. Available at <https://www-sciencedirect-com.ezproxy.is.ed.ac.uk/science/article/pii/S0148906299000170>

Cowan, G. and Boycott-Brown, T. (2003) 'The North Morecambe Field, Block 110/2a, East Irish Sea. From Gluyas, J.G and Hichens, H.M. (eds) (2003). *United Kingdom Oil and Gas Fields Commemorative Millennium Volume*. Geological Society, London, Memoir, Vol. 20, pp. 97-105. Available at <http://mem.lyellcollection.org.ezproxy.is.ed.ac.uk/content/20/1/97>

Crossrail (2018a) 'Crossrail Construction: Tunnelling - Railway Tunnels' webpage. Accessed 2017. Available at <http://www.crossrail.co.uk/construction/tunnelling/railway-tunnels/>

Crossrail (2018b) Crossrail About us: Funding' webpage. Accessed 2017. Available at <http://www.crossrail.co.uk/about-us/funding>

D

Darling, W.G., Edmunds, W.M. and Smedley, P.L. (1997) 'Isotopic evidence for paleowaters in the British Isles', *Applied Geochemistry*, vol. 12, issue 97, pp. 813–829. Available at <https://www-sciencedirect-com.ezproxy.is.ed.ac.uk/science/article/pii/S0883292797000383>

Davies, N. and Chaplow, R. (1998) 'Geotechnical characteristics of the Borrowdale Volcanic Group', *Proceedings of the Yorkshire Geological Society*, vol. 52, part 2, pp. 189–197. Available at <http://pygs.lyellcollection.org.ezproxy.is.ed.ac.uk/content/52/2/189>

Davis, A.M. (1996) 'Geophysics in offshore site investigation: a review of the state of the art'. From De Batist, M. and Jacobs, P. (eds) (1996) 'Geology of Siliclastic Shelf Seas', *Geological Society Special Publications*, No. 117, pp. 323–338. Available at <http://sp.lyellcollection.org/content/117/1/323>

Degnan, P., Bath, A., Cortés, A., Delgado, J., Haszeldine, S., Milodowski, A., Puigdomenech, I., Recreo, F., Šilar, J., Torres, T. and Tullborg, E-L. (2005) 'PADAMOT: Project Overview Report', *PADAMOT Project Technical Report*, pp. 105. Available at <http://collections.internetmemory.org/haeu/20161115170523/http://cordis.europa.eu/pub/fp5-euratom/docs/projrep-padamot_en.pdf>

Department for Business, Energy & Industrial Strategy (2017) 'Digest of United Kingdom Energy Statistics 2017, *National Statistics Publication*, July 2017. Available at <https://www.gov.uk/government/uploads/system/uploads/attachment_data/file/643414/DUKES_2017.pdf.

Department for Business, Energy & Industrial Strategy (2018) 'CONSULATION Working With Communities: Implementing Geological Disposal', January 2018. Available at <https://assets.publishing.service.gov.uk/government/uploads/system/uploads/attachment_data/file/676391/WWC_consultation.pdf>

Department for Business, Enterprise & Regulatory Reform (2008) 'Meeting the Energy Challenge: A White Paper on Nuclear Power', January 2008. Available at <https://www.gov.uk/government/uploads/system/uploads/attachment_data/file/228944/7296.pdf>

Department of Energy & Climate Change (2013a) 'MRWS - Cumbria' letter from Department of Energy & Climate Change to Cumbria Country Council, 4th March 2013. Available at <http://www.westcumbriamrws.org.uk/all_documents.asp>

Department of Energy & Climate Change (2013b) 'Nuclear Industrial Strategy: the UK's Nuclear Future', *Department of Energy and Climate Change*, London, 26th March 2013, Accessed 2018, Available at <https://www.gov.uk/government/publications/nuclear-industrial-strategy-the-uks-nuclear-future>

Dimberline, A.J., Bell, A. and Woodcock, N.H. (1990) 'A laminated hemipelagic facies from the Wenlock and Ludlow of the Welsh Basin', *Journal of the Geological Society, London*, vol. 147, pp. 693–701. Available at <http://jgs.lyellcollection.org/content/147/4/693>

Domenico, P.A. and Mifflin, M.D. (1965) 'Water from Low-Permeability Sediments and Land Subsidence', *Water Resources Research*, vol. 1, No. 4, pp. 563–566. Available at <https://agupubs.onlinelibrary.wiley.com/doi/abs/10.1029/WR001i004p00563>

Domenico, P.A. and Schwartz, F.W. (1997) 'Physical and Chemical Hydrogeology', 2nd edn, John Wiley & Sons. ISBN: 0-471-597662-7.

Downing, R.A. and Gray, D.A. (1986) 'Geothermal resources of the United Kingdom', *Journal of the Geological Society, London*, vol. 143, issue 3, pp. 499–507. Available at <http://jgs.lyellcollection.org/content/143/3/499>

Dybeck, P. and Kåwemark, B. (1996) 'Experience from eight years of operation of SFR, the final repository for LLW in Sweden'. From 'Planning and Operation of Low Level Waste Disposal Facilities', Proceedings of a Symposium, Vienna, 17-21 June 1996, pp. 305–312. Available at <http://www.iaea.org/inis/collection/NCLCollectionStore/_Public/28/038/28038144.pdf?r=1>

E

Edmunds, W.M, Robins, N.S. and Shand, P. (1998) 'The saline waters of Llandrindod and Builth, Central Wales', *Journal of the Geological Society, London*, vol. 155, pp. 627–637. Available at <http://jgs.lyellcollection.org/content/155/4/627>

Efron, N. and Read, M. (2012) 'Analysing International Tunnel Costs: An Interactive Qualifying Project', *Worcester Polytechnic Institute*. Available at <https://www.wpi.edu/Pubs/E-project/Available/E-project-043012-122558/unrestricted/Analysing_International_Tunnelling_Costs_Public_Report.pdf>

Elam, M. and Sundqvist, G. (2011) 'The Swedish KBS project: a last word in nuclear fuel safety prepares to conquer the world?' From Strandberg, U. and Andrén, M. (eds) (2011) 'Nuclear Waste Management in a Globalised World', *Routledge*. ISBN13: 978-0-415-61567-9.

Ellinas, C.P. (1990) 'Advances In Underwater Technology, Ocean Science and Offshore Engineering'. Proceedings of Aspect '90, a conference organised by the Society for Underwater Technology and held in Aberdeen, Scotland, May 30-31, *Kluwer Academic Publishers*. ISBN: 0-7923-0794-1.

Engelder, T. (1993) 'Stress Regimes in the Lithosphere', *Princeton University Press*. ISBN: 9781400863150.

Engineering ToolBox (2003) 'Altitude above Sea Level and Air Pressure' webpage, Accessed 2016, Available at <http://www.engineeringtoolbox.com/air-altitude-pressure-d_462.html>

Environment Agency (2009) 'Geological Disposal Facilities on Land for Solid Radioactive Wastes: Guidance on Requirements for Authorisation February 2009', Environment Agency. Available at <https://www.gov.uk/government/uploads/system/uploads/attachment_data/file/296504/geho0209bpjm-e-e.pdf>

Environment Agency (2016) 'What's In Your Backyard? Webpage', Accessed 2016, Available at <http://www.environment-agency.gov.uk/wiyby>

Eppelbaum, L., Kutasov, I. and Pilchin, A., (2014) 'Thermal properties of rocks and density of fluids', *Applied Geothermics*, Lecture Notes in Earth System Sciences, pp. 99-149. ISBN: 978-3-642-34022-2. Available at <http://link.springer.com/10.1007/978-3-642-34023-9>

Eurotunnel (2018) 'The Channel Tunnel – Interesting Facts' Webpage. Accessed 2017, Available at <https://www.eurotunnel.com/uk/build/>

F

Falck, W.E, and Hooker, P.J. (1990) 'Quantitative interpretation of Cl, Br and I porewater concnetration profiles in lake sediments of Loch Lomond, Scotland', *Comission of the European Communities; nuclear science and technology.* ISBN: 92-826-0516-7. Available at <https://publications.europa.eu/en/publication-detail/-/publication/fe2a54a9-65a3-44c5-a48e-df0c4e36116e/language-en>

Fetter, C.W. (2001) 'Applied Hydrogeology', 4th edn, Prentice Hall. ISBN: 978-0-130-88239-4.

Figueiredo, B., Tsang, C-F., Rutqvist, J. and Niemi, A. (2015) 'A study of changes in deep fractured rock permeability due to coupled hydro-mechanical effects', *International Journal of Rock Mechanics and Mining Sciences*, vol. 79, pp. 70–85. Available at <http://dx.doi.org/10.1016/j.ijrmms.2015.08.011>

Frape, S.K., Fritz, P. and McNutt, R.H. (1984) 'Water-rock interaction and chemistry of groundwaters from the Canadian Shield', *Geochimica et Cosmochimica Acta*, vol. 48, pp. 1617–1627. Available at <https://www.sciencedirect.com/science/article/pii/0016703784903314>

Fraser-Harris, A.P. (2012) 'Investigating the Coupled Thermo-Hydro-Chemical effects on groundwater flow caused by disposal of Higher Level Radioactive Waste using Sellafield, UK as a case study', MSc Thesis, University of Edinburgh, Edinburgh, Scotland.

Fraser Harris, A.P., McDermott, C.I., Kolditz, O. and Haszeldine, R.S. (2015) 'Modelling groundwater flow changes due to thermal effects of radioactive waste disposal at a hypothetical repository site near Sellafield, UK', *Environmental Earth Sciences*, vol. 74, issue 2, pp. 1589-1602. Available at <http://link.springer.com/10.1007/s12665-015-4156-6>

Freeze, A.R. and Cherry, J.A. (1979) 'Groundwater', 1st edn, Prentice-Hall Inc. ISBN: 0-13-365312-9.

Fritz, P. and Frape, S.K. (1982) 'Saline Groundwaters in the Canadian Shield - A first overview'. From 'Geochemistry of Radioactive Waste Disposal', *Chemical Geology*, vol. 36, issues 1–2, pp. 179–190. Available at <https://www.sciencedirect.com/science/article/pii/0009254182900456>

G

Gauthier-Lafaye, F. (2002) ‘2 billion year old natural analogs for nuclear waste disposal: the natural nuclear fission reactors in Gabon (Africa)’, C.R.Physique 3, pp. 839-849. Available at <https://www.sciencedirect.com/science/article/pii/S1631070502013518>

Ge, S., Bekins, B., Bredehoeft, J., Brown, K., Davis, E.E., Gorelick, S.M., Henry, P., Kooi, H., Moench, A.F., Rupel, C., Sauter, M., Screaton, E., Swart, P.K., Tokunaga, T., Voss, C.I. and Whitaker, F.(2003) ‘Fluid Flow in Sub-sea Floor Processes and Future Ocean Drilling’, *Eos, Transactions American Geophysical Union*, vol. 84, No. 16, pp.151–152. Available at <https://agupubs.onlinelibrary.wiley.com/doi/abs/10.1029/2003EO160002>

Geuzaine, C. and Remacle, J-F. (2009) ‘Gmsh: a three-dimensional finite element mesh generator with built-in pre- and post-processing facilities’, *International Journal for Numerical Methods in Engineering*, vol. 79, issue 11, pp. 1309-1331. Available at < https://onlinelibrary.wiley.com/doi/abs/10.1002/nme.2579 >

Gin, S. (2014) ‘Open Scientific Questions about Nuclear Glass Corrosion’, *Procedia Materials Science*, vol. 7, pp. 163–171. Available at <http://linkinghub.elsevier.com/retrieve/pii/S2211812814010657>

Gluyas, J. and Swarbrick, R. (2003) ‘Petroleum Geoscience’, 2nd edn, Blackwell Publishing. ISBN: 978-0-632-03767-4.

GoldSim Technology Group (2017a) ‘Goldsim Contaminant Transport Module User’s Guide’, Accessed 2017, Available at < https://www.goldsim.com/Web/Customers/Education/Documentation/>

GoldSim Technology Group (2017b) ‘Goldsim User’s Guide’, Accessed 2017, Available at < https://www.goldsim.com/Web/Customers/Education/Documentation/>

GoldSim Technology Group (2017c) ‘GoldSim Software’.

GoldSim Technology Group (2017d) ‘GoldSim’ webpage, Accessed 2017. Available at <www.goldsim.com/web/home/>

GoldSim Technology Group (2018) GoldSim: Help Topics.

Grasshoff, K., Kremling, K. and Ehrhardt, M. (1999) ‘Methods of Seawater Analysis’, 3rd edn, Wiley-VCH. ISBN: 3-527-29589-5.

Gu, Z., Zhu, L. and Zhong, J. (2004) ‘Modern Undersea Tunneling Technology and the Undersea Tunnel across Taiwan Strait’, *Marine Georesources & Geotechnology*, vol. 22, issue 3, pp. 151–164. Available at <http://www.tandfonline.com/doi/abs/10.1080/10641190490503980>

Gustafsson, E., Skålberg, M., Sundblad, B., Karlberg, O., Tullborg, E-L., Ittner, T., Carbol, P., Eriksson, N. and Lampe, S. (1987) ‘Radionuclide depositorion and migration within the Gideå and Finnsjön study sites, Sweden: A study of the fallout after the Chernobyl accident: Phase 1, initial survey’, *Svensk Kärnbränslehantering AB,* Technical Report No. 87-28. Available at <http://www.skb.com/publication/3271/TR87-28webb.pdf>

Gutmanis, J.C., Lanyon, G.W., Wynn, T.J. and Watson, C.R. (1998) ‘Fluid flow in faults: a study of fault hydrogeology in Triassic sandstone and Ordovician volcaniclastic rocks at Sellafield, north-west England’, *Proceedings of the Yorkshire Geological Society*, vol. 52, part 2, pp. 159–175. Available at <http://pygs.lyellcollection.org/content/52/2/159>

H

Harley, S., Rigonat, N. and Butler, I. (2016) 'Magnetic Materials: Novel Monitors of Long-Term Evolution of Engineered Barrier Systems', *Geosciences*, vol. 6, issue 4, pp. 1-15. Available at <http://www.mdpi.com/2076-3263/6/4/54>

Haszeldine, R.S. and McKeown, C. (1995) 'A model approach to radioactive waste disposal at Sellafield', *Terra Nova*, vol. 7, pp. 87-95. Available at <http://onlinelibrary.wiley.com/doi/10.1111/j.1365-3121.1995.tb00671.x/pdf>

Haszeldine, R.S. and Smythe, D.K. (1996) 'Radioactive waste disposal at Sellafield, UK: Site selection, geological and engineering problems', 1st edn, Department of Geology and Applied Geology, University of Glasgow. ISBN: 0-852-61524-8.

Hidekazu, Y. (2012) 'A reconsideration on deep sea bed disposal of high level radiological wastes – a post-Fukushima reflection on sustainable nuclear energy in Japan', *Nuclear Safety and Simulation*, vol. 3, No. 4. Available at <http://www.ijnsweb.com/?type=subscriber&action=download&file=final&ext=pdf&id=143>

Hiscock, K.M. (2005) 'Hydrogeology: Principles and Practice, 1st edn., Blackwell Publishing. ISBN: 978-0-632-05763-4.

Hiscock, K.M. & Tabatabai Najafi, M. (2011) 'Aquitard characteristics of clay-rich till deposits in East Anglia, Eastern England', *Journal of Hydrology*, vol. 405, issues 3–4, pp. 288–306. Available at <http://dx.doi.org/10.1016/j.jhydrol.2011.05.025>

Hobbs, P.R.N., Entwisle, D.C., Northmore, K.J., Sumbler, M.G., Jones, L.D., Kemp, S., Self, S., Barron, M. and Meakin, J.L. (2012) 'Engineering Geology of British Rocks and Soils - Lias Group', *British Geological Survey Internal Report*, OR/12/032. 323pp. Available at < http://nora.nerc.ac.uk/id/eprint/17270/>

Hollister, C.D. and Nadis, S. (1998) 'Burial of Radioactive Waste under the Seabed', *Scientific American*, vol. 278, No. 1, pp. 60–65. Available at <https://www.jstor.org/stable/26057623>

Houben, M.E. ten Hove, A., Peach, C.J. and Spiers, C.J. (2013) 'Crack healing in rocksalt via diffusion in adsorbed aqueous films: Microphysical modelling versus experiments', *Physics and Chemistry of the Earth*, vol. 64, pp. 95–104. Available at <http://dx.doi.org/10.1016/j.pce.2012.10.001>

Hudson, J.A., Stephansson, O., Andersson, J., Tsang, C-F. and Ling, L. (2001) 'Coupled T-H-M issues relating to radioactive waste repository design and performance', *International Journal of Rock Mechanics and Mining Sciences*, vol. 38, issue 1, pp. 143–161. Available at <https://www.sciencedirect.com/science/article/pii/S1365160900000708>

Hudson, J.A., Stephansson, O. and Andersson, J. (2005) 'Guidance on numerical modelling of thermo-hydro-mechanical coupled processes for performance assessment of radioactive waste repositories', *International Journal of Rock Mechanics and Mining Sciences*, vol. 42, issues 5–6, pp. 850–870. Available at <https://www.sciencedirect.com/science/article/pii/S1365160905000456>

Hudson, J.A. and Jing, L. (2012) 'DECOVALEX-2011 project Executive Summary', KTH Architecture and the Built Environment, Stockholm, Sweden. Available at <http://decovalex.org/resources.html>

Huyakorn, P.S. and Pinder, G.F. (1983) 'Computational Methods in Subsurface Flow', 3rd edn, Academic Press. ISBN: 978-0-323-13797-3.

I

Infrastructure UK (2010) 'Infrastructure Cost Review: Technical Report', Annual Report 2011-2012, HM Treasury. Available at <www.gov.uk/government/publications/infrastructure-cost-review>

Ingebritsen, S.E. and Manning, C.E. (1999) 'Geological implications of a permeability-depth curve for the continental crust', *Geology*, vol. 27, issue 12, pp. 1107–1110. Available at <https://pubs.geoscienceworld.org/gsa/geology/article/27/12/1107/207065/geological-implications-of-a-permeability-depth>

Institute of Nuclear Power Operations (2011) 'Special Report on the Nuclear Accident at the Fukushima Daiichi Nuclear Power Station, Special Report, Report No. 11-005. Available at <https://www.oecd-nea.org/nsd/fukushima/documents/INPO2011_11_SpecialReportonFukushimaDaiichi11-005>

International Atomic Energy Agency (2003) 'Scientific and Technical Basis for the Geological Disposal of Radioactive Wastes', Technical Report Series No. 413, Vienna, Austria. Available at <www-pub.iaea.org/MTCD/Publications/PDF/TRS413_web.pdf>

International Atomic Energy Agency (2009a) 'Classification of Radioactive Waste', IAEA Safety Standards, General Safety Guide No. GSG-1, Vienna, Austria. Available at <https://www-pub.iaea.org/books/IAEABooks/8154/Classification-of-Radioactive-Waste-General-Safety-Guide>

International Atomic Energy Agency (2009b) 'Safety Assessment for Facilities and Activities', IAEA Safety Standards, General Safety Requirements Part 4 No. GSR Part 4, Vienna, Austria. Available at <https://www-pub.iaea.org/books/iaeabooks/10884/Safety-Assessment-for-Facilities-and-Activities>

International Atomic Energy Agency (2011a) 'Disposal of radioactive waste', IAEA Safety Standards, Specific Safety Requirements No. SSR-5, Vienna, Austria. Available at <https://www-pub.iaea.org/books/iaeabooks/8420/Disposal-of-Radioactive-Waste>

International Atomic Energy Agency (2011b) 'Geological Disposal Facilities for Radioactive Waste', IAEA Safety Standards, Specific Safety Guide No. SSG-14, Vienna, Austria. Available at <https://www-pub.iaea.org/books/iaeabooks/8535/Geological-Disposal-Facilities-for-Radioactive-Waste>

International Atomic Energy Agency (2014) International Atomic Energy Agency: Radioactive Waste Disposal Facilities Webpage. Available at: http://www-ns.iaea.org/standards/documents/default.asp?s=11&l=90&sub=40&vw=1#sf.

Istok, J. (1989) ‘Groundwater Modelling by the Finite Element Method’, 1st edn, American Geophysical Union. ISBN: 0-875-90317-7.

J

Jackson, D.I., Jackson, A.A., Evans, D., Wingfield, R.T.R., Barnes, R.P. and Arthur, M.J. (1995) ‘United Kingdom offshore regional report: the geology of the Irish Sea’, British Geological Survey, London. ISBN: 0-118-84507-1.

Jackson, D.I., Johnson, H. and Smith, J.P. (1997) ‘Stratigraphical relationships and a revised lithostratigraphical nomenclature for the Carboniferous, Permian and Triassic rocks of the offshore East Irish Sea Basin’. From Meadows, N.S., Trueblood, S.P, Hardman, M. and Cowan, G (eds) (1997) ‘Petroleum Geology of the Irish Sea and Adjacent Areas’, *Geological Society Special Publication No. 124*, pp.11–32. Available at <http://sp.lyellcollection.org/content/124/1/11>

Jackson, D.I., Mulholland, P., Jones, S. and Warrington, G. (1987) ‘The Geological Framework of the East Irish Sea Basin’. From Brooks J, and Glennie K.W (1986) ‘Petroleum Geology of North West Europe’, Proceedings of the 3rd Conference, London, 26-29 October 1986, pp.191-204.

Jackson, D.I. and Mulholland, P. (1993) ‘Tectonic and stratigraphic aspects of the East Irish Sea Basin and adjacent areas: contrasts in their post-Carboniferous structural styles’. From Parker, J.R. (1993) ‘Petroleum Geology of Northwest Europe’, Proceedings of the 4th Conference, *Geological Society, London,* pp.791–808. Available at <http://pgc.lyellcollection.org/content/4/1/791>

Jiao, J.J., Shi, L. and Kuang, X. (2015) Reconstructed chloride concentration profiles below the seabed in Hong Kong (China) and their implications for offshore groundwater resources’, *Hydrogeology Journal*, vol. 23, pp. 277–286. Available at <https://link.springer.com/article/10.1007/s10040-014-1201-6>

Jing, L., Hudson, J.A. and Birkholzer, J. (2016) ‘DECOVALEX-2015 project Executive Summary’, KTH Architecture and the Built Environment, Stockholm, Sweden. Available at <http://decovalex.org/resources.html>

Johns, R.T. and Resele, G. (1997) ‘Solution and scaling of one-dimensional groundwater-solute flow with large density variations’, *Water Resources Research*, vol. 33, No. 6, pp. 1327-1334. Available at <https://agupubs.onlinelibrary.wiley.com/doi/abs/10.1029/97WR00656>

Johnson, L.H. and King, F. (2003) ‘Canister Options for the Disposal of Spent Fuel’, Technical Report 02-11, April 2003, National Cooperative for the Disposal of Radioactive Waste (NAGRA). Available at <https://www.nagra.ch/data/documents/database/dokumente/$default/Default%20Folder/Publikationen/NTBs%202001-2010/e_ntb02-11.pdf>

Joint Nature Conservation Committee (2003) ‘Irish Sea Pilot – Bottom temperature (Dec-Feb)’. Available at <http://jncc.defra.gov.uk/pdf/irish_finalreport(maps).pdf>

Jones, F.O. and Owens, W.W. (1980) ‘A Laboratory Study of Low-Permeability Gas Sands’, *Journal of Petroleum Technology*, vol. 32, issue 9, pp. 193–199. Available at <https://www.onepetro.org/journal-paper/SPE-7551-PA>

Jones, H.K., Morris, B.L., Cheney, C.S., Brewerton, L.J., Merrin, P.D., Lewis, M.A., MacDonald, A.M., Coleby, L.M., Talbot, J.C., McKenzie, A.A., Bird, M.J., Cunningham, J. and Robinson, V.K. (2000) 'The physical properties of minor aquifers in England and Wales', *British Geological Society Technical Report,* WD/00/04. 234PP. Environment Agency R&D Publication 68. Available at <http://nora.nerc.ac.uk/12663/>

K

Kim, J-S., Kwon, S-K., Sanchez, M. and Cho, G-C. (2011) 'Geological Storage of High Level Nuclear Waste', *KSCE Journal of Civil Engineering*, vol. 15, issue 4, pp. 721–737. Available at <http://link.springer.com/10.1007/s12205-011-0012-8>

King, F., Sanderson, D. and Watson, S. (2016) 'Durability of High Level Waste and Spent Fuel Disposal Containers – an overview of the combined effect of chemical and mechanical degradation mechanisms', *Radioactive Waste Management*, Technical Report 17697-TR-03. Available at <https://rwm.nda.gov.uk/publication/durability-of-high-level-waste-and-spent-fuel-disposal-containers/>

Kneller, B.C., Scott, R.W., Soper, N.J., Johnson, E.W. and Allen, P.M. (1994) 'Lithostratigraphy of the Windermere Supergroup, Northern England', *Geological Journal*, vol. 29, pp. 219–240. Available at <https://onlinelibrary.wiley.com/doi/abs/10.1002/gj.3350290304>

Kolditz, O., Beinhorn, M., Xie, M., Kalbacher, T., Bauer, S., Wang, W., McDermott, C., Chen, C., Beyer, C., Gronewold, J., Kemmler, D., Walsh, R., Du, Y., Park, C-H., Hess, M., Bürger, C. and Delfs, J-O. (2008) 'GeoSys/RockFlow Version 4.5.10(WW): Open Source Software Design Proposal'.

Kolditz, O., Bauer, S., Bilke, L., Böttcher, N., Delfs, J.O., Fisher, T., Görke, U.J., Kalbacher, T., Kosakowski, G., McDermott, C.I., Park, C.H., Radu, F., Rink, K., Shao, H., Shao, H.B., Sun, F., Sun, Y.Y., Singh, A.K., Taron, J., Walther, M., Wang, W., Watanabe, N., Wu, Y., Xie, M., Xu, W. and Zehner, B. (2012) 'OpenGeoSys: an open-source initiative for numerical simulation of thermo-hydro-mechanical/chemical (THM/C) processes in porous media', *Environmental Earth Sciences*, vol. 67, issue 2, pp. 589–599. Available at <http://link.springer.com/10.1007/s12665-012-1546-x>

Kolditz, O. & Shao, H. (2009) 'Open THMC Developer Benchmark Book: Based on OpenGeoSys Version 4.10.03'.

Konikow, L.F. and Bredehoeft, J.D. (1992) 'Ground-water models cannot be validated', *Advances in Water Resources*, vol. 15, issue 1, pp. 75–83. Available at <https://www.sciencedirect.com/science/article/pii/030917089290033X>

Krupka, K.M., Kaplan, D.I., Whelan, G., Serne, R.J. and Mattigod, S.V. (1999) 'Understanding Variation in Partition Coefficient, K_d, Values. Volume I: The K_d Model, Methods of Measurement, and Application of Chemical Reaction Codes', *United States Environmental Protection Agency*, EPA Report No. 402-R-99-004A. Available at <https://www.epa.gov/radiation/understanding-variation-partition-coefficient-kd-values>

L

Landström, O. and Sundblad, B. (1986) 'Migration of thorium, uranium, radium and Cs-137 in till soils and their uptake in organic matter and peat', *Svensk Kärnbränslehantering AB,* Technical Report No. 86-24. Available at <http://www.skb.com/publication/3236/TR86-24web.pdf>

Lee, K. and Fetter, C.W. (1994) 'Hydrogeology laboratory manual', 1st edn, Prentice Hall College Div. ISBN-13: 978-0-02369-201-7.

Lee, Y.-M. and Hwang, Y. (2009) 'A GoldSim model for the safety assessment of an HLW repository', *Progress in Nuclear Energy*, vol. 51, issues 6–7, pp. 746–759. Available at <https://www.sciencedirect.com/science/article/pii/S014919700900064X>

Lee, J.R., Woods, M.A. and Morrlock, B.S.P. (eds) (2015) 'British Regional Geology: East Anglia', 5th edn, *British Geological Survey*, Keyworth, Nottingham. ISBN: 978-0-85272-823-9.

Li, S., Tian, H., Xue, Y., Su, M., Qiu, D., Li, L. and Li, Z. (2015) 'Study on Major Construction Disasters and Controlling Technology at the Qingdao Kiaochow Bay Subsea Tunnel', *Journal of Coastal Research*, vol. 73, pp. 403–409. Available at <http://www.bioone.org/doi/10.2112/SI73-071.1>

Lide, D.R. (ed) (2004) 'CRC Handbook of Chemisty and Physics', 85th edn, CRC Press. ISBN 0-8493-0485-7.

Liu, W., Li, Y., Yang, C., Daemen, J.J.K., Yang, Y. and Zhang, G. (2015) 'Permeability characteristics of mudstone cap rock and interlayers in bedded salt formations and tightness assessment for underground gas storage caverns', *Engineering Geology*, vol. 193, pp. 212–223. Available at <https://www.sciencedirect.com/science/article/pii/S001379521500126X>

Lu, J., Wilkinson, M., Haszeldine, R.S. and Fallick, A.E. (2009) 'Long-term performance of a mudrock seal in natural CO_2 storage', *Geology*, vol. 37, no. 1, pp. 35–38. Available at <https://pubs.geoscienceworld.org/gsa/geology/article/37/1/35/193502>

Lu, J., Wilkinson, M., Haszeldine, R.S. and Boyce, A.J. (2011) 'Carbonate cements in Miller field of the UK North Sea: a natural analog for mineral trapping in CO_2 geological storage', *Environmental Earth Sciences*, vol. 62, issue 3, pp. 507–517. Available at <https://link.springer.com/article/10.1007/s12665-010-0543-1>

Lunn, R., Harley, S. and Norris, S. (eds) (2017) 'Geological Disposal of High Level Radioactive Waste - The Relationship between Engineered and Natural Barriers', *Geosciences*, Special Issue, vol. 7. Available at <www.mdpi.com/journal/geosciences/special_issues/geological_disposal>

M

Macaulay, C.I., Haszeldine, R.S. and Fallick, A.E. (1992) 'Diagenetic Pore Waters Stratified for at Least 35 Million Years: Magnus Oil Field, North Sea', *The American Association of Petroleum Geologists Bulletin*, vol. 76, no. 10, pp. 1625–1634. Available at <http://archives.datapages.com/data/bulletns/1992-93/data/pg/0076/0010/0000/1625.htm>

Mather J.D. (1985) 'Hydrogeological Characterisation of Potential Radioactive Waste Repository Host Rocks at Two Research Sites in the United Kingdom', *Hydrogeology in the*

Service of Man, Memoires of the 18th Congress of the International Association of Hydrogeologists. Available at <http://hydrologie.org/redbooks/a154/iahs_154_03_0159>

Matsuo, S. (1986) 'An overview of the Seikan tunnel project', *Tunnelling and Underground Space Technology*, vol. 1, no. 3/4, pp. 323–331. Available at <https://www.sciencedirect.com/science/article/pii/0886779886900155>

McAllister, K.R. (2013) 'Sub-Seabed Repository for Nuclear Waste - a Strategic Alternative'. Proceedings of Waste Management 2013 Conference (WM2013). Available at <http://www.wmsym.org/archives/2013/papers/13102.pdf>

McDermott, C.I. (2003) 'Inside Finite Element for Outsiders', Public Report, Groundwater Modelling Group, Centre for Applied Geosciences, University of Tübingen. Germany.

McDermott, C.I. (ed) (2015) 'Lecture Notes' produced as part of the accredited Hydrogeology 2: Simulation of Groundwater Flow and Transport Course, University of Edinburgh.

McDermott, C.I., Randriamanjatosoa, A.R.L., Tenzer, H. and Kolditz, O. (2006) 'Simulation of heat extraction from crystalline rocks: The influence of coupled processes on differential reservoir cooling', *Geothermics*, vol. 35, issue 3, pp. 321–344. Available at <https://www.sciencedirect.com/science/article/pii/S0375650506000320>

McEvoy, F.M., Schofield, D.I., Shaw, R.P. and Norris, S. (2016) 'Tectonic and climatic considerations for deep geological disposal of radioactive waste: A UK perspective', *Science of the Total Environment*, vol. 571, pp. 507–521. Available at <https://www.sciencedirect.com/science/article/pii/S0048969716314632>

McEwen, T. and Aikas, T. (2000) 'The site selection process for a spent fuel repository in Finland - Summary report', *Posiva Oy*, December 2000, Report Code - POSIVA 2000-15. ISBN: 951-652-101-0. Available at <http://www.posiva.fi/files/2613/POSIVA-2000-15_web.pdf>

McGinnes, D.F. (2002) 'Model Radioactive Waste Inventory for Reprocessing Waste and Spent Fuel', *National Cooperation for the Disposal of Radioactive Waste (NAGRA)*, Technical Report 01-01. Available at <http://www.nagra.ch/data/documents/database/dokumente/$default/Default Folder/Publikationen/NTBs 2001-2010/e_ntb01-01.pdf>

McKeown, C., Haszeldine, R.S. and Couples, G.D. (1999) 'Mathematical modelling of groundwater flow at Sellafield, UK', *Engineering Geology*, vol. 52, issues 3–4, pp. 231–250. Available at <https://www.sciencedirect.com/science/article/pii/S0013795299000083>

McLatchie, A.S., Hemstock, R.A. and Young, J.W. (1957) 'The Effective Compressibility of Reservoir Rock and Its Effects on Permeability', Proceedings of the 32nd Annual Fall Meeting of Society of Petroleum Engineers, Texas, pp. 49–51. Available at <http://www.onepetro.org/doi/10.2118/894-G>

Metcalfe, R., Crawford, M.B., Bath, A.D., Littleboy, A.K., Degnan, P.J. and Richards, H.G. (2007) 'Characteristics of deep groundwater flow in a basin marginal setting at Sellafield, Northwest England: ^{36}Cl and halide evidence', *Applied Geochemistry*, vol. 22, issue 1, pp. 128–151. Available at <https://www.sciencedirect.com/science/article/pii/S0883292706002551>

Metcalfe, R. and Rochelle, C.A. (1999) 'Chemical containment of waste in the geosphere', *Geological Society, London, Special Publications*, vol. 157, issue 1, pp. vii–xvi. Available at <http://sp.lyellcollection.org/content/157/1/vii>

Metcalfe, R., Watson, S.P., Rees, J.H., Humphreys, P. and King, F. (2008) 'Gas Generation and Migration from a Deep Geological Repository for Radioactive Waste: A Review of Nirex/NDA's Work', Technical Report No. NWAT/NDA/RWMD/2008/002, produced for the *Environment Agency*. Available at <https://assets.publishing.service.gov.uk/government/uploads/system/uploads/attachment_data/file/296497/geho1108bozn-e-e.pdf>

Meteorological Office (2017) 'Annual Average Rainfall 1981-2010' webpage, Accessed 2016, Available at <https://www.metoffice.gov.uk/public/weather/climate/>

Meybeck, M., Chapman, D.V. and Helmer, R. (eds) (1989) 'Global Freshwater Quality: A First Assessment', 1st edn, World Health Organisation, Wiley-Blackwell. ISBN-13: 978-0-63117-314-4.

Michie, U. (1996) 'The geological framework of the Sellafield area and its relationship to hydrogeology', *Quarterly Journal of Engineering Geology and Hydrogeology*, vol. 29, pp. S13–S27. Available at <http://qjegh.lyellcollection.org/content/29/Supplement_1/S13>

Miller, W., Alexander, R., Chapman, N., McKinley, I. and Smellie, J. (1994) 'Natural analogue studies in the geological disposal of radioactive wastes', *NAGRA*, Technical Report 93-03. Available at <http://www.nagra.ch/data/documents/database/dokumente/$default/Default Folder/Publikationen/NTBs 1991-1993/e_ntb93-03.pdf>

Min, K-B., Rutqvist, J., Tsang, C-F. and Jing, L. (2005) 'Thermally induced mechanical and permeability changes around a nuclear waste repository - a far-field study based on equivalent properties determined by a discrete approach', *International Journal of Rock Mechanics and Mining Sciences*, vol. 42, issues 5-6, pp. 765–780. Available at <https://www.sciencedirect.com/science/article/pii/S1365160905000419>

Mosé, R., Siegel, P. and Ackerer, P. (1994) 'Application of the mixed hybrid finite element approximation in a groundwater flow model: Luxury or necessity?', *Water Resources Research,* vol. 30, No. 11, pp. 3001-3012. Available at <https://agupubs.onlinelibrary.wiley.com/doi/abs/10.1029/94WR01786>

N

National Research Council (1992) 'Ground Water at Yucca Mountain: How high can it rise?', National Academy Press. ISBN10: 0-309-04748-X.

Neuzil, C.E. (1986) 'Groundwater Flow in Low-Permeability Environments', *Water Resources Research*, vol. 22, no. 8, pp. 1163–1195. Available at <https://agupubs.onlinelibrary.wiley.com/doi/abs/10.1029/WR022i008p01163>

Neuzil, C.E. (2003) 'Hydromechanical coupling in geologic processes', *Hydrogeology Journal*, vol. 11, pp. 41–83. Available at <https://link.springer.com/article/10.1007/s10040-002-0230-8>

Nguyen, T.S., BörgessonL., Chijimatsu, M., Hernelind, J., Jing, L., Kobayashi, A. and Rutqvist, J. (2008) 'A case study on the influence of THM coupling on the near field safety of a spent fuel repository in sparsely fractured granite', *Environmental Geology*, vol. 57, issue 6, pp. 1239–1254. Available at <http://link.springer.com/10.1007/s00254-008-1565-9>

Niemi, A., Yang, Z., Carrera, J., Power, H., McDermott, C.I., Rebscher, D., Wolf, J.L., May, F., Figueiredo, B. and Vilarrasa, V. (2017) 'Mathematical Modelling: Approaches for Model Simulation'. From Niemi, A., Bear, J. and Bensabat, J. (eds) (2017) 'Geological Storage of CO_2 in Deep Saline Aquifers', pp. 144–150, Springer Nature. ISBN: 978-94-024-0994-9.

Nirex (1987) 'The Way Forward: A Discussion Document', *United Kingdom Nirex Limited*, Harwell, Oxfordshire. Available at <http://www.geos.ed.ac.uk/homes/rsh/The_Way_Forward_United_Kingdom_Nirex_Limited_1987_-_colour.pdf>

Nirex (1989a) 'Deep Repository Project: Preliminary Environmental and Radiological Assessment and Preliminary Safety Report', *United Kingdom Nirex Limited*, Harwell, Oxfordshire, Nirex Report No. 071.

Nirex (1989b) 'Thermal Data for use in Modelling and their Preliminary Application', *United Kingdom Nirex Limited*, Harwell, Oxfordshire, Nirex Report No. SA/97/074, 2nd revision.

Nirex (1997a) 'An Assessment of the Post-closure Performance of a Deep Waste Repository at Sellafield: Volume 1: Hydrogeological Model Development - Conceptual Basis and Data', *United Kingdom Nirex Limited*, Harwell, Oxfordshire, Report No. S/97/012.

Nirex (1997b) 'An Assessment of the Post-closure Performance of a Deep Waste Repository at Sellafield: Volume 2: Hydrogeological Model Development - Effective Parameters and Calibration', *United Kingdom Nirex Limited*, Harwell, Oxfordshire, Report No. S/97/012.

Nirex (1997c) 'An Assessment of the Post-closure Performance of a Deep Waste Repository at Sellafield: Volume 3: The Groundwater Pathway', *United Kingdom Nirex Limited*, Harwell, Oxfordshire, Report No. S/97/012.

Nirex (1997d) 'An Assessment of the Post-closure Performance of a Deep Waste Repository at Sellafield: Volume 4: The Gas Pathway', *United Kingdom Nirex Limited*, Harwell, Oxfordshire, Report No. S/97/012.

Nirex (1997e) 'Sellafield Geological and Hydrogeological Investigations: The Derivation of Freshwater and Environmental Heads, Hydraulic Conductivity and Borehole Chloride Values with Uncertainty Limits for use in Nirex 97 Groundwater Modelling', *United Kingdom Nirex Limited*, Harwell, Oxfordshire, Report No. SA/97/065.

Nirex (1997f) 'Sellafield Geological and Hydrogeological Investigations: The Quaternary of the Sellafield Area', *United Kingdom Nirex Limited*, Harwell, Oxfordshire, Report No. SA/97/002.

Nirex (2002) 'Options for Radioactive Waste Management that have been Considered by Nirex', *United Kingdom Nirex Limited*, Harwell, Oxfordshire. Report No. N/049. Available at <https://tools.nda.gov.uk/publication/012-options-for-radioactive-waste-management-that-have-been-considered-by-nirex-2002/>

Nirex (2005a)' Review of 1987-1991 Site Selection for an ILW/LLW Repository', *United Kingdom Nirex Limited*, Harwell, Oxfordshire. Report No. 477002. Available at <https://tools.nda.gov.uk/publication/review-of-1987-1991-site-selection-for-an-ilwllw-repository/>

Nirex (2005b) 'Review of CoRWM Document No. 625: Sub seabed disposal', *United Kingdom Nirex Limited*, Harwell, Oxfordshire. Report No. 471699. Available at <https://rwm.nda.gov.uk/publication/nirex-review-of-corwm-document-no-625-sub-seabed-disposal-april-2005/>

Nirex (2005c) Review of CoRWM Document No. 927: Sub seabed disposal of radioactive waste - legal considerations', *United Kingdom Nirex Limited*, Harwell, Oxfordshire. Report No. 471717. Available at <https://rwm.nda.gov.uk/publication/nirex-review-of-corwm-document-no-927-sub-seabed-disposal-of-radioactive-waste-legal-considerations-april-2005/>

Nirex (2005d) 'Specification for Waste Packages Containing Vitrified High Level Waste and Spent Nuclear Fuel', *United Kingdom Nirex Limited*, Harwell, Oxfordshire. Report No. N/124. Available at <http://www.nda.gov.uk/publication/n124-specification-for-waste-packages-containing-vitrified-high-level-waste-and-spent-nuclear-fuel-december-2005/?download>

Nuclear Decommissioning Authority (2010a) 'Geological Disposal: Generic disposal system designs', NDA Report No. NDA/RWMD/048. Available at <https://rwm.nda.gov.uk/publication/geological-disposal-generic-disposal-facility-designs-december-2010/>

Nuclear Decommissioning Authority (2010b) 'Geological Disposal: Generic Environmental Safety Case main report', NDA Report No. NDA/RWMD/021. Available at <http://www.nda.gov.uk/publication/geological-disposal-generic-environmental-safety-case-main-report-december-2010/>

Nuclear Decommissioning Authority (2010c) 'Geological Disposal: Radionuclide behaviour status report', NDA Report No. NDA/RWMD/034. Available at <https://rwm.nda.gov.uk/publication/geological-disposal-radionuclide-behaviour-status-report-december-2010/>

Nuclear Decommissioning Authority (2010d) 'Geological Disposal: An overview of the generic disposal system safety case', NDA Report No. NDA/RWMD/010. Available at <https://rwm.nda.gov.uk/publication/geological-disposal-an-overview-of-the-generic-disposal-system-safety-case-december-2010/>

Nuclear Decommissioning Authority (2013a) '2013 UK Radioactive Waste Inventory: Scope and Conventions', *Department of Energy & Climate Change*, URN 14D044, NDA/ST/STY(14)0008. Available at <https://ukinventory.nda.gov.uk/wp-content/uploads/sites/18/2014/02/14D044_NDASTSTY140008_-_Scope_and_Conventions.pdf>

Nuclear Decommissioning Authority (2013b) 'Geological Disposal: Overview of international siting processes', September 2013. Available at < https://rwm.nda.gov.uk/publication/geological-disposal-overview-of-international-siting-processes/>

Nuclear Decommissioning Authority (2013c) 'Radioactive Wastes in the UK: A Summary of the 2013 Inventory', *Department of Energy & Climate Change*. ISBN: 978-1-905985-33-3. Available at <https://ukinventory.nda.gov.uk/wp-content/uploads/sites/18/2014/02/14D039-NDASTSTY140006-UKRWI-2013-High-Level-Summary.pdf>

Nuclear Decommissioning Authority (2014) 'Implementing Geological Disposal: A Framework for the long-term management of higher activity radioactive waste', *Department of Energy & Climate Change*, URN 14D/235. Available at <https://www.gov.uk/government/publications/implementing-geological-disposal-annual-report-april-2013-march-2014>

Nuclear Decommissioning Authority (2017a) 'Annual Report & Accounts 2016/17'. Available at <https://www.gov.uk/government/publications/nuclear-decommissioning-authority-annual-report-and-accounts-2016-to-2017>

Nuclear Decommissioning Authority (2017b) 'Radioactive Wastes in the UK: A summary of the 2016 Inventory'*, Department for Business, Energy & Industrial Strategy*. ISBN: 978-1-905985-36-4. Available at <https://ukinventory.nda.gov.uk/document-library/?filter-taxs[wds_document_category]=175>

Nuclear Decommissioning Authority (2017c) 'Radioactive Wastes in the UK: UK Radioactive Waste Inventory Report', *Department for Business, Energy & Industrial Strategy*. ISBN: 978-1-905985-33-3. Available at <https://ukinventory.nda.gov.uk/document-library/?filter-taxs[wds_document_category]=175>

Nuclear Decommissioning Authority (2018) 'Governments consider views on geological disposal' web-article, Accessed 2018, Available at <www.gov.uk/government/news/governments-consider-views-on-geological-disposal>

Nuclear Energy Agency (2008) 'Moving Forward with Geological Disposal of Radioactive Waste: A Collective Statement by the NEA Radioactive Waste Management Committee (RWMC)', *Organisation for Economic Co-operation and Development (OECD)*. ISBN: 978-92-64-99057-9. Available at <https://www.oecd-nea.org/rwm/reports/2008/nea6433-statement.pdf>

O

O'Sullivan, M.J., Pruess, K. and Lippmann, M.J. (2001) 'State of the art of geothermal reservoir simulation', *Geothermics*, vol. 30, pp. 395–429. Available at <https://www.sciencedirect.com/science/article/pii/S0375650501000050>

Ontario Power Generation (2018) 'What is the deep geological repository (DGR?)' webpage, Accessed 2018. Available at <http://opgdgr.com/>

OpenGeoSys (2017) 'OpenGeoSys: Open-Source Multi-Physics' webpage, Accessed 2017. Available at <www.f.org>

Ophori, D.U. (1998) 'The significance of viscosity in density-dependent flow of groundwater', *Journal of Hydrology*, vol. 204, issues 1–4, pp. 261–270. Available at <https://www.sciencedirect.com/science/article/pii/S0022169497001169>

P

Park, Y.J., Sudicky, E.A. and Sykes, J.F. (2009) 'Effects of shield brine on the safe disposal of waste in deep geologic environments', *Advances in Water Resources*, vol. 32, issue 8, pp. 1352–1358. Available at <http://dx.doi.org/10.1016/j.advwatres.2009.06.003>

Parsons Brinckerhoff (2010) 'Geological Disposal Facility Ventilation Study', *Radioactive Waste Management Directorate*. Available at <https://tools.nda.gov.uk/publication/geological-disposal-facility-ventilation-study-september-2010/>

Pharaoh, T.C., Merriman, R.J., Webb, P.C. and Beckinsale, R.D. (1987) 'The concealed Caledonides of eastern England: preliminary results of a multidisciplinary study', *Proceedings of the Yorkshire Geological Society*, vol. 46, issue 4, pp. 355–369. Available at <http://pygs.lyellcollection.org/cgi/doi/10.1144/pygs.46.4.355>

Phillips, O.M. (1991) 'Flow and Reactions in Permeable Rocks', 1st edn, Cambridge University Press. ISBN: 0-521-38098-7.

Posiva Oy (2003) 'ONKALO Underground Characterisation and Research Programme (UCRP)', Report No. POSIVA 2003-03. Available at <www.posiva.fi/files/1299/POSIVA_2003-03.pdf>

Posiva Oy (2009a) 'Olkiluoto Site Description 2008 Part 1', Report No. POSIVA 2009-01. Available at <http://www.posiva.fi/files/1035/Posiva2009-01_web_part1.1rev.pdf>

Posiva Oy (2009b) 'Olkiluoto Site Description 2008 Part 2', Report No. POSIVA 2009-01. Available at <http://www.posiva.fi/files/914/Posiva2009-01_web_part2.pdf>

Posiva Oy (2012) 'Safety Case for the Disposal of Spent Nuclear Fuel at Olkiluoto – Synthesis 2012', Report No. POSIVA 2012-12. Available at <www.posiva.fi/files/2992/Posiva_2012-12web2.pdf>

Posiva Oy (2017) 'Final Disposal' webpage. Accessed 2017, Available at <www.posiva.fi/en/final_disposal#.WtBz02eWzoo>

Post, V.E.A., Groen, J., Kooi, H., Person, M., Ge, S. and Edmunds, W.M. (2013) 'Offshore fresh groundwater reserves as a global phenomenon', *Nature*, vol. 504, pp. 71–78. Available at <www.nature.com/articles/nature12858>

Powers, D.W., Lambert, S.J., Shaffer, S-E., Leslie, R.H. and Weart, W.D. (eds) (1978) 'Geological Characterization Report, Waste Isolation Pilot Plant (WIPP) Site, Southeastern New Mexico – Volume II', *Department 4510 Waste Management Technology*, Sandia Laboratories, New Mexico. Available at <www.iaea.org/inis/collection/NCLCollectionStore/_Public/10/456/10456382.pdf>

Public Health England (2017) 'UK maps of radon' webpage, Accessed 2018, Available at <http://www.ukradon.org/information/ukmaps>

Pulkkanen, V. and Nordman, H. (2010) 'Modelling of Near-Field Radionuclide Transport Phenomena in a KBS-3V Type of Repository for Nuclear Waste with GoldSim Code – and Verification Against Previous Methods', Posiva Oy, Working Report No. 2010-14. Available at <www.posiva.fi/files/1203/WR_2010-14web.pdf>

R

Radioactive Materials Management (2003) ‘Cost Estimate for a Deep Geologic Repository for Used Nuclear Fuel: Report of a Study carried out for Ontario Power Generation, New Brunswick Power, Hydro-Québec and Atomic Energy of Canada Limited’, Report 1106/MD18085/REP/02. Available at <www.nwmo.ca/~/media/Site/Files/PDFs/2015/11/17/23/24/1031_costestimate_deepgeologicalrep.ashx?la=en>

Radioactive Waste Management (2012) ‘Thermodynamic Sorption Modelling in Support of Radioactive Waste Disposal Safety Cases: NEA Sorption Project Phase III’, *Nuclear Energy Agency*. ISBN: 978-92-64-117781-9. Available at <www.oecd-nea.org/rwm/docs/2013/6914-sorption-III>

Radioactive Waste Management (2016a) ‘Geological Disposal: Engineered Barrier System Status Report’, *Nuclear Decommissioning Authority*, Report no. DSSC/452/01. ISBN: 978-1-84029-565-8. Available at <http://rwm.nda.gov.uk/publication/geological-disposal-engineered-barrier-system-status-report/>

Radioactive Waste Management (2016b) ‘Implementing Geological Disposal: Providing Information on Geology, National Geological Screening Guidance’, *Nuclear Decommissioning Authority*. Available at <www.gov.uk/government/publications/national-geological-screening-guidance>

Ranjram, M., Gleeson, T. and Luijendijk, E. (2015) ‘Is the permeability of crystalline rock in the shallow crust related to depth, lithology or tectonic setting?’, *Geofluids*, vol. 15, issues 1–2, pp. 106–119. Available at <www.onlinelibrary.wiley.com/doi/abs/10.1111/gfl.12098>

Rechard, R.P., Cotton, T.A. and Voegele, M.D. (2014) ‘Site selection and regulatory basis for the Yucca Mountain disposal system for spent nuclear fuel and high-level radioactive waste’, *Reliability Engineering and System Safety*, vol. 122, pp. 7–31. Available at <www.sciencedirect.com/science/article/pii/S0951832013001865>

Ronczka, M., Hellman, K., Günther, T., Wisén, R. and Dahlin, T. (2017) ‘Electric resistivity and seismic refraction tomography: a challenging joint underwater survey at Äspö Hard Rock Laboratory’, *Solid Earth*, vol. 8, issue 3, pp. 671–682. Available at <www.solid-earth.net/8/671/2017/>

Rutqvist, J. and Stephansson, O. (2003) ‘The role of hydromechanical coupling in fractured rock engineering’, *Hydrogeology Journal*, vol. 11, issue 1, pp. 7–40. Available at <www.link.springer.com/article/10.1007/s10040-002-0241-5>

Rutqvist, J., Barr, D., Datta, R., Gens, A., Millard, A., Olivella, S., Tsang, C-F. and Tsang, Y. (2005) ‘Coupled thermal–hydrological–mechanical analyses of the Yucca Mountain Drift Scale Test—Comparison of field measurements to predictions of four different numerical models’, *International Journal of Rock Mechanics and Mining Sciences*, vol. 42, issues 5–6, pp. 680–697. Available at <www.sciencedirect.com/science/article/pii/S1365160905000353>

Rutqvist, J., Chijimatsu, M., Jing, L., Millard, A., Nguyen, T.S. Rejeb, A., Sugita, Y. and Tsang, C-F. (2005) ‘A numerical study of THM effects on the near-field safety of a hypothetical nuclear waste repository—BMT1 of the DECOVALEX III project. Part 3: Effects of THM coupling in sparsely fractured rocks’, *International Journal of Rock Mechanics and Mining Sciences*, vol. 42, issues 5–6, pp. 745–755. Available at <https://www.sciencedirect.com/science/article/pii/S1365160905000390>

Rutqvist, J., Barr, D., Birkholzer, J.T., Chijimatsu, M., Kolditz, O., Liu, Q., Oda, Y., Wang, W. and Zhang, C. (2008) 'Results from an International Simulation Study on Coupled Thermal , Hydrological, and Mechanical (THM) Processes near Geological Nuclear Waste Repositories', *Lawrence Berkeley National Laboratory*. Available at <www.tandfonline.com/doi/abs/10.13182/NT08-A3974>

Rutqvist, J. (2015) 'Fractured rock stress-permeability relationships from in situ data and effects of temperature and chemical-mechanical couplings', *Geofluids*, vol. 15, issues 1–2, pp. 48–66. Available at <www.onlinelibrary.wiley.com/doi/abs/10.1111/gfl.12089>

S

Salter, I. and Wilson, W. (2006) 'Sub-sea disposal of radioactive waste'. *International Journal of Nuclear Law*, vol. 1, No. 2, pp. 199–205. Available at <www.inderscienceonline.com/doi/abs/10.1504/IJNUCL.2006.010262>

Savage, D. (ed) (1995) 'The scientific and regulatory basis for the geological disposal of radioactive waste', Wiley. ISBN: 978-471-96090-4.

Schlumberger (2016) 'Common Data Access: UKOilandGasData' website. Accessed 2016 and 2017 via the University of Edinburgh, Available at <www.ukoilandgasdata.com>.

Schulze-Makuch, D. (2005) 'Longitudinal Dispersivity Data and Implications for Scaling Behaviour', *Ground Water*, Review Paper, vol. 43, issue 3, pp. 443–456. Available at <www.onlinelibrary.wiley.com/doi/abs/10.1111/j.1745-6584.2005.0051.x>

Schulze-Makuch, D., Carlson, D.A., Cherkauer, D.S. and Malik, P. (1999) 'Scale Dependency of Hydraulic Conductivity in Heterogeneous Media', *Ground Water*, vol. 37, issue 6, pp. 904–919. Available at <www.onlinelibrary.wiley.com/doi/abs/10.1111/j.1745-6584.1999.tb01190.x>

Schwartz, F.W. and Zhang, H. (2003) 'Fundamentals of Ground Water', 1st edn., John Wiley & Sons. ISBN: 9780--471-13785-6.

Sekiya, M. and Yamasaki, M. (2015) 'Antoine Henri Becquerel (1852-1908): a scientist who endeavoured to discover natural radioactivity', *Radiological Physics and Technology*, vol. 8, issue 1, pp. 1-3. Available at <https://link.springer.com/article/10.1007%2Fs12194-014-0292-z>

Sharland, S.M., Agg, P.J., Naish, C.C. and Wikramaratna, R.S. (2008) 'Gas Generation by Metal Corrosion and the Implications for Near-field Containment in Radioactive Waste Repositories', *AEA Technology Group Report*. Available at <www.iaea.org/inis/collection/NCLCollectionStore/_Public/26/053/26053342.pdf>

SKB (1992) 'Treatment and final disposal of nuclear waste: Siting of a deep repository', *Svensk Kärnbränslehantering AB*, Background Report to RD&D-Programme 92. Available at <www.iaea.org/inis/collection/NCLCollectionStore/_Public/26/038/26038212.pdf>

SKB (1995) 'General Siting Study 95: Siting of a deep repository for spent nuclear fuel', *Svensk Kärnbränslehantering AB*, Technical Report No. 95-34. Available at <http://inis.iaea.org/search/search.aspx?orig_q=RN:27042307>

SKB (2001) ‘Feasibility studies - Östhammar, Nyköping, Oskarshamn, Tierp, Hultsfred and Älvkarleby: Summary Report’, *Svensk Kärnbränslehantering AB*, Technical Report No. TR-01-12. Available at <www.skb.se/upload/publications/pdf/TR-01-16.pdf>

SKB (2005a) ‘Preliminary safety evaluation for the Forsmark area: Based on data and site descriptions after the initial site investigation stage’, *Svensk Kärnbränslehantering AB*, Technical Report No. TR-05-16. Available at <www.skb.se/publikation/998963/TR-05-16.pdf>

SKB (2005b) ‘Preliminary safety evaluation for the Simpevarp subarea: Based on data and site descriptions after the initial site investigation stage’, *Svensk Kärnbränslehantering AB*, Technical Report No. TR-05-12. Available at <www.skb.se/publikation/923452/TR-05-12.pdf>

SKB (2006) ‘Long-term safety for KBS-3 repositories at Forsmark and Laxemar – a first evaluation: Main Report of the SR-Can project’, *Svensk Kärnbränslehantering AB*, Technical Report No. TR-06-09. Available at <www.skb.se/upload/publications/pdf/TR-06-09.pdf>

SKB (2009) ‘Final repository for spent fuel in Forsmark – basis for decision and reasons for site selection’, *Svensk Kärnbränslehantering AB*, SKBdoc 1221293 (English Translation of SKBdoc 1207622).

SKB (2011) ‘Long-term safety for the final repository for spent nuclear fuel at Forsmark repository for spent nuclear fuel at Forsmark - Volume 1’, *Svensk Kärnbränslehantering AB*, Technical Report No. TR-11-01. Available at <www.skb.se/upload/publications/pdf/TR-11-01_vol1.pdf>

SKB (2017a) ‘Costs from and including 2018 for the radioactive residual products from nuclear power: Basis for fees and guarantees for the period 2018-2020’, *Svensk Kärnbränslehantering AB*, Technical Report No. TR-17-02. Available at <www.skb.se/upload/publications/pdf/TR-17-02.pdf>

SKB (2017b) ‘The Final Repository SFR’ webpage, Accessed 2017, Available at <www.skb.com/our-operations/sfr/>

SKB (2018a) ‘How Forsmark was selected’ webpage, Accessed 2018, Available at <www.skb.com/future-projects/the-spent-fuel-repository/how-forsmark-was-selected/>

SKB (2018b) ‘Extending the SFR’ webpage, Accessed 2018, Available at <www.skb.se/upload/publications/pdf/Fact-sheet_Extending_the_SFR.pdf>

SKB (2018c) ‘The Spent Fuel Repository’ webpage, Accessed 2018, Available at <www.skb.com/future-projects/the-spent-fuel-repository/>

SOEST (2015) SOEST: Webpage. Available at: https://www.soest.hawaii.edu/oceanography/courses/OCN623/Spring 2015/Salinity2015web.pdf.

Sorenson, K.B (ed) (2015) ‘Safe and Secure Transport and storage of Radioactive Materials’, Woodhead Publishing. ISBN: 978-1-78242-309-6.

Spycher, N.F., Sonnenthal, E.L. and Apps, J.A. (2003) ‘Fluid flow and reactive transport around potential nuclear waste emplacement tunnels at Yucca Mountain, Nevada’, *Journal of*

Contaminant Hydrology, vols. 62–63, pp. 653–673. Available at <www.sciencedirect.com/science/article/pii/S0169772202001833>

Stephan, P. (2010) 'VDI Heat Atlas', 2nd edn, VDI-verlag GmbH Düsseldorf. ISBN: 978-3-540-77876-9. Available at <www.springer.com/gb/book/9783540778769>

Stephansson, O., Hudson, J.A. and Jing, L. (2004) Coupled Thermo-Hydro-Mechanical-Chemical Processes in Geo-Systems: Fundamentals, Modelling, Experiments and Applications - Volume 2', Elsevier Ltd. ISBN: 978-0-080-44525-0.

Stephens, M.B (2010) 'Forsmark site investigation. Bedrock geology – overview and excursion guide', *Svensk Kärnbränslehantering AB*, Report No. R-10-07. Available at <www.skb.se/upload/publications/pdf/R-10-04.pdf>

Stober, I. and Bucher, K. (1999) 'Origin of salinity of deep groundwater in crystalline rocks', *Terra Nova*, vol. 11, issue 4, pp. 181–185. Available at <www.onlinelibrary.wiley.com/doi/full/10.1046/j.1365-3121.1999.00241.x>

Stober, I. and Bucher, K. (2015) 'Hydraulic conductivity of fractured upper crust: insights from hydraulic tests in boreholes and fluid-rock interaction in crystalline basement rocks', *Geofluids*, vol. 15, issues 1–2, pp. 161–178. Available at <www.onlinelibrary.wiley.com/doi/abs/10.1111/gfl.12104>

Stormont, J.C. (1997) 'In situ gas permeability measurements to delineate damage in rock salt', *International Journal of Rock Mechanics and Mining Sciences*, vol. 34, No. 7, pp. 1055–1064. Available at <www.sciencedirect.com/science/article/pii/S1365160997901994>

Streffer, C., Gethmann, C.F., Kamp, G., Kröger, W., Rehbinder, E. and Renn, O. (2011) 'Radioactive Waste: Technical and Normative Aspects of its Disposal', Springer. ISBN: 978-3-642-22925-1. Available at <www.springer.com/gp/book/9783642229244>

Stuart, I.A. and Cowan, G. (1991) 'The South Morecambe Gas Field, Blocks 110/2a, 110/3a, 110/8a, UK East Irish Sea'. From Abbotts, I.L (ed) (1991), 'United Kingdom Oil and Gas Fields', *25 Years Commemorative Volume*, Geological Society Memoir, vol. 14, pp. 527–541. Available at <http://mem.lyellcollection.org/content/14/1/527>

T

Tecplot (2018) 'Tecplot: home' webpage, Accessed 2015, Available at <www.tecplot.com/>

The Crown Estate (2017) 'Energy, Minerals & Infrastructure: cables and pipelines', webpage, accessed 2017 (page removed 2018). New page available 2018 at <www.thecrownestate.co.uk/en-gb/what-we-do/on-the-seabed/cables-and-pipelines/>

Thomas, R. and Ward, D. (1972) 'Effect of Overburden Pressure and Water Saturation on Gas Permeability of Tight Sandstone Cores', *Journal of Petroleum Technology*, vol. 24, issue 2. Available at <www.onepetro.org/journal-paper/SPE-3634-PA>

Tideway (2015) 'Themes Tideway Tunnel Fact Sheet', *Bazalgette Tunnel Limited (BTL)*, accessed 2018, available at <www.tideway.london/media/1450/tideway_press_pack_sept_2015.pdf>

Tóth, J. (1963) ‘A Theoretical Analysis of Groundwater Flow in Small Drainage Basins’, *Journal of Geophysical Research*, vol. 68, No. 16, pp. 4795–4812. Available at <www.dx.doi.org/10.1029/JZ068i016p04795>

Tsang, C-F. (ed) (1987) ‘Coupled Processes Associated with Nuclear Waste Repositories’, 1st edn, Academic Press. ISBN: 0-12-701620-1.

Tsang, C-F. (1991) ‘Coupled Hydromechanical-Thermochemical Processes in Rock Fractures’, *Reviews of Geophysics*, vol. 29, issue 4, pp. 537–551. Available at <https://agupubs.onlinelibrary.wiley.com/doi/abs/10.1029/91RG01832>

Tsang, C-F., Bernier, F. and Davies, C. (2005) ‘Geohydromechanical processes in the Excavation Damaged Zone in crystalline rock, rock salt, and indurated and plastic clays - in the context of radioactive waste disposal’, *International Journal of Rock Mechanics & Mining Sciences*, vol. 42, pp. 109–125. Available at <www.sciencedirect.com/science/article/pii/S1365160904002679>

Tsang, C-F, Stephansson, O., Jing, L. and Kautsky, F. (2009) ‘DECOVALEX Project: from 1992 to 2007’, *Environmental Geology*, vol. 57, issue 6, pp. 1221–1237. Available at <https://link.springer.com/article/10.1007/s00254-008-1625-1>

Tsang, C-F. and Niemi, A. (2013) ‘Deep hydrogeology: a discussion of issues and research needs’, *Hydrogeology Journal*, vol. 21, issue 8, pp. 1687–1690. Available at <https://link.springer.com/article/10.1007%2Fs10040-013-0989-9>

Tsang, C-F. and Niemi, A. (2017) ‘Overview of Processes Occurring During CO_2 Geological Storage and Their Relevance to Key Questions and Performance’. From Niemi, A., Bear, J. and Bensabat, J. (eds) (2017) ‘Geological Storage of CO_2 in Deep Saline Aquifers’, pp. 26–27, Springer Nature. ISBN: 978-94-024-0994-9.

Tuniz, C. (2012) ‘Radioactivity: A Very Short Introduction’, 1st edn, Oxford University Press. ISBN: 978-0-19-969242-2.

U

U.S. Department of Energy (2010) ‘U.S. Department of Energy’s Motion to Withdraw’, *United States of America Nuclear Regulatory Commission*, March 3rd 2010. Available at <www.energy.gov/sites/prod/files/edg/media/DOE_Motion_to_Withdraw.pdf>

U.S. Department of Energy (2012) Waste Isolation Pilot Plant: Geotechnical Analysis Report for July 2010 - June 2011’, Report No. DOE/WIPP-12-3484. Available at <www.wipp.energy.gov/library/cra/CRA-2014/references/Others/US_DOE_2012_Geotechnical_Analysis_Report_DOE_WIPP_12_3484.pdf>

U.S. Department of Energy (2016) ‘Transuranic Waste Acceptance Criteria for the Waste Isolation Pilot Plant: Revision 8.0’, Report No. DOE/WIPP-02-3122. Carlsbad Field Office. Available at <www.wipp.energy.gov/library/wac/WAC.pdf>

UK Parliament (1987) ‘Channel Tunnel Act 1987 - Chapter 53’*, Her Majesty’s Stationery Office*. Available at <www.legislation.gov.uk/ukpga/1987/53>

UK Parliament (1997) 'Town and Country Planning Act 1990 - Appeal by United Kingdom Nirex Limited Proposed Rock Characterisation Facility on Land at and Adjoining Longlands Farm, Gosforth, Cumbria (Local Authority Application Number 4/94/9011)' letter, 17th March 1997. Available at <www.westcumbriamrws.org.uk/all_documents.asp>

United Nations (2017) 'The Paris Agreement' webpage, accessed 2017, available at <www.unfccc.int/process/the-paris-agreement/what-is-the-paris-agreement>

University of Edinburgh (2018) 'High Performance Computing' webpage, accessed 2018, available at <www.ed.ac.uk/information-services/research-support/research-computing/ecdf/high-performance-computing>

V

van Genuchten, M.T. and Alves, W.J. (1982) 'Analytical Solutions of the One-Dimensional Convective-Dispersive Solute Transport Equation', *Technical Bulletins 157268,* United States Department of Agriculture, Economic Research Service. Available at <https://ideas.repec.org/p/ags/uerstb/157268.html>

Vopálka, D., Lukin, D. and Vokál, A. (2006) 'Modelling of Processes Occurring in Depp Geological Repository – Development of New Modules in the GoldSim Environment', *Czechoslovak Journal of Physics*, vol. 56, pp. 623–628. Available at <https://link.springer.com/article/10.1007/s10582-006-1074-6>

W

Warrington, G. (1997) 'The Penarth Group-Lias Group succession (Late Triassic-Early Jurassic) in the East Irish Sea Basin and neighbouring areas: a stratigraphical review'. From Meadows, N.S., Trueblood, S.P., Hardman, M. and Cowan, G. (eds) (1997) 'Petroleum Geology of the Irish Sea and Adjacent Areas', *Geological Society Special Publication*, No. 124, pp. 33-46. Available at <http://sp.lyellcollection.org/content/124/1/33>

Waste Isolation Pilot Plant (2018) 'Home' webpage, accessed 2018, available at <www.wipp.energy.gov/>

Watanabe, N., Wang, W., McDermott, C.I., Taniguchi, T. and Kolditz, O. (2010) 'Uncertainty analysis of thermo-hydro-mechanical coupled processes in heterogeneous porous media', *Computational Mechanics*, vol. 45, issue 4, pp. 263–280. Available at <https://link.springer.com/article/10.1007/s00466-009-0445-9>

Wilson, A.A. (1990) 'The Mercia Mudstone Group (Trias) of the East Irish Sea Basin', *Proceedings of the Yorkshire Geological Society*, vol. 48, part 1, pp. 1–22. Available at <http://pygs.lyellcollection.org/content/48/1/1>

Winograd, I.J. (1990) 'The Yucca Mountain project: Another perspective', *Environmental Science and Technology*, vol. 24, issue 9, pp. 1291–1293. Available at <https://pubs.acs.org/doi/pdf/10.1021/es00079a602>

Wladis, D., Jönsson, P. and Wallroth, T. (1997) 'Regional characterization of hydraulic properties of rock using well test data', *Svensk Kärnbränslehantering AB*, Technical Report No. TR-97-29. Available at <www.skb.com/publication/13749/TR97-29webb.pdf>

Wollenberg, H.A. and Flexser, S. (1984) 'Contact zones and hydrothermal systems as analogues to repository conditions', *In: Smellie, J .A. T. (editor) Natural analogues to the conditions around a final repository for high level radioactive waste.* Proceedings of the natural analogue workshop held at Lake Geneva, U.S.A. *SKB Technical Report,* TR 84-18. Available at <https://www.sciencedirect.com/science/article/pii/0009254186900355/>

Woodcock, N.H. and Pharaoh, T.C. (1993) 'Silurian facies beneath East Anglia', *Geological Magazine*, vol. 130, issue 5, pp. 681–690. Available at <www.cambridge.org/core/journals/geological-magazine/article/div-classtitlesilurian-fades-beneath-east-angliadiv/E80A5415E273D4C161A7A73B7AA3C9BA>

Y

Yaliz, A. and Chapman, T.J. (2003) 'The Lennox Oil and Gas Field, Block 110/15, East Irish Sea'. From Gluyas J.G. and Hichens, H.M. (eds) (2003) 'United Kingdom Oil and Gas Fields', Commemorative Millennium Volume, *Geological Society*, London, Memoir, vol. 20, pp. 87-96. Available at <http://mem.lyellcollection.org/content/20/1/87>

Yaliz, A. and McKim, N. (2003) 'The Douglas Oil Field, Block 110/13b, East Irish Sea'. From Gluyas J.G. and Hichens, H.M. (eds) (2003) 'United Kingdom Oil and Gas Fields', Commemorative Millennium Volume, *Geological Society*, London, Memoir, vol. 20, pp. 63-75. Available at <http://mem.lyellcollection.org/content/20/1/61>

Yaliz, A. and Taylor, P. (2003) 'The Hamilton and Hamilton North Gas Fields, Block 110/13a, East Irish Sea'. From Gluyas J.G. and Hichens, H.M. (eds) (2003) 'United Kingdom Oil and Gas Fields', Commemorative Millennium Volume, *Geological Society*, London, Memoir, vol. 20, pp. 77-86. Available at <http://mem.lyellcollection.org/content/20/1/77>

Yeh, G-T. (1981) 'On the Computation of Darcian Velocity and Mass Balance in the Finite Element Modelling of Groundwater Flow', *Water Resources Research,* vol. 17, No. 5, pp. 1529-1534. Available at <https://agupubs.onlinelibrary.wiley.com/doi/abs/10.1029/WR017i005p01529>

Yoo, C. (2016) 'Effect of water leakage in tunnel lining on structural performance of lining in subsea tunnels', *Marine Georesources & Geotechnology*, vol. 35, issue 3, pp. 305-317. Available at <www.tandfonline.com/doi/full/10.1080/1064119X.2016.1162235>

Z

Zheng, J., Zheng, L., Liu, H-H. and Ju, Y. (2015) 'Relationships between permeability, porosity and effective stress for low-permeability sedimentary rock', *International Journal of Rock Mechanics & Mining Sciences*, vol. 78, pp. 304–318. Available at <http://dx.doi.org/10.1016/j.ijrmms.2015.04.025>

Appendix A

A.1: Fundamental Process Laws

A.1.1: Liquid Flow

Liquid is most commonly transported due to a pressure differential (advection). The flux of liquid, such as groundwater, through a porous medium can be described using (Equ. A.1) (Hiscock 2005), and is based on Darcy's Law. The underlying assumptions of Darcy's Law are presented within section 2.8.3.

$$F_{gw} = K\frac{\partial h}{\partial x} \qquad (A.1)$$

Where F_{gw} is the groundwater flux (m/s), K is the hydraulic conductivity (m/s), h is the hydraulic head (m), and x is the distance in the x-direction (m). The hydraulic conductivity K (Equ. A.2) itself comprises the fluid properties of density ρ (kg/m^3), acceleration due to gravity g (m/s^2), and the dynamic viscosity μ (Pa s), and the geometric component of intrinsic permeability k (m^2) of the host rock formation (Domenico & Schwartz 1997; McDermott et al. 2006).

$$K = \frac{\rho\, g}{\mu}k \qquad (A.2)$$

A.1.2: Heat Transport

Heat can be transported via conduction (temperature driven), convection (due to fluid advection) and radiation (from electromagnetic waves). Radiation is not considered significant within the sub-surface and is therefore typically ignored within groundwater related thermal process simulations e.g. by (Rutqvist, Barr, et al. 2005). The flux of heat through a saturated rock mass as a result of conduction can be described through (Equ.A.3), based on Fourier's Law (Cengel & Boles 2011). The underlying assumptions of Fourier's Law are presented within section 2.8.3.

$$F_{heat} = \lambda_m\frac{\partial T}{\partial x} \qquad (A.3)$$

Where F_{heat} is the heat flux (W/m^2), λ_m is the thermal conductivity of the medium (W/mK), T is the temperature (K), and x is the distance in the x-direction (m). The thermal conductivity λ_m (Equ.A.4) itself comprises the thermal conductivity of the fluid λ_w (W/mK), and the thermal conductivity of the solid λ_r (W/mK), where n_e is the effective porosity (-) (McDermott et al. 2006).

$$\lambda_m = n_e\lambda_w + (1 - n_e)\lambda_r \quad \text{(A.4)}$$

A.1.3: Mass transport

Mass can be transported via diffusion (concentration driven) or convection (as a result of fluid advection). Mass can also be stored (i.e. not transported) via sorption, and can be removed from the sub-surface system via radioactive decay (conversion of mass to energy). The flux of mass through a saturated rock mass as a result of diffusion can be described through (Equ.A.5) and is based on Fick's first Law (Hiscock 2005). The underlying assumptions of Fick's Law are presented within section 2.8.3.

$$F_{mass} = \frac{D_e}{R_f}\frac{\partial C}{\partial x} \quad \text{(A.5)}$$

Where F_{mass} is the mass flux (kg/m^{2}s), D_e is the effective diffusion coefficient (m^2/s), C is the mass concentration (kg/m^3) (Phillips 1991), R_f is the retardation factor and represents the effect of chemical processes on the rate of mass transport (Domenico & Schwartz 1997), discussed further in section A.3.3.3, and x is the distance in the x-direction (m). The effective molecular diffusion coefficient D_e (m^2/s) itself comprises the effective porosity n_e (-), and the diffusion coefficient $D_{m(mass)}$ (m^2/s) (Equ.A.6) (Domenico & Schwartz 1997).

$$D_e = n_e D_{m(mass)} \quad \text{(A.6)}$$

A.2: Derivation of the Three-Dimensional Process Equations

Groundwater flow, mass transport and heat transport are all based on the laws of the conservation of energy, with groundwater flow and mass transport involving the transportation of mass, whilst heat transport involves the transportation of energy.

Considering the mass, or energy, balance in words (Equ.A.7) over a control volume (Figure A.0.1) allows the three-dimensional groundwater flow, heat transport and mass transport equations to be derived as follows.

$$\begin{aligned} &mass\ or\ energy\ input - mass\ or\ energy\ output \\ &\qquad = change\ in\ mass\ or\ energy\ storage \end{aligned} \quad \text{(A.7)}$$

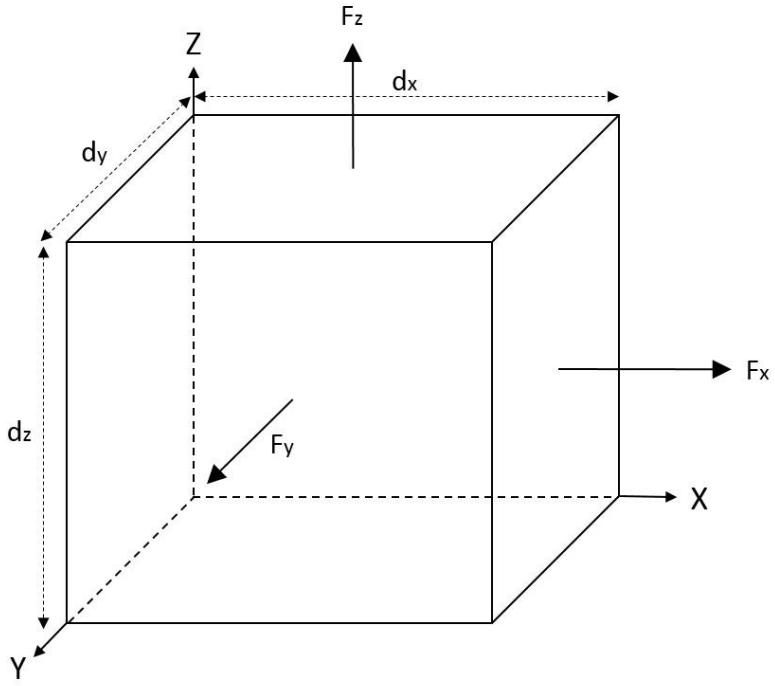

Figure A.0.1: Representative Control Volume, adapted from (Anderson & Woessner 1992).

Considering the flux into the control volume within the x, y and z orientations (whether that be groundwater, heat or mass) leads to (Equ.A.8)

$$F_{in} = F_x dydz + F_y dxdz + F_z dxdy \qquad (A.8)$$

Considering the flux out of the control volume within the x, y and z orientations (whether that be groundwater, heat or mass) leads to (Equ.A.9)

$$F_{out} = (F_x + \frac{\partial F_x}{\partial x} dx)dydz + (F_y + \frac{\partial F_y}{\partial y} dy)dxdz + (F_z + \frac{\partial F_z}{\partial z} dz)dxdy \qquad (A.9)$$

Subtracting the flux out (Equ.A.9) from the flux in (Equ.A.8) of the control volume leads to the differential form of the mass or energy balance equation (Equ.A.10) over the control volume, where the right hand term represents the *change in stored energy or mass*.

$$-\frac{\partial F_x}{\partial x} - \frac{\partial F_y}{\partial y} - \frac{\partial F_z}{\partial z} = change\ in\ stored\ energy\ or\ mass \qquad (A.10)$$

When the *change in stored energy or mass* equals zero, the system can be said to be in 'steady state' however, when it does not equal zero, the system can be said to be 'transient', and must include a mass or energy source or sink (Anderson & Woessner 1992). In addition, Equ.A.10 assumes that mass or energy changes linearly along the specified axis of the control volume, considered justified for sufficiently small control volumes (McDermott 2015).

A.3: Three-Dimensional Process Equations

The three-dimensional liquid flow, heat transport and mass transport equations are all derived using the method described in section A.2. For further information on the derivation of the three dimensional equations for groundwater flow, heat transport or mass transport, the reader is referred to (Freeze & Cherry 1979).

A.3.1: Liquid Flow

The three-dimensional balanced saturated liquid flow equation is presented (Equ.A.11) (Niemi et al. 2017).

$$S_s \frac{\partial P}{\partial t} - \nabla \cdot \left(\frac{k}{\mu} (\nabla P + \rho g \nabla z) \right) = Q \qquad (A.11)$$

Where S_s is the storage coefficient (Pa^{-1}), P is the fluid pressure (Pa), t is time (s), k is the intrinsic permeability (m^2), μ is the dynamic viscosity (Pa s), ρ is the fluid density (kg/m^3), g is the acceleration due to gravity (m/s^2), z is the elevation head (m), and Q is the source/sink term (m^3/s) for the volumetric balance equation (Watanabe et al. 2010).

A.3.2: Heat Transport

The three-dimensional balanced heat transport equation is presented (Equ.A.12) (Niemi et al. 2017).

$$D_T \Delta T - c_w \rho_w \nabla \cdot (v_a T) - \rho Q_T = c_m \rho_m \frac{\partial T}{\partial t} \qquad (A.12)$$

Where D_T is the heat diffusion-dispersion tensor for the porous medium (W/mK), T is the temperature (K), c_w is the specific heat capacity of fluid (J/kg K), ρ_w is the fluid density (kg/m^3), v_a is the advective fluid velocity (m/s), ρ is the density of the saturated porous rock (kg/m^3), Q_T is the heat source or sink (J/kg K), c_m is the specific heat capacity of the saturated porous rock (J/kg K), ρ_m is the density of the saturated porous rock (kg/m^3), and t is time (s) (McDermott et al. 2006).

The heat diffusion-dispersion tensor D_T (W/mK) comprises two terms (Equ.A.13); an effective heat diffusion coefficient $D_{m(heat)}$ (W/mK) (Equ.A.14), and a heat dispersion coefficient β (J/K m^2) (Equ.A.15) due to advective velocity v_a (m/s) (McDermott et al. 2006) both of which operate at *approx.* 1.00E-06 (W/mK) (Phillips 1991), and where α is the thermal diffusivity (J/K m^2) (McDermott et al. 2006)

$$D_T = D_{m(heat)} + v_a \beta \qquad (A.13)$$

$$D_{m(heat)} = \frac{\lambda_m}{c_m \rho_m} \quad \text{(A.14)}$$

$$\beta = \alpha \frac{c_w \rho_w}{c_m \rho_m} \quad \text{(A.15)}$$

Equ.A.12 assumes that both the solid and fluid are at the same temperature within the control volume (McDermott 2015).

A.3.3: Mass Transport

The three-dimensional balanced mass transport equation is presented (Equ.A.16) (Niemi et al. 2017).

$$\frac{\partial C}{\partial t} = \nabla \cdot \left(\frac{D}{R_f} \nabla C \right) - \frac{v_a}{R_f} \cdot \nabla C + C_s + C_r + C_\lambda \quad \text{(A.16)}$$

Where C is the solute concentration (kg/m^3), t is time (s), D is the hydrodynamic dispersion tensor (m^2/s), v_a is the advective fluid velocity (m/s), R_f is the retardation factor (section A.3.3.1), C_s is a concentration source term (Kg/m^{3}s), such as input from a chemical spill, C_r is a concentration source term due to chemical reactions (Kg/m^{3}s), and C_λ is a concentration source term due to radioactive decay (Kg/m^{3}s) (section A.3.3.2).

The hydrodynamic dispersion tensor D is itself a function of the dispersity α (m), advective velocity v_a (m/s), and the effective molecular diffusion coefficient D_e (m^2/s) (previously outlined in Equ.A.6) (Domenico & Schwartz 1997).

$$D = \alpha \, | \, v_a \, | + D_e \quad \text{(A.17)}$$

A.3.3.1: Retardation Factor (R_f)

The retardation factor R_f (Equ.A.18) describes the degree to which the transportation of mass (contaminants) is slowed down relative to that of groundwater (Krupka et al. 1999), with a R_f of 1 representing a contaminant traveling the same speed as groundwater, whilst a R_f of 2 describes a contaminant travelling half the speed of groundwater. A larger retardation factor is considered advantageous for deep geological disposal as it grants more time for radioactive decay within the sub-surface environment.

$$R_f = 1 + \frac{\rho_b \, K_d}{n_e} \quad \text{(A.18)}$$

Where ρ_b is the bulk density of the aquifer material (kg/m^3), n_e is the effective porosity (-), and K_d is the partition coefficient (m^3/kg), and describes the propensity of a contaminant to partition to the solid phase through the process of sorption (Domenico & Schwartz 1997). The

analytical solution and method used to validate the retardation calculation is presented within section B.2.11.

K_d within Equ.A.18 can be expressed in different ways. Firstly as Equ.A.19 where K_{oc} is the partition coefficient of a compound between organic carbon and water (m^3/kg), and f_{oc} which is the weight fraction of organic carbon (-). f_{oc} indicates that mineralogy, and therefore lithology, plays a key role in determining the partition coefficient (Savage 1995). Secondly, K_d can also be expressed through Equ.A.20 (assuming a linear Freundlich sorption isotherm) where *S* is the quantity of mass sorbed on the surface (kg/kg) or (-), and *C* is the equilibrium concentration (kg/m^3) (Domenico & Schwartz 1997).

$$k_d = K_{oc} f_{oc} \qquad (A.19)$$

$$k_d = \frac{S}{C} \qquad (A.20)$$

Equ.A.20 can also be expressed graphically (Figure A.0.2) in which a concentration (X), such as limited by solubility, would achieve a proportional amount of mass sorption (Blue Lines).

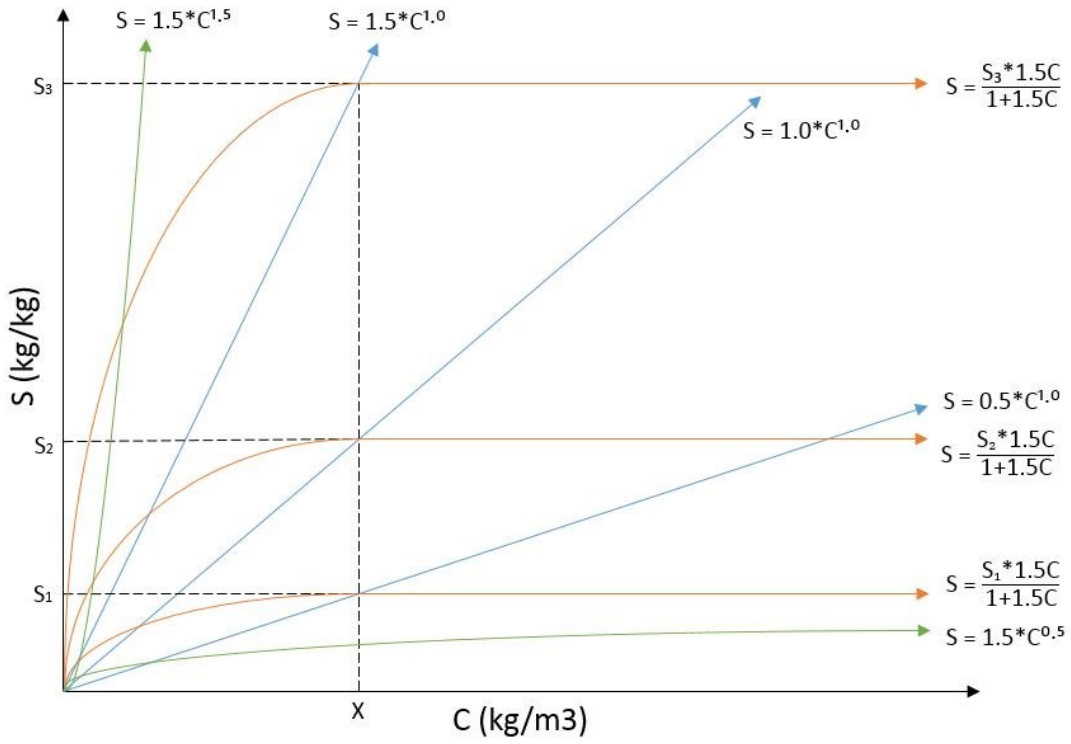

Figure A.0.2: Illustration of 1) Blue Line: Freundlich Linear Sorption Isotherms with Kd's of 0.5, 1 and 1.5, 2) Green Line: Freundlich Non-linear Sorption Isotherms with Kd's of 0.5 and 1.5, and 3) Orange Line: Langmuir Non-Linear Sorption Isotherms with Kd's of 1.5 and increasing maximum sorption capacity (S_1, S_2 and S_3). Adapted from (Domenico & Schwartz 1997).

A.3.3.2: Radioactive Decay (C)

The concentration source term (C_λ) due to radioactive decay (kg/m^{3}s) in Equ.A.16 can be expressed as follows (Equ.A.21)

$$C_\lambda = -\lambda(n_e C + \rho_b s) \quad \text{(A.21)}$$

$$\lambda = \frac{ln(2)}{T_{0.5}} \quad \text{(A.22)}$$

$$s = K_d\, C \quad \text{(A.23)}$$

Where $-\lambda$ is the radioactive decay constant (s^{-1}), n_e is the effective porosity (-), C is the mass concentration (kg/m^3), ρ_b is the bulk density (kg/m^3), and s is the mass fraction of sorbed chemical (-) (McDermott 2015; Anderson & Woessner 1992). The radioactive decay constant is itself defined in (Equ.A.22) where $T_{0.5}$ is the radioactive half-life (s) (Domenico & Schwartz 1997), whilst the mass fraction of sorbed chemicals s is defined in (Equ.A.23) where K_d is the partition coefficient, discussed in section A.3.3.1 (McDermott 2015).

A.3.3.3: Representing the dominant transport process through the Peclet Number (P_e)

The advective-dispersive term (first term on the right of Equ.A.17) is typically in the order of 1.00E-06 m^2/s, whilst the diffusive term (second term on the right of Equ.A.17) is in the order of 1.00E-09 m^2/s (Phillips 1991). The advective-dispersive term therefore typically dominates mass transportation in more permeable formations, such as sandstones and along fractures, whilst the diffusive term dominates in low permeability formations such as clays, salts and through undisturbed crystalline matrix.

The ratio of diffusion/dispersion dominated mass transport (or conductive heat transport) to advective dominated mass/heat transport is described through the grid Peclet Number P_e (-) (Equ.A.24) (Anderson & Woessner 1992), where v_a is the advective velocity (m/s), x is the grid size (m), and D is the hydrodynamic dispersion tensor (m^2/s).

$$P_e = \frac{|\, v_a \,|\Delta x}{D} \approx \frac{\Delta x}{\alpha} \quad \text{(A.24)}$$

When the Peclet Number is greater than 1, mass transport can be considered primarily a result of advecting groundwater, whilst a value much less than 1 indicates diffusion/dispersion dominated solute transport. Due to very slow rates of fluid movement and solute transport via diffusion, these formations are often considered advantageous for deep geological disposal containment.

A.4: Coupling of the Processes

The processes of liquid flow, heat transport and mass transport are coupled through a series of material properties, both solid and liquid, which enable groundwater flow at geologically and hydrogeologically variable sites to be simulated. The key couplings will now be explained.

A.4.1: Advective Velocity

The advective velocity v_a (m/s) of groundwater can be obtained by dividing the groundwater flux (Equ. 2.1.) through by the effective porosity n_e (-) (Equ.A.25).

$$v_a = \frac{F_{gw}}{n_e} \qquad (A.25)$$

The advective velocity term, once calculated for groundwater flow, is then passed on for use within the three-dimensional heat transport equation (Equ.A.12), and the three-dimensional mass transport equation (Equ.A.16), thus coupling the three processes in a staggered approach i.e. one process is solved fore before another.

A.4.2: Material Fluid Properties

Both fluid density ρ (kg/m^3) and dynamic viscosity μ (Pa s), included within the advective velocity v_a term through the hydraulic conductivity K, are dependent on the temperature T (K) and mass concentration C (kg/m^3) of the fluid, and as such are key components within the coupling process. Specific fluid density and dynamic viscosity functions for use within this research are presented within section B.1.3.1.

The specific heat capacity c_w (J/kg K) and specific heat conductivity λ_w (W/mK) of the fluid both enable the transport of heat throughout the system, changing the temperature, which affects the fluid properties of density and viscosity. The material fluid properties of specific heat capacity and conductivity thus control the coupling of the liquid flow, heat transport and mass transport processes. The specific heat capacity and heat conductivity will be applied as constants for the purpose of this research as discussed further in section B.1.3.2.

A.4.3: Material Medium Properties

Both effective porosity n_e (-) and intrinsic permeability k (m^2) are included within the advective velocity v_a term, and as such, are used to couple liquid flow, heat transport and mass transport and will be applied per lithological unit, discussed further in section B.1.4.

Heat dispersion β (J/K m^2) (Equ.A.15) located within the diffusion-dispersion tensor of the heat transport equation (Equ.A.12), and mass dispersion α (m) (Equ. A.17) located within the hydrodynamic dispersion tensor of the mass transport equation (Equ.A.16) involve the spread

of mass or heat energy via the advective velocity term v_a, but can also be used as a tool to ensure numerical stability, discussed further in section B.1.8.

The specific storage coefficient S_s (Pa^{-1}), located within the groundwater flow equation (Equ.A.11) describes the release of water (as pressure) from storage under transient groundwater conditions and therefore controls the volume of water through which heat energy or mass is transported, and will also be applied per lithological units as values can vary markedly.

A.4.4: Material Solid Properties

The mass density ρ_r (kg/m^3), thermal capacity c_w (J/K), and thermal conductivity of the rock mass λ_r (W/mK) are all located within the heat transport equation (Equ.A.12) and as such, control the transfer of heat energy throughout the entire system, and will be applied per lithological unit as discussed in section B.1.5.

A.4.5: Material Chemical Properties

The diffusion coefficient D_e (m^2/s), is located within the hydrodynamic dispersion tensor D (m^2/s) (Equ.A.17) of the mass transport equation (Equ.A.16) and as such, controls the transfer of mass throughout the system. A uniform diffusion coefficient of 1.99E-09 m^2/s has been applied to the entire model domain.

A.4.5: Geological Parameters

Geological processes are incorporated into the model via host rock geometries and material properties. All material medium properties and material solid properties will therefore be lithologically dependent, represented through different material groups within the model. The applied material properties have been outlined within the site specific results and discussion chapters (Chapters 5 to 7), and associated appendices.

Appendix B

B.1: TH Model Construction

B.1.1: Geometry (GEO)

The geometry (either 1D, 2D, or 3D) defines the spatial domain required for model simulation, subdividing the domain into material groups (MAT) of interest to which properties can be assigned. The decision of this research is to run the TH models as two dimensional (2D) simulations in the X-Z orientation, based on 2D geological cross-sections, such as those provided by the British Geological Survey (BGS). This is due to the availability of 2D geological cross sections over 3D geological interpretations, and the excess computational resources required for 3D simulation.

The simulation of 2D rather than 3D groundwater flow is also considered conservative within the context of this research, as pressure can only dissipate within two-dimensions, resulting in steeper pressure gradients, and faster groundwater flow. Furthermore, 2D groundwater simplifications still achieves the objective of this research, which is to characterise regional groundwater flow patterns, and to identify hydrogeological/geological features of importance, rather than to undertake detailed radionuclide fate and transportation risk assessments.

Finally, the geometry will extend to *approx.* 30 km in length, and between 2 and 4 km depth, to ensure the *'regional'* groundwater flow system is captured (see section 2.3.4), including the key topographical features. *'Edge effects'* must also be accounted for within this domain which is the artificial disturbance of groundwater, close to the boundaries due to the applied boundary conditions, rather than the coupled process interactions under investigation.

B.1.2: Mesh (MSH)

The mesh (MSH) discretises the geometric domain (GEO) into a series of 1D, 2D or 3D *'elements'*, depending on the dimensions of the geometry (in the case of this research, 2D). 2D elements can take the form of either rectangles or triangles, with triangles selected for this research, in line with a previous Sellafield model developed by (Fraser Harris et al. 2015). Mesh development will occur using the commonly used open source meshing software 'Gmsh' (Geuzaine & Remacle 2009).

The density of elements in the mesh will be increased in areas for which a rapid change in the numerical solution is anticipated, such as along a narrow fault, or around the repository where

radiogenic heat emission and decay will be simulated. For this reason element density is also a tool used to ensure numerical stability (section B.1.8).

Faults will be represented as equivalent continuous porous mediums, an approach which has received much attention within geoscientific literature e.g. (Domenico & Schwartz 1997; Schulze-Makuch et al. 1999), and has been commonly used within historic geological disposal post-closure assessments (Nirex 1997b). The continuous porous medium approach is considered legitimate for porous media within the 'macroscopic regime' where the influence from individual pores (microscopic regime) is not detected (Figure B.0.1). Furthermore, the continuous porous medium approach is also considered legitimate to represent discrete fracture networks when considered over a large enough area (macroscopic regime). This is because the rock mass can be considered to behave in an equivalent porous medium (similar to the upscaling of porous medium from flow between grains to meter scale). Therefore, as this research simulates regional scale groundwater flow, the equivalent continuous porous medium approach to both porous medium and discrete fracture networks is considered appropriate.

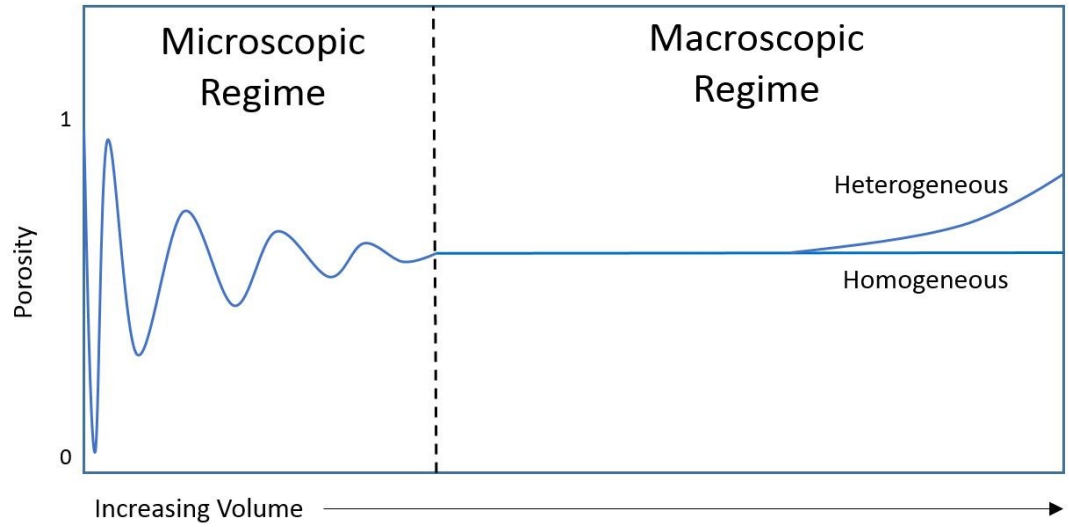

Figure B.0.1: Illustration of the Continuous Porous Medium Approach. Image adapted from (Domenico & Schwartz 1997)

Faults were represented as 50 m wide fault damaged zones, in line with previous research undertaken at Sellafield by (Fraser Harris et al. 2015). All faults and thin hydrogeological units were designed to have a minimum of one full element within the material group of interest.

B.1.3: Material Fluid Properties (MFP)

B.1.3.1: Fluid Density & Dynamic Viscosity

Fluid density and dynamic viscosity are key fluid properties involved in coupling thermo-hydro-chemical processes (section A.4). Examples show groundwater densities can range from *approx.* 1,000 kg/m^3 for freshwater, to 1,300 kg/m^3 for brines within the same region, whilst viscosities can range from *approx.* 0.0014 Pa s for freshwater, to 0.0032 Pa s for brines (Ophori 1998). These fluid properties can have a major influence on controlling regional groundwater movement, such as in West Cumbria (section 2.5.6), and there variations across the model domain will be captured.

A fluid density function and a dynamic viscosity function, previously defined for Sellafield (Nirex 1997a) are presented within Equ.B.1 & Equ.B.2 respectively, and applied to the OpenGeoSys code by (Fraser Harris et al. 2015), where ρ is the density of the fluid (kg/m^3), C is the chloride concentration (mg/l), T is the temperature (°C), and μ is the dynamic viscosity (Pa.s).

$$\begin{aligned}\rho(C,T) = {} & (998.2063 + 0.001266C - 1.19 \times 10^{-9}C^2) \\ & + (-0.22644 - 2.82 \times 10^{-6}C + 7.20 \times 10^{-12}C^2)(T-20) \\ & + (-0.00361 + 2.68 \times 10^{-8}C - 7.17 \times 10^{-14}C^2)(T-20)^2\end{aligned} \quad \text{(B.1)}$$

$$\begin{aligned}\mu(C,T) = {} & (1.002 \times 10^{-3} + 2.43 \times 10^{-9}C + 1.08 \times 10^{-14}\,C^2) \\ & \times \exp(-0.02358(T-20) + 0.000107(T-20)^2)\end{aligned} \quad \text{(B.2)}$$

Equ.B.1 & B.2 were derived under conditions of 20 °C and for atmospheric pressure (Nirex 1997a). The effect of temperature on fluid density is however considered greater than that of pressure, and thus the above equations are considered appropriate. This is because density is anticipated to vary by *approx.* 24 kg/m^3 over the expected 1 to 500 bar pressure range (based on a temperature of 0 ^{o}C) (Stephan 2010), but by *approx.* 41 kg/m^3 over the expected 8 to 100 ^{o}C temperature range (based on a pressure of 1 bar) (Stephan 2010). In addition viscosity is anticipated to vary by *approx.* 8.7E-05 Pa s over the expected 1 to 500 bar pressure range (based on a temperature of 0 ^{o}C) (Stephan 2010), but by *approx.* 1.1E-03 Pa s over the expected 8 to 100 ^{o}C temperature range (based on a pressure of 1 bar) (Stephan 2010).

Due to the absence of site specific density and viscosity functions for the Thetford and Tynwald Basin sites, the Nirex defined functions for Sellafield will be applied.

The variation in the fluid density and viscosity functions between sites is currently unknown, however (Watanabe et al. 2010) suggests that the influence of viscosity and density uncertainty

on coupled process modelling is typically much less than those generated from uncertainties in material properties, such as permeability, which can span 2 or 3 orders of magnitude (section 2.7.1). As the lithology and therefore material properties will also vary between sites, the use of the Sellafield derived viscosity and density functions within the Thetford and Tynwald Basin models are considered legitimate, however, it is recommended any future site specific investigations focus on defining fluid property functions for the individual sites.

B.1.3.2: Specific heat capacity and heat conductivity of a fluid

A constant specific heat capacity c_w of 4.28E+03 (J/kg K) (Kolditz et al. 2008) and a constant specific heat conductivity λ_w of 6.00E-01 (W/mK) (Eppelbaum et al. 2014) will be applied. This is justified as fluid heat capacity is only expected to vary by *approx.* 21 J/kg K over the 10 to 100 °C temperature range based on pure water at a pressure of 1 bar (Stephan 2010) i.e. < 0.5 %, and heat conductivity by 0.0956 W/mK (Stephan 2010) i.e. *approx.* 15 %. Furthermore (Watanabe et al. 2010) suggests that dynamic viscosity (section A.4.2) is a more influential fluid parameter than heat capacity or conductivity when simulating coupled process fluid flow. Variations of dynamic viscosity will be captured across the model domain (see B.1.3.1). It is however recommended that future research focus on defining site specific fluid heat capacity and conductivity functions for the individual sites.

B.1.4: Material Medium Properties (MMP)

B.1.4.1: Intrinsic Permeability, Effective Porosity & Storage

Intrinsic permeability k (m^2), effective porosity n_e (-) and storage S_s (Pa^{-1}) (section A.4.3), are lithologically dependent and are all expected to vary significantly over the modelled domain (Domenico & Mifflin 1965; Batu 1998), with values for permeability reported to range over 10 orders of magnitude from 3.00E-09 m^2 for gravel, to 3.00E-21 m^2 for unfractured crystalline rock (Domenico & Schwartz 1997), with effective porosity reported to range over 6 orders of magnitude from 1.00E-01 for sandstone to 5.00E-07 for crystalline rock (Domenico & Schwartz 1997), and with specific storage reported to range over 4 orders of magnitude from 2.00E-06 Pa^{-1} for plastic clay to 3.30E-010 Pa^{-1} for unfractured rock (Domenico & Schwartz 1997). As such, these material medium properties have been applied per hydrogeological unit as described within the site chapters (Chapter 5 to 7), and are based on site specific information where available, otherwise generic literature derived ranges have been used.

Where a statistically significant range of permeability values have been provided, such as for Sellafield (Nirex 1997b), the *'most-likely'* permeability values have been based on 50th percentile permeability values, and 95th percentile permeability values in the case of the *'high'* permeability modelled scenario using Equ.B.3.

$$k = 10^{N(P,m,\sigma)} \quad \text{(B.3)}$$

Where k is the permability (m^2), and where N is a function giving the inverse of the normal distribution, with a mean m permeability (m^2), and a standard deviation σ for a given probability P. For example, for a hydrological unit with a mean log10 permeability (m^2) of -16, and a standard deviation log10 permeability (m^2) of 1, a value of 1.00E-016 m^2 has been applied to the '*most-likely'* permeability scenario, and a value of 4.41-015 m^2 has been applied to the *'high'* permeability model scenario.

Where a statistically insignificant/unknown permeability range has been provided, such as is the case for absolute permeability ranges provided in (Domenico & Schwartz 1997), a permeability value from the centre/middle of the logarithmic range has been applied to the '*most-likely'* permeability scenario. In addition, the highest permeability value of the logarithmic range has been applied to the *'high'* permeability model scenario. For example, from a permeability range of 1.00E-016 to 1.00E-014 m^2, a value of 1.00E-015 m^2 has been applied to the '*most-likely'* permeability scenario, and a value of 1.00E-014 m^2 has been applied to the *'high'* permeability model scenario.

This approach to permeability value selection involves a degree of judgement, especially where mixed lithological units have been identified. Although not ideal, the approach is considered legitimate for the aims of this research, from which further site specific research and data collection can be guided.

Finally, where literature values of specific storage have been presented with respect to hydraulic head ($S_{s\ head}$) (-), the conversion to specific storage with respect to pressure head ($S_{s\ pressure}$) (Pa^{-1}) (Equ.B.4), has involved an assumption of freshwater density (ρ_f) of 1000 kg/m^3.

$$Ss_{pressure} = \frac{Ss_{head}}{\rho_f g} \quad \text{(B.4)}$$

B.1.4.2: Heat and Mass Dispersion

Heat and mass transportation are considered difficult to solve numerically, and as a result can lead to a phenomenon called 'numerical dispersion', which involves the artificial dispersion of heat or mass across the mesh due to numerical errors (Anderson & Woessner 1992). To minimise numerical dispersion, the mesh should ideally be designed so that the Peclet number P_e (section A.3.3.3) is less or equal to two (Anderson & Woessner 1992), although acceptable solutions have been reported up to 10 (Huyakorn & Pinder 1983).

Heat and mass dispersion values will be applied as either 10 or 50 for each hydrogeological unit, depending on which value most closely satisfies the Peclet number. The applied heat and

mass dispersion values have been reported within Appendix sections C.1., D.1., and E.1. for the individual sites.

B.1.5: Material Solid Properties (MSP)

B.1.5.1: Mass Density, Thermal Capacity & Thermal Conductivity

The mass density of a rock ρ (kg/m^3), thermal capacity c_r (J/K) and thermal conductivity λ_r (W/mK) are lithologically dependent, and are expected to vary significantly over the modelled domain, with the thermal conductivity of rocks ranging between 1.2 and 5.9 W/mK (Eppelbaum et al. 2014), and reported densities between 2,090 and 2,750 kg/m^3 (Eppelbaum et al. 2014). Material solid properties have therefore been applied and documented, per hydrogeological unit, within the site specific chapters (Chapters 5 to 7).

B.1.6: Boundary Conditions (BC)

Boundary conditions must be defined at nodes, most commonly, although not exclusively, along a domain boundary. The boundary conditions control the movement of pressure, mass or heat, into and out of the model, and thus typically represent the interaction between the model and the wider field of study (Anderson & Woessner 1992). Where no boundary exists, no pressure, mass or heat can enter or leave the model domain.

Boundary conditions have been applied to the TH models with known values of pressure, temperature and mass concentration as described in sections B.1.6.1 to B.1.6.3. The application of radiogenic heat emission as a temperature boundary has been discussed separately in section 8.3.2.

B.1.6.1: Pressure Boundaries

Onshore surface pressure boundaries will be calculated using Equ.B.5 (Engineering ToolBox 2003) where P_a is atmospheric pressure at sea level, reported as 101325 Pa (Lide 2004), and h is the elevation above sea level (m).

$$P_{onshore\ surface} = P_a(1 - 2.26E\text{-}05\ h)^{5.25588} \quad \text{(B.5)}$$

Offshore seabed pressure boundaries will be calculated using Equ.B.6 where P_a and h are as described for Equ.B.5, $\rho_{seawater}$ is the density of seawater, typically reported as 1,025 kg/m^3 (Grasshoff et al. 1999), and g is acceleration due to gravity, reported at 9.81 m/s^2.

$$P_{offshore\ seabed} = P_a + (\rho_{seawater} \times g \times h) \quad \text{(B.6)}$$

Sub-surface pressure boundaries will be calculated using Equ.B.7 where $P_{onshore\ surface/offshore\ seabed}$ (Pa) is either Equ.B.5 or Equ.B.6 depending on the location of the sub-surface pressure boundary, ρ_{water} is the density of the water, typically reported as 1,000 kg/m^3 for freshwater

and 1,025 kg/m^3 for seawater (Grasshoff et al. 1999), and where g and h are as described for Equ.B.6.

$$P_{subsurface} = P_{onshore\ surface/offshore\ seabed} + (\rho_{water} \times g \times h) \quad \text{(B.7)}$$

An illustration of the pressure boundary nomenclature is presented within Figure B.0.2.

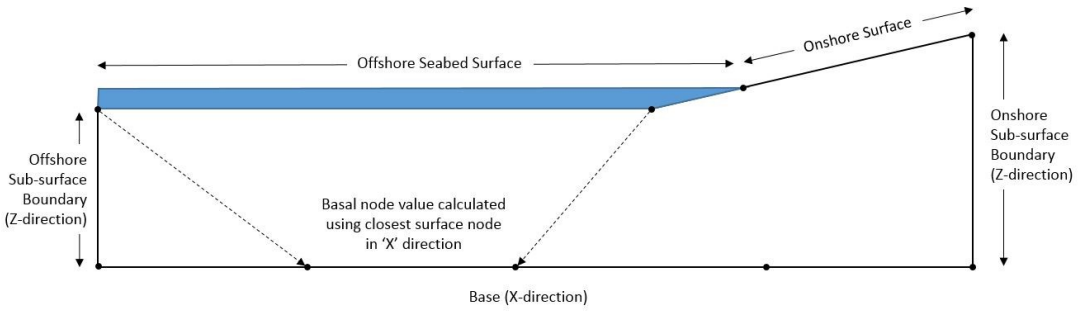

Figure B.0.2: Graphic, none site specific, illustration of the boundary nomenclature.

B.1.6.2: Temperature Boundaries

Sub-surface temperature boundaries will be calculated based on Equ.B.8 where $T_{onshore\ surface/\ offshore\ seabed}$ is the temperature (°C) at either the onshore surface, or offshore seabed depending on the location of the temperature boundary, with offshore seabed temperatures typically reported as 8.5 °C such as for the Irish Sea seabed between December 2002 and February 2003 (Joint Nature Conservation Committee 2003). ΔT is the geothermal gradient, reported as 0.025 °C/m for typical continental settings (Downing & Gray 1986), and h is the distance below ground level (m).

$$T_{subsurface} = T_{onshore\ surface/offshore\ seabed} + (\Delta T \times h) \quad \text{(B.8)}$$

Temperature boundaries running along the base of the model domain have been calculated so that specific h and $T_{onshore\ surface/offshore\ seabed}$ values of the surface nodes have been applied to those basal nodes that most closely match the surface nodes x-orientation. An illustration of the temperature boundary nomenclature and application of surface node values to basal node values is presented within Figure B.0.2.

B.1.6.3: Mass Concentration Boundaries

Mass concentration (C_m) boundaries (kg/m^3) will be calculated based on Equ.B.9, where Cl is in mg/l, typically reported as 19,350 mg/l for seawater (Grasshoff et al. 1999), and ρ_{water} is the density of freshwater, reported as 1000 kg/m^3.

$$C_m = \left(\frac{Cl}{1000}\right) + \rho_{water} \quad \text{(B.9)}$$

Chloride was chosen as it makes up the majority of dissolved ions in groundwater by weight (*approx.* 55.4% for seawater). It is however recommended that any future work also includes sodium within the mass boundary calculations, as sodium and chloride together make up 86 % of total salinity by weight (SOEST 2015). The percentage difference between using just 'Cl' and 'Cl+Na' on mass concentration (kg/m^3) is however < 1 %, and thus is only considered a minor source of uncertainty. The density of groundwater can however be expected to range between 1,000 and 1,200 kg/m^3 across a regional setting. The use of freshwater density could create an error of up to 20 % in the mass concentration calculation. The use of freshwater density is however considered a conservative approach as groundwater with a lower mass concentration will have a lower density and viscosity, and will therefore flow faster (considered a negative attribute for radionuclide containment).

B.1.7: Initial Conditions (IC)

Initial pressure, temperature and mass concentration values across the model domain are required for the finite element method to solve. An illustration of the spatial and temporal position of the initial conditions within a numerical model, along with the boundary conditions, are presented within Figure B.0.3.

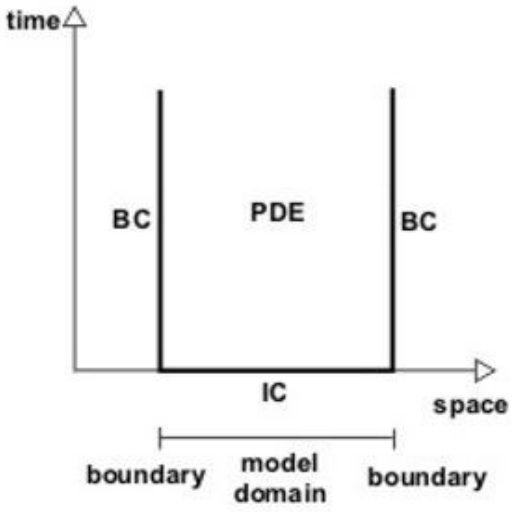

Figure B.0.3: Graph showing the relationship in space and time between partial differential equations (PDE or EQS), boundary conditions (BC) and initial conditions (IC).

The modelled scenarios will undergo a two stage process. The first stage will involve the models being run to quasi-steadystate conditions, which is the point where only small changes are observed in the solution over time. This will be achieved by using gradational and lithological specific initial conditions. The distribution of pressure, mass and temperature at

the end of the quasi-steadystate model simulation will then form the initial conditions for the transient model (i.e. the solution changes with respect to time, such as is required for radiogenic heat emission and decay, discussed in Chapter 9).

B.1.8: Numerical Control (NUM)

Mesh density and distribution (see section B.1.2), and mass and heat dispersion (section B.1.4.2) are critical parameters in ensuring numerical stability. This is in addition to timestep length, which must allow migrating groundwater to jump cleanly across an element within the specified timestep, whilst capturing the process of interest (see section 9.1) (McDermott 2003). A faster migrating groundwater requires a smaller timestep than a slower migrating groundwater (Anderson & Woessner 1992).

Time step length will be applied to each TH modelled scenario individually to enable numerical stability. Timestep length will be reduced within the transient model scenario to ensure the full effect of radiogenic heat emission and decay, and particle transportation is captured.

B.2: Reactive C (Goldsim) Model Construction

The C modelling was undertaken to verify the radionuclide retardation calculations. This section will present how the C models were constructed. The C models were run deterministically (GoldSim Technology Group 2018) with the results reported as the absolute particle travel distance over 10,000 years. A summary of the results and C model input files are presented within Appendix F.

B.2.1: Geometry (GEO)

The geometry for the reactive C models were be based on worst-case 1D 'streak-lines' of groundwater particles released from the theoretical deep geological repository within the TH model (see section 3.4.3).

The worst case streak-line (see section 3.4.3) were converted into an advection equivalent GoldSim compatible format. This was done by the average advective velocity (v_a) per hydrogeological unit (m/s) being converted into a volumetric flow rate (Q) per hydrogeological unit (m^3/s) using Equ.B.10 to B.12. Where x is the particle travel distance per hydrological unit (m), t is the time per hydrological unit (s), n_e is the effective porosity per hydrological unit (-), and A is the pathway cross-sectional area (m^2), assumed to be 1.

$$v_a = \frac{x}{t} \qquad (B.10)$$

$$q = v_a \times n_e \quad \text{(B.11)}$$

$$Q = q \times A \quad \text{(B.12)}$$

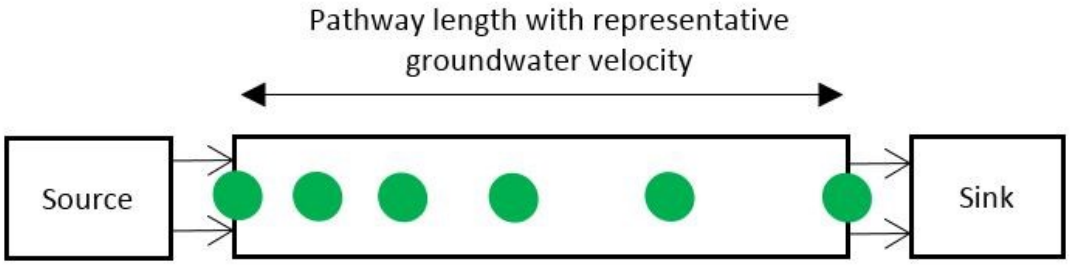

Figure B.0.4: Coneptual image of the conversion of the 'worst-case' streak-line to a GoldSim compatible format.

All the material groups encountered within the TH (OpenGeoSys) models were included within the C models. The use of a 1D model is considered appropriate to validate the retardation factor of radionuclides traveling along a discrete, pre-determined pathway.

B.2.2: Mesh (MSH)

The GoldSim pathway is subdivided into a number of user defined cells, considered analogous to nodes (which define the limits of the elements, see section B.1.2). Each cell is linked to another through advective and diffusive mass flux links (GoldSim Technology Group 2017a). The array of cells behaves as a mesh, with the mass transport equation solved for using the finite difference method (section 3.2.5). The number of cells in a pathway is analogous to the mesh density (section B.1.2), and can therefore also be used as a tool to control numerical stability (section B.1.8), as was the case in this research.

Cell number was selected for the reactive C GoldSim models to ensure the Peclet number (section A.3.3.3) was matched, and thus, the solution was numerically stable using (Equ.B.13), where the dispersivity α (m) is set to 0.5% of the pathway length (see section B.2.4). All GoldSim models were therefore simulated with 100 cell, the maximum allowed.

$$Cell\ no. = \frac{pathway\ length}{\propto \times 2} \quad \text{(B.13)}$$

B.2.3: Material Chemical Properties (MCP)

The radionuclides selected for analysis are listed in Table B.0.1 and are considered to represent a range of sub-surface radionuclide fate and transportation behaviours (see section 2.3.2).

Table B.0.1: Summary of selected radionuclides for use within the GoldSim contaminant transportation models, along with their respective half-lives.

Periodic Group	**Radioelement**	**Radionuclide**	**Half-lives (yrs)**
Alkali Metals	Cs	135	2.3E+06
Alkaline Earth Metals	Sr	90	28.79
Transition & Post Transition Metals	Tc	99	2.11E+05
	Ni	59	1.01E+05
Non-metals	Cl	36	3.01E+05
	Se	79	2.95E+05
Lanthanides	Eu	152	13.54
Actinides	Am	241	432.2
	U	238	4.47E+09

Maximum radionuclide solubility (mol/m^3), which includes the effects of organic complexants (see section 2.3.2) for unshielded intermediate level waste (Chambers & Williams 2010), has been presented in Table B.0.2. Also presented is the minimum sorption coefficients per radionuclide of each main lithological type (section 2.3.1). Where more than 1 oxidation state is likely, such as for Tc, Se and U, the oxidation state with the highest solubility has been applied in line with (Nirex 1997c), which is considered a conservative approach.

A source porosity of 1 has been assumed for the purpose of the initial radionuclide mass dissolution rate calculation. In reality, the higher activity waste packages will be vitrified, creating very low initial porosities, however, uncertainties exist around the rate of glass dissolution, which can vary over several orders of magnitude, depending on the experimental/environmental conditions (Gin 2014). Instantaneous radionuclide exposure has been assumed, with no engineered barriers to delay the release of dissolved radionuclides, representing a worst case scenario.

The conservative sorption values for higher and lower strength rocks are based on data elicitation (compilation) undertaken by Serco representatives (Nirex 2003; Chambers & Williams 2010). Sorption values (partition coefficients) are treated as a linear sorption isotherm, and thus assume the equilibrium concentration and amount of mass sorbed to be proportional (see section A.3.3.1). No sorption has been conservatively assumed for evaporitic

rocks due to the competition for sorption sites form the dissolved ions already within the dense, fully saturated groundwaters (section 2.3.1). All lithological units are assumed to be chemically and physically homogenous, with the effects of anion exclusion and molecular filtration excluded (see section 2.3.1 for anion exclusion and molecular filtration description).

Finally, although the effect of radiogenic heat on solubility and sorption has not been explicitly modelled, selection of worst case sorption and solubility values will cover most of this uncertainty, which is considered less than an order of magnitude over 20 to 80 °C (Nirex 1997c).

Table B.0.2: Summary of far-field sorption values and near-field and far-field solubility values for use within the GoldSim models

Periodic Group	**Radionuclide**	**Formation**	**Sorption/Kd** *(m^3/kg)* Higher Strength Rock, Table 5 (Chambers & Williams 2010), Lower Strength Rock, Table 6 (Chambers & Williams 2010). Evaporitic rock (Nuclear Decommissioning Authority 2010c)	**Near-field Solubility** *(mol/m^3),* including organic complexants (corrected using SEF's for unshielded ILW vaults with cellulose loading 3.94 wt%) Table 3 (Chambers & Williams 2010)
			Minimum	*Maximum*
Alkali Metals	Cs	Higher strength	1.00E-04	Unlimited
		Lower strength	1.00E-03	
		Evaporites	none	
Alkaline Earth Metals	Sr	Higher strength	1.00E-06	Unlimited
		Lower strength	3.00E-04	
		Evaporites	none	
Transition Metals	Tc (mix)	Higher strength	1.00E-06	5.00E-02
		Lower strength	1.00E-06	
		Evaporites	none	
	Ni	Higher strength	1.00E-03	6.75E+02
		Lower strength	5.00E-04	
		Evaporites	none	
Non-Metals	Cl	Higher strength	none	Unlimited
		Lower strength		
		Evaporites		
	Se(mix) (reduced)	Higher strength	1.00E-06	1.00E+03
		Lower strength	1.00E-06	
		Evaporites	none	

Lanthanides	Eu	Higher strength	none	Unlimited
		Lower strength		
		Evaporites		
Actinides	Am	Higher strength	1.00E-02	1.94E+04
		Lower strength	1.00E-03	
		Evaporites	none	
	U(mix) (reduced)	Higher strength	1.00E-06	8.89E+05
		Lower strength	1.00E-04	
		Evaporites	none	

B.2.4: Material Fluid Properties (MFP)

Dispersion and diffusion values were required for GoldSim simulation however, the processes do not affect the retardation factor (section 2.3.3), which was the focus of this modelling. Dispersion was therefore set very low to 0.005 of the pathway length to ensure the retardation, as a result of advective velocity, was the focus. For comparison, in-field dispersion values typically operate between 0.40 and 0.92 (Schulze-Makuch 2005). Similarly, diffusion was also reduced, with greater reduction required for pathways with lower groundwater velocities. Applied dispersion and diffusion values are presented for each site within Appendix F.

B.2.5: Material Medium Properties (MMP)

Effective porosity will be applied per hydrological unit encountered within the streakline, as listed for each individual site in Appendix sections C.1., D.1., and E.1.

B.2.6: Material Solid Properties (MSP)

Dry bulk density will be applied per hydrological unit encountered within the streakline, as listed for each individual site in Appendix sections C.1., D.1., and E.1.

B.2.7: Boundary Conditions (BC)

B.2.7.1: Groundwater Boundary Conditions

The average volumetric flow rate (m^3/yr) per encountered hydrogeological unit was calculated using Equ.B.10 to B.12, with these values used to define hydraulic head at the start and end of the model pathway.

B.2.7.2: Mass Boundary Conditions

Initial radioactive mass (section B.2.8), located within the repository, is dissolved away using the applied solubilities per radionuclide (Table B.0.2), and transported out of the repository into the pathway using the calculated groundwater volumetric flow rate (section B.2.7.1). The

rate of mass transport into the pathway forms the first mass concentration boundary condition, whilst the the mass boundary at the end of the pathway is an open boundary.

B.2.8: Initial Conditions (IC)

The initial mass of radionuclide within the repository is presented within Table B.0.3, and represents the weighted average density (tonne/m^3) contributing to >90% of the activity per radionuclide waste stream. The original data set was supplied by the Nuclear Decommissioning Authority upon request (2017). The initial mass per radionuclide will be applied to a hypothetical 1 m^3 source, justified as all radionuclide waste volumes exceed this volume initially.

Table B.0.3: Summary of initial radionuclide mass for use within the GoldSim contaminant transportation models

Selected radionuclide	**Initial Mass (tonnes)**
Am^{241}	2.65
Cl^{36}	1.38
Cs^{135}	2.65
Eu^{152}	2.50
Ni^{59}	0.99
Se^{79}	2.65
Sr^{90}	2.65
Tc^{99}	2.37
U^{238}	1.88

B.2.9: Source Terms (ST)

Mass is removed from each cell via radioactive decay. The rate of decay per radionuclide is calculated using the radionuclide specific half-lives (Table B.0.1) and Equ.A.21.

B.2.10: Numerical Control (NUM)

The reactive C models will be run for 2 million years with 10 year time steps over the first 20,000 years and 1,000 year timesteps thereafter to capture the full range of radionuclide behaviours. The element size (cell number along the pathway) was set so that the Peclet Number was satisfied (section B.2.2).

B.2.11: Determining the Retardation Factor

The characteristics of the breakthrough curve (such as simulated by Goldsim) vary depending on whether the source behaves as a pulse (single injection), or a continuous source (open-tap). The nature of the source also determines the point on the breakthrough curve used to represent the retardation factor i.e. the point of average linear velocity (v_a). An illustration of breakthrough curves and the retardation point for an unreactive pulse source and a continuous source are presented within Figure B.0.5.

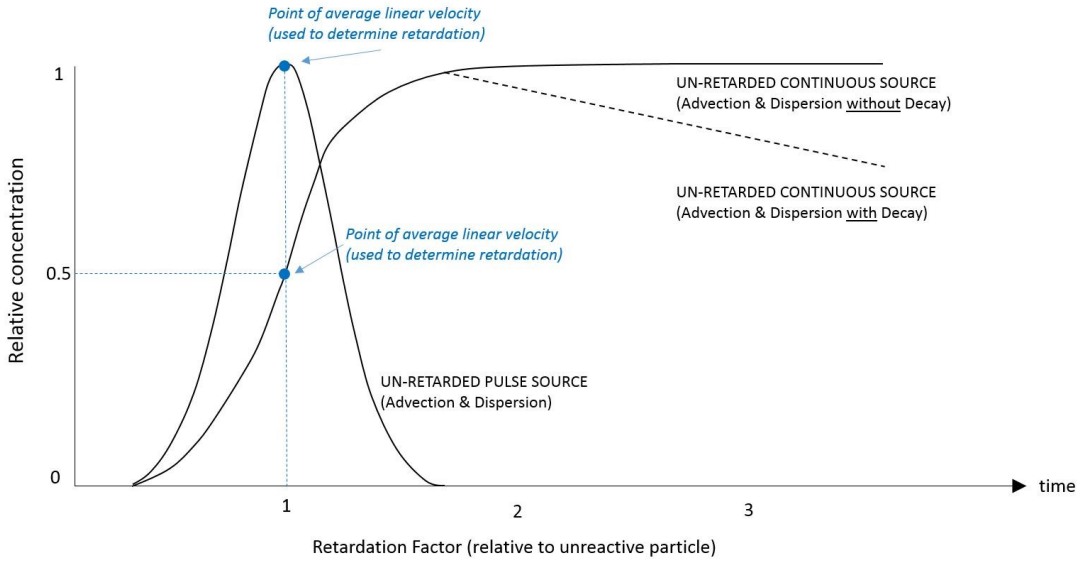

Figure B.0.5: Image of an unretarded breakthrough curve for 1) a pulse source, 2) a continuous source. Circles represent point of average linear velocity used to determine the retardation factor.

In reality, the pulse source and continuous source represent the two end member source scenarios, with finite sources often being depleted over time, such as a result of solubility constraints and/or groundwater flow rate. Therefore, for simplicity within this research, where the release of contaminants out of a source is limited by solubility, the breakthrough curve and retardation factor was considered from the position of a 'continuous source', and where solubility is not a limiting factor, it was considered from the position of a 'pulse source'.

B.2.12: Analytical Solution for a Continuous-Decaying Source

The retardation factor of the released radionuclides was determined through comparison to an analytical solution for a continuous-decaying source, Equation C13 from (van Genuchten & W. J. Alves 1982) (Equ.B.14), where C_b is the initial dissolved mass within the source (kg/m^3), and $E(x,t)$ is the breakthrough function (-). Equ.B.14 assumes that 1) all the source material is decayable, 2) there is no initial mass within the pathway, and 3) that there are no additional source terms within the pathway.

$$c(x,t) = C_b\, E(x,t) \qquad \text{(B.14)}$$

$$E(x,t) = e^{-\lambda t}\left\{\frac{1}{2}exp\left[\frac{(v-w)x}{2D}\right]\ erfc\left[\frac{Rx-wt}{2(DRt)^{\frac{1}{2}}}\right] + \frac{1}{2}exp\left[\frac{(v+w)x}{2D}\right]\ erfc\left[\frac{Rx+wt}{2(DRt)^{\frac{1}{2}}}\right]\right\} \qquad \text{(B.15)}$$

Within Equ.B.15 x is distance (m), t is time (s), λ is the decay rate for mass in the source (s^{-1}), v is the advective velocity (m/s), D is the hydrodynamic dispersion tensor (m) and is determined using Equ.A.17, and R is the retardation factor (-). The equations representing u (Equ.B.16) and w (Equ.B.17) are presented below, where μ is the decay rate for mass in the pathway (s^{-1}).

$$u = v\left(1 + \frac{4\mu D}{v^2}\right)^{\frac{1}{2}} \qquad \text{(B.16)}$$

$$w = v\left[1 + \frac{4D}{v^2}(\mu - \lambda R)\right]^{\frac{1}{2}} \qquad \text{(B.17)}$$

Where more than one lithological medium is encountered along a pathway, the hydrodynamic dispersion tensor *(D)* will be determined using the weighted (distance) average for dispersion *(α)* and effective porosity *(n_e)*.

Finally, both the analytical solution, and the GoldSim determined breakthrough curves will be normalised to '1' of the maximum breakthrough concentration to enable direct comparison and thus, does not require C_b (Equ.B.14), reducing the analytical solution down to Equ.B.15.

B.2.13: Assumptions & Simplifications of C models

This section presents a summary of the assumptions and simplifications applied to the C 'Goldsim' models:

1. Initial radionuclide mass within the source of the reactive C models assumed pure radionuclide substance with densities obtained from reported waste streams (section B.2.8) within a 1 m^3 area. It also assumed a source porosity of 1 for dissolution (section B.2.3), with dissolved radionuclides immediately available for transport. These were conservative assumptions with the purpose of minimising the effect of the engineered barrier facility, to ensure the natural barrier was tested in isolation,

2. Reactive C models simulated particle transport along a 1D section (section B.2.1), with minimal dispersion or diffusion active (section B.2.4), and no anion exclusion or

molecular filtration (section 2.3.1). This led to an overestimation of radionuclide concentrations as mass cannot spread out laterally, but enabled the retardation factor, as a result of advective transport, to be more clearly identified.

3. Maximum solubility values were applied per radioelement, and conservatively assumed the effects of organic complexants for unshielded waste (section B.2.3), under equilibrium conditions. Furthermore, where variable valance states were likely (propensity of an element to form a chemical compound or molecule), the highest solubility of the different valance states was conservatively applied,

4. Minimum sorption values were applied per lithological classification i.e. higher strength, lower strength or evaporitic rock (section B.2.3), so all higher strength rocks for example were assumed to behave in a similar geochemical manner. Each material groups along the reactive C model pathway was assumed chemically and physically homogenous,

5. Sorption/partion coefficient values were applied to the reactive C models assuming a linear sorption isotherm i.e. the equilibrium concentration and amount of mass sorped are proportional (sections 2.3.3.2, A.3.3.1 & B.2.3). This approach is justified as more advanced sorption knowledge would require site specific information (data collection) and batch experiments,

6. The reactive C models were based on streak-lines generated within the TH models, without the effect of radiogenic heat emission. The applied solubility and sorption ranges were valid up to temperatures of 80 °C (section B.2.3) and thus covered much of the temperature range anticipated as a result of radiogenic heat emission. The change in particle pathway as a result of radiogenic heat emission has not been accounted for within the reactive C models,

7. Radionuclides were assumed to decay (Table B.0.1), with no daughter products generated (section 2.3.2). No additional radionuclide mass was added through source terms (C_s) or from reactions (Cr) within the reactive C models (section A.3.3),

8. When solubility constraints limited the release of radionuclide mass into the pathway within the reactive C models, the breakthrough curve was treated as a ‘continuous source’, however, when solubility did not control the mass release rate, the breakthrough curve was treated as a ‘pulse source’ (section B.2.11). The difference in the retardation factor between the two methods was within 20 %. This error was

considered suitable for the purpose of this research, which was to determine the magnitude retardation potential, itself anticipated to range over 2 orders of magnitude,

9. The individual radioelements released into the reactive C pathway are not considered to react, or to be influenced by each other within the pathway,

10. The analytical solution for the continuous-decaying source, used to determine the retardation factor within the GoldSim models assumed 1) all the source material is decayable, 2) there is no initial mass within the pathway, and 3) that there are no additional source terms within the pathway (Appendix B.2.11),

11. The Hydrodynamic Dispersion Tensor for the continuous-decaying source analytical solution was determined from the weighted (distance) average of dispersion and effective porosity from along the pathway (Appendix B.2.11),

B.3: Model Run Scripts

Provided within the electronic appendix:

- startup.sh
- runAModel.sh
- modelArray.sh

(Used to run the OpenGeoSys models on the Eddie3 compute cluster in parallel)

B.4: OpenGeoSys Source Code

Provided within the electronic appendix.

(Source OpenGeoSys code as adapted by (Fraser Harris et al. 2015), see section B.1.3.1)

B.5: Geometry Outline Files

Provided within the electronic appendix:

- Sellafield_Geo_tec.dat
- Tynwald Basin_Geo_tec.dat
- Thetford_Geo_tec.dat

(Used to visually delineate the geometry of the TH models within Tecplot)

B.6: Process Alterations Files

Provided within the electronic appendix:

- ADVECTIVE_VELOCITY.equ
- EISB10_ADVECTIVE_VELOCITY_X1.equ
- EISB10_ADVECTIVE_VELOCITY_Y1.equ

- EISB10_ADVECTIVE_VELOCITY_Z1.equ
- N3_ADVECTIVE_VELOCITY_X1_Y1_Z1.equ
- S10_ADVECTIVE_VELOCITY_X1.equ
- S10_ADVECTIVE_VELOCITY_Y1.equ
- S10_ADVECTIVE_VELOCITY_Z1.equ

(Used to convert Darcy Flux to Advective Velocity within Tecplot, Note: EISB10=Tynwald Basin, N3=Thetford, S10=Sellafield)

- EISB10_Hydrodynamic_Dispersion.equ
- N3_Hydrodynamic_Dispersion.equ
- S10_Hydrodynamic_Dispersion.equ

(Used to plot Hydrodynamic Dispersion within Tecplot, Note: EISB10=Tynwald Basin, N3=Thetford, S10=Sellafield)

Appendix C

Full Sellafield model input and output scripts are provided electronically within Appendix C.0.

C.1: Sellafield Model Material Property Inputs

Table C.0.1: Summary of material group data input for the Sellafield Model.

Model Component	MMP	MMP	MMP	MMP	MMP	MMP	MSP	MSP	MSP
Formation	POROSITY	PERMEABILITY (X-direction) (most-likely & *high*)	PERMEABILITY (Z-direction) (most-likely & *high*)	MASS DISPERSION (Isotropic)	HEAT DISPERSION (Isotropic)	STORATIVITY	DENSITY	THERMAL CAPACITY	THERMAL CONDUCTIVITY
Units	*decimal*	m^2	m^2	*m*	*m*	Pa^{-1}	Kg/m^3	*J/kg/K*	*W/m/K*
QUATERNARY UNDIFFERENTIATED	0.175[1]	1.42E-14[14] *1.41E-13*[14]	1.06E-15[14] *3.96E-15*[14]	50		1.00E-07[10]	2.76E+03[9]	845[9]	2.51[6]
ENNERDALE GRANOPHYRE, ESKDALE GRANITE AND ESKDALE GRANODIORITE UNDIFFERENTIATED	0.010[1]	8.71E-18[14] *1.39E-17*[14]		50		3.35E-10[10]	2.60E+03[2]	790[7]	2.42[8]
ENNERDALE GRANOPHYRE AND ESKDALE GRANITE FAULTED		1.00E-14[14] *4.41E-13*[14]		10		1.00E-09[10]			
ORMSKIRK AND CALDER SANDSTONE UNDIFFERENTIATED	0.201[1]	1.08E-14[14] *6.55E-13*[14]	2.74E-15[14] *2.07E-13*[14]	50		1.73E-08[11]	2.09E+03[9]	845[93]	3.3[9]

ORMSKIRK AND CALDER SANDSTONE FAULTED		2.52E-15[14] *4.36E-12[14]*	4.20E-15[14] *1.85E-12[14]*	10				
ST BEES SANDSTONE UNDIFFERENTIATED	0.095[1]	1.13E-15[14] *1.27E-14[14]*	2.57E-16[14] *1.00E-15[14]*	50		2.33E+03[9]	845[9]	3.1[9]
ST BEES SANDSTONE FAULT MATERIAL		7.91E-15[14] *1.90E-13[14]*	2.28E-15[14] *1.08E-13[14]*	10				
BROCKRAM BRECCIA UNDIFFERENTIATED	0.030[1]	4.74E-18[14] *5.71E-17[14]*		50	1.02E-08[12]	2.63E+03[9]	1133[9]	2.5[9]
BROCKRAM BRECCIA FAULT MATERIAL		7.73E-17[14] *2.50E-14[14]*	1.26E-15[14] *9.22E-14[14]*	10				
ST BEES SHALES AND EVAPORITES UNDIFFERENTIATED	0.037[1]	3.66E-17[14] *2.96E-15[14]*		50	1.00E-08[12,13]	2.76E+03[9]	845[9]	3.1[9]
ST BEES SHALES AND EVAPORITES FAULTED				10				
CARBONIFERER OUS LIMESTONE UNDIFFERENTIATED	0.013[1]	4.65E-16[14] *2.27E-14[14]*		50	1.02E-08[12]	2.17E+03[9]	1133[93]	2.7[9]
CARBONIFERER OUS LIMESTONE FAULT MATERIAL		1.00E-14[14] *2.64E-12[14]*		10				
FLEMING HALL (BVG) UNDIFFERENTIATED	0.011[1]	5.67E-18[14] *3.50E-17[14]*		50	3.35E-10[10]	2.69E+03[4]	729[6]	2.51[6]
FLEMING HALL (BVG) FAULT MATERIAL		4.54E-18[14] *1.20E-16[14]*		10	1.00E-09[10]	2.67E+03[5]		

BLEAWATH (BVG) UNDIFFERENTIATED		2.47E-18[14] *9.86E-18*[14]	50	3.35E-10[10]	2.71E+03[9]	885[6]	2.58[6]
BLEAWATH (BVG) FAULT MATERIAL		1.75E-18[14] *1.20E-15*[14]	10	1.00E-09[10]			
MOORSIDE (BVG) UNDIFFERENTIATED		3.91E-18[14] *3.62E-17*[14]	50	3.35E-10[10]		971[6]	2.43[6]
MOORSIDE (BVG) FAULT MATERIAL		1.75E-18[14] *1.20E-15*[14]	10	1.00E-09[10]			
BORROWDALE VOLCANIC GROUP UNDIFFERENTIATED		5.76E-18[14] *3.54E-17*[14]	50	3.35E-10[10]		843[9]	2.5[9]
BORROWDALE VOLCANIC GROUP FAULT MATERIAL		1.75E-18[14] *1.20E-15*[14]	10	1.00E-09[10]			
REPOSITORY	*Values assigned same as Fleming Hall Undifferentiated*						

[1](Nirex 1997b) Table 3.2. [2] (Best 2002) Figure 9.1. [3](Nirex 1989b) Figure 8.2. [4](Davies & Chaplow 1998) Table 4. [5](Davies & Chaplow 1998) Table 2. [6](Nirex 1989b) Table 3.1. [7](Eppelbaum et al. 2014) Table 2.9. [8](Domenico & Schwartz 1997) Table 9.4. [9](Nirex 1989b) Figure 8.1. [10](Batu 1998) Table 2-14. [11](Allen et al. 1997) Table 7.7.5. [12](McKeown et al. 1999) Table 1. [13](Jones et al. 2000) Table 7.5. [14](Nirex 1997b) Table 5.2.

C.2: Sellafield Model Run Log

Table C.0.2: Summary table of Sellafield model run log and initial conditions.

Step Number	Processes	Initial Conditions	Iterations	Time step length	Reloads
		(Starting elevation (m relative to sea level), starting value, gradient of value)	*count*	*years*	*count*
1	H	H onshore: 100 m, 100156 pa, 10055 pa H offshore: -35 m, 453259 pa, 10055 pa	10	1	1
2	C	Generated using python script (available in Appendix C.4.1<inputs<THC<Mass_IC_setter), which weighted mass concentration values linearly across the model domain based on distance from known values. Known mass values obtained from BH2, 3, 4, 9A/B & 10 (Bath et al. 2006). Mass concentration values also used in calibration (section 4.4), across the model domain			
3	THC *(reload)*	H: reloaded from output of step 1 T onshore: 0 m, 8.5 ºC, 0.025 ºC T offshore: -35 m, 8.5 ºC, 0.025 ºC C: reloaded from output of step 2	300	100	1
4	THC *(quasi-steadystate)*	H: reloaded from output of step 3	200	100	1

		T: reloaded from output of step 3 C: reloaded from output of step 3			
5	THC *(repository temperature generation)*	H: reloaded from output of step 4 T: reloaded from output of step 4 C: reloaded from output of step 4	10,000	1, 3, 10, 30, 100 and every 100 thereafter for 1st reload. 100 year basic timestep for the 2nd to 5th reloads.	5

C.3: Sellafield Calibration

C.3.1: Freshwater Head Equation

Equ.C.1 was obtained from (Nirex 1997a) where h_f is freshwater head (m), P is pressure (Pa), P_A is atmospheric pressure (Pa), ρ_f is the density of freshwater (kg/m^3), g is the gravity (m/s^2) and z is elevation (m aOD).

$$h_f = \frac{P - P_A}{\rho_f g} + z \qquad (C.1)$$

C.3.2: Mass Concentration Equation

Equ.C.2 was used for mass concentration calibration where C is the concentration (mg/L), C_m is the mass concentration (kg/m^3), and ρ_f is the density of freshwater (kg/m^3).

$$C = \left(C_m - \rho_f\right) \times 1000 \qquad (C.2)$$

C.3.3: Mass, Temperature & Pressure Calibration Spreadsheet

Provided within the electronic appendix for:

- Most likely permeability steadystate calibration.xlsx
- High permeability steadystate calibration.xlsx

C.4: Sellafield OpenGeoSys Model Input & Output Files

C.4.1: Most-Likely Permeability Model Input & Output Files

Provided within the electronic appendix.

- Inputs [Folder]
  Input files of model runs for 1) Hydraulics only [Folder], 2) THC [Folder] and 3) the temperature curves as a result of radiogenic heat emission [Folder]
- Outputs [Folder]
  Output files of model runs for 1) Hydraulics only [Folder], 2) THC [Folder] and 3) the temperature curves as a result of radiogenic heat emission [Folder]

C.4.2: High Permeability Model Input & Output Files

Provided within the electronic appendix.

- Inputs [Folder]
  Input files of model runs for 1) Hydraulics only [Folder], 2) THC [Folder] and 3) the temperature curves as a result of radiogenic heat emission [Folder]
- Outputs [Folder]
  Output files of model runs for 1) Hydraulics only [Folder], 2) THC [Folder] and 3) the temperature curves as a result of radiogenic heat emission [Folder]

C.4.3: Input Spreadsheets

Provided within the electronic appendix.

- BC_IC.xlsx
  Used to calculate boundary conditions and initial conditions
- Permeability.xlsx
  Used to calculate permeability values
- Mass concentration used within Mass Setter.xlsx
  Used to develop mass concentration initial conditions

C.5: Sellafield OpenGeoSys Workings for Reporting

C.5.1: Most-Likely Permeability Workings

Provided within the electronic appendix.

- Advection_Diffusion_Calc [Folder]
  Used to calculate the percentage of the far-field domain that has a 'slow' advective groundwater velocity.
- Radiogenic_heat_emission [Folder]
  Used to determine the area and degree to which groundwater velocity is affected by radiogenic heat emission, including the increase in radionuclide travel distance as a result of heat emission.
- Streaklines_Calc [Folder]
  Used to determine the particle travel distance under baseline (no heat generation) conditions

C.5.2: High Permeability Workings

Provided within the electronic appendix.

- Advection_Diffusion_Calc [Folder]
  Used to calculate the percentage of the far-field domain that has a 'slow' advective groundwater velocity
- Radiogenic_heat_emission [Folder]
  Used to determine the area and degree to which groundwater velocity is affected by radiogenic heat emission, including the increase in radionuclide travel distance as a result of heat emission.
- Streaklines_Calc [Folder]
  Used to determine the particle travel distance under baseline (no heat generation) conditions

Appendix D

Full Tynwald Basin model input and output scripts are provided electronically within Appendix D.0.

D.1: Tynwald Basin Model Material Property Inputs

Table D.0.1: Summary of material group data input for the Tynwald Basin Model.

Model Component	MMP	MMP	MMP	MMP	MMP	MMP	MSP	MSP	MSP
Formation	POROSITY	PERMEABILITY (X-direction) (most-likely & *high*)	PERMEABILITY (Z-direction) (most-likely & *high*)	MASS DISPERSION (Isotropic)	HEAT DISPERSION (Isotropic)	STORATIVITY	DENSITY	THERMAL CAPACITY	THERMAL CONDUCTIVITY
Units	*decimal*	m^2	m^2	*m*	*m*	Pa^{-1}	Kg/m^3	*J/kg/K*	*W/m/K*
QUATERNARY UNDIFFERENTIATED	0.175[1]	1.42E-14[18] *1.41E-13*[18]	1.06E-15[18] *3.96E-15*[18]	50		1.00E-07[14]	2.09E+03[3]	845[3]	3.1[3]
ELSWICK MUDSTONE UNDIFFERENTIATED	0.091[10]	4.40E-18[10] *1.51E-17*[10]	2.57E-18[10] *7.73E-18*[10]	50		1.00E-06[15]	2.76E+03[9]	845[9]	2.51[6]
ELSWICK MUDSTONE FAULTED				10					
WORTON HALITE UNDIFFERENTIATED	0.006[12]	1.00E-18*** *1.00E-17*		50		1.02E-10[16]			2.07[6]
WORTON HALITE FAULTED				10					
DOWBRIDGE MUDSTONE UNDIFFERENTIATED	0.091[10]	4.40E-18[10] *1.51E-17*[10]	2.57E-18[10] *7.73E-18*[10]	50		1.00E-06[15]			2.51[6]
DOWBRIDGE MUDSTONE FAULTED				10					

PREESALL HALITE UNDIFFERENTIATED	0.006[12]	1.00E-18*** *1.00E-17*	50	1.02E-10[16]			2.07[6]
PREESALL HALITE FAULTED			10				
CLEVELEY MUDSTONE UNDIFFERENTIATED	0.074[13]	1.00E-18*** *1.00E-17*	50	1.00E-08[15,16]			2.29[6]
CLEVELEY MUDSTONE FAULTED			10				
MYTHOP HALITE UNDIFFERENTIATED	0.074[13]	1.00E-18*** *1.00E-17*	50	1.00E-08[15,16]			2.29[6]
MYTHOP HALITE FAULTED			10				
BLACKPOOL MUDSTONE UNDIFFERENTIATED	0.091[10]	4.40E-18[10] *1.51E-17[10]*	2.57E-18[10] *7.73E-18[10]*	50	1.00E-06[15]		2.51[6]
BLACKPOOL MUDSTONE FAULTED				10			
ROSSALL HALITE UNDIFFERENTIATED	0.074[13]	1.00E-18*** *1.00E-17*	50	1.00E-08[15,16]			2.29[6]
ROSSALL HALITE FAULTED			10				
ANSDELL MUDSTONE UNDIFFERENTIATED	0.091[10]	4.40E-18[10] *1.51E-17[10]*	2.57E-18[10] *7.73E-18[10]*	50	1.00E-06[15]		2.51[6]
ANSDELL MUDSTONE FAULTED				10			
FLYDE HALITE UNDIFFERENTIATED	0.074[13]	1.00E-18*** *1.00E-17*	50	1.00E-08[15,16]			2.29[6]
FLYDE HALITE FAULTED			10				

ORMSKIRK AND CALDER SANDSTONE UNDIFFERENTIATED	0.201[1]	1.08E-14[18] *6.55E-13*[18]	2.74E-15[18] *2.07E-13*[18]	50	1.73E-08[17]	2.09E+03[9]	845[9]	3.3[9]
ORMSKIRK AND CALDER SANDSTONE FAULTED		2.52E-15[18] *4.36E-12*[18]	4.20E-15[18] *1.85E-12*[18]	10				
ST BEES SANDSTONE UNDIFFERENTIATED	0.095[1]	1.13E-15[18] *1.27E-14*[18]	2.57E-16[18] *1.00E-15*[18]	50		2.33E+03[9]	845[9]	3.1[9]
ST BEES SANDSTONE FAULT MATERIAL		7.91E-15[18] *1.90E-13*[18]	2.28E-15[18] *1.08E-13*[18]	10				
PERMIAN UNDIFFERENTIATED	0.037[1]	3.66E-17[18] *2.96E-15*[18]		50	1.00E-08[15,16]	2.76E+03[9]	845[9]	3.1[9]
PERMIAN FAULTED				10				
WESTPHALIAN COAL MEASURE UNDIFFERENTIATED	0.1[11]	1.7E-16[11] *1.7E-15*[11]	1.7E-17[11] *1.7E-16*[11]	50	3.50E-09[11]	2.17E+03[9]	1133[9]	2.7[9]
WESTPHALIAN COAL MEASURE FAULTED		1.7E-15 *1.7E-14*****	1.7E-16 *1.7E-15*****	10				
NAMURIAN UNDIFFERENTIATED	0.03[11]	6.00E-15[11] *6.00E-14*[11]	6.00E-16[11] *6.00E-15*[11]	50	1.02E-08[11]			
NAMURIAN FAULTED		6.00E-14 *6.00E-13*****	6.00E-15 *6.00E-14*****	10				
DINANTIAN LIMESTONE UNDIFFERENTIATED	0.013[1]	4.65E-16[18] *2.27E-14*[18]		50	1.02E-08[16]			
DINANTIAN LIMESTONE FAULTED		1.00E-14[18] *2.64E-12*[18]		10				
BORROWDALE VOLCANIC GROUP UNDIFFERENTIATED	0.011[1]	5.76E-18[18] *3.54E-17*[18]		50	3.35E-10[14]	2.71E+03[9]	843[9]	2.5[9]
BORROWDALE VOLCANIC GROUP FAULT MATERIAL		1.75E-18[18] *1.20E-15*[18]		10	1.00E-09[14]			

REPOSITORY	*Values assigned same as Mythop Halite*

[1](Nirex 1997b) Table 3.2. [2] (Best 2002) Figure 9.1. [3](Nirex 1989b) Figure 8.2. [4](Davies & Chaplow 1998) Table 4. [5](Davies & Chaplow 1998) Table 2. [6](Nirex 1989b) Table 3.1. [7](Eppelbaum et al. 2014) Table 2.9. [8](Domenico & Schwartz 1997) Table 9.4. [9](Nirex 1989b) Figure 8.1. [10](Armitage et al. 2015) Table 1. [11](Cai & Ofterdinger 2014) Table 1. [12](Cosenza et al. 1999) Pg.510. [13](Liu et al. 2015) Table 2. [14](Batu 1998) Table 2-14. [15](Jones et al. 2000) Table 7.5. [16](McKeown et al. 1999) Table 1. [17](Jones et al. 2000) Table 7.7.5. [18](Nirex 1997b) Table 5.2.

** High permeability (m^2) values calculated from [84](Nirex 1997b) Table 5.2 using Equ.B.3, and a probability of 0.95.

*** An intrinsic permeability of $2.00E^{-21}$ m^2 has been reported for the Phenoblastic Salt in the Amelie Mine (Cosenza et al. 1999), $1.00E^{-21}$ m^2 for undisturbed rock salt at the Waste Isolation Plant, New Mexico (Stormont 1997) and between $1.00E^{-20}$ and $1.00E^{-22}$ m^2 for permeability to brine (Cosenza et al. 1999). However, permeabilities is for these clean halite units will be capped at 1.00E-18 m^2 to enable numerical stability for the *'most-likely'* model, and will be simply be raised by one order of magnitude for the *'high permeability'* model, which also accounts for possible salt dissolution.

**** As no high permeability values are available for the Westphallain Coal Measures Faulted the Namurian Faulted, the most likely permeability has been raised by one order of magnitude to obtain a high permeability.

D.2: Tynwald Basin Model Run Log

Table D.0.2: Summary table of Tynwald Basin model run log and initial conditions.

Step Number	**Processes**	**Initial Conditions**	**Iterations**	**Time step length**	**Reloads**
		(Starting elevation (m relative to sea level), starting value, gradient of value)	*count*	*years*	*count*
1	H	H: -25 m, 352,706 pa, 11,221 pa	10	1	1
2	HC *(reload)*	H: reloaded from output of step 1 C Quaternary: -25 m, 1019.4 kg/m^3, 2.0 kg/m^3 C Mercia Mudstone: -100 m, 1200 kg/m^3, 0 kg/m^3 C Remainder: -200 m, 1174 kg/m^3, 0 kg/m^3	1	1	1
3	C (altered)	Mass distribution obtained from step 2, and then corrected using a python script (available in Appendix D.5.1<inputs<THC<EISB10_IC) which weighted mass concentration values linearly across a small area of the model domain, based on distance from known values. This was done in order to simulate an area of freshwater. Mass density values along the lake district boundary fault were based on BH10 from Sellafield, justified as both have the Ormskirk/Calder Sandstone outcropping at the surface.			
4	THC *(reload)*	H: reloaded from output of step 1 T onshore: -1 m, 8.5 ºC, 0.025 ºC T offshore: -30 m, 8.5 ºC, 0.025 ºC	1	1	1

		C: reload from output of step 3			
5	THC *(quasi-steadystate)*	H: reloaded from output of step 4 T: reloaded from output of step 4 C: reloaded from output of step 4	10	100	1
4	THC *(repository temperature generation)*	H: reloaded from output of step 5 T: reloaded from output of step 5 C: reloaded from output of step 5	10,000	1, 3, 10, 30, 100 and every 100 thereafter for 1st reload. 100 year basic timestep for the 2nd to 5th reloads.	5

D.3: Tynwald Basin Mass Concentration Boundary Calculation

An average mass concentration for the lower half of the southwest boundary condition, and the base of the northeastern mass concentration boundary, was calculated using data provided in Table D.0.3. This data was converted into Kg/m^3 Cl equivalent using Equ.D.1 & Equ.D.2. The upper half of the southwest boundary (next to the Mercia Mudstone Group) was assumed to be fully saturated with respect to salt to the presence of offshore bedded halites.

Table D.0.3: Summary of salinity measurements obtained from oil and gas wells within the Irish Sea Basin (Barnes et al. 2005; Yaliz & McKim 2003; Yaliz & Taylor 2003; Yaliz & Chapman 2003; Cowan & Boycott-Brown 2003; Bastin et al. 2003).

Field	**Depth to crest**	**Resource Type**	**Reservoir**	**Temperature**	**Salinity**	**Mass Concentration***
	m			Degrees Celcius	ppm (NaCl)	(Kg/m^3) (Cl equivalent)

Douglas	652	Oil	Ormskirk sandstone	30	270 000	1164
Hamilton	701	Gas	Ormskirk sandstone	30	300 000	1182
Hamiltion North Fields	792	Gas	Ormskirk sandstone	30	300 000	1182
Lennox	762	Oil & Gas	Ormskirk sandstone	30	280 000	1170
North Morecambe	899	Gas	Ormskirk and St Bees sandstone	33	270 000	1164
South Morecambe	671	Gas	Ormskirk and St Bees sandstone	33	300 000	1182

$$Cl_{ppm} = NaCl_{ppm} \times \frac{Molar\ Mass\ of\ Cl}{Molar\ Mass\ of\ NaCl} \quad (D.1)$$

$$Cl_{\frac{kg}{m3}} = \left(\frac{Cl_{ppm}}{1000}\right) + 1000 \quad (D.2)$$

D.4: Tynwald Basin OpenGeoSys Model Input & Output Files

D.4.1: Most-Likely Permeability Model Input & Output Files

Provided within the electronic appendix.

- Inputs [Folder]
  Input files of model runs for 1) Hydraulics only [Folder], 2) THC [Folder] and 3) the temperature curves as a result of radiogenic heat emission [Folder]
- Outputs [Folder]
  Output files of model runs for 1) Hydraulics only [Folder], 2) THC [Folder] and 3) the temperature curves as a result of radiogenic heat emission [Folder]

D.4.2: High Permeability Model Input & Output Files

Provided within the electronic appendix.

- Inputs [Folder]

Input files of model runs for 1) Hydraulics only [Folder], 2) THC [Folder] and 3) the temperature curves as a result of radiogenic heat emission [Folder]

- Outputs [Folder]
  Output files of model runs for 1) Hydraulics only [Folder], 2) THC [Folder] and 3) the temperature curves as a result of radiogenic heat emission [Folder]

D.4.3: Input Spreadsheets

Provided within the electronic appendix.

- BC_IC.xlsx
  Used to calculate boundary conditions and initial conditions
- Mass concentration used within mass setter.xlsx
  Used to develop mass concentration initial conditions

D.5: Tynwald Basin OpenGeoSys Workings for Reporting

D.5.1: Most-Likely Permeability Workings

Provided within the electronic appendix.

- Advection_Diffusion_Calc [Folder]
  Used to calculate the percentage of the far-field domain that has a 'slow' advective groundwater velocity.
- Radiogenic_heat_emission [Folder]
  Used to determine the area and degree to which groundwater velocity is affected by radiogenic heat emission, including the increase in radionuclide travel distance as a result of heat emission.
- Streaklines_Calc [Folder]
  Used to determine the particle travel distance under baseline (no heat generation) conditions

D.5.2: High Permeability Workings

Provided within the electronic appendix.

- Advection_Diffusion_Calc [Folder]
  Used to calculate the percentage of the far-field domain that has a 'slow' advective groundwater velocity.
- Radiogenic_heat_emission [Folder]
  Used to determine the area and degree to which groundwater velocity is affected by radiogenic heat emission, including the increase in radionuclide travel distance as a result of heat emission.
- Streaklines_Calc [Folder]
  Used to determine the particle travel distance under baseline (no heat generation) conditions.

Appendix E

Full Thetford model input and output scripts are provided electronically within Appendix E.0.

E.1: Thetford Model Material Property Inputs

Table E.0.1: Summary of material group data input for the Thetford Model.

Model Component		MMP	MMP	MMP	MMP	MMP	MMP	MSP	MSP	MSP
Formation	Age	POROSITY	PERMEABILITY (X-direction) (most-likely & *high*)	PERMEABILITY (Z-direction) (most-likely & *high*)	MASS DISPERSION (Isotropic)	HEAT DISPERSION (Isotropic)	STORATIVITY	DENSITY	THERMAL CAPACITY	THERMAL CONDUCTIVITY
Units		*decimal*	*m^2*	*m^2*	*m*	*m*	*Pa^{-1}*	*Kg/m^3*	*J/kg/K*	*W/m/K*
LOWESTOFT GLACIAL TILL	Quaternary	0.18[9]	1.00E-16[2] *2.00E-13[2]*		10	10	1.00E-07[14]	1.99E+03[8]	845[7]	3.10[7]
CHALK	Cretaceous	0.01[5]	1.00E-16[6] *1.00E-15[6]*	5.00E-17[6] *5.00E-16[6]*	10	10	1.00E-09[15]	1.72E+03[10]	959[11]	1.79[4]
ANCHOLME GROUP & GAULT CLAY	Jurassic	0.04[5]	5.70E-16 *6.78E-14* See Table E.0.4	1.21E-18 *2.40E-16* See Table E.0.4	10	10	4.00E-08[16]	2.56E+03[11]	838[11]	1.82[4]

GREAT & INFERIOR OOLITE	Jurassic	0.15[13]	1.00E-15[6] *1.00E-14*[6]	5.00E-16[6] *5.00E-15*[6]	10	10	1.00E-07[17]	2.71E+03[11]	851[11]	3.50[4]
LIAS GROUP & MERCIA MUDSTONE-PENARTH GROUP	Jurassic, Triassic, Permian	0.0275[5]	1.66E-17 *3.59E-16* See Table E.0.3	1.07E-18 *2.12E-16* See Table E.0.3	10	10	1.00E-06[18]	2.21E+03[3,12]	845[3]	2.04[4]
UPPER CALEDONIDE BASEMENT	Silurian	5.00E-05[5] (0.01 used for R_f calc.)*	8.00E-16[2] *1.00E-14*[2]		50	50	1.00E-09[14]	2.71E+03[3]	843[3]	3.40[4]
LOWER CALEDONIDE BASEMENT		5.00E-06[5]	1.00E-18[2] *2.00E-17*[2]				3.55E-10[14]			
RESPOSITORY	*Values assigned same as Upper Caledonide Basement*									

[1](Meybeck et al. 1989) Table 1.5. [2](Domenico & Schwartz 1997) Table 3.2. [3](Nirex 1989b) Figure 8.1. [4](Banks et al. 2013) Table 3. [5](Domenico & Schwartz 1997) Table 2.2. [6](Domenico & Schwartz 1997) Table 3.4. [7](Nirex 1989b) Figure 8.2. [8](Hiscock & Tabatabai Najafi 2011) Table 3. [9](Nirex 1997b) Table 3.2. [10](Allen et al. 1997) Table 4.1.4. [11](Eppelbaum et al. 2014) Table 2.7. [12](Hobbs et al. 2012) p.g.105. [13](Allen et al. 1997). [14](Batu 1998) Table 2-14. [15](Allen et al. 1997) Table 4.1.6 & Table 4.1.7. [16](Jones et al. 2000) Table 5.8. [17](Allen et al. 1997) Table 6.1.2. [18](Jones et al. 2000) Table 6.3 & Table 7.5.

* Porosity of 0.01 used for the retardation calculation for the Upper Caledonide Basement as solute transportation would be via a fracture, not through the matrix. Therefore a higher porosity is required.

E.2: Thetford Model Run Log

Table E.0.2: Summary table of Thetford model run log and initial conditions.

Step Number	**Processes**	**Initial Conditions**	**Iterations**	**Time step length**	**Reloads**
		(Starting elevation (m relative to sea level), starting value, gradient of value)	*count*	*years*	*count*
1	H	H: 41.31 m, 100830 pa, 9810 pa	10	1	1
2	THC *(reload)*	H: reloaded from output of step 1 T: 41.31 m, 9.78 ºC, 0.025 ºC C: 41.31m, 1000 kg/m^3, 0.009407976 kg/m^3	1	1	1
3	THC *(quasi-steadystate)*	H: reloaded from output of step 2 T: reloaded from output of step 2 C: reloaded from output of step 2	10	100	20
4	THC *(repository temperature generation)*	H: reloaded from output of step 3 T: reloaded from output of step 3 C: reloaded from output of step 3	10,000	1, 3, 10, 30, 100 and every 100 thereafter for 1st reload. 100 year basic timestep for the 2nd to 5th reloads.	5

E.3: Thetford Model Combined Lithological Permeability Calculation

The average horizontal (k_x) and vertical (k_z) permeability of combined hydrogeological units has been calculated using Equ.E.1 & Equ.E.2 (Lee & Fetter 1994), where *k* is the hydraulic conductivity (m/s) and *b* is the thickness (m). These equations assume homogeneous and isotropic units.

$$K_x = \frac{1}{b}\sum_{i=1}^{n} k_i b_i \qquad (E.1)$$

$$K_z = \frac{b}{\sum_{i=1}^{n} \frac{b_i}{k_i}} \qquad (E.2)$$

The results were then converted from m/s to m^2 using Equ.E.3 where *k* is the intrinsic permeability in m^2, K is the hydraulic conductivity in m/s, μ is the dynamic viscosity and is assumed to be 0.001 N/ms as per fresh water, ρ is the density and is assumed to be 1000 kg/m^3 as per fresh water, and g is the acceleration due to gravity and is assumed to be 10 m/s^2.

$$k = \left(\frac{\mu}{\rho g}\right) K \qquad (E.3)$$

Table E.0.3: Inputs for use in the Mercia Mudstone-Penarth Group & Lias Group permeability calculation.

Formation	Interpreted Primary Lithology	Thickness	Hydraulic Conductivity (most-likely)	Hydraulic Conductivity (conservative)
Units		m	*m/s*	*m/s*
Whitby Mudstone	Mudstone	20	1.00E-11[1]	2.00E-09[1]
Marlstone Formation	Ironstone	3	5.00E-09[3]	5.00E-08[3]
Dyrham Formation	Siltstone	5	1.00E-09[2]	1.40E-08[2]
Charlmouth Mudstone	Mudstone	50	1.00E-11[1]	2.00E-09[1]
Mercia mudstone - Penarth Group	Mudstone	50	1.00E-11[1]	2.00E-09[1]

Permeability values were obtained from (Domenico & Schwartz 1997) where [1] is a typical value taken from unweather marine clay and shale from Table 3.2, [2] is a typical value taken from siltstone from Table 3.2, and [3] is a typical value taken from limestone, dolomite vertical conductivity from Table 3.4.

Table E.0.4: Inputs for use in the Ancholme Group & Gault Clay permeability calculation.

Formation	Interpreted Primary Lithology	Thickness	Hydraulic Conductivity (most-likely)	Hydraulic Conductivity (conservative)
Units		m	*m/s*	*m/s*
Gault	Clay	15	1.00E-11[2]	2.00E-09[2]
Carstone	Sandstone	10	5.00E-08[3]	6.00E-06[3]
Sandringham Sands Formation (Runcton & Roxham Member)	Sandstone	6	5.00E-08[3]	6.00E-06[3]
Kimmerage Clay Formation	Mudstone	50	1.00E-11[1]	2.00E-09[1]
Amphill Clay Formation	Mudstone	25	1.00E-11[1]	2.00E-09[1]
West Walton Formation	Siltstone	10	1.00E-09[4]	1.40E-08[4]
Oxford Clay Formation	Mudstone	40	1.00E-11[1]	2.00E-09[1]
Kellaways Formation - Sandstone	Sandstone	2	5.00E-08[3]	6.00E-06[3]
Kellaways Formation - Mudstone	Mudstone	2	1.00E-11[1]	2.00E-09[1]

Permeability values were obtained from (Domenico & Schwartz 1997) where [1] is a typical value taken from unweather marine clay and shale from Table 3.2, [2] is a typical value taken from unweather marine clay from Table 3.2, [3] is a typical value taken for sandstone from Table 3.2, and [4] is a typical value taken from siltstone from Table 3.2.

E.4: Thetford OpenGeoSys Model Input & Output Files

E.4.1: Most-Likely Permeability Model Input & Output Files

Provided within the electronic appendix.

- Inputs [Folder]
  Input files of model runs for 1) Hydraulics only [Folder], 2) THC [Folder] and 3) the temperature curves as a result of radiogenic heat emission [Folder]
- Outputs [Folder]
  Output files of model runs for 1) Hydraulics only [Folder], 2) THC [Folder] and 3) the temperature curves as a result of radiogenic heat emission [Folder]

E.4.2: High Permeability Model Input & Output Files

Provided within the electronic appendix.

- Inputs [Folder]

Input files of model runs for 1) Hydraulics only [Folder], 2) THC [Folder] and 3) the temperature curves as a result of radiogenic heat emission [Folder]

- Outputs [Folder]
  Output files of model runs for 1) Hydraulics only [Folder], 2) THC [Folder] and 3) the temperature curves as a result of radiogenic heat emission [Folder]

E.4.3: Input Spreadsheets

Provided within the electronic appendix.

- BC_IC_K.xlsx
  Used to calculate boundary conditions, initial conditions and the permeability of mixed lithology hydrogeological units

E.5: Thetford OpenGeoSys Workings for Reporting

E.5.1: Most-Likely Permeability Workings

Provided within the electronic appendix.

- Advection_Diffusion_Calc [Folder]
  Used to calculate the percentage of the far-field domain that has a 'slow' advective groundwater velocity.
- Radiogenic_heat_emission [Folder]
  Used to determine the area and degree to which groundwater velocity is affected by radiogenic heat emission, including the increase in radionuclide travel distance as a result of heat emission.
- Streaklines_Calc [Folder]
  Used to determine the particle travel distance under baseline (no heat generation) conditions

E.5.2: High Permeability Workings

Provided within the electronic appendix.

- Advection_Diffusion_Calc [Folder]
  Used to calculate the percentage of the far-field domain that has a 'slow' advective groundwater velocity.
- Radiogenic_heat_emission [Folder]
  Used to determine the area and degree to which groundwater velocity is affected by radiogenic heat emission, including the increase in radionuclide travel distance as a result of heat emission.
- Streaklines_Calc [Folder]
  Used to determine the particle travel distance under baseline (no heat generation) conditions.

Appendix F

Reactive C (GoldSim) model results summary and files. Reactive C models were used to validate the radionuclide retardation calaculations.

F.1: Sellafield GoldSim Model Output Files

F.1.1: Most Likely Permeability GoldSim Model Files

Provided within the electronic appendix. (Model and results summary provides within Figures F.0.1 & F.0.2).

F.1.2: High Permeability GoldSim Model Files

Provided within the electronic appendix. (Model and results summary provides within Figures F.0.3 & F.0.4).

F.2: Tynwald Basin GoldSim Model Output Files

F.2.1: Most Likely Permeability GoldSim Model Files

Provided within the electronic appendix. (Model and results summary provides within Figures F.0.5 & F.0.6).

F.2.2: High Permeability GoldSim Model Files

Provided within the electronic appendix. (Model and results summary provides within Figures F.0.7 & F.0.8).

F.3: Thetford GoldSim Model Output Files

F.3.1: Most Likely Permeability GoldSim Model Files

Provided within the electronic appendix. (Model and results summary provides within Figures F.0.9 & F.0.10).

F.3.2: High Permeability GoldSim Model Files

Provided within the electronic appendix. (Model and results summary provides within Figures F.0.11 & F.0.12 for pathway 1, and Figures F.0.13 & F.0.14 for pathway 2).

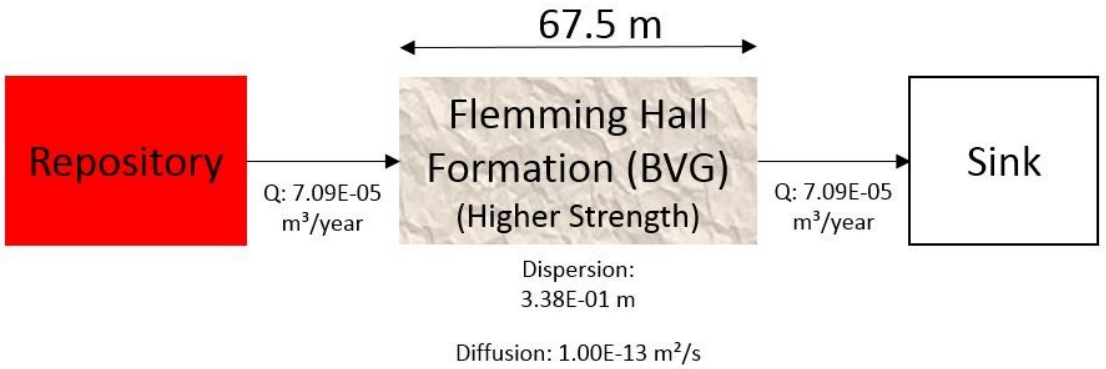

Figure F.0.1: Structure of GoldSim model based on the longest pathway (67.5 m) simulated for the Sellafield model with most-likely permeability values.

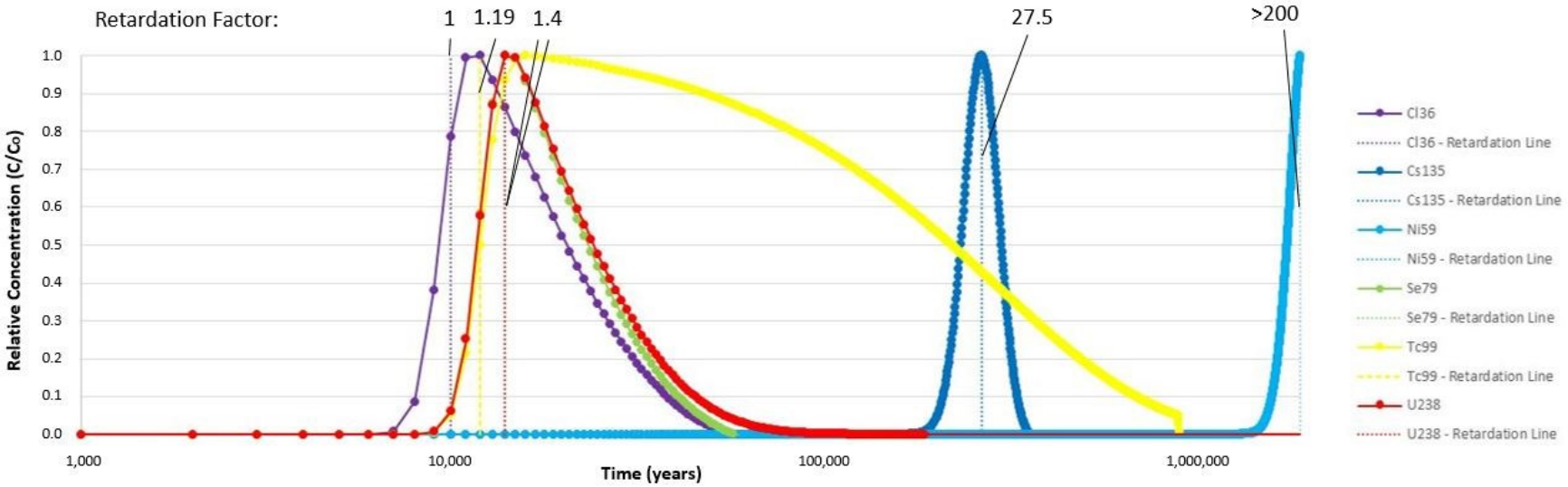

Figure F.0.2: Relative concentration radionuclide breakthrough curves and retardation factors (R_f) based on the maximum particle travel distance (streak-line) at Sellafield when run with most likely permeabilities (see Figure 4.14.C). No Am241, Eu152, or Sr90 was detected. Comparisons to the analytical solution are provided within electronic Appendix F.1.1.

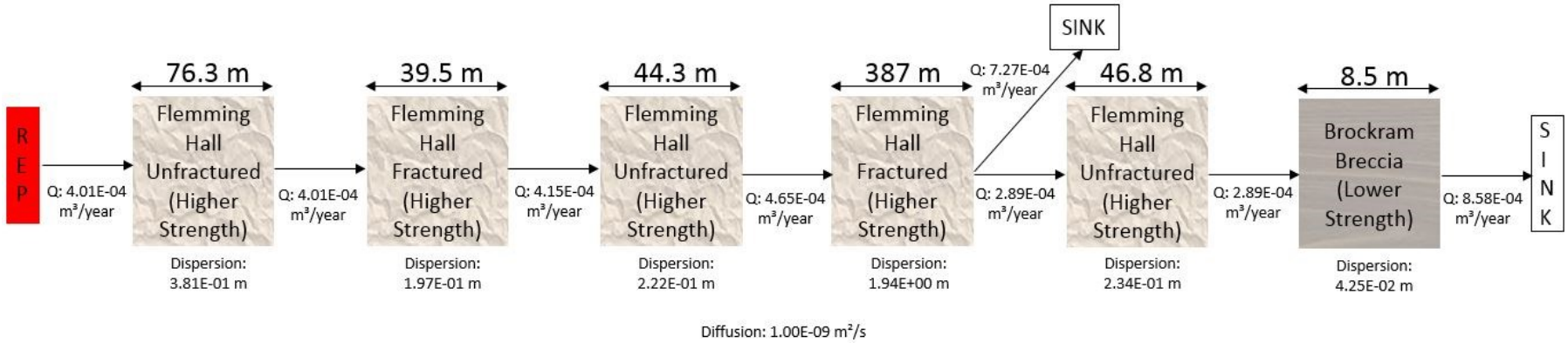

Figure F.0.3: Structure of GoldSim model based on the longest pathway (602 m) simulated for the Sellafield model with high permeability values.

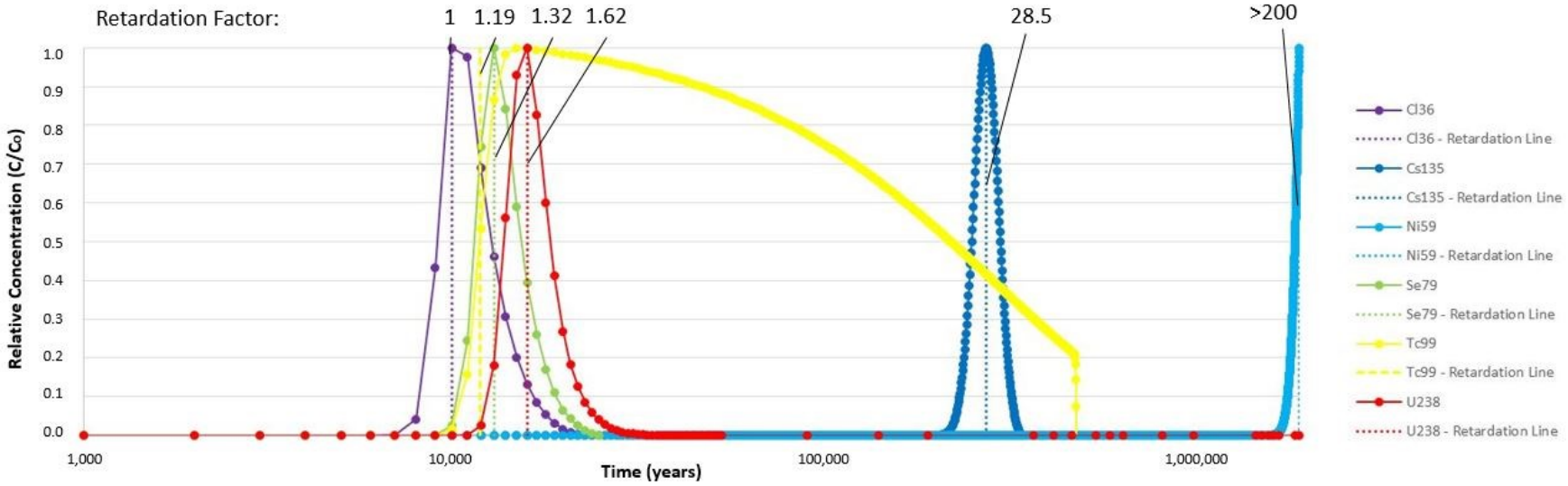

Figure F.0.4: Relative concentration radionuclide breakthrough curves and retardation factors (Rf) based on the maximum particle travel distance (streak-line) at Sellafield when run with high permeabilities (see Figure 4.15.C). No Am241, Eu152, or Sr90 was detected. Comparisons to the analytical solution are provided within electronic Appendix F.1.2

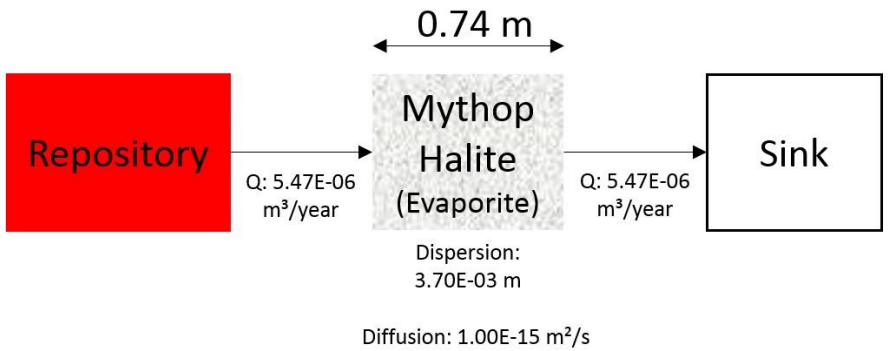

Figure F.0.5: Structure of GoldSim model based on the longest pathway (0.74 m) simulated for the Tynwald Basin model with most-likely permeability values.

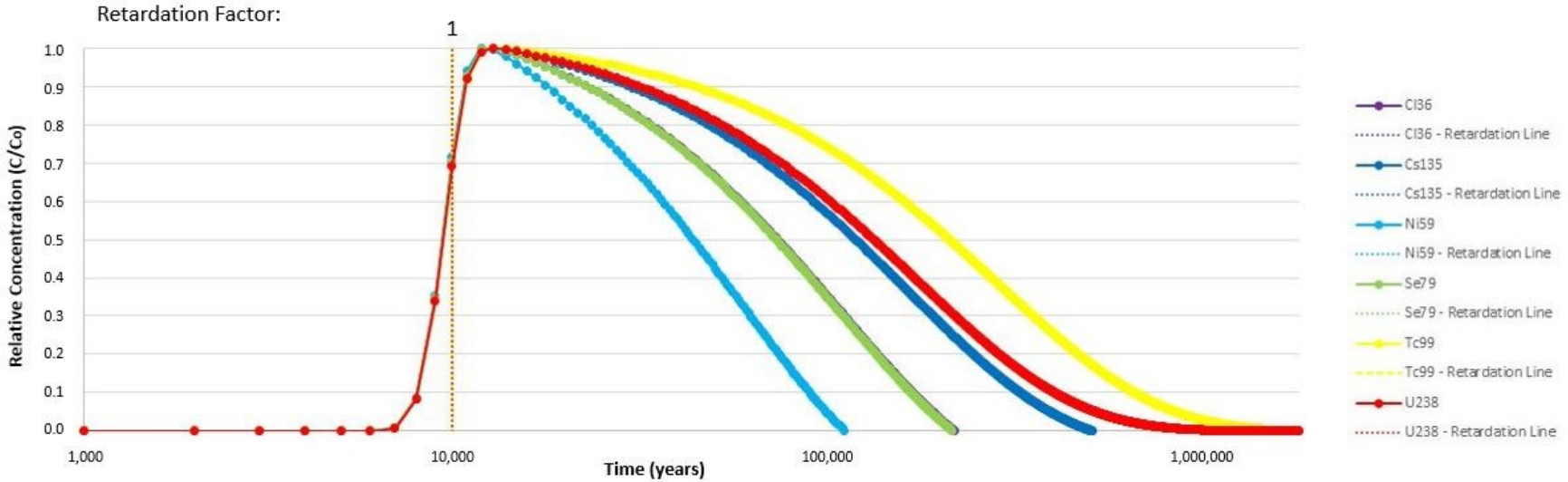

Figure F.0.6: Relative concentration radionuclide breakthrough curves and retardation factors (Rf) based on the maximum particle travel distance (streak-line) within the Tynwald Basin when run with most likely permeabilities (see Figure 4.14.C). No Eu152 or Sr90 was detected. Am241 was detected but decayed away rapidly making retardation determination difficult and as such has not been reported here. Comparisons to the analytical solution are provided within electronic Appendix F.2.1.

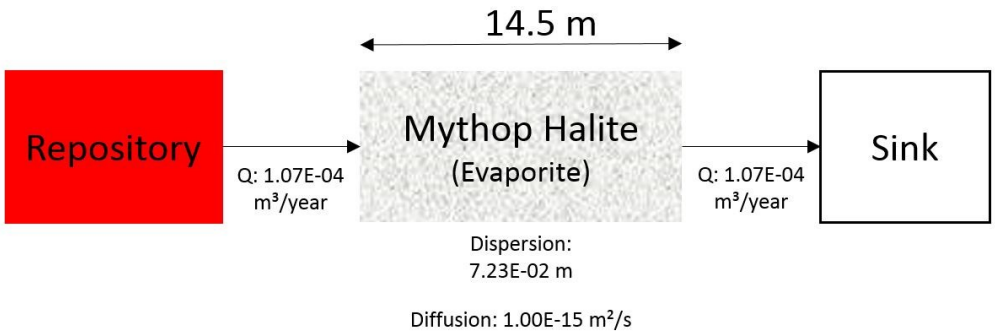

Figure F.0.7: Structure of GoldSim models based on the longest pathway (14.5 m) simulated for the Tynwald Basin model when populated with high permeability values.

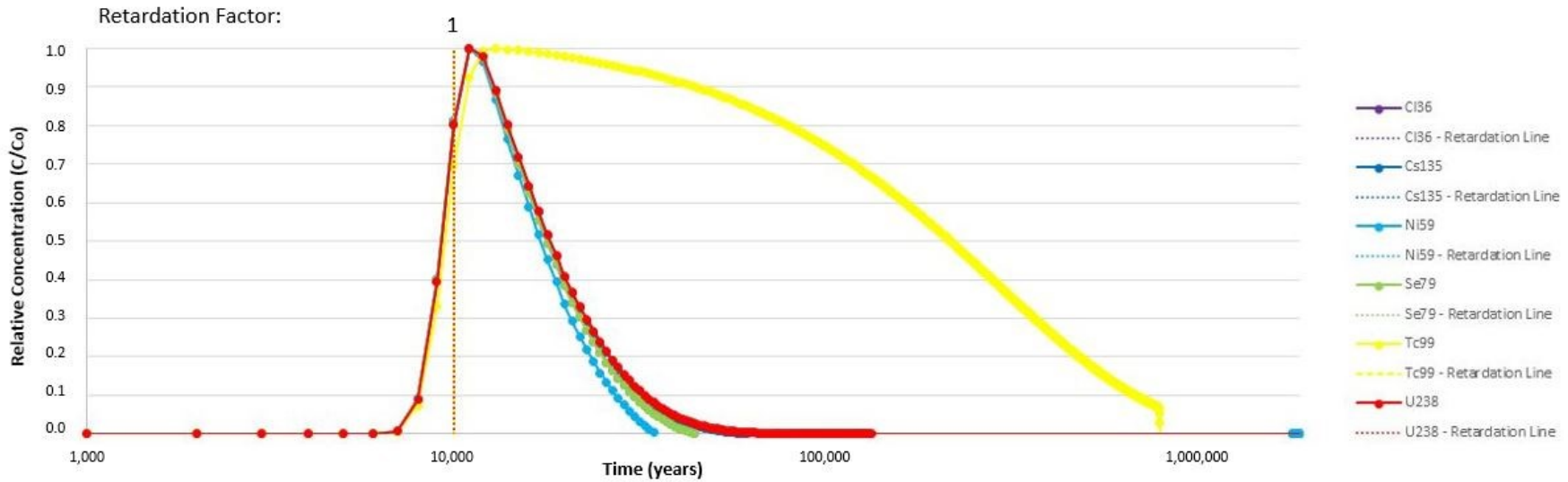

Figure F.0.8: Relative concentration radionuclide breakthrough curves and retardation factors (Rf) based on the maximum particle travel distance (streak-line) within the Tynwald Basin when run with high permeabilities (see Figure 4.15.C). No Eu152 or Sr90 was detected. Am241 was detected but decayed away rapidly making retardation determination difficult and as such has not been reported here. Comparisons to the analytical solution are provided within electronic Appendix F.2.2.

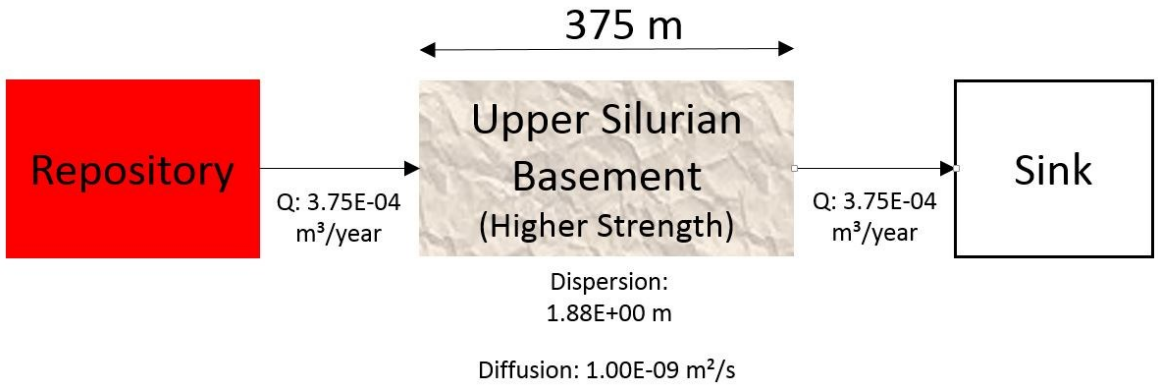

Figure F.0.9: Structure of GoldSim model based on the longest pathway (375 m) simulated for the Thetford model with most-likely permeability values.

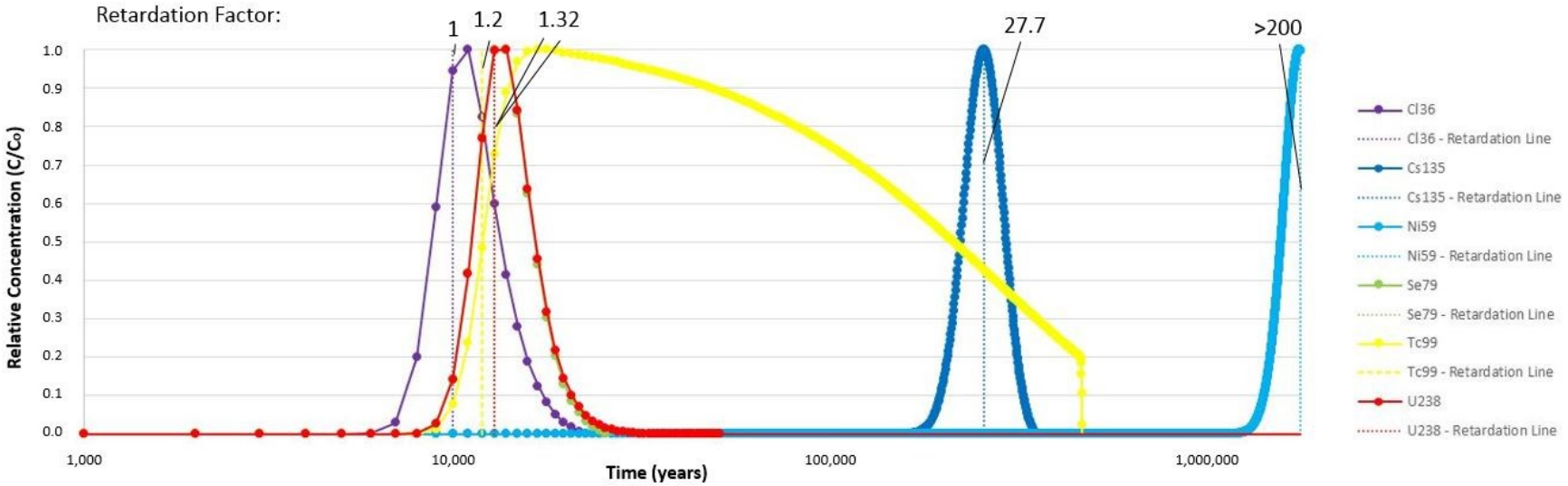

Figure F.0.10: Relative concentration radionuclide breakthrough curves and retardation factors (Rf) based on the maximum particle travel distance (streak-line) at Thetford when run with most likely permeabilities (see Figure 4.14.C). No Am241, Eu152, or Sr90 was detected. Comparisons to the analytical solution are provided within electronic Appendix F.3.1.

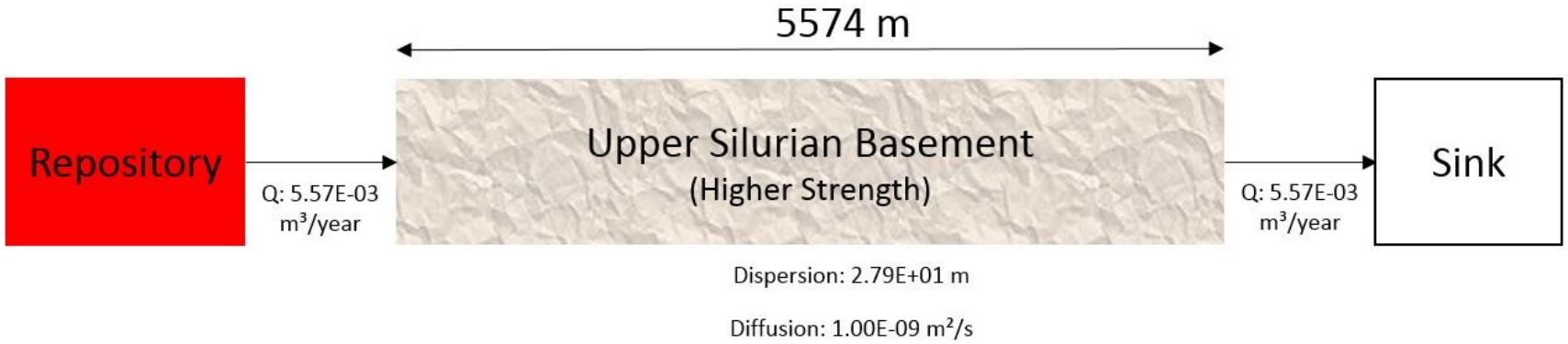

Figure F.0.11: Structure of GoldSim model based on the longest pathway (5574 m) simulated for Pathway 1 of the Thetford model with high permeability values.

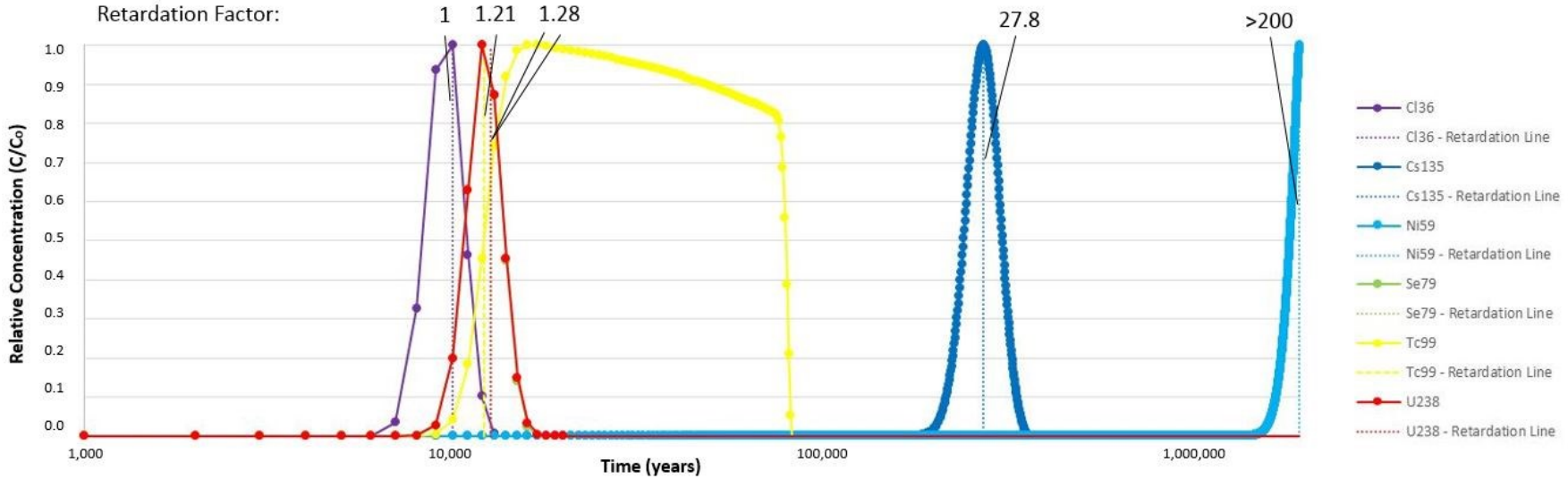

Figure F.0.12: Relative concentration radionuclide breakthrough curves and retardation factors (Rf) based on the maximum particle travel distance (streak-line) along pathway 1 at Thetford when run with high permeabilities (see Figure 4.15.C). No Am241, Eu152 or Sr90 was detected. Comparisons to the analytical solution are provided within electronic Appendix F.3.2.

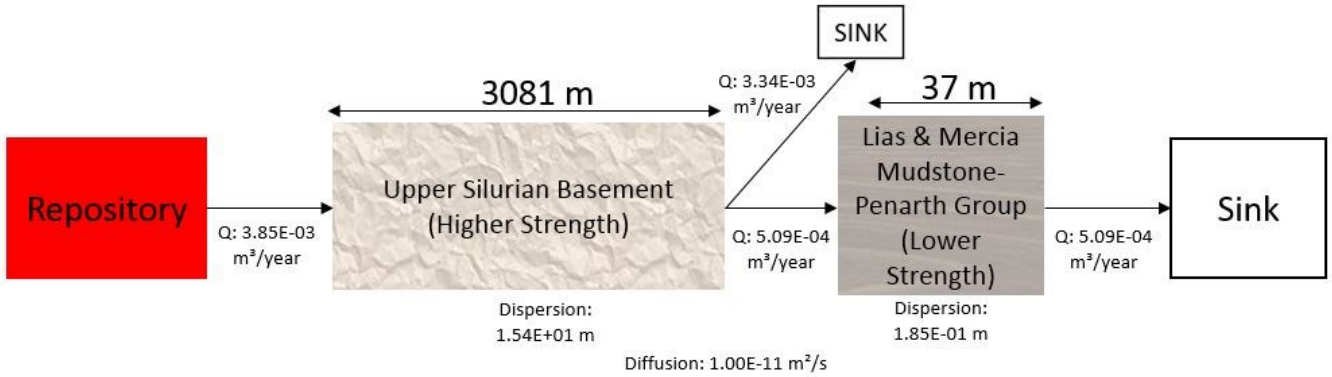

Figure F.0.13: Structure of GoldSim model based on the longest pathway (5574 m) simulated for Pathway 2 of the Thetford model with high permeability values.

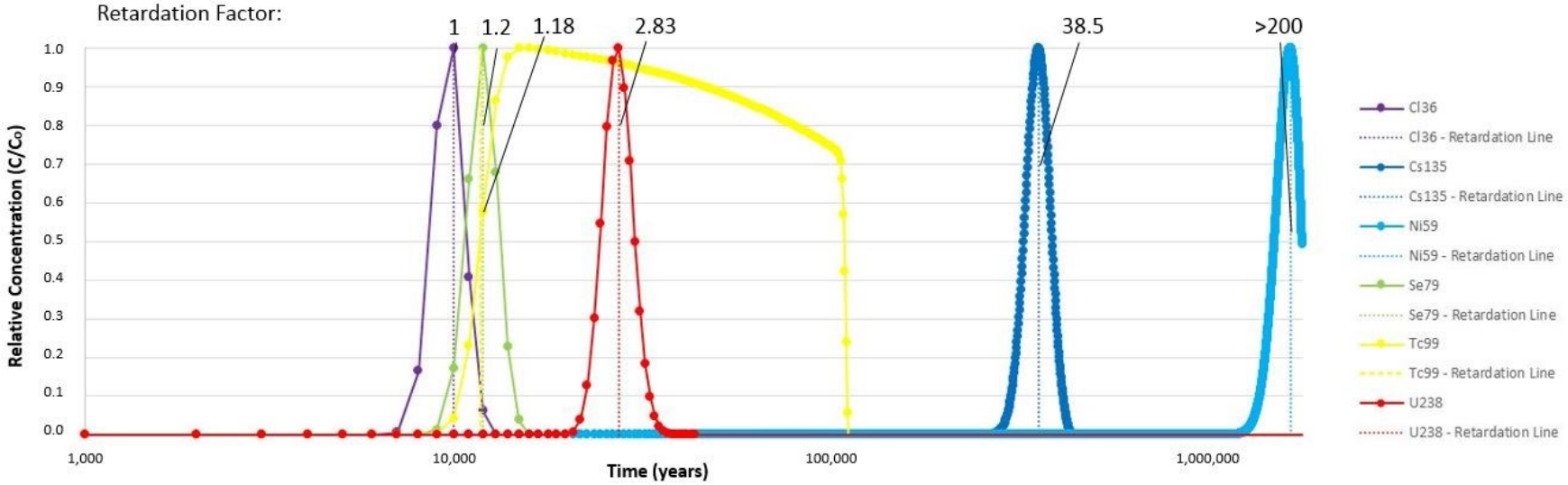

Figure F.0.14: Relative concentration radionuclide breakthrough curves and retardation factors (Rf) based on the maximum particle travel distance (streak-line) along pathway 2 at Thetford when run with high permeabilities (see Figure 4.15.C). No Am241, Eu152 or Sr90 was detected. Comparisons to the analytical solution are provided within electronic Appendix F.3.2.

Appendix G: Evaluating Radioactive Waste Disposal offshore the UK: hydrogeological containment, tunneling principles, and socio-economic factors

This appendix will introduce the concept of offshore sub-seabed radioactive waste disposal (section G.1), discuss whether radionuclide containment is as good offshore as it is onshore (section G.2), the technical feasibility of offshore deep geological disposal facility construction (section G.3), provide preliminary economic predictions for an offshore facility (section G.4), discuss the legal, political and social implications (section G.5), and finally conclusions (section G.6).

This appendix is not intended to provide an exhaustive discussion on all aspect of sub-seabed disposal, nor is it intended to undertake a safety case appraisal of offshore disposal, but is intended to stimulate debate and research within this re-emerging, and increasingly important topic within a UK context.

G.1: Introduction

"Curiously, the search for a suitable nuclear graveyard has been confined almost exclusively to sites on the continents, despite the fact that geological formations below the world's oceans, which cover some 70 percent of the planet's surface, may offer even greater potential" (Hollister & Nadis 1998)

Disposal of radioactive waste within an offshore, sub-seabed deep geological disposal facility is not a new concept (Hollister & Nadis 1998). Historically considered sub-seabed disposal options, within the deep ocean floor (4-5 km below sea surface), included: 1) waste emplacement within relatively soft, hundreds of meters thick, unconsolidated pelagic muds; 2) in the underlying consolidated sediments; or 3) even deeper within basalt of the oceanic crust (Hollister & Nadis 1998). Benefits include long term stable geological formations (over hundreds of millions of years), enormous sorption and dilution capacity, far away from human settlements, and secure access points (Hollister & Nadis 1998). Problems however included unproven emplacement technologies, the requirement for major international cooperation, and legal and social acceptance (McAllister 2013). These problems resulted in deep sub-seabed disposal being side-lined in favour of onshore disposal, within an engineered facility situated 200–1,000 m below the ground surface (see section 1.1.5). The technical and political risks

for this type of onshore disposal were considered less than for deep offshore disposal (McAllister 2013). The concept of shallower sub-seabed disposal facility development, within the continental shelf, has however come to fruition, with the development of the Swedish Final Repository for Short-Lived (low and intermediate level) Radioactive Waste (SFR). The SFR opened in 1988 and is located 50—60 m below the Baltic seabed (SKB 2017b; SKB 2018b; Dybeck & Kawemark 1996). A further extension to the SFR site is currently planned down to a depth of 120 m in order to increase capacity (SKB 2018b).

Up until 2016 no country had publically considered disposing of its heat producing higher activity waste legacy (see section 1.1.4) offshore, with the operational Waste Isolation Pilot Plant (section 2.5.1) and the chosen Forsmark (section 2.5.3) and Olkiluoto (section 2.5.4) sites all situated onshore, albeit the latter two in coastal regions.

Several reports have been published over the past few years re-appraising sub-seabed disposal. These have been published in light of the siting difficulties encountered with the onshore Yucca Mountain disposal facility (section 2.5.2) (Hollister & Nadis 1998; McAllister 2013; Bala 2014), and also because of the Fukushima disaster in Japan (Hidekazu 2012). The UK's decision to extent the national geological screening programme 20 km offshore England, Wales and Northern Ireland (up to the territorial boundary) in 2016 (Radioactive Waste Management 2016b), has therefore-launched the question of sub-seabed disposal feasibility in a serious way. This raises a number of overarching questions, which will be discussed within this chapter, including:

1. Is the containment performance as good offshore as it is onshore?
2. Is it technically feasible to construct an offshore deep geological disposal facility?
3. Would offshore geological disposal facility construction be economically viable?
4. Will an offshore geological disposal facility be legally, politically and socially acceptable?

This appendix will explore these questions by analysing relevant literature, UK and international analogies, and considering fundamental hydrogeological and engineering principles.

G.2.: Is the containment performance as good offshore as it is onshore?

G.2.1: Beneficial Hydrogeological Characteristics

The role of groundwater as part of a multi-barrier containment system was summarised within section 1.1.5 and detailed throughout Chapter 2. In addition, the groundwater characteristics considered beneficial to radionuclide containment and isolation were presented within section 2.3.6. The beneficial hydrogeological characteristics (section 2.3.6) are considered applicable to both onshore and offshore scenarios given the inclusion of the '*seaward dipping and offshore sediments'* hydrogeological regime (section 2.3.7).

G.2.2: Sub-seabed hydrogeological processes

Offshore hydrogeological systems are less well understood than onshore systems as historically far fewer offshore studies have been conducted (Jiao et al. 2015; Post et al. 2013). Where deeper offshore hydrogeological data (> 500 m bgl) has been collected this has been primarily secondary data through oil and gas investigations (Bjørlykke 1993; Bjørlykke 1994; Bjørlykke & Høeg 1997; Gluyas & Swarbrick 2003). These studies, typically undertaken in deep sedimentary basins, paint a picture of fluid flow driven by very long duration geological processes such as compaction, diagenesis, cementation, and mechanical stresses. These processes result in groundwater velocities several orders of magnitude lower than shorter-term onshore predominately pressure driven systems (Bjørlykke 1993; Bjørlykke & Høeg 1997; Ge et al. 2003). In some cases, ancient waters in deep hydrocarbon basins have been tracked isotopically to show that gases and waters diffuse extraordinarily slowly, such as through mudrock seals, at rates of a metre per million years (Lu et al. 2009; Lu et al. 2011). Furthermore, studies have also shown that water layering has remained static and un-moving for tens of millions of years (Macaulay et al. 1992), considered a beneficial characteristic for deep geological disposal.

Forces such as uplift, subsidence and erosion, in addition to glacial groundwater flushing, can however cause changes to pressure driven flow over time (McEvoy et al. 2016), affecting both on and offshore groundwater systems. Glacial flushing is of particular concern for the deep geological disposal of radioactive waste because it can force fresh glacial melt water through the sub-surface, facilitating the faster transport of released radionuclides away from the repository environment. The effect of glacial flushing is dependent on the geological and hydrogeological characteristics of each site. For example, the presence of a near-surface low permeability geological unit, or that of a dense hydrogeological brine formation, can reduce the influence of glaciation on the wider groundwater system (Park et al. 2009). In the UK, glacial flushing has volumetrically replaced pre-existing sub-surface water down to *approx.*

500 m (Degnan et al. 2005). This depth will be greater in settings with strong coupling between near-surface and deeper groundwater systems (section 2.3.6). Such locations may be characterised by fractures open to depth, connecting shallow surface flow to deeper waters.

Groundwater often becomes stratified within offshore sedimentary basins as a results of mass density differences, and trapping from over and under pressurised zones (with respect to hydrostatic pressure) (Gluyas & Swarbrick 2003; Bjørlykke 1993). The elevated densities of these groundwater strata are derived from a mixture of palaeo-seawater trapped before burial, and from ongoing water-rock interactions, dissolving minerals, and increasing the ion (electrically charged particle) content of the waters (Frape et al. 1984; Stober & Bucher 1999). The ion content of the groundwater may increase to the point of the formation of 'dense brines', such as have been found in the Canadian Shield (Fritz & Frape 1982) and the Baltic Shield of Sweden (Bein & Arad 1992). Dense brines have been found to reduce the upward vertical velocity of groundwater flow under groundwater (glacial) flushing conditions, controlling the regional groundwater flow system (Park et al. 2009; Johns & Resele 1997). Because of this control, and their long formation times, dense brines often illustrate hydrogeologically stable environments (Park et al. 2009) and as such, are often considered advantageous environments for deep geological disposal facility development. Dense brines can be found in both onshore and offshore settings.

The average upwards migration of fluids within offshore deep sedimentary basins, driven by geologically slow compaction of sediment, is reported to be less than that of the rate of basin subsidence (Bjørlykke 1993). This results in very low rates of groundwater discharge to the surface (sea-floor). This is in contrast to onshore groundwater systems driven by gravity flow, with typically much faster recharge and discharge often along fractures, faults or diffusion of dissolved ions through matrix formations. Although higher permeability faults can also act as conduits through which deeper, thermally heated waters may ascend within offshore sedimentary basins, the release of porewaters into these faults is often considered limited by the low rate of mechanical compaction (Bjørlykke 1993). Selection of an offshore location with a thick, low permeability geological unit near to the surface, acting as a seal to decouple and prevent the downward penetration of gravity driven flow, and as a top seal to reduce upward outflow, would further limit the rate of discharge towards the surface. This would also reduce the influence of glacial flushing within the area of the repository, enhancing natural barrier containment potential.

If small quantities of radionuclides were eventually to be released to the ocean, the great amount of seawater would act to disperse and reduce the concentration further (Chapman et

al. 1986). However, based on current technologies, this would be almost impossible to remediate if required, and as such, a site with appropriate geological and hydrogeological characteristics would be required to minimise this performance failure. It should however be noted for comparison that onshore geological disposal facility designs also have the potential to discharge to the oceans, either via groundwater base flow or overland flow, but that discharge would more likely be, at least initially, contained to a particular groundwater basin, offering an improved opportunity for remediation.

It can therefore be argued that the likelihood of radionuclide release at the surface, either onshore or offshore, is entirely site dependent, however, offshore settings with their reduced local and regional groundwater flow rates, have the potential to offer greater long term containment and isolation of radioactive waste. This would grant more time for radionuclide decay. This containment and isolation potential can be increased with selection of a site with a low permeability unit near the surface, acting as a laterally extensive top seal, reducing the effect of glacial flushing, and reducing or eliminating discharge to the oceans.

G.2.3: Potentially suitable locations offshore the UK

Six far-field hydrogeological regimes have been previously identified (section 2.3.7) which encompass the beneficial groundwater characteristics (section 2.3.6). The hydrogeological regimes which are specifically applicable to offshore settings (Nirex 1987) include 1) offshore sediments (including sedimentary basins and modified basin limbs) (Figure G.0.1), 2) offshore basement beneath sedimentary cover (Figure G.0.2) and 3) offshore hard rocks (Figure G.0.3).

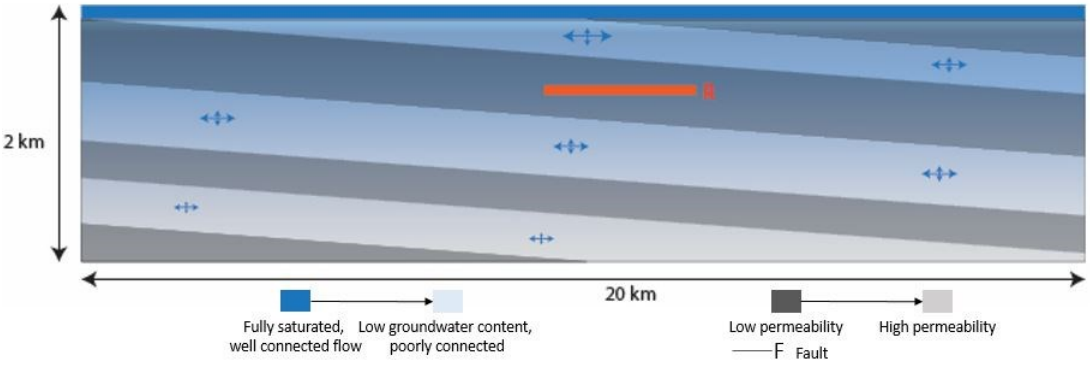

Figure G.0.1: Illustration of offshore sediments hydrogeological regime. Blue arrows represent the direction and magnitude of groundwater flow whilst the orange rectangle R represents the repository.

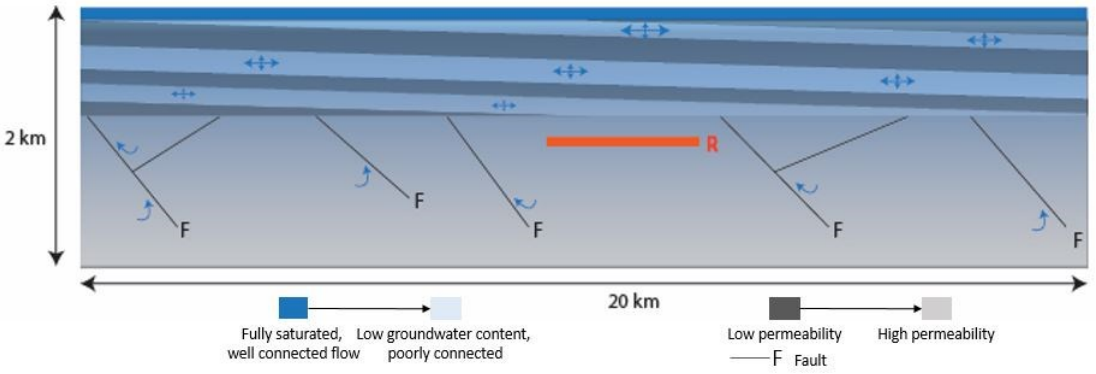

Figure G.0.2: Illustration of offshore Basement rock beneath sedimentary cover hydrogeological regime. Blue arrows represent the direction and magnitude of groundwater flow whilst the orange rectangle R represents the repository.

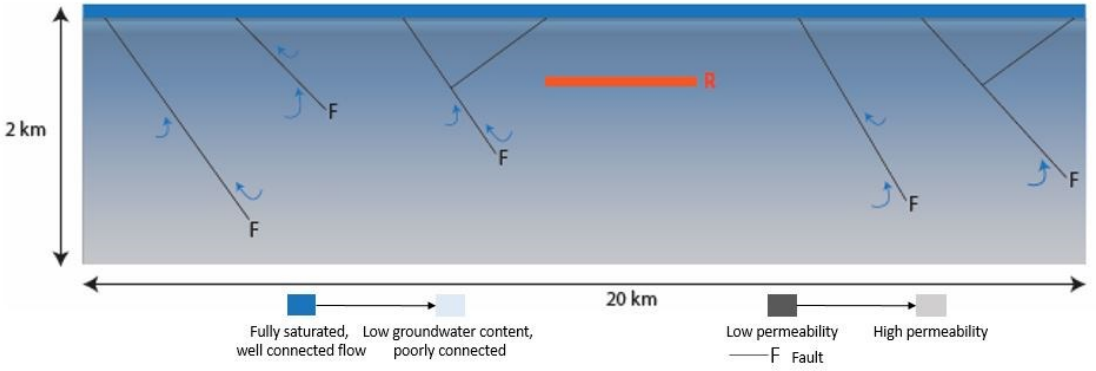

Figure G.0.3: Illustration of offshore hard rocks with low topographic relief hydrogeological regime. Blue arrows represent the direction and magnitude of groundwater flow whilst the orange rectangle R represents the repository. Potentially permeable faults connect to seabed with no sediment seal.

Locations offshore around the UK identified as demonstrating these types of geological, and therefore hydrogeological formations, include locations beneath the Irish Sea, Southern North Sea, and the English Channel (see Figure 2.19). These areas present an interesting opportunity for the UK, and should form the focus of future deep geological facility research moving forward.

Investigations undertaken for the purpose of a rock characterisation facility at Sellafield, UK, (section 2.5.6) identified an offshore dense brine formation beneath the Irish Sea (Black & Brightman 1996) with a purported residence time of >2 Ma (Bath et al. 2006). This residence time transcends quaternary glaciation events implying some degree of hydrogeological stability. The dense brines of the East Irish Sea Basin have already been the focus of a previous geological disposal facility scoping study (Barnes et al. 2005) which concluded that due to the

expected low flow rates and long travel times, the location could offer very good potential for deep geological disposal.

The eastern portion of the East Irish Sea Basin could thus provide an ideal location to focus future offshore site specific investigations, and hence has been chosen for investigation as part of this research (section 2.6). The reasons for this are: 1) a *'potentially suitable sedimentary formation'* which comprises thick, low permeability, flat lying, regionally continuous bedded evaporates (forming a seal to inflow of shallow groundwater, or outflow of leachates from a repository); 2) the presence of 'dense brines'; and 3) the proximity to the nations higher activity waste legacy stockpile at Sellafield.

Furthermore, historic mine workings associated with the Sandwith Anhydrite Mine offshore West Cumbria, to the north of St Bees Head, could offer the opportunity for initial rock characterisation testing, however ultimately any repository development would have to avoid such mined areas. A clear question next is can the site be accessed from onshore safely and at a reasonable cost?

G.3: Is it technically feasible to construct an offshore deep geological disposal facility?

G.3.1: Land vs offshore geological disposal facility access

Historically, Nirex Ltd (now Radioactive Waste Management Ltd) considered that an offshore geological disposal facility could be accessed either via an offshore man-made structure, such as a shaft, or from an onshore facility via connecting sub-seabed (drift) tunnel(s) (Figure G.0.4) (Nirex 1989a; Nirex 2002; Nirex 2005b).

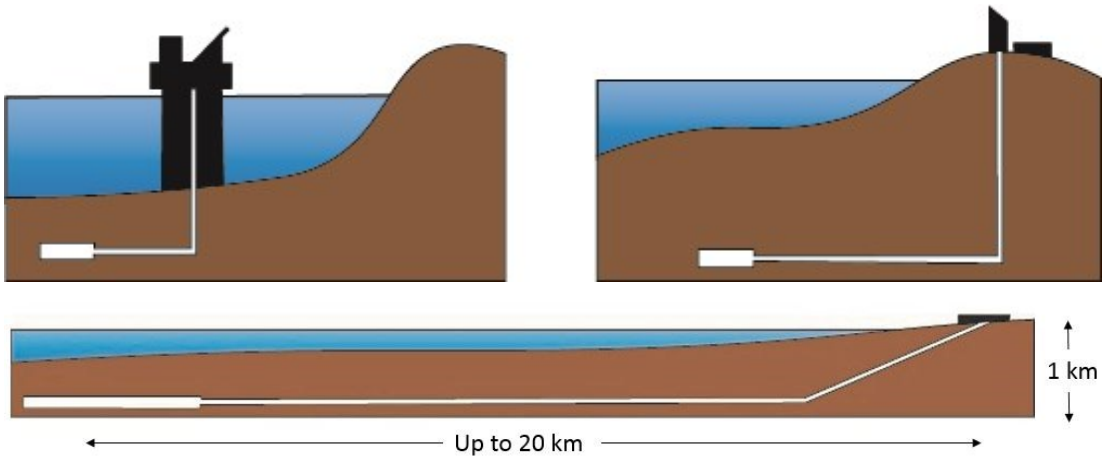

Figure G.0.4: Not to scale conceptual illustrations, redrawn and modified from (Nirex 1989a) of an offshore geological disposal facility with offshore access (top left), and offshore geological disposal facility with land based

access (top right). Below, conceptual illustration of offshore geological disposal facility proposed in this review, accessed by an extended horizontal drift tunnel.

A review undertaken on the disposal of low and intermediate level waste (section 1.1.3) offshore using an offshore shaft access system suggested engineering feasibility (Beale & Taylor 1989). However, the geological conditions required for shaft stability were ultimately considered too restrictive, and the idea was shelved (Nirex 2002). This has resulted in land based access via drift tunnel(s), up to a maximum of 20 km in length, as the only offshore geological disposal facility option under consideration (Radioactive Waste Management 2016b).

G.3.2: International sub-seabed construction experience

Internationally the precedence of sub-seabed engineering has already been proven with multiple projects exceeding 20 km in length. These include the Channel Tunnel with a total tunnel length of 50.5 km and a sub-seabed section of 37.9 km (Eurotunnel 2018); and the Seiken tunnel in Japan with a total length of 53.85 km and a sub-seabed section of 23.3 km (Matsuo 1986). Longer sub-seabed tunnels have also been proposed such as the 73 km long Haenam-Jeju tunnel in South Korea (Yoo 2016), and the 220 km Taiwan Strait tunnel (Gu et al. 2004). All these offshore tunnels are however shallower, by at least 50 m (Eurotunnel 2018), than a drift tunnel would be required to descend as a minimum.

Although challenges exist with offshore site investigations and construction (Li et al. 2015), most notably through the encountering of transmissive hydrogeological features (Anagnostou 2014), almost continuous technological advancements (Ellinas 1990; Davis 1996) have resulted in strong sub-seabed predictive capabilities. These technologies enable the most transmissive features to be avoided, or their effects mitigated against. Recent advances include: 1) the use of P-Cable (http://pcable.com/), improving the resolution of seismic imaging within the upper 1 km; 2) geological forecasting through the use of radar and advanced borehole drilling such as used in the Qingdao Kiaochow Bay Tunnel, China (Li et al. 2015); and 3) combined electrical resistivity and seismic refraction tomography, such as at the Äspö Hard Rock Laboratory, Sweden (Ronczka et al. 2017).

The greatest abundance of transmissive features are typically associated with the upper 300 m where glacial isostatic rebound, weathering, and mineral dissolution have physically and chemically altered the rock mass (Rutqvist & Stephansson 2003; Coli & Pinzani 2014; Wladis et al. 1997). Tunnelling projects are typically constructed within this near surface region and as a result experienced groundwater inflow (Coli & Pinzani 2014). Deeper than around 500

m, standard crustal stress regimes mean that vertical stress becomes greater than the minimum horizontal stress, such that horizontal fractures close, and vertical fractures become in compression and open (Engelder 1993). The sub-surface stress regime is however setting and lithology dependent (Rutqvist 2015; Ingebritsen & Manning 1999; Stober & Bucher 2015), with clay rich lithologies showing greater permeability reduction with depth than fractured crystalline rocks (Zheng et al. 2015; Jones & Owens 1980; McLatchie et al. 1957; Thomas & Ward 1972). Development of an offshore deep geological disposal facility and connecting drift tunnel would therefore benefit from greater construction depth i.e > 500 m, overlain by abundant clay rich rock to reduce vertical permeability. Associated costs are provided within section G.4.

G.3.3: Mine site analogy for the purpose of offshore deep geological disposal facility ventilation design

In many respects a geological disposal facility can be considered similar in layout to that of a mine site, with a large underground space for operations connected via service tunnels to a supporting surface facility. In the case of an offshore facility, access and egress of personnel, waste, equipment and services would be via long (up to a maximum length of 20 km) drift tunnel, compared to vertical shafts, or a combination of shafts and shorter drift tunnels for onshore facility (Nuclear Decommissioning Authority 2010a). The long access drift tunnel(s) potentially required for an offshore facility raises questions around appropriate ventilation, especially as the development of offshore ventilation shafts would create vertical pathways for groundwater and radionuclide migration, and thus should be avoided.

Although no offshore mine site with a 20 km long connecting sub-seabed tunnel has been identified during this research, Boulby Potash Mine in East Yorkshire, UK, extends 7—8 km offshore beneath the North Sea. Boulby has >1,000 km of subterranean tunnels of which 65—70% are located offshore (Boulby 2017). The mine also extends to depths of *approx.* 1.4 km and is ventilated by a series of fans and booster fans controlled from a surface ventilation facility (Boulby 2017). Furthermore the ability of the international community to ventilate and cool very deep mines, such as the 3.3 km deep South African Mponeng Gold Mine (AngloGoldAshanti 2017), suggests an appropriate ventilation system could be designed in the case of an offshore facility by specialist ventilation engineers, improving radionuclide safety.

The cost of construction and operation of ventilation systems on mine sites is reported to be high (typically 15—22% of total mine costs (Petrov and Popov (2004) reported in Acuna

Duhart 2010)). However, operational mine sites are 'profit' driven operations as opposed to 'safety' driven operations and as such, the improved offshore radiological containment may outweigh the additional cost of ventilating the long access tunnel(s) and offshore geological disposal facility.

G.4: Would offshore deep geological disposal facility construction be economically viable?

The cost of an offshore geological disposal facility can most simply be approximated as the cost of an onshore geological disposal facility, plus the additional sub-seabed tunnel connecting the onshore surface facility to the offshore repository. Section G.4 will therefore firstly discuss onshore geological disposal facility cost estimates (section G.4.1) for which most information currently exists, followed by offshore cost estimates (section G.4.2).

G.4.1: Onshore deep geological disposal facility cost estimates

Economic predictions for development of an onshore geological disposal facility within the UK range from £10.95 billion to £37.25 billion (Nuclear Decommissioning Authority 2017a). These estimates are for the existing waste legacy, excluding waste from the new generation of proposed nuclear power stations. The most-likely cost estimate is however placed at £14.75 billion (Nuclear Decommissioning Authority 2017a). To put these values into context, the NDA's most-likely economic 'discounted' provision for decommissioning the UK's entire nuclear power network stands at *approx.* £164 billion (Nuclear Decommissioning Authority 2017a) i.e. a disposal facility would form 9 % of the total anticipated decommissioning cost. For clarification, the onshore disposal facility design includes onshore and underground facilities, and a 5.5 m diameter drift tunnel extending 3.3 to 4 km length depending on rock type and depth (Nuclear Decommissioning Authority 2010a). Therefore a section of total possible offshore drift tunnel length has already been accounted for within onshore disposal cost estimates.

Direct comparison to other international deep geological disposal facility cost estimates is problematic given the variation in waste stream content and volume between countries. The cost of a deep geological repository in Canada for used nuclear fuel has however been previously estimated at $12.7 billion (£9.6 billion) (Radioactive Materials Management 2003), whilst the Swedish deep geological disposal facility at Forsmark is estimated at SEK 36,675 million (£3.2 billion) (SKB 2017a). The low cost of Forsmark is considered a result of the segregation of radioactive waste into three separate repositories; the 'SFR' for short-lived LLW and ILW (see section G.1) which will take 200,000 m^3 of radioactive waste post extension (SKB 2017b); a 'SFL' for long lived LLW and ILW (although this is still within the

planning stages); and the deep geological disposal facility at Forsmark for HAW (SKB 2017a) taking a calculated 23,000 m^3 of HAW based on a capacity of 6,000 canisters, each with a volume of 3.7 m^3 (SKB 2017b). The segregation of the waste into three separate sites therefore reduces the total volume of waste required for final deep geological disposal at Forsmark to <5 % of that of the UK (see section 1.1.4).

In addition to the cost of siting, design, construction, operation and decommissioning of a UK geological disposal facility, costs will also be incurred in the transportation and associated re-packaging of the waste (Sorenson 2015). Transportation will take place from the storage facility at Sellafield (Cumbria), out along public roads, or via waterways to the final repository site. Development of a drift tunnel directly from Sellafield out beneath the Irish Sea to an offshore disposal facility would remove the need for external transportation, thus removing some of these extra costs. The cost savings by removing the need for re-packaging and extra transportation within this scenario can be approximated at £700 million. This estimate is based on Swedish cost estimates for transportation, encapsulation and storage, corrected for reduction in activity/process, and based on an onshore geological disposal facility cost estimate of £14.75 billion.

Table G.0.1: Breakdown of cost saving for geological disposal facility (GDF) development offshore Sellafield within the East Irish Sea Basin.

Activity/Process	**% contribution to total onshore GDF cost (SKB 2017a)**	**Amount and Justification for reduction**	**% reduction to total GDF cost**
Transportation	4	50% reduction as outwards transport not required	2
Encapsulation	11	10% reductions in both encapsulation and storage - some reduction but large scale encapsulation, verification and storage still required	1.1
Storage	17		1.7
Total			4.8

Furthermore, this may prove a more publically acceptable solution as discussed within section G.5, by removing the risk posed by the transportation of highly radioactive waste across the public transportation network.

G.4.2: Offshore Geological Disposal Facility Cost Estimates

A sub-seabed drift tunnel connecting the onshore surface facility to the offshore repository could extend a maximum of 20 km offshore, up to the UK's territorial water limit (Radioactive Waste Management 2016b). However, if an offshore disposal facility is located close to the

coast, the length of the drift tunnel may be no greater than for an onshore disposal facility, resulting in similar associated costs.

Unfortunately no international comparative studies of sub-seabed tunnelling costs have been identified to enable cost estimation of an extended sub-seabed drift tunnel. Furthermore, when comparative onshore tunnelling costs have been identified, these have been of limited scope e.g.(Infrastructure UK 2010). (Efron & Read 2012) suggests that this is because tunnelling costs are highly variable and dependent on numerous internationally dependent factors including geology, tunnel type and design, location, length, depth, tunnel face area, materials/plant, local labour costs, local health and safety regulations, environmental regulations, client knowledge, and government and public support schemes. This is assumed to cause a similar problem for sub-seabed tunnel cost comparisons. Therefore, to minimise the number of extraneous variables, two modern UK based tunnelling analogies will be discussed instead to ensure comparable labour costs, plant/material costs and health, safety and environmental regulations; Crossrail and the Thames Tideway Tunnel.

G.4.2.1: Crossrail Cost Analogy

The London based onshore Crossrail project involves two twin bored 6.2 m diameter tunnels extending 21 km in length, and reaching a maximum depth of 40 m below ground level (Crossrail 2018a). Although an offshore repository could reach a similar length, a repository would descend deeper, to a depth of 200-1,000 m. Crossrail and a geological disposal facility are however comparable in the respect both are/would be high grade construction projects. Crossrail in order to avoid underground services through central London, and a geological disposal facility to ensure radionuclide containment through geological mitigation and security of flowing features.

In addition to depth, differences also arise over the number of bored tunnels. International experience suggests a single bored tunnel, rather than the Crossrail twin bored tunnel, however, due to the requirement for waste, personnel and ventilation segregation (Parsons Brinckerhoff 2010; Nuclear Decommissioning Authority 2010a), the possibility of twin bored drift tunnel is not excluded. Finally an offshore geological disposal facility would be constructed under the seabed where enhanced management against encountered transmissive features would be required (see section G.3.2) compared to Crossrail.

The total cost of Crossrail is anticipated to be around £14.8 billion (Crossrail 2018b), including 10 new passenger boarding and disembarking stations (Crossrail 2018a), not required in the case of a geological disposal facility. Based on the list of awarded contracts (Crossrail 2018b),

although difficult to segregate, all excavation work including planning, control and management comprises slightly less than a third of the total costs, the station construction is slightly more than a third and system-wide infrastructure makes up the remainder.

The twin-bored tunnel construction costs (33%) can therefore be approximated to £4.9 billion. This equates to £230 million/km. Assuming a 16.7 km length twin bored tunnel (20 km max. length subtract 3.3 km already accounted for within onshore geological disposal facility cost estimates), the £230 million/km would add an extra £3.9 billion onto the cost of an onshore geological disposal facility. This would increase the cost of a geological disposal facility by *approx.* 21%.

G.4.2.2: Themes Tideway Tunnel Cost Analogy

Another high grade construction project through central London, the Thames Tideway Tunnel, consists of a single bored 7.2 m wide tunnel, situated at a depth of between 35 and 65 m. The tunnel will extend a total length of 25 km (Tideway 2015). Again, similarities to an offshore geological disposal facility involve the high grade construction required and likely single bored tunnel. Differences are associated with depth of burial and onshore construction.

Cost estimates for the Thames Tideway Tunnel are £4.2 billion (Tideway 2015), including a number of pumping stations and sewage treatment works, not required for a geological disposal facility (Tideway 2015). Again assuming similar division of costs i.e. *approx.* 30 % on tunnelling costs, the single bored tunnel costs can be approximated at £56 million/km. Assuming a 16.7 km length single bored tunnel as described above, this would add an additional £0.9 billion onto the cost of an onshore geological disposal facility. This would increase the overall cost estimates by *approx.* 6%.

G.4.2.3: Offshore Geological Disposal Facility Cost Estimates & Uncertainty: Summary

Cost estimates, based on the anecdotal Crossrail and Themes Tideway Tunnel projects, rather than directly analogous construction projects, suggest a mark-up of between 6 and 21 %. These cost estimates are considered conservative as the repository may not extend the full 20 km offshore. Furthermore, if repository construction were offshore from Sellafield, assuming cost estimates based on the Thames Tideway alone, much of the extra sub-seabed tunnelling costs could be offset by the reduced cost of waste transportation and associated packaging as discussed above.

Finally, costs estimated for an offshore geological disposal facility are still well within the cost uncertainty range for an onshore disposal facility development (discussed above) thus suggesting economic feasibility. However this research only presents preliminary cost

estimates and further research must be carried out, in conjunction with any potential developer, to constrain the costs further.

G.5: Will it be legally, politically and socially acceptable?

G.5.1: Ownership and Volunteering Communities

The decision to extend the search area up to 20 km off the coast of the UK would place an offshore geological disposal facility within the legal subsoil of 'territorial waters' (UK Parliament 1987). The ownership of mining rights, resources and seabed access of the territorial waters are controlled by the UK, and are leased through The Crown Estate. Although The Crown Estate do not currently have a specific policy for offshore geological disposal facility development, the granting of servitudes and leases for storage of materials would be required prior to any operations or construction. This is also the policy for any potential Carbon Capture and Store site (The Crown Estate 2017), another large scale sub-surface geo-engineering project, although CO_2 emplacement is achieved via borehole injection rather than mining.

The UK government opted for a 'volunteerism' based approach to site selection, however following rejection of an application for a rock characterisation facility at the site (see section 2.5.6), the UK has been left with no willing host community. In January 2018, the Nuclear Decommissioning Authority relaunched the search for a volunteer host community (Guardian 2018). The search started with a draft document outlining how communities should be represented (Department for Business Energy & Industrial Strategy 2018). No clear indication was however given within the document as to whom a host community, in the case of an offshore geological disposal facility, would be/comprise. A request has been filled to the Nuclear Decommissioning Authority for clarification of this point, and a response is currently awaited.

If the Crown Estate could however be the host community in on offshore scenario, disposal within territorial waters could remove the requirement for an onshore volunteering host community, enabling faster final disposal to be achieved.

G.5.2: Marine Pollution and Safety

The marine environment (including marine life and the wider aquatic ecosystem) is protected through a number of international and domestic laws including: 1) the 1982 United Nations Convention on the Law of the Sea (UNCLOS); 2) the 1992 Convention for the Protection of the Marine Environment of the North-East Atlantic (OSPAR Convention); 3) the 1972 Convention on the Prevention of Marine Pollution by Dumping of Wastes and Other Matter;

and 4) the 1996 Protocol (London Protocol) (McAllister 2013; Salter & Wilson 2006). International opinion on the legality of offshore disposal is mixed. Firstly, the 1996 London Protocol (London Dumping Convention) voted to classify disposal of nuclear material below the seabed as 'ocean dumping', thus making it illegal (Hollister & Nadis 1998; McAllister 2013). However, a review undertaken into the legality of disposing of radioactive waste within an offshore disposal facility, accessed via a sub-seabed tunnel from an onshore surface facility, concluded that disposal would not be legally precluded (Salter & Wilson 2006). This review stated that sub-seabed disposal is not classed as 'dumping' as long as protection of the marine environment is 'scientifically and technically demonstrated' (Salter & Wilson 2006). International interpretation of this law is therefore mixed, and requires clarification, and possible re-appraisal of the legality of offshore disposal facility development.

G.5.3: Public Concerns and Practicalities

The disposal of radioactive waste within an offshore geological disposal facility could bypass the historically encountered 'volunteerism' based political stalemate (section G.5.1). However, on the other hand, research undertaken by the University of East Anglia suggests that oceans are commonly perceived as a *'global resource'* and as such, public opposition to offshore geological disposal facility development may still arise (Nirex 2005b). These concern have also been highlighted by (Bala 2014; Hollister & Nadis 1998; Nirex 2005b; Nirex 2005c) and thus illustrate a serious and ongoing area of uncertainty to successful offshore geological disposal facility development. For example, (Hollister & Nadis 1998) notes a bill passed in the house of representatives in America in the mid- 1990's prohibiting sub-seabed disposal, or federal funding of activities, including research, into sub-seabed disposal, illustrating the emotive nature of the subject.

An offshore geological disposal facility with connecting sub-seabed tunnel would require a 1 km^2 surface facility (Nuclear Decommissioning Authority 2010a). Development of an offshore facility within 20 km of a current coastal nuclear facility, namely Sellafield in the UK, would thus provide immediate access to a secure offshore space. Furthermore, development within 20 km of Sellafield where the higher activity waste (section 1.1.4) stockpile is currently located would remove the need for further re-packaging and transportation of the waste (see section G.4.1). This may prove a socially and politically more acceptable option, not only speeding up final disposal, but also improving the long term security of the waste packages.

G.6: Conclusions

In conclusion, containment potential is entirely site specific, however, the low groundwater flow rates and long residence times characterising offshore groundwater flow could provide enhanced long term radionuclide containment and isolation, for as little as a 5% cost mark-up, compared to an onshore disposal facility.

Offshore disposal, within territorial waters, could provide a faster final disposal solution, potentially removing the need for volunteering host community. Furthermore, disposal offshore of Sellafield, within the East Irish Sea Basin, would remove the requirement for further radioactive waste transportation, and associated re-packaging.

The engineering feasibility of an offshore disposal facility, constructed up to 20 km offshore the coast, has already been demonstrated through numerous international sub-seabed construction projects, including the offshore Swedish Final Repository for Short-Lived Radioactive Waste; the offshore Boulby Potash Mine in East Yorkshire, and the 50.5 km long England-France Channel Tunnel.

Previously identified potentially suitable sedimentary formations offshore the UK include: the East Irish Sea Basin; Southern North Sea; and the English Channel. All of which warrant further investigation as part of the on-going national site selection programme.

Further research is however required on the design and implementation of an appropriate ventilation system for the offshore facility, improved offshore tunnelling and construction cost estimates, and the legality and social opposition that may arise to offshore disposal.

G.7: Summary

This appendix has provided a high level discussion on the technical, legal, economic, social and political feasibility of offshore deep geological disposal facility construction, and has highlighted areas around the UK for which future offshore investigations should be focused.